MAHLE GmbH (Ed.)

Pistons and engine testing

MAHLE GmbH (Ed.)

Pistons and engine testing

With 269 illustrations and 20 tables

VIEWEG+
TEUBNER

Bibliographic information published by the Deutsche Nationalbibliothek
The Deutsche Nationalbibliothek lists this publication in the Deutsche Nationalbibliografie; detailed bibliographic data are available in the Internet at http://dnb.d-nb.de.

This book is based on the 1st edition of the German book „Kolben und motorische Erprobung“ edited by MAHLE GmbH.

1st Edition 2012

Editor:
© MAHLE GmbH, Stuttgart 2012

Editorial Office: Ewald Schmitt | Elisabeth Lange

Vieweg+Teubner Verlag is a brand of Springer Fachmedien.
Springer Fachmedien is part of Springer Science+Business Media.
www.viewegteubner.de

Cover design: KünkelLopka Medienentwicklung, Heidelberg
Typesetting: Klementz publishing services, Freiburg
Printing company: AZ Druck und Datentechnik, Berlin
Printed on acid-free paper
Printed in Germany

ISBN 978-3-8348-1590-3

Preface

Dear readers,

The second volume of the MAHLE Knowledge Base, a series of technical books, is both a broader and a more in-depth companion to the first volume, “Cylinder components.” In this volume, MAHLE specialists share their broad, extensive technical knowledge on the subject of the piston, its design, layout, and testing. The many illustrations, graphs, and tables provide a vivid visual overview of the subject, making your work in this area easier every day.

Never before have the requirements that international legislation and customers place on modern engines, and therefore on the piston, been so great, and sometimes so contradictory. That is why you will find so many details about the piston–its function, requirements, different types, design guidelines–as well as about simulating operational durability with finite element analysis, about piston materials, piston cooling, and component testing. Engine testing, however, is still the most important element in the component development program, as is the validation of new simulation programs and systematic development of design specifications. Learn more about it here–with the scientific depth and meticulousness you expect–in the extensive chapter on “Engine testing.”

This second volume of the technical books series is, once again primarily directed to the engineers and scientists in the areas of development, design, and maintenance of engines. However, professors and students in the subjects of mechanical engineering, engine technology, thermodynamics, and vehicle construction, as well as any readers with an interest in modern gasoline and diesel engines, will also find valuable information on the following pages.

I wish you much enjoyment and many new insights from this reading.

Stuttgart, November 2011

Heinz K. Junker

Acknowledgment

We would like to thank all authors for contributing to this technical book.

Dipl.-Ing. Ingolf Binder
Dipl.-Ing. Karlheinz Bing
Dipl.-Ing. Thomas Deuß
Dipl.-Ing. Holger Ehnis
Dr.-Ing. Rolf-Gerhard Fiedler
Dipl.-Ing. Rudolf Freier
Dipl.-Ing. Matthias Geisselbrecht
Dr.-Ing. Wolfgang Ißler
Dipl.-Ing. Peter Kemnitz
Dr.-Ing. Reiner Künzel
Dipl.-Ing. Ditrich Lenzen
Dr. Kurt Maier
Dipl.-Ing. Olaf Maier
Dr.-Ing. Uwe Mohr
Dipl.-Ing. Helmut Müller
Dr. Reinhard Rose
Dipl.-Ing. Wilfried Sander
Dipl.-Ing. Volker Schneider
Dr.-Ing. Wolfgang Schwab
Dipl.-Ing. Bernhard Steck
Peter Thiele
Dr.-Ing. Martin Werkmann

Contents

1 Piston function, requirements, and types

1.1 Function of the piston

1.1.1 The piston as an element of power transmission

In the cylinder of an engine, the energy bound up in the fuel is rapidly converted into heat and pressure during the combustion cycle. The heat and pressure values increase greatly within a very short period of time. The piston, as the moving part of the combustion chamber, has the task of converting this released energy into mechanical work.

The basic structure of the piston is a hollow cylinder, closed on one side, with the segments piston crown with ring belt, pin boss, and skirt; **Figure 1.1**. The piston crown transfers the gas forces resulting from the combustion of the fuel-air mixture via the pin boss, the piston pin, and the connecting rod, to the crankshaft.

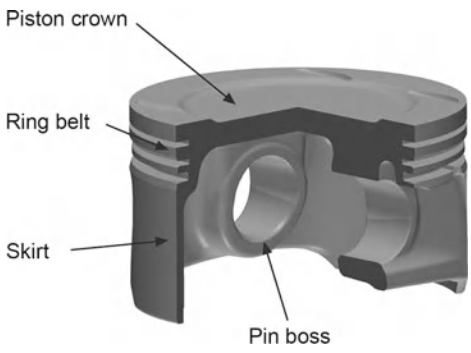

Figure 1.1: Gasoline engine pistons for passenger cars

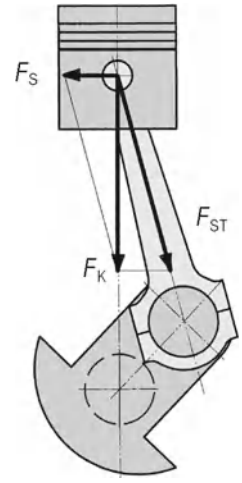

Figure 1.2: Forces on the piston

The gas pressure against the piston crown and the oscillating inertial forces, referred to in the following as the inertia force, of the piston and the connecting rod constitute the piston force F_K; **Figure 1.2**. Due to the redirection of the piston force in the direction of the connecting rod (rod force F_{ST}), an additional component arises–following the force parallelogram–, namely the lateral force F_S, also known as the normal force. This force presses the piston

MAHLE GmbH (Ed.), *Pistons and engine testing,* DOI 10.1007/978-3-8348-8662-0_1,

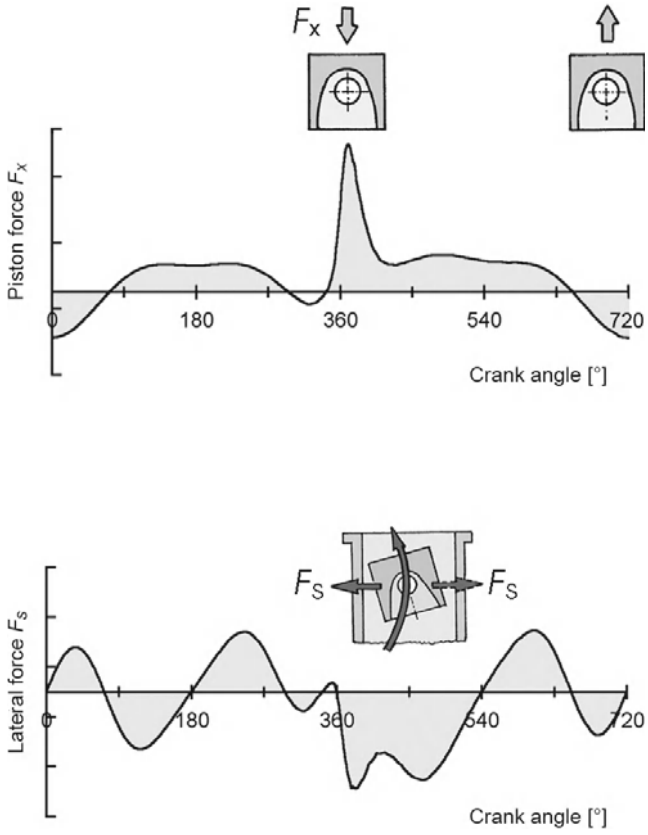

Figure 1.3:
Force curves

skirt against the cylinder bore. During a combustion cycle, the lateral force changes direction several times, which presses the piston from one side of the cylinder bore to the other, due to the existing piston clearance. **Figure 1.3** shows the piston force and lateral force curves as a function of the crank angle.

1.1.2 Sealing and heat dissipation

As a moving and force-transmitting component, the piston, together with the piston rings, must reliably seal the combustion chamber against gas passage and the penetration of lubricating oil under all load conditions. It can fulfill this task only if a hydrodynamic lubricating film is present between the piston rings or skirt and the cylinder bore. The stoppage of the piston at the two dead center points, where the lubricating film isn't fully functional, is particularly problematic. The piston rings must remain functional over very long running periods. Average sliding speeds are typically 10 to 12 m/s.

In four-stroke engines, the piston crown also supports the mixture formation. For this purpose, it has a partially jagged shape, with exposed surfaces (such as the bowl rim) that absorb heat and reduce the load capacity of the component. In two-stroke engines with

outlet ports, the piston also acts as a sliding valve and is thermally highly loaded due to the combustion gases flowing out at high speed.

In order for the piston to be able to withstand the briefly occurring, extreme combustion temperatures, it must dissipate the heat sufficiently; Chapter 5.6. The heat in the cylinders is primarily dissipated by the piston rings, but also by the piston skirt. The inner contour transfers heat to the air in the housing and to the oil. Additional oil can be applied to the piston for improved cooling; Chapter 5.

1.1.3 Variety of tasks

The most important tasks that the piston must fulfill are:
- Transmission of force from and to the working gas
- Variable bounding of the working chamber (cylinder)
- Sealing off the working chamber
- Linear guiding of the conrod (trunk piston engines)
- Heat dissipation
- Support of charge exchange by drawing and discharging (four-stroke engines)
- Support of mixture formation (by means of suitable shape of the piston surface on the combustion chamber side)
- Controlling charge exchange (in two-stroke engines)
- Guiding the sealing elements (piston rings)
- Guiding the conrod (for top-guided conrods)

As the specific engine output increases, so do the requirements on the piston at the same time.

1.2 Requirements on the piston

Fulfilling different tasks such as
- structural strength,
- adaptability to operating conditions,
- low friction,
- low wear,
- seizure resistance and simultaneous running smoothness,
- low weight with sufficient shape stability,
- low oil consumption, and
- low pollutant emissions values

result in partly contradictory requirements, both in terms of design and material. These criteria must be carefully coordinated for each engine type. The optimal solution can therefore be quite different for each individual case.

Table 1.1: Operating conditions and solution approaches for piston design and materials

Operating conditions	Requirements on the piston	Design solution	Material solution
Mechanical load a) Piston crown/combustion bowl Max. gas pressure, two-stroke gasoline engine: 3.5–8.0 MPa Max. gas pressure, four-stroke gasoline engine: Naturally aspirated engine: 6.0–9.0 MPa Turbo: 9.0–12.0 MPa Max. gas pressure, diesel engine: Naturally aspirated engine: 8.0–10.0 MPa Turbo: 14.0–24.0 MPa b) Piston skirt Lateral force: approx. 10% of the max. gas force	High static and dynamic strength, even at high temperatures	Sufficient wall thickness, shape-stable design, consistent “force flow” and “heat flow”	Various AlSi casting alloys, warm-aged (T5) or age-hardened (T6), cast (partly with fiber reinforcement), or forged; Forged steel
c) Pin boss Permissible surface pressure temperature-dependent	High surface pressure in the pin bores; low plastic deformation	Bushing	Specialty brass or bronze bushings
Temperatures: Gas temperatures in the combustion chamber of up to 2,000°C, exhaust 600–900°C Piston crown/bowl rim, 200–400°C, for ferrous materials 350–500°C Pin boss: 150–260°C Piston skirt: 120–180°C	Strength must also be retained at high temperature. Identification mark: Strength at elevated temperatures, durability, high thermal conductivity, scaling resistance (steel)	Sufficient heat-flow cross sections, cooling channels	As above
Acceleration of piston and connecting rod at high rpm: partly much greater than 25,000 m/s^2	Low mass, resulting in small inertia forces and inertia torques	Lightweight construction with ultra-high material utilization	AlSi alloy, forged
Sliding friction in the ring grooves, on the skirt, in the pin bearings; at times poor lubrication conditions	Low frictional resistance, high wear resistance (affects service life), low seizing tendency	Sufficiently large sliding surfaces, even pressure distribution; hydrodynamic piston shapes in the skirt area; groove reinforcement	AlSi alloys, tin-plated, graphited, coated skirt, groove protection with cast-in ring carrier or hard anodizing
Contact alteration from one side of the cylinder to the other (primarily in the area of the top dead center)	Low noise level, moderate “piston tipping” in cold or warm engine, low impulse loading	Low running clearance, elastic skirt design with optimized piston shape, pin bore offset	Low thermal expansion. Eutectic or hypereutectic AlSi alloys

The operating conditions of the piston and the resulting design and material requirements are summarized in **Table 1.1**.

1.2.1 Gas pressure

The piston is subjected to an equilibrium of gas, inertia, and supporting forces. The supporting forces are the resultant of the conrod and lateral forces. The maximum gas pressure in the combustion cycle has critical significance for the mechanical loads. The maximum gas pressures that occur depending on the combustion process (gasoline, diesel, two-stroke, four-stroke) and charge intake (naturally aspirated/turbocharger) are shown in **Table 1.1**. At a speed of 6,000 rpm in a gasoline engine, for example, at a maximum gas pressure in the combustion cycle of 75 bar, each piston (D = 90 mm) is subjected to a load of about 5 metric tons, 50 times per second.

In addition to the maximum gas pressure, the rate of pressure increase also affects the stress on the piston. The values for diesel engines are about 6 to 12 bar/1 CAD (crank angle degree), but can be significantly higher in case of combustion faults. The rates of pressure increase in gasoline engines are in the range of 3 to 6 bar/1 CAD. Especially if unsuitable fuels are used (octane number too low), combustion faults can occur under high load, known as “knocking.” Pressure increase rates of up to 30 bar/1 CAD are possible. Depending on the knock intensity and period of operation, it can lead to significant damage to the piston and failure of the engine. As a prevention method, modern gasoline engines are equipped with knock control systems.

1.2.2 Temperatures

The temperature of the piston and cylinder is an important parameter for operational safety and service life. The peak temperatures of the exhaust gas, even if present only for a short time, can reach levels in excess of 2,200°C. The exhaust gas temperatures range between 600 to 850°C for diesel engines, and 800 to 1,050°C for gasoline engines.

The temperature of the fresh intake mixture (air or mixture) can be in excess of 200°C for turbocharged engines. Charge air cooling reduces this temperature level to 40–60°C, which in turn lowers the component temperatures and improves filling of the combustion chamber.

Due to their thermal inertia, the piston and the other parts in the combustion chamber do not exactly follow these temperature fluctuations. The amplitude of the temperature fluctuations is only a few °C at the piston surface, and drops off rapidly toward the interior. The piston crown, which is exposed to the hot combustion gases, absorbs different amounts of heat, depending on the operating point (rpm, torque). For non-oil-cooled pistons, the heat is primarily conducted to the cylinder wall by the compression ring, and to a much lesser degree,

by the piston skirt. For cooled pistons, in contrast, the engine oil carries off a large portion of the accumulating heat; Chapter 7.2.

Heat flows that lead to characteristic temperature fields result from the material cross sections that are determined by the design. Typical temperature distributions for gasoline and diesel engine pistons are shown in **Figures 1.4** and **1.5**.

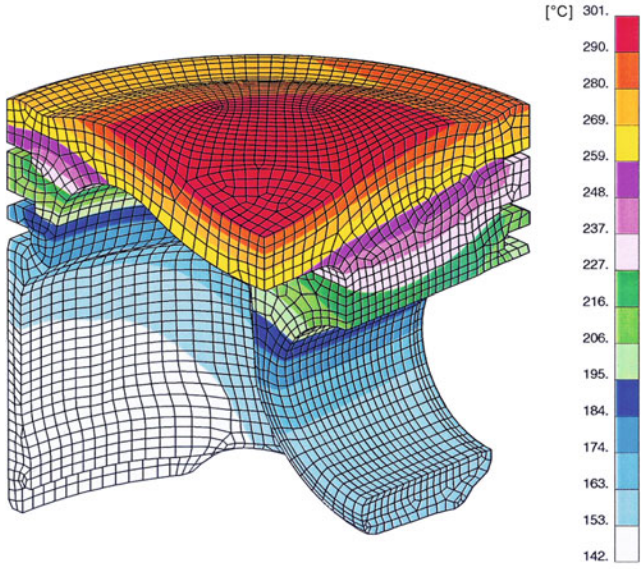

Figure 1.4:
Temperature distribution in a gasoline engine piston

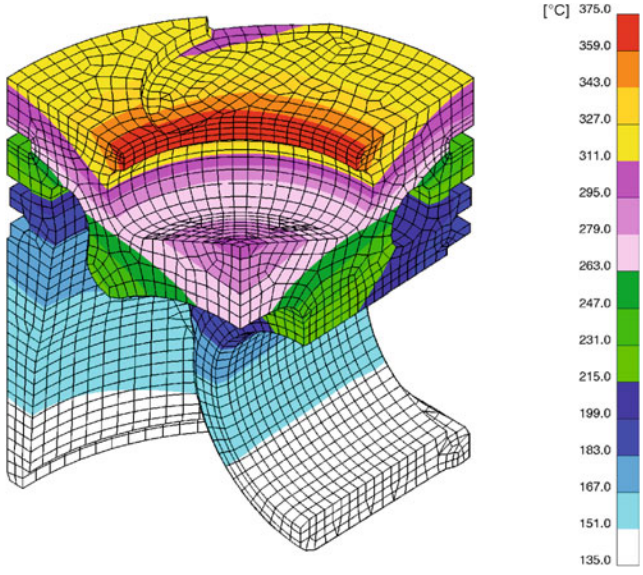

Figure 1.5:
Temperature distribution in a diesel engine piston with cooling channel

The temperature levels and distributions in the piston essentially depend on the following parameters:

- Operating process (gasoline/diesel)
- Operating principle (four-stroke/two-stroke)
- Combustion process (direct/indirect injection)
- Operating point of the engine (speed, torque)
- Engine cooling (water/air)
- Design of the piston and cylinder head (location and number of gas channels and valves, type of piston, piston material)
- Piston cooling (yes/no)
- Intensity of cooling (spray jet cooling, cooling channel, cooling channel location, etc.)

The strength properties of the piston materials, particularly of light alloys, are very dependent on the temperature. They determine the level and distribution of the temperatures in the piston and the stresses that can be withstood. High thermal loads cause a drastic reduction in the fatigue resistance of the piston material. The critical locations for diesel engines with direct injection are the boss zenith and the bowl rim; and for gasoline engines, the transition area from the boss connection to the piston crown.

The temperatures in the first piston ring groove are also significant in terms of oil coking. If certain limit values are exceeded, the piston rings tend to “lock up” (coking) due to residue build-up in the piston ring groove, which leads to an impairment of their functionality. In addition to the maximum temperatures, the piston temperatures are significantly dependent on the engine operating conditions (such as speed, brake mean effective pressure, ignition angle, injection quantity). **Table 7.2.3** in Chapter 7.2 shows typical values for passenger car gasoline and diesel engines in the area of the first piston ring groove.

1.2.3 Piston mass

The piston, equipped with piston rings, piston pin, and circlips, together with the oscillating connecting rod portion, constitute the oscillating mass. Depending on the engine type, free inertia forces and/or inertia torques are thus generated that can no longer be compensated at times, or that require extreme efforts to do so. This characteristic gives rise to the desire to keep the oscillating masses as low as possible, particularly in high-speed engines. The piston and the piston pin account for the greatest proportion of the oscillating masses. Any weight reduction undertaking must therefore start with these components.

About 80% of the piston mass is located in the area from the center of the piston pin to the upper edge of the crown. The remaining 20% is in the area from the center of the piston pin to the end of the skirt. The determination of the compression height *KH* is therefore of great significance, because it predetermines about 80% of the piston mass.

For pistons of gasoline engines with direct injection, the piston crown can be used to support mixture formation and can thus be shaped accordingly. These pistons are taller and heavier. The center of gravity is thus shifted upward.

Piston mass m_K can best be compared (without piston rings and piston pin) when related to the comparative volume D^3, as shown in **Figure 1.6**. The compression height, however, must always be taken into consideration. Mass figures ("X factors") for proven piston designs m_K/D^3 are shown in **Table 1.2**.

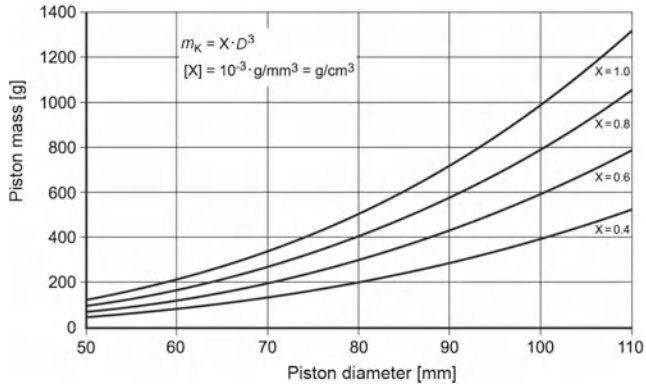

Figure 1.6:
Piston mass m_K (without piston rings and piston pin) for passenger car engines, as a function of the piston diameter

Table 1.2: Mass figures for passenger car pistons <100 mm in diameter, made of aluminum base alloys

Operating principle	Mass figure m_K/D^3 [g/cm³]
2-stroke gasoline engine with manifold injection	0.50–0.70
4-stroke gasoline engine with manifold injection	0.40–0.60
4-stroke gasoline engine with direct injection	0.45–0.65
4-stroke diesel engine	0.90–1.10

1.2.4 Friction and wear

The design, shape, and installation clearance are not the only factors that ensure flawless operation of the piston in the cylinder. The friction forces on the skirt and the skirt lubrication play a decisive role in smooth piston running behavior.

Certain roughness values must be maintained at the piston skirt and the honed cylinder surface. They

- enhance running-in characteristics,
- prevent abrasive wear,

- are a prerequisite for the formation of a hydrodynamic lubricating film between the piston skirt and the cylinder wall, and
- prevent the piston from seizing, i.e., local fusing between the piston and the cylinder due to lack of clearance or lubricating oil.

Roughness values of R_a = 2.5–5 µm are aimed for on the piston skirt.

Figure 1.7 shows the location and shape of the boundary lubrication gap between piston and cylinder. The hydrodynamic lubrication behavior is disturbed only at the reversal points (top and bottom dead center) of the piston, due to the change in direction of the piston motion.

Protective coatings on the running surfaces, such as MAHLE GRAFAL®, reduce friction and improve resistance to seizing.

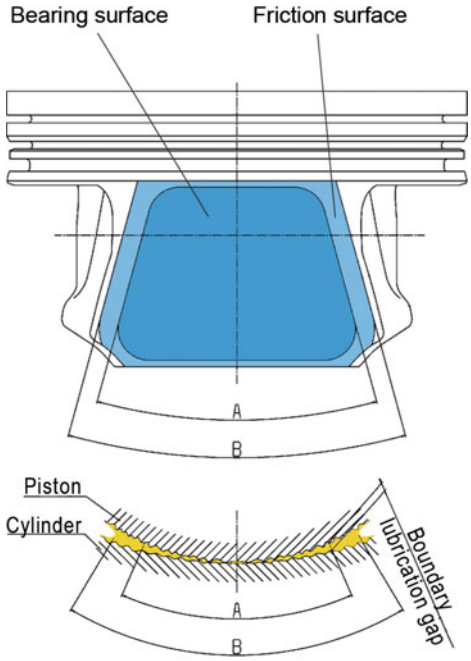

Figure 1.7:
Boundary lubrication gap between piston and cylinder

1.2.5 Blow-by

One of the primary functions of the piston and the piston rings is to seal off the pressurized combustion chamber from the crankcase. Due to the clearance between the piston and the cylinder, combustion gases (blow-by) can enter the crankcase during the kinematic motion sequence. In addition to the resulting energy loss, escaping leakage gas also poses a risk to the piston and piston ring lubrication due to contamination and displacement of the lubricating film, and due to oil coking as a result of overheated temperatures at the locations in

contact with the combustion gases. Increased blow-by values also require greater crankcase ventilation.

Sealing against gas penetration is mainly accomplished by the first piston ring, which is a compression ring. For naturally aspirated engines, the quantity of blow-by is a maximum of 1%; for turbocharged engines, it is a maximum of 1.5% of the theoretical air intake volume.

1.3 Piston types

The various operating principles of combustion engines give rise to a wide variety of engine types. Each engine type requires its own piston variant, characterized by its construction, shape, dimensions, and material.

The most significant piston types in engine design are described in the following. There are also new development paths, such as pistons for very low-profile engines, or pistons made of composite materials with local reinforcement elements.

1.3.1 Pistons for four-stroke gasoline engines

Modern gasoline engines employ lightweight designs with symmetrical or asymmetrical skirt contours and potentially different wall thicknesses for the thrust and antithrust sides. These piston types are characterized by low weight and particular flexibility in the center and lower skirt areas.

1.3.1.1 Controlled-expansion pistons

Controlled-expansion pistons are pistons with insert strips that control thermal expansion. They are installed in gray cast iron crankcases. The main target of controlled-expansion piston designs, and many inventions in this field, was and still is to reduce the relatively large differences in thermal expansion between the gray cast iron crankcase and the aluminum piston. The known solutions range from Invar strip pistons to autothermic or Autothermatik pistons.

Due to various adverse properties–notch effects due to cast-in strips, increased piston mass, and higher cost–controlled-expansion pistons are fading more and more into the background. For completeness' sake, however, older piston types are addressed briefly.

Autothermic pistons

Autothermic pistons, **Figure 1.8**, are slotted at the transition from the piston crown to the skirt, at the height of the oil ring groove. They are characterized by their particularly quiet

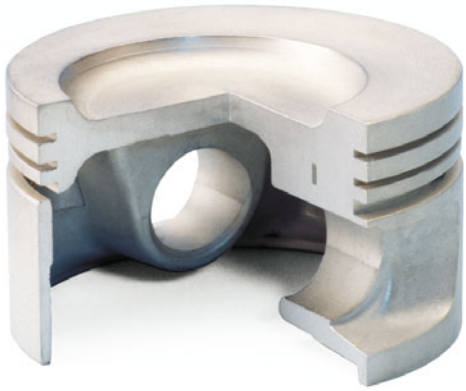

Figure 1.8: Autothermic piston

Figure 1.9: Autothermatik piston

running behavior. The unalloyed steel strips cast in between the skirt and the pin boss, together with the light alloy that surrounds them, form control elements. They reduce the thermal expansion of the skirt in the direction that is critical for the guiding of the piston in the cylinder. Due to their relatively low load capacity (slits), however, autothermic pistons are no longer up to date.

Autothermatik pistons

Autothermatik pistons, **Figure 1.9**, operate according to the same control principle as autothermic pistons. In the case of Autothermatik pistons, however, the transition from the crown to the skirt is not slotted. The transition cross sections are dimensioned such that they barely constrain the heat flow from the piston crown to the skirt and, on the other hand, do not significantly degrade the effectiveness of the steel strips through the connection of the skirt to the rigid crown. This piston design thus combines the high strength of the nonslotted piston with the advantages of the control strip design. Autothermatik pistons are still used to some extent in gasoline and naturally aspirated diesel engines.

1.3.1.2 Box-type pistons

This piston type, **Figure 1.10**, is characterized by its low mass, optimized support, and box-like, often slightly oval skirt design. The box-type piston was designed for use in modern passenger car gasoline engines and is compatible with both aluminum and gray cast iron crankcases. With a flexible skirt design, the difference in thermal expansion between the gray cast iron crankcase and the aluminum piston can be compensated very well in the elastic range. If the box width is different on the thrust and anti-thrust sides, the piston is referred to as an asymmetrical duct piston. Box-type pistons are cast or forged.

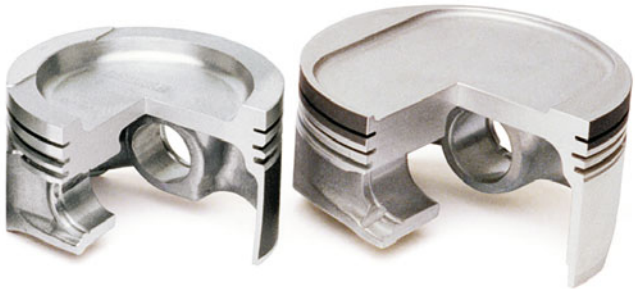

Figure 1.10:
Asymmetrical duct pistons

In addition to the classical box-type piston with vertical box walls, new shapes have recently been established, with box walls that are tapered toward the top. One example is the EVOTEC® piston; Chapter 1.3.1.3.

Pistons for engines with very high specific power output (greater than 100 kW/l) may have a cooling channel; **Figure 1.11**.

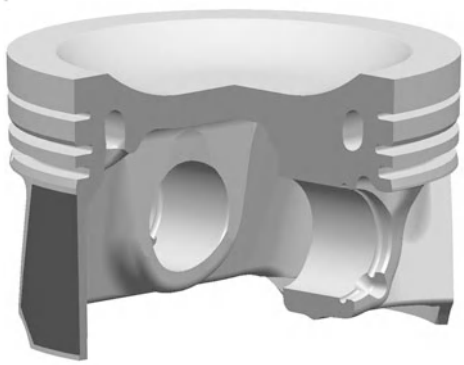

Figure 1.11:
Piston with cooling channel for gasoline engines

1.3.1.3 EVOTEC® pistons

The greatest current potential for reducing the piston mass in four-stroke gasoline engines is the EVOTEC® design, which is primarily used in conjunction with trapezoidal supports; **Figure 1.12**.

Box walls set at a steep angle allow particularly deep cast protrusions behind the ring grooves in the boss area, with good elasticity in the lower skirt area. The connection of the box walls far inside the piston crown–combined with supporting ribs in the piston window between the ring area and the box wall–provides excellent structural stiffness with very small cross sections.

Another significant feature of this piston concept is the asymmetric design of the box walls. In order to accommodate the higher lateral force load on the thrust side, the spacing of the box walls is smaller on the thrust side. The shorter lever arm between the box wall and the

Figure 1.12: EVOTEC® piston

contact area between the piston and the cylinder reduces the bending moment load. This allows smaller cross sections, even with extremely high lateral forces, which are preferred for turbocharged gasoline engines with direct injection. In order to provide the required elasticity and good guiding properties, the anti-thrust side, which experiences significantly lower loads, features greater spacing between the box walls.

1.3.1.4 Forged aluminum pistons

In engines with very high power densities–such as highly loaded turbocharged gasoline engines–cast pistons reach their limits. MAHLE forged pistons are a particularly good fit for this area of application; **Figure 1.13**. Their strength advantage in the temperature range of up to about 250°C improves the load capacity for lateral forces, and increases the load capacity of the boss and the fracture toughness. Forged pistons are therefore especially

Figure 1.13:
Forged aluminum piston

well suited for high-speed concepts and turbocharged engines. Due to the high ductility of the forged material, they also react more tolerantly to peak pressures that can arise if an engine is operated very close to the knock limit. This allows lower ring land widths, among other things, and therefore lower compression heights. Since the manufacturing process is very stable, the forged pistons can be designed to the limit in order to minimize component weight.

One disadvantage, compared to cast counterparts, is the higher product cost of the forged piston. Limited design flexibility is another. Undercuts, in particular, cannot be incorporated in the design.

Motorsport pistons are all special designs; **Figure 1.14**. The compression height *KH* is very low, and the overall piston is extremely weight-optimized. Only forged pistons are employed in this field. Weight optimization and piston cooling are critical design criteria. In Formula 1, specific power outputs of greater than 200 kW/l and speeds of more than 19,000 rpm are common. The service life of the pistons matches the extreme conditions.

Figure 1.14:
Forged piston for Formula 1

1.3.2 Pistons for two-stroke engines

For pistons of two-stroke engines, **Figure 1.15**, the thermal load is particularly high due to the more frequent heat incidence–one expansion stroke for every revolution of the crankshaft. It also needs to close off and expose the intake, exhaust, and scavenging ports in the cylinder during its up-and-down motion, thus controlling the gas exchange. This leads to high thermal and mechanical loads.

Two-stroke pistons are equipped with one or two piston rings, and their external design varies from open window-type pistons to full-skirt piston models. This depends on the shape of the scavenging ports (long channels or short loop-shaped scavenging passage). The pistons are typically made of the hypereutectic AlSi alloy MAHLE138.

Figure 1.15:
Piston and cylinder for a two-stroke engine

1.3.3 Pistons for diesel engines

1.3.3.1 Ring carrier pistons

Ring carrier pistons, **Figure 1.16**, have been in use since 1931. The first, and at times even the second piston ring are guided in a ring carrier that is securely joined to the piston material by metallic bonding.

The ring carrier is made of an austenitic cast iron with a similar coefficient of thermal expansion to that of the piston material. The material is particularly resistant to frictional and impact wear. The first piston ring groove, which is the most vulnerable, and the piston ring inserted in it are thereby effectively protected against excessive wear. This is particularly advantageous at high operating temperatures and pressures, which are particularly prevalent in diesel engines.

Figure 1.16:
Ring carrier piston

1.3.3.2 Cooling channel pistons

In order to cool the area around the combustion chamber most effectively, and thereby address the increased temperatures that result from higher power outputs, there are various types of cooling channels. The cooling oil is generally fed through fixed ports in the crankcase. Chapter 5 gives an overview of possible cooling variants.

Figure 1.17 shows a cooling channel piston with ring carrier for a passenger car diesel engine. The annular hollow spaces are formed by casting around salt cores, which are then dissolved and washed away with water.

1.3.3.3 Pistons with cooled ring carrier

The piston with "cooled ring carrier," **Figure 1.18**, is a new cooled piston variant for diesel engines. The cooled ring carrier significantly improves the cooling of the first piston ring groove and the thermally highly loaded combustion bowl rim. The intensive cooling of this ring groove makes it possible to replace the usual double keystone ring with a rectangular ring.

1.3.3.4 Pistons with bushings in the pin bore

One of the most highly stressed areas of the piston is the piston pin bearing. Temperatures of up to 240°C can occur in this area, a range at which the strength of the aluminum alloy starts to drop off considerably.

For extremely stressed diesel pistons, measures such as form bores, pin bore relief, or oval pin bores are no longer sufficient to increase the load capacity of the boss. For this reason,

Figure 1.17: Salt-core cooling channel piston with ring carrier for a passenger car diesel engine

Figure 1.18: Piston for passenger cars with cooled ring carrier

Figure 1.19: Ring carrier piston for a commercial vehicle diesel engine with piston pin bore bushings

Figure 1.20: FERROTHERM® piston

MAHLE has developed a reinforcement of the pin bore, using shrink-fit bushings made of a material with higher strength (e.g., CuZn31Si1); **Figure 1.19**.

1.3.3.5 FERROTHERM® pistons

In FERROTHERM® pistons, **Figure 1.20**, the guiding and sealing functions are implemented separately. The two parts, piston crown and piston skirt, are movably connected to each other through the piston pin. The piston crown, made of forged steel, transfers the gas pressure to the crankshaft via the piston pin and connecting rod.

The light aluminum skirt only bears the lateral forces that arise due to the angle of the connecting rod, and can therefore support the piston head with an appropriate design. In addition to this “shaker cooling” via the skirt, closed cooling channels can also be incorporated in the piston crown. The outer cooling gallery of the steel piston crown is closed by split cover plates.

Due to its design, the FERROTHERM® piston exhibits good wear values in addition to high strength and temperature resistance. Its consistently low oil consumption, small dead space, and relatively high surface temperature provide good conditions for maintaining low exhaust emissions limits. FERROTHERM® pistons are used in highly loaded commercial vehicle engines.

Figure 1.21: MONOTHERM® piston for a commercial vehicle engine

Figure 1.22: Optimized MONOTHERM® piston for a commercial vehicle engine

1.3.3.6 MONOTHERM® pistons

The MONOTHERM® piston, **Figure 1.21**, emerged from the development of the FERROTHERM® piston. This piston type is a single-piece forged steel piston that is greatly weight-optimized. With a small compression height (to less than 50% of the cylinder diameter) and machining above the pin boss spacing (internal), the piston mass, including the piston pin, is nearly that of the mass of a comparable aluminum piston with piston pin. In order to improve the piston cooling, the outer cooling gallery is closed off by two cover plate halves. The MONOTHERM® piston is used in commercial vehicle engines with peak cylinder pressures of up to 20 MPa.

1.3.3.7 Optimized MONOTHERM® pistons

In optimized MONOTHERM® pistons, **Figure 1.22**, the piston skirt is connected to the pin boss on the side, just as a conventional MONOTHERM® piston is. The upper edge of the piston skirt is additionally connected to the inner contour of the piston.

The advantages of the optimized MONOTHERM® piston are:

- Stiffening of the structure, resulting in reduced deformation and greater load capacity
- Reducing the secondary piston motion, resulting in both a reduced tendency to cavitate and improved guide properties, particularly for the piston rings
- Smoothing of surface pressure on the skirt
- Additional surface and additional cross section for heat dissipation
- Advantages in forging and machining

The optimized MONOTHERM® piston is used for peak cylinder pressures of up to 25 MPa.

1.3.3.8 MonoXcomp® pistons

In order to be able to handle continuously increasing specific power output levels, peak cylinder pressures, and thermal stresses, MAHLE has developed the MonoXcomp® piston; **Figure 1.23**. Similar to the familiar piston types in the large piston segment (Chapter 1.3.4, Composite pistons for large engines), the MonoXcomp® piston is a composite piston, i.e., consisting of several parts:

- The piston crown with integrally formed antifatigue shaft and screw thread
- The thrust sleeve, which features a nut thread and an elastically deformable part with contact zone for transmitting power to the piston skirt, and
- The piston skirt with the counterpart to the contact zone. It has an integrally formed antifatigue collar, and the interior is deformable like a Belleville spring washer.

The ability to use different materials for the piston crown, piston skirt, and thrust sleeve enables the optimal utilization of material potentials. Particularly for piston crowns, the use of highly temperature-resistant and oxidation-resistant materials allows for extreme loads.

The structure, which is very rigid due to its closed form, reduces deformations in the piston and thereby enables thin walls and peak cylinder pressures greater than 25 MPa. The thin walls in the bowl area, in turn, improve the piston cooling and thus allow greater heat flow.

The multicomponent design additionally makes it possible to incorporate a very large exterior cooling gallery. This is especially important for the cooling of the highly stressed bowl rim. There is a second cooling channel in the interior, which effectively reduces the piston crown temperature. Both cooling galleries are connected by channels.

A prerequisite for the secure screw connection between dynamically loaded components is the elastic tensioning, applied over great elongation lengths. This means that external influences, such as temperature distributions, inertia forces, and combustion forces, which lead to different deformation states, have only a slight effect on the tension situation in the screw joint.

Figure 1.23:
MonoXcomp® piston for a commercial vehicle engine

In comparison with the large-bore piston, the compression height for commercial vehicle pistons is significantly lower (up to less than 60% of the cylinder diameter for MonoXcomp® pistons), which prevents the fitting of the typically used antifatigue bolts. In the MonoXcomp® piston concept, therefore, the required expansion has been distributed evenly across all piston components, such that the total expansion of typical antifatigue bolts is achieved overall. The targeted compliance that is set in the screw joint of the MonoXcomp® piston ensures the minimum required bolt force at all times. This prevents the piston crown from lifting off, even at high speeds of 3,000 rpm, for example, and prevents the screw joint from loosening.

1.3.3.9 MonoWeld® pistons

The portfolio of steel pistons was complemented with the new friction-welded MonoWeld® piston; **Figure 1.24**. The structure is stiffer than the optimized MONOTHERM® piston, making for an increased thermal load capacity. Compared to the MonoXcomp® piston, the MonoWeld® piston has no cooling gallery in its interior.

The MonoWeld® piston is suitable for peak cylinder pressures of up to 25 MPa.

Figure 1.24:
MonoWeld® piston for a commercial vehicle engine

1.3.3.10 Electron-beam-welded pistons

The basis is a forged aluminum alloy piston for highly loaded engines. Forging provides significantly higher and more consistent strength values than casting. On the other hand, the casting process allows the use of ring carriers and the incorporation of salt cores to form cooling channels.

Figure 1.25:
Electron-beam-welded piston with cooling channel for a high-performance diesel engine

Electron-beam welding makes it possible to combine forged piston bases with cast ring bands, in order to unite the advantages of both manufacturing methods. **Figure 1.25** shows an example of an electron-beam-welded piston with ring carrier and cooling channel.

1.3.4 Composite pistons for large engines

1.3.4.1 Areas of application and design types

The composite piston enables the incorporation of cooling channels and the combination of the properties of various materials in one piston. The performance range of four-stroke engines with composite pistons extends from 500 to 30,000 kW, with up to 20 cylinders. Areas of application include power generation units, main and auxiliary ship drives, and heavy-construction and railroad vehicles.

There are many variants of composite pistons. Common to them all is a design consisting of two main components: the piston crown with the ring belt (upper part of piston) and the piston skirt with the pin boss (lower part of piston). The two parts are screwed together with appropriate threaded fasteners.

The connection between the upper and lower parts of the piston can be designed as a central screw joint–with only one screw, **Figure 1.30** and **Figure 1.26 left**–or as a multiple screw joint. The multiple screw joint is essentially divided into models with four single screws, of

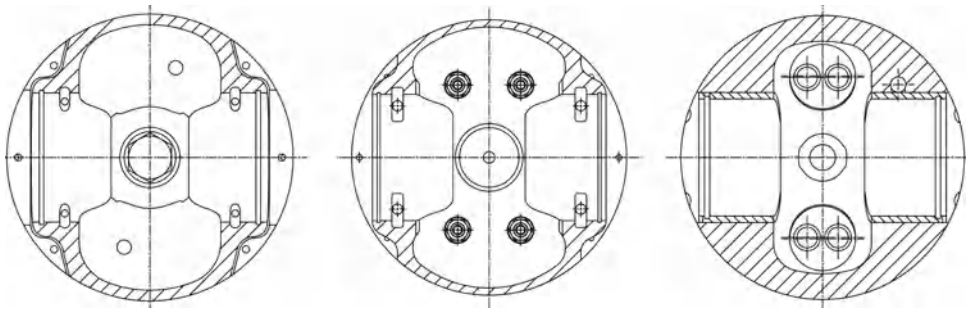

Figure 1.26: Types of screw joints–bottom views

which each has its own backing piece, **Figure 1.26 center**, and twin screw joints, i.e., two screws for each backing piece, **Figure 1.26 right**.

The selection of the screw joint type is based on the geometric ratios of the piston. For example, the component size, cavity geometry, cooling principle, and design of the upper part (bore cooling or shaker cooling) have a great influence.

1.3.4.2 Piston upper part

The piston upper part is made of forged steel and can be designed with shaker cooling or bore cooling; **Figure 1.27**. The bore-cooled variant is characterized by increased rigidity, with the efficient heat transfer remaining unchanged. The increased rigidity makes a design with only one contact surface possible.

If heavy fuel oil is used, the piston ring grooves are inductively hardened or chrome-plated to reduce wear.

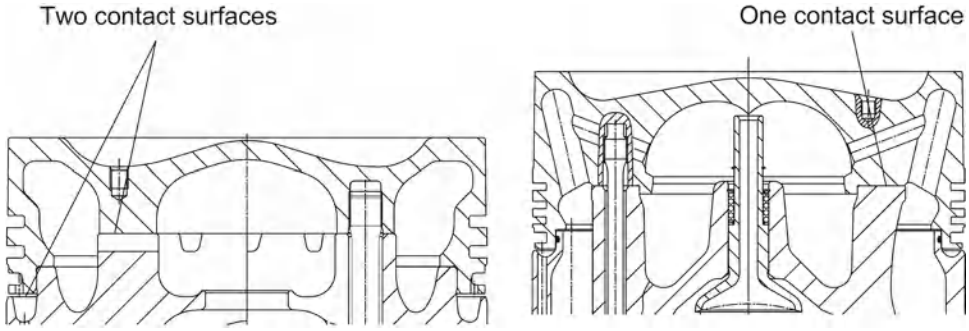

Figure 1.27: Piston upper part with shaker cooling (left) and bore cooling (right)

1.3.4.3 Piston lower part made of forged aluminum alloy

Forged aluminum skirts, **Figure 1.28**, are suitable for low and medium peak cylinder pressures, exhibit a low mass, and are easy to machine.

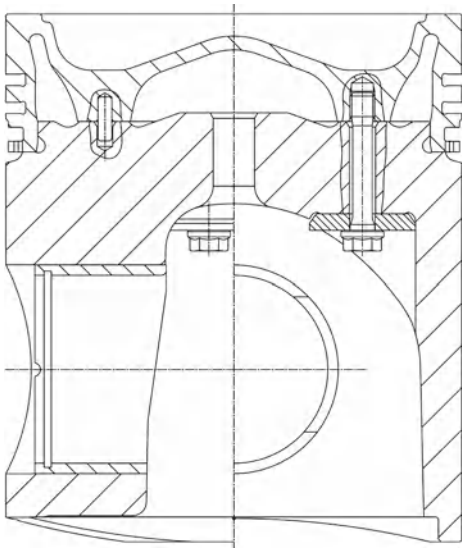

Bild 1.28:
Composite piston with steel crown, aluminum skirt, pin bore bushings, backing piece, and antifatigue bolt

1.3.4.4 Piston lower part made of nodular cast iron

Key features of a composite piston with nodular cast iron piston skirt, **Figure 1.29**, are low cold piston clearance and the resulting low secondary piston motion as well as high seizure resistance. The casting process, in contrast to forged steel, allows for undercuts and therefore a lighter design. With an appropriate design, it is suitable for peak cylinder pressures greater than 20 MPa. Compared to pistons with aluminum skirts, however, the mass is increased due to the higher material density.

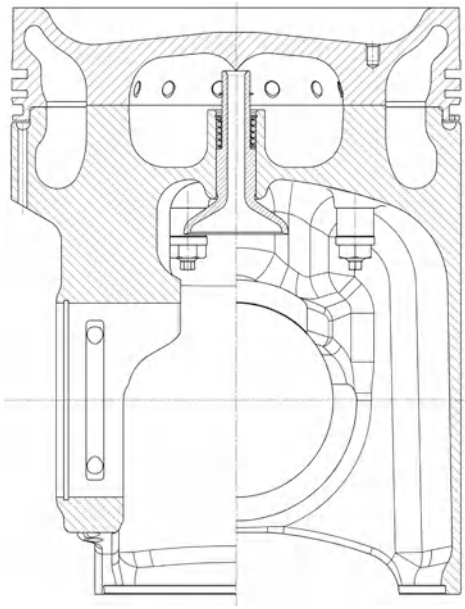

Figure 1.29:
Composite piston with steel crown and nodular cast iron piston skirt, backing piece, and antifatigue bolts

1.3.4.5 Piston lower part made of forged steel

Piston lower parts made of forged steel, **Figure 1.30**, provide ultra-high component strength and, related to the process, a material with extremely few defects. They are suitable for ultra-high stresses greater than 24 MPa. Similar to pistons with nodular cast iron piston skirts, they provide the advantage of low cold piston clearance, resulting in low secondary piston motion.

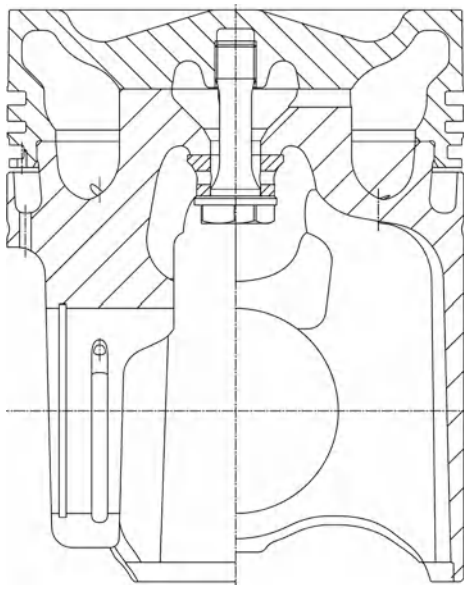

Figure 1.30:
Composite piston with steel crown and forged steel piston skirt, backing piece, and antifatigue bolt

2 Piston design guidelines

Due to the operational requirements of typical internal combustion engines (two-stroke, four-stroke, gasoline, and diesel engines), aluminum-silicon alloys are generally the most appropriate piston materials. Large-bore pistons and commercial vehicle pistons, or their crowns or upper parts, however, are often made of steel.

2.1 Terminology and major dimensions

Functional divisions of the piston are the piston crown, the ring belt with top land, the pin boss, and the piston skirt; **Figure 2.1**. Additional functional elements, cooling channels, and ring carriers indicate the type of piston design. The piston rings, piston pin, and–depending on the design–the pin retaining system are all part of the piston assembly.

In order to keep the masses as low as possible, a careful design of the piston and good piston cooling are necessary. Important dimensions and typical values are shown in **Figure 2.2** and **Table 2.1**.

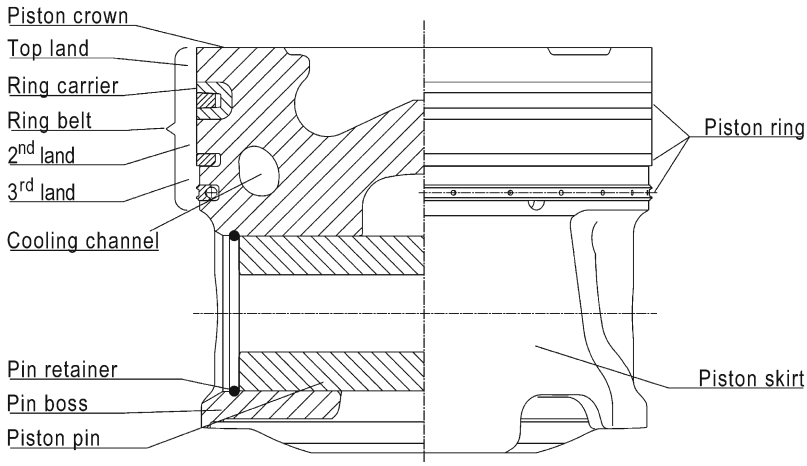

Figure 2.1: Important piston terminology

MAHLE GmbH (Ed.), *Pistons and engine testing,* DOI 10.1007/978-3-8348-8662-0_2,

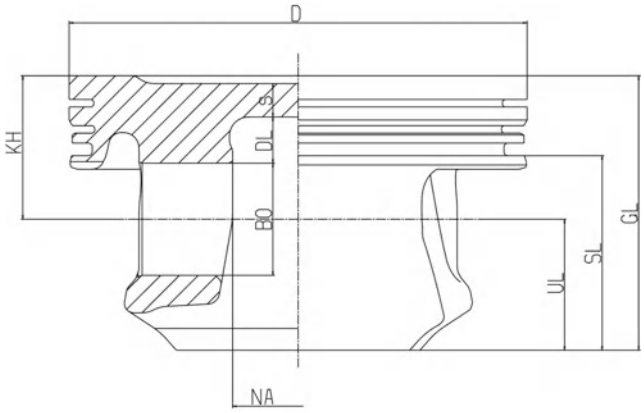

Figure 2.2:
Important piston dimensions

BO: Pin bore Ø (piston pin Ø)
KH: Compression height
NA: Pin boss spacing
D: Piston Ø
s: Crown thickness
DL: Expansion length
SL: Skirt length
GL: Total height
UL: Lower height

Table 2.1: Major dimensions of light-alloy pistons

	Gasoline engines		Diesel engines*
	Two-stroke	**Four-stroke (passenger cars)**	**Four-stroke (passenger cars)**
Diameter D [mm]	30–70	65–105	65–95
Total height GL/D	0.8–1.0	0.6–0.7	0.8–0.95
Compression height KH/D	0.4–0.55	0.30–0.45	0.5–0.6
Pin diameter BO/D	0.20–0.25	0.20–0.26	0.3–0.4
Top land height [mm]	2.5–3.5	2–8	6–12
Second ring land height St/D*	0.045–0.06	0.040–0.055	0.055–0.1
Groove height for first piston ring [mm]	1.2 and 1.5	1.0–1.75	1.75–3.5
Skirt length SL/D	0.55–0.7	0.4–0.5	0.5–0.65
Pin boss spacing NA/D	0.25–0.35	0.20–0.35	0.25–0.35
Crown thickness s/D or s/DMu, max**	0.055–0.07	0.06–0.10	0.14–0.23

* Values for diesel engines apply to ring carrier pistons, ** Diesel

2.1.1 Crown shapes and crown thickness

The piston crown forms part of the combustion chamber. Pistons for gasoline engines can be flat, raised, or sunken. For diesel engine pistons, the combustion chamber bowl is located in the piston crown. The geometry of the piston crown is also affected by the number and location of the valves; **Figure 2.3**. The maximum gas pressure and the quantity of heat to be dissipated determine the thickness of the piston crown (crown thickness). The piston crown, or the bowl rim for diesel engines, is the part of the piston that is exposed to the greatest thermal stress.

The values listed in **Table 2.1** for the crown thickness s apply in general to pistons with flat, convex, or concave crowns.

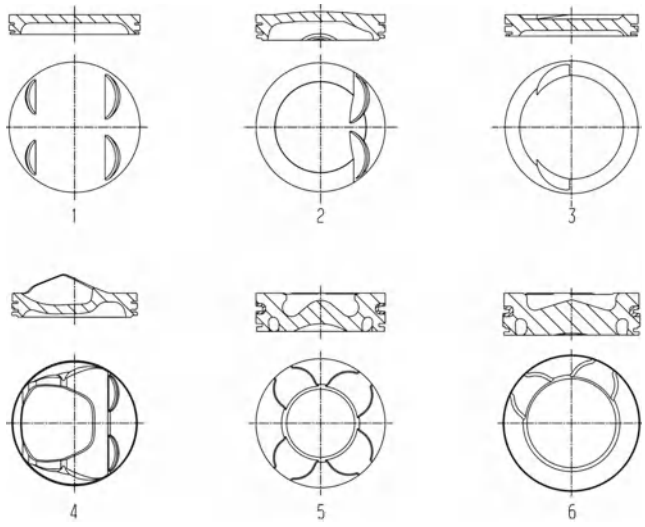

Figure 2.3:
Examples of piston crown shapes of various pistons for gasoline and diesel engines (1–3 for four-stroke gasoline engines with multi-point injection, 4 for four-stroke gasoline engines with direct injection, 5–6 for four-stroke diesel engines with direct injection)

2.1.2 Compression height

The compression height is the distance between the center of the piston pin and the upper edge of the top land. The goal is to have as low a compression height as possible, in order to keep the piston mass and the height of the engine as low as possible. The number and height of piston rings, the required ring lands, the piston pin diameter, and the top land width, however, result in a minimum compression height; a lower height is not possible. For diesel engine pistons, in addition to the combustion chamber depth, the conrod eye radius and the required minimum crown thickness below the combustion cavity generally determine the compression height.

Reducing the compression height also has disadvantages. For high power output and gas pressures, higher temperatures in the pin bore and higher stresses on the piston crown are the result of the low compression height. Cracks in the pin bore or the piston crown may then occur. Accordingly, for diesel engine pistons, a large expansion length is advantageous for the load capacity of the bowl rim.

2.1.3 Top land

In the piston ring zone, the distance between the edge of the piston crown and the top side of the first piston ring groove is called the top land. Its dimensions are a compromise between the following requirements: low piston mass and minimal dead volume for reducing fuel consumption and exhaust gas emissions, on one side; on the other side, the first piston ring, which is a compression ring, requires a temperature range that is still compatible with its function. This, in turn, depends greatly on the combustion process, the material, and the

geometry of the first piston ring and its piston ring groove, as well as the location of the water jacket on the cylinder.

For gasoline engines, the top land width is 4–10% of the piston diameter, tending to decrease in order to further reduce the hydrocarbon emissions caused by gaps.

For passenger car diesel engines with direct injection, this value is 8–15% of the piston diameter.

For commercial vehicle diesel engines with direct injection, it is 8–13% of the piston diameter for aluminum pistons, and 6–10% for steel pistons.

2.1.4 Ring grooves and ring lands

The piston ring zone, in general, consists of three ring grooves that hold the piston rings. The piston rings seal off the combustion chamber and control lubricating oil consumption. Their surface must therefore be of the highest quality. Poor sealing leads to blow-by of combustion gases into the crankcase, to heating due to the contact of the hot gas flow on the surfaces, and to destruction of the critical oil film on the running surfaces of the sliding and sealing partners. The piston ring must not impact the groove root diameter of the piston when it is pressed into the groove so that it is flush with the outer diameter of the piston, that is, it requires radial clearance.

Current lubricating oils permit groove temperatures of over 200°C in gasoline engine pistons, and up to 280°C in diesel engine pistons, without the piston rings binding due to residue build-up in the first piston ring groove.

For diesel engine pistons, which develop significantly greater combustion pressures than gasoline engines, the first piston ring groove is made much more wear-resistant by casting in a ring carrier. Ring carriers are typically made of Ni-resist, an austenitic cast iron with a thermal expansion coefficient that is approximately the same as aluminum. The ring carrier forms a permanent metallic bond with the piston through the established process of Al-fin composite casting. This process also enables better heat flow.

The ring land is the part of the ring belt of a piston that is located between two piston ring grooves. The second ring land, in particular, which is severely loaded by the gas pressure, must be sized sufficiently to prevent fracture of the ring land. Its height depends on the maximum gas pressure of the engine and the land temperature. For gasoline engine pistons, the ring land width is 4–6% of the piston diameter, for turbocharged passenger car diesel engines it is 5.5–10%, and for commercial vehicle pistons about 10%. The third or remaining ring lands can be smaller, due to the lower pressures they are subjected to.

2.1.5 Total height

The total height GL of the piston, relative to the piston diameter, depends on the compression height and the guide length on the skirt. For small, high-revving engines in particular, the total height is kept as low as possible in order to obtain low piston mass.

2.1.6 Pin bore

2.1.6.1 Surface roughness

The pin bore/piston pin sliding system must be in perfect condition in order to ensure reliable engine operation. If the surface roughness is too low, particularly when starting, this can cause galling of the pin bore. Therefore, depending on the pin bore diameter, a surface roughness of R_a = 0.63–1.0 µm is desired for the pin bore. Pistons with piston pins that move only in the piston (shrink-fit connecting rods) generally have slightly greater surface roughness values, in order to increase oil retention, particularly under less than ideal running conditions.

Other detailed measures are often necessary in order to ensure lubrication under all operating conditions. These include oil pockets (slots) or circumferential oil channels for improved lubrication in the pin bore.

2.1.6.2 Fitting clearance

The clearance of the piston pin in the pin boss is important for smooth running and low wear of the bearing surfaces. The fitting clearance increases with increasing operating temperature, which is caused by the greater heating of the piston relative to the pin, and possibly the different thermal expansion of the piston and pin materials. For pistons of Al alloy, this increase can be approximated as:

increase in clearance = 0.001 x pin diameter [mm]

The increase in clearance for a 30 mm diameter piston pin is therefore approximately 30 µm.

Previously, very tight clearances were typical, so that the piston pin could be inserted only in a preheated piston. Today, the clearance is considerably greater, and the piston pin is inserted into the pin bore at room temperature. This prevents deformation of the skirt due to shrinkage stresses and potential galling of the piston pin in the piston when starting at low temperatures.

When designing the minimum clearance, **Table 2.2**, in gasoline engines, differentiation must be made between a floating pin bearing or a piston pin with a shrink fit in the pin end bore. The floating piston pin is the standard design and is the variant that can be specifically most highly loaded in the pin boss.

Table 2.2: Minimum pin clearance for gasoline engines [mm] (not suitable for motorsport engines)

Floating configuration of the piston pin	Piston pin shrink fit
0.002–0.005	0.006–0.012

With shrink-fit connecting rods, the piston pin is seated in the small end bore with some interference. This makes the automatic assembly of the piston, piston pin, and connecting rod easier, because no special piston pin circlip is needed. The shrink-fit conrod design is not suitable for modern diesel engines and gasoline engines with turbocharging.

2.1.6.3 Tolerances

Similar considerations apply to matching the piston pin and piston as for the piston and cylinder. In order to facilitate assembly–aided by lower production tolerances for the pin bore and piston pin–only one defining group is typically used. The tolerance for piston pins is 4–8 µm, depending on the pin diameter. The pin bore tolerance is about 1 µm greater in each case.

2.1.6.4 Offset

The kinematics of the crank mechanism of a reciprocating piston engine leads to multiple contact alteration of the piston on the cylinder wall during a working cycle. After the top dead center point, the gas pressure presses one side of the piston skirt against the cylinder wall. This zone is known as the thrust side, and the opposite side of the skirt is the antithrust side.

An offset of the piston pin axis relative to the piston axis (pin bore offset) causes a change in the contact behavior of the piston as the side changes, and decisively affects the lateral forces and impacts. By calculating the piston motion, the location and amount of offset from the piston axis can be optimized, thus drastically reducing piston running noise and the risk of cavitation on the cylinder liner.

2.1.7 Piston skirt

The piston skirt, as the lower part of the piston, guides the piston in the cylinder. It can fulfill this task only if it has suitable clearance to the cylinder. Sufficient skirt length and tight guidance keep the tipping of the piston low during contact alteration from one cylinder wall to the other.

For diesel engine pistons, the full-skirt piston was previously dominant, with its closed skirt, interrupted only in the area of the pin bore. This design is still sometimes used for pistons in two-stroke gasoline engines. Aluminum diesel pistons for commercial vehicle engines still

feature a full-skirt design at times, with only a slight setback in the area of the pin boss, but window-type pistons are used across the board in passenger cars.

Gasoline engine pistons have a wide range of designs for the piston skirt; **Figure 2.4**. In order to keep inertia forces low, they now have only relatively narrow skirt contours, which led to the box-type piston, sometimes with different running surface widths (asymmetrical duct pistons) and/or slanted box walls (including EVOTEC® pistons).

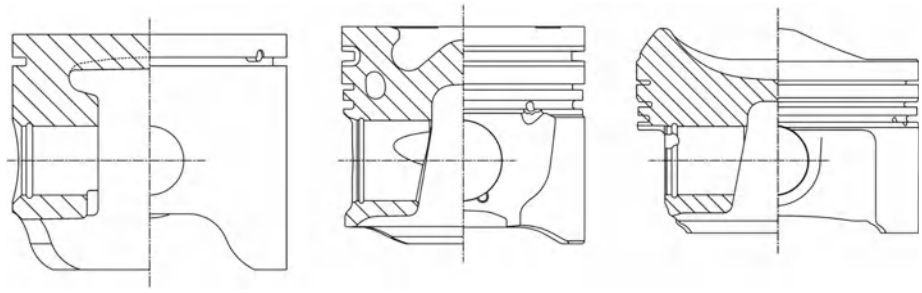

Full-skirt piston for two-stroke gasoline engine

Window-type piston for passenger car diesel engine

Box-type piston for passenger car gasoline engine

Figure 2.4: Skirt forms

The piston skirt must meet a few requirements related to its strength. First, it must bear the lateral forces without major deformations, and second, it should elastically adapt to the deformations of the cylinder. The piston crown deflects under the temperature and peak cylinder pressure, and deforms the piston skirt to an oval in the thrust and antithrust direction. This increases the diameter in the direction of the piston pin, and reduces it along the thrust-antithrust axis. Residual skirt narrowing due to plastic deformation, however, should be avoided. Remedial measures for at-risk pistons include greater wall thickness, oval interior piston shape, or small circumferential length of the piston skirt.

The lower end of the piston skirt should protrude out of the cylinder only a little or not at all (lower edge of pin bore). The protrusion must be considered appropriately when designing the piston profile.

2.2 Piston profile

2.2.1 Piston clearance

The piston deforms and stretches under the influence of forces, primarily the gas pressure and gas temperatures. This change in shape must be considered in advance in order to prevent binding at operating temperatures. This is done with a piston shape that deviates from the ideal circular cylinder. The piston must therefore be installed with some clearance in the cold state, which takes the expected deformation and the secondary piston motion into consideration.

Local clearance in the cold state is made up of the difference of the cylinder diameter and the piston, imagined as a circular cylinder (the fitting clearance), as well as the deviation of the piston from this circular cylinder shape. The piston profile (fine piston contour) deviates from the ideal circular cylinder in the axial direction (conicity, barrel shape) and in the circumferential direction (ovality).

2.2.2 Ovality

Pistons typically have a slightly smaller diameter in the piston pin axis than in the thrust-antithrust axis. The difference is the (diametric) ovality; **Figure 2.5**.

The oval shape of the crown and skirt provides many design opportunities. The skirt ovality creates space for thermal expansion in the piston pin axis direction. The ovality can be varied to generate an even wear pattern with sufficient width. It is typically (diametric) 0.3–0.8% of the piston diameter.

In addition to the normal ovality, ovalities with superposition are also possible, such as double or tri-ovality. For double ovality, in the form of a positive (double oval plus) or negative (double oval minus) superposition, the local piston diameter is greater or less than for normal ovality; **Figure 2.5, left**. The positive superposition widens the wear pattern relative to normal ovality, and the negative makes it narrower. Tri-ovality widens the wear pattern, which is limited due to a significantly reduced local piston diameter starting at about 35° from the thrust-antithrust axis; **Figure 2.5, right**.

The resulting running surfaces in the thrust and antithrust direction should not be too narrow, so that the specific pressures between the piston and cylinder remain low. In order to prevent hard bearing surfaces and the risk of galling, the bearing surface should not, however, extend out to the box walls. **Figure 1.7** (Boundary lubrication gap between piston and cylinder) in Chapter 1.2.4 (Friction and wear) shows the bearing surface of an advantageous piston profile.

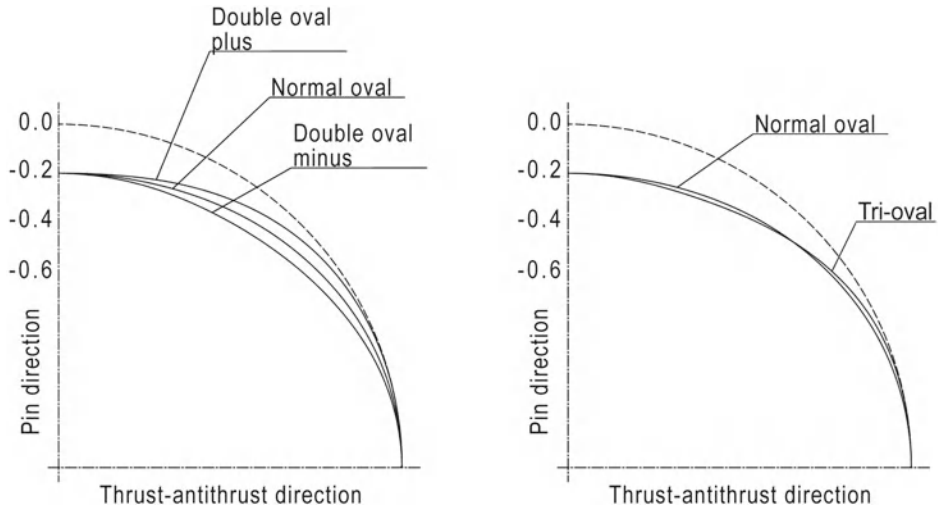

Figure 2.5: Ovality and superposition, double oval (left), tri-oval (right)

Further opportunities for optimizing the piston profile are provided by different ovalities in the thrust and antithrust direction, as well as ring belt offsets and so-called corrections.

In contrast to the essentially round pistons described above, with ovalities in the order of (diametric) a few 100 µm, the diameter in the running axis of an oval piston is about 1.3 times the diameter in the pin axis. The displacement is thereby increased by about 40% for the same length of the engine block and same cylinder spacing. While the production of the piston is unproblematic, machining the cylinder bore presents great difficulties, which is why oval pistons are very rare. The piston rings are fixed, like those in two-stroke engine pistons, and therefore do not rotate.

2.2.3 Skirt and ring belt tapering

The piston is tapered slightly at the upper and lower skirt ends, in order to promote the formation of the wedge of lubricating oil that acts as a bearing.

The greater taper in the area of the piston rings compensates for the great thermal expansion due to high temperatures in this area and for the deformation due to gas pressure. It also prevents the piston ring belt from impacting the cylinder due to secondary piston motion. For noise-sensitive gasoline engines, in particular, there should be no contact between the piston ring belt and the cylinder.

All of these aspects require optimized machining forms of the lateral surface for the various piston designs. The final piston profile can be verified only with extensive engine testing. **Figure 2.6** shows a detail from a piston profile drawing.

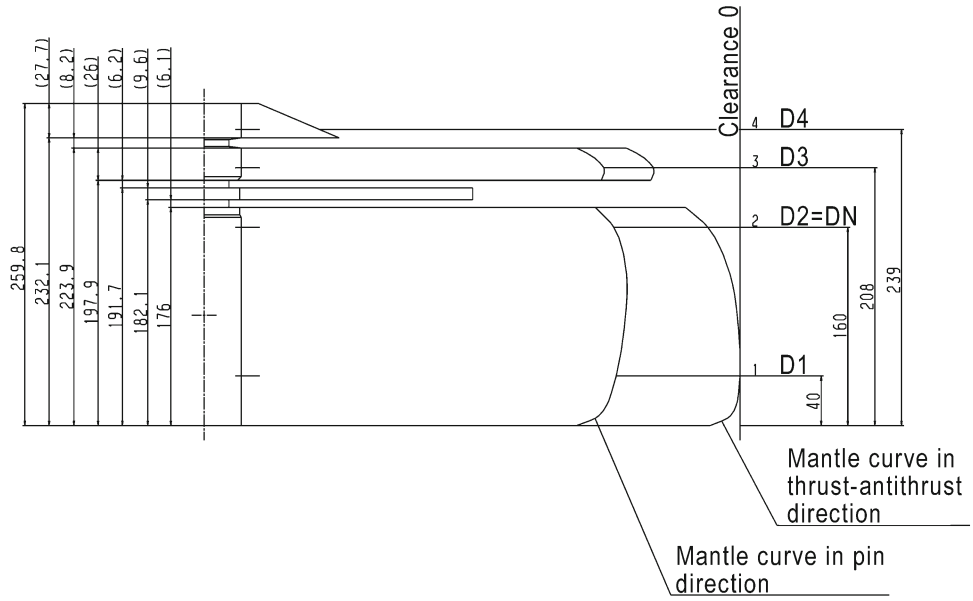

Figure 2.6: Piston profile

2.2.4 Dimensional and form tolerances

The piston diameter is typically determined absolutely at one of at least three measuring planes. This reference measuring plane is designated as *DN*. It is preferably located at the point with the tightest clearance between the piston and cylinder (DN = D1) or in an area with a stable shape (DN = D2). The dimensional tolerance (diametric) is 8–18 µm, depending on the piston diameter.

The outer contour of the piston is manufactured by NC-controlled precision turning. A funnel-shaped tolerance band results from the elasticity of the piston, as shown schematically in **Figure 2.7** (Piston profile, dimensional and form tolerances). Deviations from the nominal form are called form tolerances. The form tolerances of the diameters D1, D2, D3, and D4 for passenger car and commercial vehicle pistons are about 7 µm in the skirt area (diametric) relative to DN, and 10–15 µm in the ring belt area (diametric). The principle of the sliding scale applies. The tolerance band for the form tolerances shifts according to the actual diameter in the classification plane.

2.2.5 Fitting clearance

The fitting clearance is the difference between the cylinder diameter and the largest piston diameter D1. The fitting clearance should be as small as possible, so that consistently smooth running is achieved under all operating conditions. Due to the difference in thermal

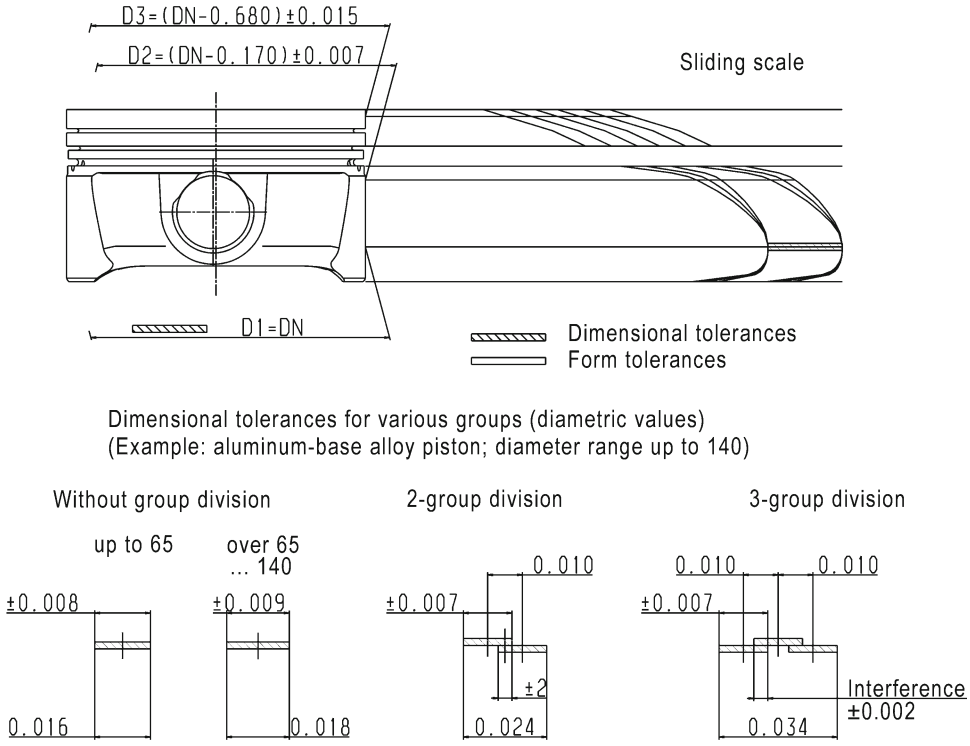

Figure 2.7: Piston profile, dimensional and form tolerances

expansion, this goal is most difficult to achieve for the combination of an aluminum piston and gray cast iron cylinder. Previously, cast-in steel strips were often used to reduce thermal expansion. **Table 2.3** gives an overview of the (diametric) clearances at the skirt for various piston designs.

Table 2.3: Typical fitting clearances for light-alloy pistons [‰ of nominal diameter]

	Gasoline engines			Diesel engines
	Two-stroke	Four-stroke (passenger cars)		Four-stroke (passenger cars)
Engine block material	Aluminum-base alloy	Aluminum-base alloy	Gray cast iron	Gray cast iron
Fitting clearance	0.6–1.3	0.1–0.2	0.3–0.5	0.6–0.9
Clearance at upper skirt end	1.4–4.0*	1.0–1.3	1.7–2.2	1.9–2.4

* Only for single-ring designs and high-performance engines (skirt end close to top land)

The fitting clearance decreases with increasing operating temperature, which is caused by the greater heating of the piston relative to the cylinder, and possibly the different thermal expansion of the piston and cylinder materials. At operating temperature, the piston runs in the cylinder with interference. Due to the ovality, the interference is limited to the elastically adaptable area of the skirt.

2.2.6 Defining group

One defining group for the piston and cylinder makes piston installation easier in mass production. If the highest priority is the economic efficiency of production, then slightly wider bands must be used for the dimensional tolerances than for division into several groups, e.g., (diametric) 18 µm compared to (diametric) 14 µm for a two-group division; **Figure 2.7**.

When pistons up to 140 mm in diameter are divided into several classes, overlap zones of 2 µm are required at the group boundaries. The pistons in the overlapping zones can be assigned to the larger or smaller defining group, as desired. This ensures that the desired quantity can be supplied for each defining group.

2.2.7 Skirt surface

Besides the skirt contour, the surface of the skirt running surface also has a great influence on the sliding behavior of the piston. If the surface roughness is too low, the piston may not run in properly. Skirt roughness profiles with roughness values of R_a = 2.5–5 µm (R_z = 10–20 µm), generated precisely by diamond turning, provide good results.

Thin metal layers of tin (0.8–1.3 µm) or synthetic resin graphite coatings (10–40 µm) further improve the boundary lubrication properties, particularly in the critical run-in process or when starting the engine under less than ideal conditions, such as during cold start. In some cases, an antifriction phosphate coating (about 0.5 µm) is additionally applied prior to graphite coating.

3 Simulation of piston operational fatigue strength using FEA

Today's requirements for modern combustion engines can be met only with highly efficient combustion and charging processes. Modern engines can now achieve specific power output and peak cylinder pressures in the combustion chamber that were previously unheard of outside of motorsport. This exposes the pistons to extreme loads, but the high requirements for service life and cost efficiency remain unchanged for these components. They are the decisive variables in the current global competitive environment.

One prerequisite in the run-up to extensive engine testing is simulation, particularly of operating loads, and verification of the operational fatigue strength of the piston. Precise, physically based approaches and the use of efficient calculation methods are therefore critical. In the industrial environment, the finite element analysis (FEA) has become established as a standard process. The special application of this method to the piston engine component is described in the following.

3.1 Modeling

The basis for FE analysis is modeling, using discretization or meshing, that is, the partitioning of the affected structure into so-called volume elements. All the individual parts of the entire model are meshed, typically in three dimensions, including all significant details, and with only minor simplifications.

Due to the processing capacity of current computers, symmetries (the use of half or quarter models) are no longer imperative. The initial geometry created by design can nearly always be implemented in full detail. Powerful mesh generators and user interfaces with refined graphics (known as preprocessors) effectively support modeling. Modern software running on multiprocessor computers allows models with a large quantity of volume elements to be processed, or solved.

In the case of piston calculations, the entire model includes not only the piston, but also the piston pin, the connecting rod small end, and the cylinder; **Figure 3.1**. The cylinder and connecting rod small end are fixed to the appropriate interfaces for the calculation. For the piston and piston pin components, which move during engine operation, support is provided solely by contact conditions. Interactions and load application can thus be shaped under

MAHLE GmbH (Ed.), *Pistons and engine testing,* DOI 10.1007/978-3-8348-8662-0_3,

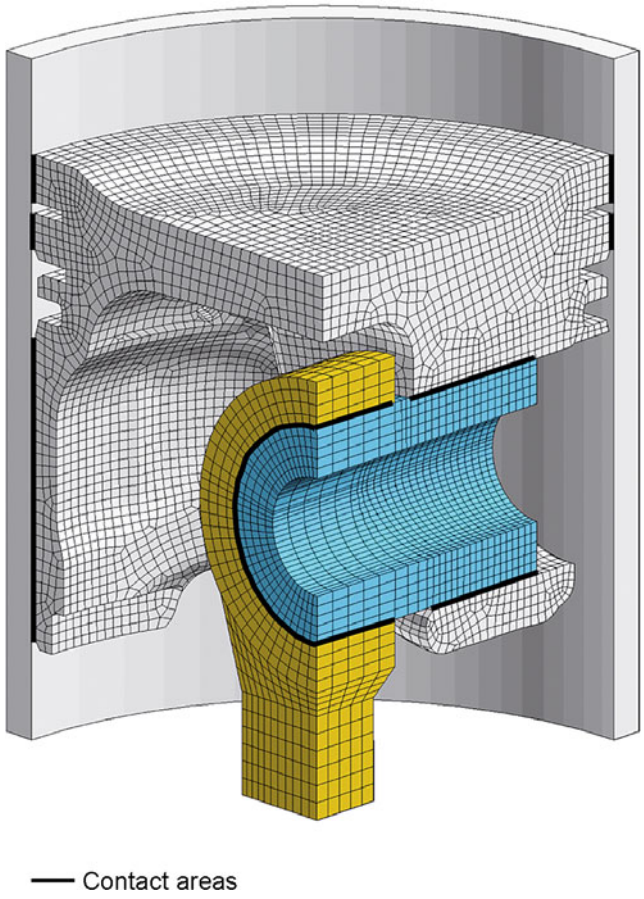

Figure 3.1:
FE model of a piston, with piston pin and connecting rod small end

conditions that are close to reality. Within the contact definitions, any existing refined profiles of the contact surfaces, such as the piston skirt profile or the pin bore profile, can also be taken into consideration.

The application of the load to the model is depicted in the following Chapters 3.2 and 3.3. The assignment of material properties concludes the modeling process. Depending on the component, the application, and the load, both purely linear-elastic material properties and elastic-plastic properties are used.

3.2 Boundary conditions from engine loading

First, loads are differentiated as either thermal or mechanical; see Chapters 3.2.1 and 3.2.2. Next it is determined whether the load on the piston should be treated as dynamic, or simplified as a static load.

The operating load on the piston is given by the operating principle of the engine (e.g., four-stroke gasoline or four-stroke diesel process). Due to the cyclical sequence of the strokes for this operating principle, the load is considered to be cyclical. The cyclical loads include:

- The temperature from the combustion process
- The gas force from the cylinder pressure
- The inertia force, and
- The lateral force

Loads, which do not originate directly in the engine operating principle are either static, such as internal stresses (Chapter 3.3), or they result from changes in engine operation. These could be randomly caused (e.g., road profile for passenger cars), or definitively prescribed (e.g., acceptance run, exhaust gas test cycle).

3.2.1 Thermal loads

The thermal load from the gas temperatures in the combustion process is also a cyclical load on the piston. It acts primarily during the expansion stroke on the combustion chamber side of the piston.

In the other strokes, depending on the operating principle, the thermal load on the piston is reduced, interrupted, or even has a cooling effect during gas exchange. In general, heat transfer from the hot combustion gases to the piston occurs primarily by convection, and only a slight portion results from radiation.

In relation to the expansion stroke, the duration over which the thermal load from combustion acts is very short. Therefore, only a very small portion of the component mass of the piston, near the surface on the combustion side, follows the cyclical temperature fluctuations. Nearly the entire mass of the piston, therefore, reaches a quasi-static temperature, which can, however, have significant local variations. A temperature field is established; see Chapter 3.4. In the simulation, the cyclical temperature fluctuations at the surface can be taken into consideration, but this requires a great deal of computational effort. It is generally omitted.

The thermal boundary conditions required to simulate the quasi-static temperature field in the piston are determined using a cycle simulation. They may be supplemented by any temperature measurements from engine tests; see Chapter 7.2. Additional knowledge about heat transfer that is dependent on the contact pressure allows suitable heat transfer coefficients to be defined for all relevant surfaces and contact areas of the piston. In combination with the corresponding ambient temperatures, they are used to describe the local heat flow.

An alternative to determining the thermal boundary conditions required to simulate the quasi-static temperature field in the piston is the use of the CFD method. It allows numerical simulation of the combustion process.

Using the CFD method, for example, the consequences of nonhomogenous mixture preparation and the corresponding nonuniform heat generation in the combustion chamber can be described. It also allows near-realistic modeling of the complex conditions on the piston-side walls of the combustion chamber, particularly in a direct injection diesel engine. A practical example of the high spatial resolution of the boundary conditions for simulating the temperature field is the detailed consideration of the interaction between the wedge-shaped flame jets and the contour of the piston bowl; **Figure 3.2**.

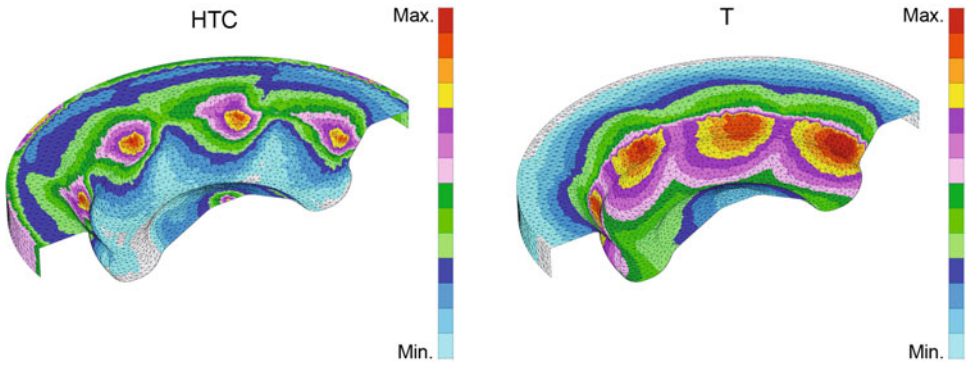

Figure 3.2: Distribution of heat transfer coefficients (HTC, left) and gas temperature (T, right) on the piston crown of a commercial vehicle engine, from a CFD analysis

Due to the multihole nozzles used in this combustion process, nearly any pattern can occur at the circumference of the piston bowl. Without the support of the CFD method, such relationships can be modeled only at a simplified level with reasonable effort.

3.2.2 Mechanical loads

The cyclical loading of the piston due to
- the gas force from the cylinder pressure,
- the inertia force from the oscillating motion of the piston, and
- the lateral force from the support of the gas force by the inclined connecting rod, and the inertia force of the oscillating connecting rod

determines the mechanical load.

According to the fundamental principles of machine dynamics, the correct superposition of these dynamic forces, as a function of the kinematic relationships in the crank mechanism, can be determined at any given point in time, and can be defined as an external force in the simulation of the operating loads. In the simulation of the operating load on the piston, the external forces acting on the piston are considered to be static at the point in time that is under analysis.

In order to avoid neglecting any combination of these forces–so-called load cases–that may be critical, a practical number of appropriately selected points in time are analyzed. This includes primarily the times at which individual components of the mechanical load reach a maximum. For example, the effect of the piston's inertia force is at a maximum at the dead centers of the crank mechanism. Other examples include the maximum of the cylinder pressure, or the lateral force, which in turn can act in two different directions. Because the same position of the crank mechanism elements occurs for all of these cases, the time is defined on the basis of the angular position of the crankshaft. For example, in the four-stroke cycle, two revolutions of the crankshaft are needed for the entire process, which corresponds to 720 degrees of crank (shaft) angle.

3.2.2.1 Gas force

Simulation of the gas force is intended to represent the effect of gas pressure on a piston at operating temperature. The gas pressure is applied to the simulation model over the entire piston crown, down to the lower flank of the top ring groove. The force distribution of the longitudinal force generated thus runs through the piston pin to the connecting rod small end.

3.2.2.2 Inertia force

The oscillating motion of the piston in the cylinder generates accelerations that reach a maximum at the top dead center (TDC).

In this context, the length of the connecting rod relative to the crank radius of the crankshaft pin, known as the stroke-connecting rod ratio, plays a decisive role. As the length of the connecting rod increases, the acceleration of the piston and the lateral forces decrease. Maximizing the length of the connecting rod is therefore a recognized design principle. In order to achieve this while minimizing overall dimensions, the compression height of the piston must also be reduced as much as possible. This has corresponding consequences for the piston design; see Chapter 2, **Figure 2.2**. The accelerations are linearly dependent

on the stroke-connecting rod ratio of the crank mechanism, and quadratically dependent on the engine speed. This means that the effects of the inertia forces in high-speed engines increase significantly.

The resulting acceleration force is applied to the connecting rod by the piston, by means of the piston pin. In the FE model, the acceleration is applied globally to the piston and piston pin. The model is fixed in the axial direction at the connecting rod small end.

3.2.2.3 Lateral force

The conversion of the piston's linear motion into the crankshaft's rotational motion leads to force components in the crank mechanism, which press the piston against the cylinder wall. Due to the lateral deflection of the connecting rod big end and the resulting inclined position of the connecting rod, these are known as lateral forces. In a crank mechanism that is not offset (cylinder axis and conrod axis are collinear), the greatest lateral forces occur in the expansion stroke. In high-speed engines, however, they can also occur in other crank angle ranges as a result of inertia forces. In the simulation, the lateral forces of interest are transmitted into the piston via the connecting rod small end and the piston pin. The piston then presses against the cylinder.

As already indicated in the simulation of the gas force, the simulation of lateral forces is a purely static consideration at first. This approach is correct if the piston runs in the cylinder without clearance, but this is not always the case in practice. Disregarding the operating conditions for a cold start, in which the installation clearance is fully present for a short period, additional conditions can occur, depending on the application, in which there is a running clearance between the piston and the cylinder. This includes, in addition to most applications of steel or nodular cast iron as a piston material, all thin-walled lightweight pistons, such as are preferred for use in gasoline engines and especially in motorsport applications. These piston types become deformed under the operating conditions during engine load. Despite the typical interference under full-load conditions, this often leads to dynamic clearance conditions between the piston and cylinder.

These effects can be depicted using appropriate simulation tools (in this case, the structural dynamic simulation of the piston secondary motion). The resulting additional dynamic loads in the static approaches of the lateral force thus can be taken into account for the FE analysis in a physically correct manner.

3.3 Boundary conditions due to manufacturing and assembly

Pistons with design features, such as pin bore bushings or ring carrier inserts, as well as composite pistons, are made up of several parts that are connected to each other using various methods: casting, joining or pressing a shrink fit, and bolting. These joining and assembly methods cause internal stresses, which must be considered in a precise strength analysis. Such loads act statically on the piston and must be included in relaxation processes and for problems dealing with creep under load.

3.3.1 Casting process/solidification

Internal stresses in the component are an unavoidable characteristic of casting. They arise due to differences in wall thicknesses and different local cooling conditions; they are therefore present in the piston as well. Heat treatment after the casting process, however, reduces these stresses. Both processes–the casting process and the heat treatment–can be modeled using a numerical casting simulation, and the resulting internal stresses can be considered as well.

3.3.2 Inserts

Aluminum pistons for diesel engines usually have a cast-in ring carrier made of austenitic cast iron with lamellar graphite (Niresist), which is intended to reduce ring side wear in the top ring groove; see Chapter 1.3.3. Cast-in and composite stresses arise during the casting-in of this ring carrier. The aluminum alloy shrinks onto the ring carrier during solidification and final cooling, thus generating primarily compressive stresses in the ring carrier.

3.3.3 Pressed-in components

The combustion pressures in a passenger car diesel engine currently reach about 200 bar, while commercial vehicle diesel engines reach about 250 bar, and even greater than 250 bar in large-bore engines. This leads to high stresses in the pin boss. Particularly for pistons made of aluminum or composite pistons with aluminum skirts, therefore, it may be necessary to increase the load capacity of the pin boss by shrinking in a pin bore bushing made of a suitable material, such as bronze or special brass. The shrink-in process generates compressive stresses in the pin bore bushing, and tensile stresses in the surrounding aluminum alloy, primarily at the bottom of the pin boss (nadir).

3.3.4 Bolt connections

Bolt connections in composite pistons must be analyzed under the described thermal and mechanical loads. Analysis of the assembled state at room temperature, as well as the consideration of friction at the various support contact surfaces, is also required.

Depending on the process used for tightening the bolts (hydraulic, torque control, or angular control) the prestressing force of the bolts is calculated and adjusted at room temperature for the simulation of the bolt connection in the FE model. The prestressing force is then superimposed on the thermal and mechanical loads (gas force, inertia force, lateral force).

With this approach, it is possible to establish

- whether the bolt prestressing force increases or decreases in the piston at operating temperature,
- how clearances and inclinations on the support contact surfaces affect the distribution of the prestressing force,
- whether the piston crown lifts off from the piston skirt in the area of the bolt, and
- how clearances affect the stress amplitudes from the mechanical loads.

3.4 Temperature field and heat flow due to temperature loading

The extent of the temperature field and the resulting temperature gradients are determined by the cooling of the piston. Pistons are generally categorized as having no cooling, spray-oil cooling, or cooling-channel cooling. The partially filled cooling channels and cooling cavities, together with the oscillating piston motion, lead to extensive turbulence in the engine oil cooling medium. This turbulence generates high relative velocities of the cooling medium at the channel wall, which in turn improves heat transfer at the wall. This condition is referred to, in a simplified manner, as the “shaker effect.” The piston is then said to have “shaker cooling.”

With regard to component strength, the temperatures at the piston crown (gasoline pistons), at the bowl rim (diesel pistons), in the support area (transition from the pin boss to the piston crown), and in the pin bore are of interest. The temperatures in the top ring groove and the cooling channel are also significant in terms of oil coking. Typical temperature values for passenger car engines are:

- Center of piston crown (gasoline engine, manifold injection) 270–310°C
- Piston crown bowl (gasoline engine, direct injection) 270–350°C
- Bowl rim (diesel engine, direct injection) 350–400°C

- Support area 200–250°C
- Pin bore (zenith) 200–250°C
- Top ring groove (spray-jet cooling, salt-core cooling channel) 200–280°C
- Top ring groove (cooled ring carrier) 180–230°C
- Cooling channel (zenith) 250–300°C

Numerical simulation of the temperature field allows detailed analysis of the heat flows in the piston. Depending on the piston cooling method used in each case, typical values for the percentual distribution of the total heat flow to the piston crown are shown in **Table 3.1** for various areas of the piston. In the uncooled piston, the heat flow to the cooled cylinder liner (through the ring grooves, the piston rings, and the piston skirt) dominates the heat flow pattern, while the heat flow into the engine oil by convection is predominant in the cooled piston types.

Table 3.1: Distribution of heat flow for various piston types

Piston type	Uncooled piston	Oilspray cooling	Oilspray cooling	Salt-core cooling channel	Cooled ring carrier	MONO-THERM® ring channel	2-chamber cooling cavity
Operating principle	Gasoline	Gasoline	Diesel	Diesel	Diesel	Diesel	Diesel
Heat flow [%] Cooling channel	0	0	0	40–50	50–60	75–90	90–100
Ring belt	50–60	15–25	50–55	25–45	10–30	0–10	0–5
Skirt	10–15	5–10	10–15	5–10	5–10	0	0
Inner shape	10–20	50–60	20–30	5–15	5–15	0–10	0–5
Window/ cast undercut	5–10	0–5	0–5	0–5	0–5	0	0
Pin boss	5–10	0–5	0–15	0–10	0–10	0	0

The typical temperature distribution in a gasoline engine piston, with a temperature gradient from the piston crown to the skirt, generates a thermal deformation as shown in **Figure 3.3**. This deformation characteristic must be taken into consideration when fine machining is done on the outer diameter, and defines the barrel shape used for the piston skirt. The prominent inclination at the zenith of the pin bore is typical for these deformation patterns. This wedge-shaped gap between the pin boss zenith and the piston pin is completely closed under the gas force load.

Pistons with cooled ring carriers are used in passenger car diesel engines, in order to reduce the temperature at the bowl rim and in the top ring groove. **Figure 3.4** shows a comparison

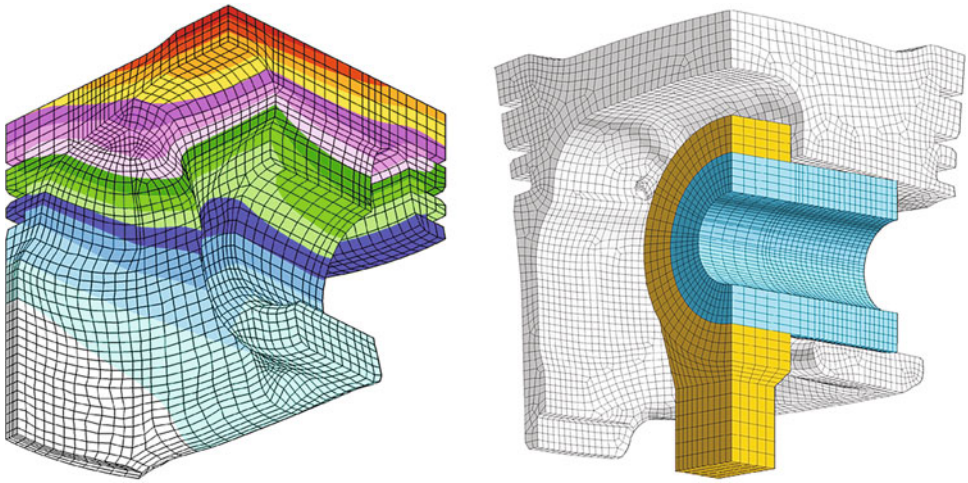

Figure 3.3: Temperature distribution (left) and thermal deformation (right) of a piston in a passenger car gasoline engine with spray jet cooling (deformation shown magnified)

of the cooling effect of a cooled ring carrier (left) and a so-called salt-core cooling channel (right). The advantageous effect of the cooled ring carrier on the bowl rim temperature, and especially on the temperature in the top ring groove, is evident.

For commercial vehicles, MONOTHERM® pistons are also used in engines with the highest power ratings. It is a single-piece forged steel piston. It has a skirt that is directly connected to the pin boss, and which can be open or closed at the top. **Figure 3.5** shows the tempera-

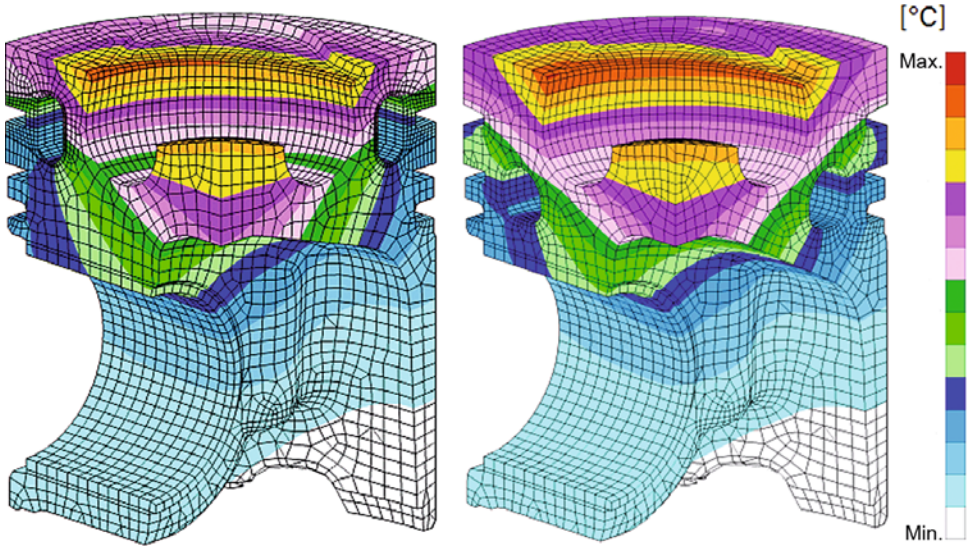

Figure 3.4: Comparison of cooling effect for cooled ring carriers (left) and salt-core cooling channels (right) on a passenger car diesel piston

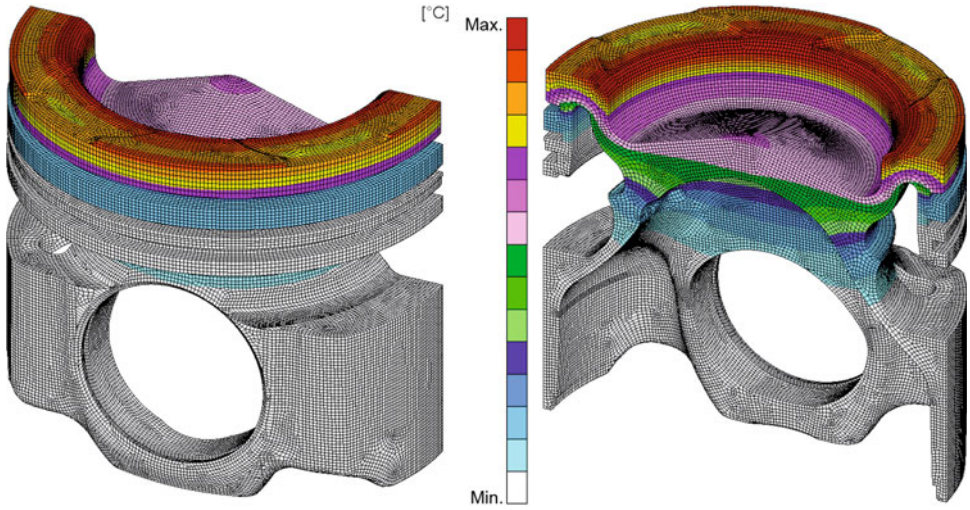

Figure 3.5: Temperature distribution in a MONOTHERM® piston with a closed skirt

ture distribution in a MONOTHERM® piston with a closed skirt. The greatly reduced heat flow in the skirt, and the resulting low skirt temperatures, is typical for this type of piston.

For large-bore engines, a significantly longer service life is required, and the cylinder pressures reach levels greater than 250 bar. Under such conditions, piston cooling is decisively significant. Therefore, large-bore pistons are nearly always designed as composite pistons, with a crown part made of heat-resistant steel, and a skirt made of either aluminum, nodular cast iron, or forged steel. With this design, it is possible to make the cooling cavities large, and accordingly effective for cooling. This is accomplished, for example, by using concentric 2-chamber systems, which cover nearly the entire crown of the piston. The heat balances in **Table 3.1** show that the cooling in this piston is very effective. The heat flowing into the piston due to combustion can thus be dissipated nearly 100% by the cooling oil.

The thermal deformations caused by the severe temperature gradients in the piston crown are shown in **Figure 3.6** for a piston with shaker cooling. The temperature in the bolt connection affects the relaxation behavior in the high-strength bolt material used here. If temperatures greater than 180 to 200°C occur over large areas of the bolt, then relaxation must be anticipated, leading to a reduction in bolt prestressing force during operation.

The skirts of composite pistons are hardly affected by the temperature load–with the exception of the area of the bolt connection's countersunk holes. The temperature here can increase the stresses in the radii of the countersunk holes, if the axial gaps are poorly designed. For bolt connections in composite pistons, the distribution of the bolt prestressing force at the inner support contact face must not drop below 20 to 25% of the prestressing force under temperature loading. This can be achieved by suitably designing the axial gap at the outer support contact face.

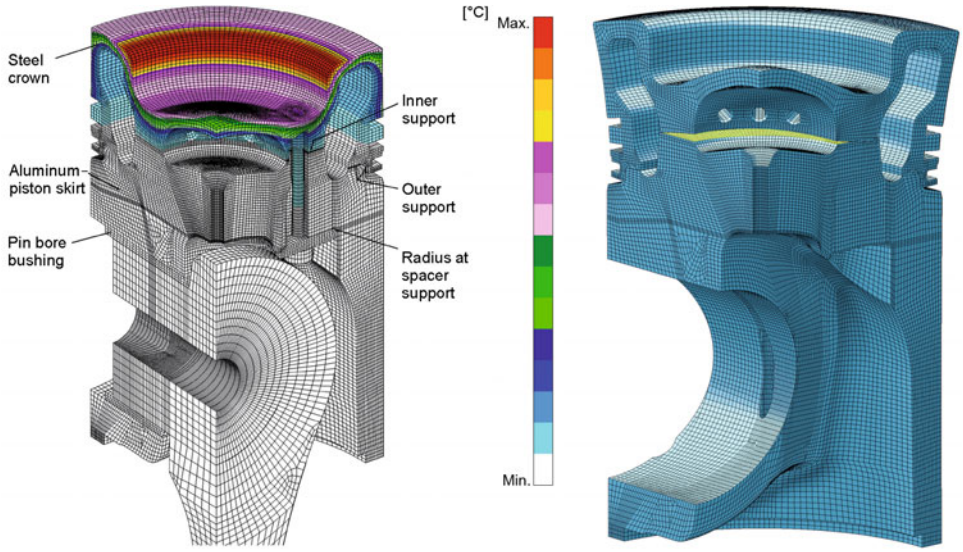

Figure 3.6: Temperature distribution (left) and thermal deformation (right) of a large-bore piston with shaker cooling (deformation shown magnified)

3.5 Stress behavior

3.5.1 Stresses due to temperature loading

The temperature distributions shown in Chapter 3.4 for various pistons show significant temperature gradients. This is especially true at the piston crown and the bowl rim. The piston expands greatly in the hot areas, whereas expansion is less in the cooler areas. The thermal stresses thus induced–primarily compressive stresses–are greatest at the crown and bowl area, and can exceed the yield point of the piston material there.

In order to consider the fact that the yield point has been exceeded in the FEA, complex analysis using the nonlinear elastic-plastic behavior of the material is necessary. Exceeding the yield point, however, affects only limited, localized areas of the piston. These areas also have very low stiffness, due to the high temperatures that are typically present there. The repercussions for the global stress and deformation behavior of the entire piston are therefore correspondingly small.

The numerical complexity can be reduced by determining the thermal stresses under linear-elastic conditions, considering the temperature-dependent physical material data. The stresses thus determined are then locally converted into an elastic-plastic behavior at the highly stressed locations of interest, and are analyzed for strength and service life according to the methods described in Chapter 3.6.

Figure 3.7 shows the distribution of the thermally induced stresses in a piston for a gasoline engine with manifold injection. The temperatures on the nearly flat piston crown are approximately 280 to 300°C, which generate compressive stresses in the internal crown area.

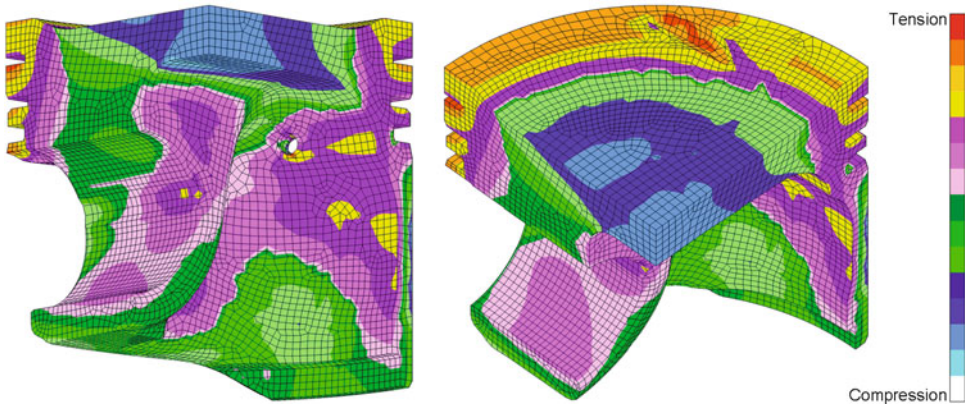

Figure 3.7: Thermally induced stresses in a piston for a passenger car gasoline engine with manifold injection

Figure 3.8 shows the thermally induced stresses in an aluminum piston with a cooled ring carrier for a passenger car diesel engine with direct injection. The undercut bowl shape reveals a significant concentration of compressive stresses at the bowl rim. The level of the bowl rim stresses, together with the high temperatures (up to 400°C) lead to the yield point at the bowl rim being exceede.

In general, bowl rims have better strength and temperature performance when the bowl rim radius is greater. The same applies to a small undercut for the bowl as well as to obtuse angles and flat bowl shapes, which are preferably used for commercial vehicle pistons.

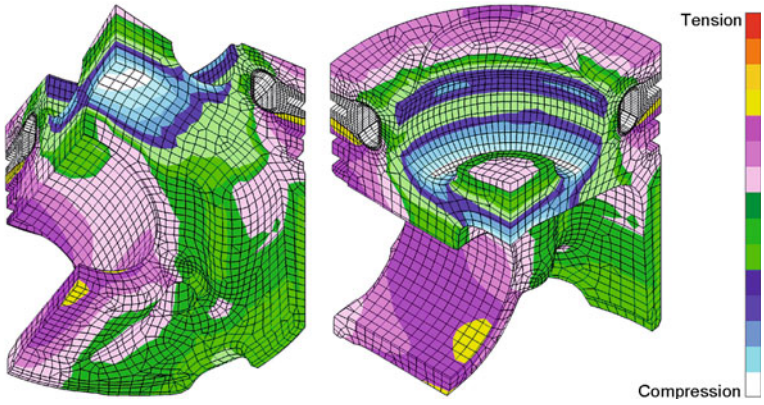

Figure 3.8: Thermally induced stresses in a piston with cooled ring carrier

MONOTHERM® pistons (made of steel) also have high thermally induced compressive stresses at the bowl rim and in the cooling channel area. Compared to pistons made of aluminum, however, this has little effect on the strength, as long as the temperatures in these areas are less than the scaling limit. Long-term temperatures greater than 450 to 500°C cause scaling, and therefore damage the surface. Such defect locations can be the starting point for cracks in the bowl rim of a steel piston.

Composite pistons with shaker cooling generally have the greatest thermally induced stresses in the steel crown. The stress maxima are located in the wall of the outer cooling cavity, the top ring groove, and at the bowl rim.

3.5.2 Stresses due to mechanical loading

For all mechanical loads, the “temperature” load case, assumed to be quasi-static, is superimposed in order to calculate the correct resulting stresses in the piston analysis.

As a reaction to the gas force load, the piston presses against the piston pin and the cylinder. For aluminum pistons, the stiff piston pin dominates the deformation behavior of the system, because the piston has a lower stiffness due to its highly temperature-dependent material properties. The structure bends; the piston is deformed “around the piston pin.” This deformation generates stresses induced by the gas force in addition to the temperature stresses, and causes a “saddle-shaped” curve in the piston ring grooves.

Figure 3.9 shows the distribution of the stress amplitudes, as calculated from the cyclical gas force loads on a piston. This general stress distribution from the gas pressure can be explained by the “bending around the piston pin” and applies, in the broadest sense, to all pistons: under gas force load, circumferential tensile stresses arise at the bowl rim along the pin axis, while compressive stresses predominate in the thrust-antithrust direction.

Under gas force load, for all piston variants, the pin boss and support area and the transition of the support area into the piston crown are clearly loaded by compressive stresses; **Figure 3.10**. In aluminum pistons, in particular, the load limit of the pin bosses can be exceeded due to high local pressures and temperatures. This limit can be increased, to a certain degree, by the use of special pin bore profiles that deviate from the round, cylindrical pin bore by 10 to 100 µm. The design of the pin bore profile, however, also affects the stress at other areas on the piston, such as the bowl rim, bowl ground, cooling channel, or support.

In composite pistons, high compressive stresses due to gas force also arise in the support area. The force distribution of the gas force, from the combustion chamber, through the crown and the contact surfaces, into the skirt and then into the piston pin, can be significantly affected by the radial location of the support contact surfaces. Surface pressures and displacements (relative motions) arise under gas force loads at the support contact surfaces in each expansion stroke. These are caused by the different deformations of the piston’s crown and skirt. This can lead to wear at the contact surfaces.

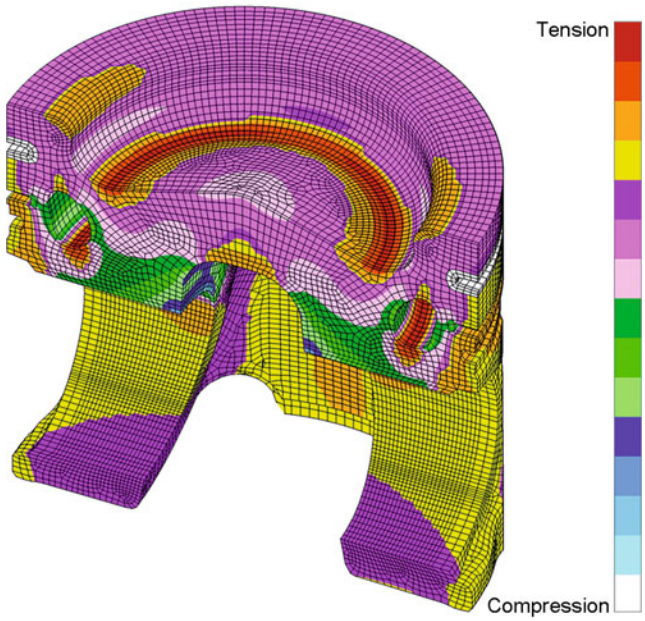

Figure 3.9:
Stress amplitudes due to gas force loading on a commercial vehicle piston with salt-core cooling channel

The bolt connection is particularly important for composite pistons in order to minimize the amplitudes from the gas force, particularly in the skirt's countersunk holes. This is done by appropriately designing the bolted parts (ball spacer, optimized countersunk depth) and by placing the bolt bores outside of the force distribution of the gas force as much as possible (central bolt joint, twin bolt joint).

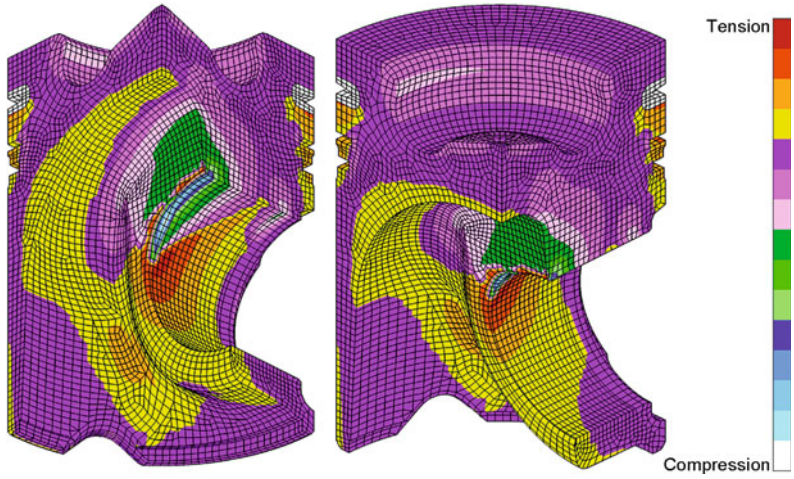

Figure 3.10: Stresses under temperature and gas force in a passenger car diesel piston with spray-jet cooling

At TDC, the effect of inertia force contributes to relieving the contact load due to gas force in the pin boss and the small end bore. **Figure 3.11** shows the stress distribution due to the temperature and inertia forces at the gas exchange TDC for a passenger car gasoline piston, which is primarily concentrated at the side of the pin bore.

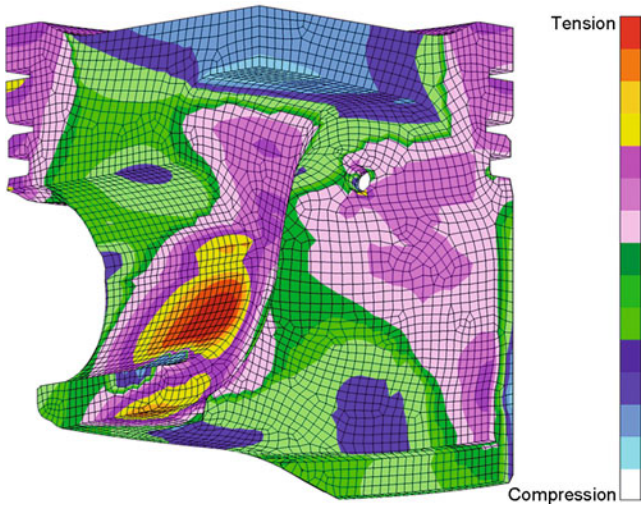

Figure 3.11: Stresses from temperature and inertia force loads in a gasoline engine piston at top dead center gas exchange

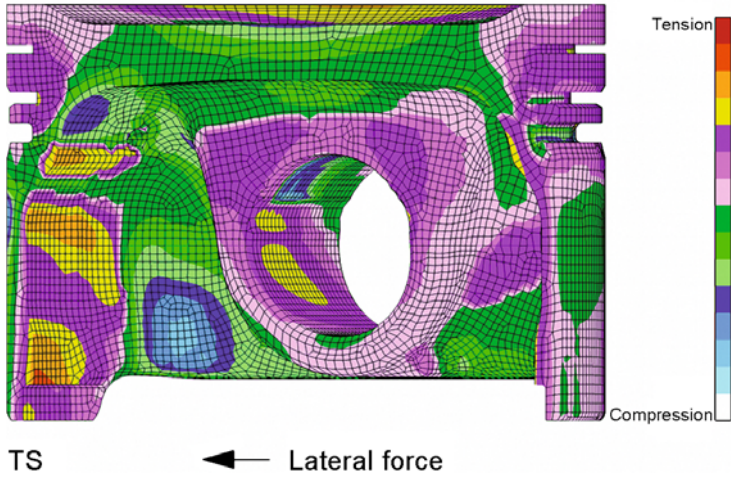

Figure 3.12: Stresses due to temperature, gas force, and lateral force loads on a gasoline engine piston

Figure 3.12 shows the distribution of stresses under the effects of temperature, gas force, and the maximum lateral force on a passenger car gasoline piston. The location with the greatest stress amplitudes can be easily identified at the transition from the piston skirt to the pin boss. The level of the maximum compressive stresses is greatly influenced by the degree of skirt ovality. Reducing the deformation of the piston prior to full contact with the cylinder, by using a piston skirt with less ovality, significantly reduces the stress amplitudes without requiring increased wall thickness in the skirt area.

3.5.3 Stresses due to manufacturing and assembly

Figure 3.13 shows the stress distribution from the joining process of a shrink-fit pin bore bushing, using the example of a piston for a passenger car diesel engine with direct injection. The bushing is not shown in the illustration. The joining process generates tensile stresses in the circumferential direction, across broad areas of the pin boss circumference, with maxima at the equator and the nadir (exterior). These must be taken into consideration when designing the boss shape and wall thicknesses.

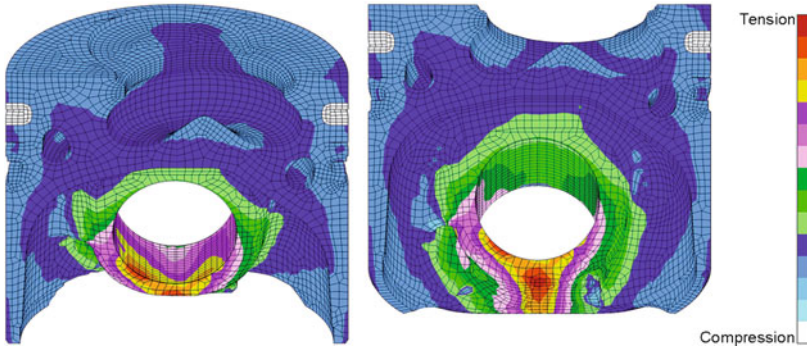

Figure 3.13: Cold shrink fit of the pin boss, stress distribution

3.6 Numerical verification of operational fatigue strength

While steel and cast iron have pronounced fatigue resistance, aluminum materials lose fatigue strength with increasing numbers of cycles. This material behavior needs to also be taken into consideration in the strength assessment. For steel pistons, the stresses are determined in a linear-elastic FEA under full-load conditions, considering all load case combinations, and are analyzed for fatigue resistance, based on the temperature and surface condition (stress-life method).

For today's highly stressed aluminum pistons, the evaluation based on a defined number of load cycles (limiting number of cycles: 50 million) is no longer possible considering a minimum safety factor due to the lack of fatigue resistance, as indicated above, at the highly stressed component locations. The cyclic plastification that occurs primarily in the highly thermally stressed bowl area, must be taken into consideration, and this requires a different approach.

Numerical verification of the operational fatigue strength is an important instrument for reducing the time, and therefore the cost, required for development. It is possible to develop the product close to its final contours at an early stage by considering variants used in series production, and thus reducing the number of engine tests. Service life analysis provides, among others, the following opportunities:

- Assessment of geometric influences (e.g., bowl rim radius, cooling gallery location, pin-bore profiles)
- Effects of load changes (e.g., power, torque, and engine speed)
- Comparison of customer release procedures
- Correlation between release engine tests and field applications
- Establishing inspection intervals
- Parameter studies for developing reasonable engine test programs

Verification of operational fatigue strength is performed using the "local strain approach," analyzing local, transient stresses and deformations (strain-life method); **Figure 3.14**.

The load-versus-time sequences are typically defined for customer-specific engine release test procedures, or by the load spectrum of the MAHLE engine test lab. These are primarily alternating load programs and thermal shock tests, which are intended to cover nearly all conditions of the series application within less time under more severe conditions.

The stress distribution in a piston under engine operating loads is known for a static temperature field from the finite element analysis. In addition to the full-load state, partial-load states can also be calculated as needed, and analyzed for critical levels of equivalent stresses (mean stress and stress amplitude). Residual stresses are taken into account in the service life analysis, as are the existing knowledge gained from engine testing, field findings, and strain gage measurements on identical or similar components in the laboratory.

With regard to materials, cyclic stress-strain curves and total strain controlled strain-life curves as a function of temperature are necessary. The isothermal material parameters for the temperature range from RT (room temperature) to 400°C are based on zero mean strain tests (strain ratio $R_\varepsilon = -1$) and are based on the saturated material state at the 50% service life cycle.

In order to describe the local stress-strain situation, starting with the initial loading curve and continuing after load reversal with the hysteresis branches (doubling the stress-strain curve, according to Masing), the "true" (elastic-plastic) stresses and strains are iteratively determined from the calculated elastic stresses at the highly loaded component locations, using

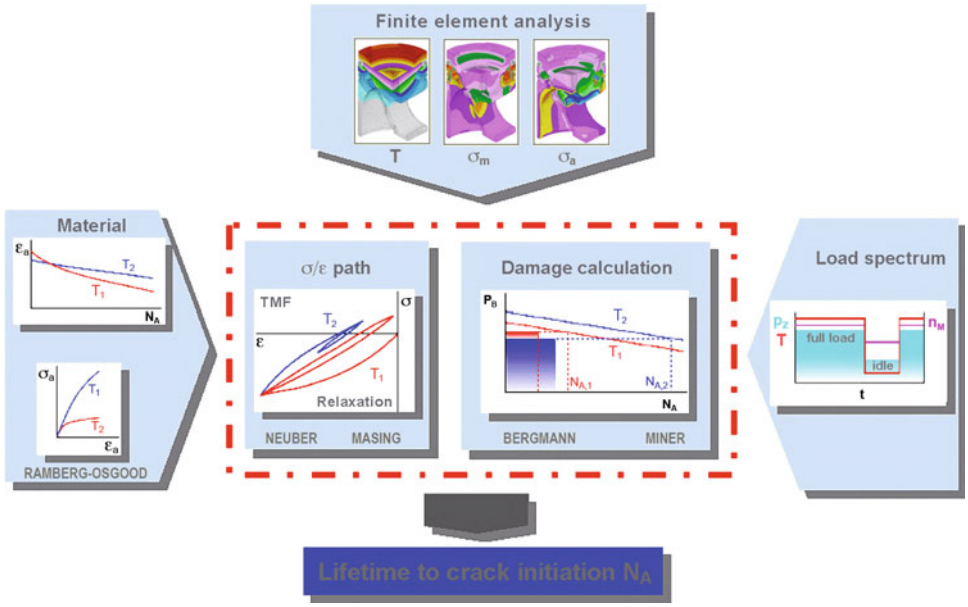

Figure 3.14: Service life concept (schematic)
Definitions: T_1: Temperature 1
T_2: Temperature 2
σ_m: Mean stress
σ_a: Stress amplitude
ε_a: Strain amplitude
p_z: Maximum gas pressure in working cycle
n_M: Engine speed
Remark: The symbols apply only to **Figure 3.14**.

the Neuber approximation. The mathematical formulation of the cyclic stress-strain curve follows the Ramberg-Osgood material law and the hyperbolic curve according to Neuber. The effect of mean stress is described by a damage parameter PB, according to Bergmann.

Here, nonzero mean stresses are transformed into zero mean stresses. In addition to converting the stress into P_B values (damage parameter according to Bergmann), the temperature-dependent ε/N lines are also described as P-Wöhler lines. The effect of the load spectrum is analyzed using a damage calculation based on the linear damage hypothesis according to Palmgren-Miner, which states that damage is accumulated starting from the 1st load cycle. Failure occurs at a defined sum of damage. The application of the operational fatigue strength assessment is performed at MAHLE using the proprietary MAFAT computer program. The result is the local service life up to crack initiation. The qualitative effects of gas pressure and temperature on the service life are shown, using the example of a passenger car diesel piston, in **Figure 3.15**: 10% reduction in gas pressure leads to nearly 3 times the service life, while a 10°C lower component temperature approximately doubles the service life.

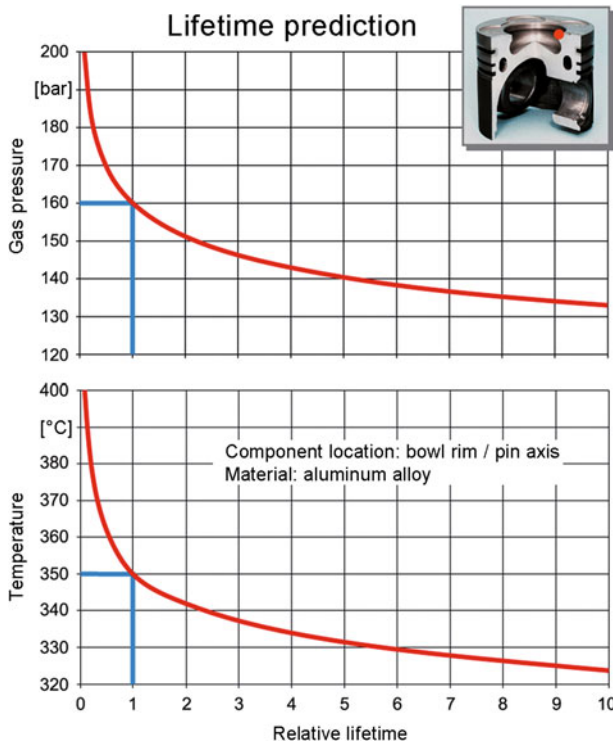

Figure 3.15:
Effect of gas pressure and component temperature on the service life of a passenger car diesel piston

Figure 3.16 shows the close agreement between the analysis and engine test results, based on the example of a gasoline piston. The failure locations are situated in the center of the crown and at the valve pocket intersection, and coincide with the lowest service life values on this piston.

Another comparison is shown in **Figure 3.17**, using the example of a heavy duty diesel piston. The piston failure, with cracks occuring in the bowl floor, again matches the service life prediction.

In the damage calculation, the high-cycle stress due to the maximum gas pressure load acting for a large number of load cycles, and the low-cycle damage due to temperature changes under operating conditions with relatively few events are separated (HC or HCF: high-cycle fatigue, and LC or LCF: low-cycle fatigue). When the operating conditions change, a transient temperature and a change in material properties occurs. At present, the LCF stress is considered as isothermal by using the higher temperature of the two load cases to define the LC stress range. According to the latest TMF (thermomechanical fatigue) fundamental research, under thermal-mechanical loading, this can lead to a nonconservative service life estimate. Because of the temperature and stress gradients present in the piston, the out-of-phase processes are of primary interest: while compressive stresses build up at the combustion bowl rim during heating due to the constraint of the surrounding material, tensile stresses during cooling resulting from reversed plastification may lead to crack initiation.

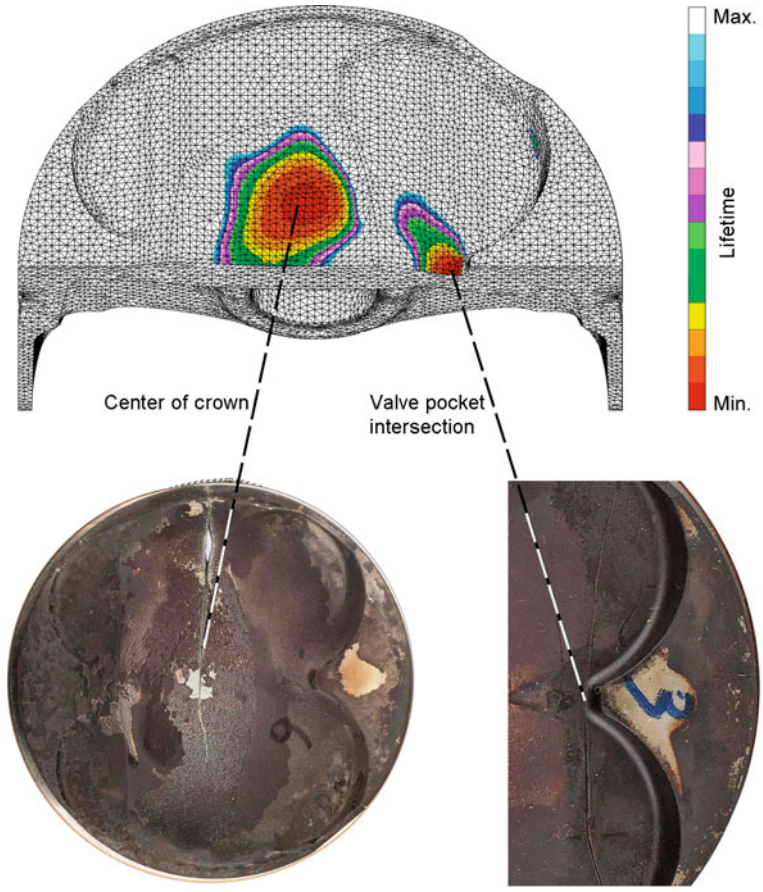

Figure 3.16: Comparison of numerical simulation and engine test (passenger car gasoline piston)

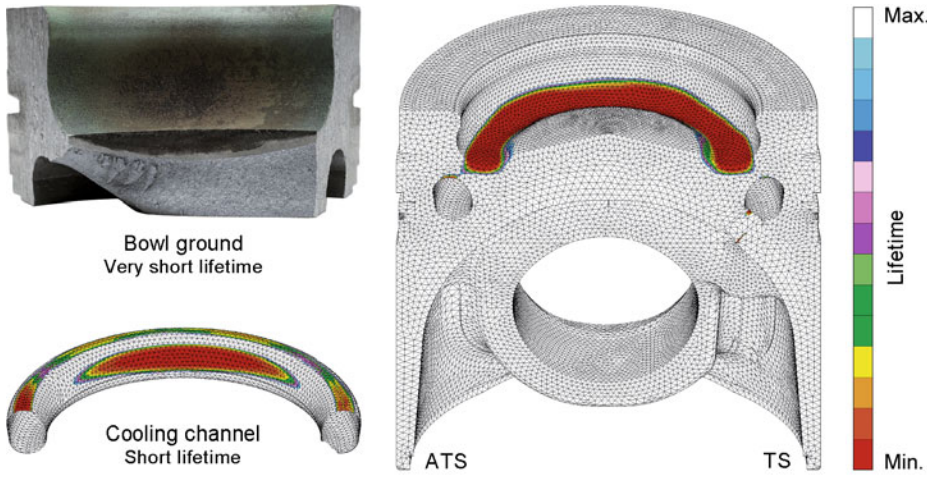

Figure 3.17: Comparison of numerical simulation and engine test (heavy duty diesel piston)

Current research and development activities focus on the simulation of near-engine conditions. Baseline material tests are performed on in-house TMF test benches. Because the transient LC loads–with the exception of the shutdown or stopping process–are simultaneously superimposed on the mechanical loads (HC loads), this must also be taken into consideration in the numerical simulation. One potential method is to investigate the microstructural damage process under various loading conditions.

One practical approach uses models for cyclic plasticity (Chaboche, Jiang, etc.) that describe material-dependent deformation behavior for monotone and cyclic stresses, creep, relaxation, and cyclic creep. Changes in the deformation model for LCF stresses can be used to adapt the viscoplastic material law to include the effect of HCF. The service life of components under cyclic load is often determined by the formation and growth of microcracks. A cycle-dependent damage parameter can be developed on the basis of elastic-plastic fracture mechanics of microcracks, and includes the effects of isothermal and thermomechanical stresses, dwell times, creep effects, etc., resulting in a prediction of the service life.

4 Piston materials

4.1 Requirements for piston materials

The functions of the piston and the loads that act on it present a very special set of requirements for the piston material.

If low piston weight is the goal, then a low-density material is preferred. Besides its design shape, the strength of the material is the deciding factor for the load capacity of the piston. The change in loads over time requires both good static and dynamic strength. Temperature resistance is likewise important, due to the thermal loads.

The thermal conductivity of the material is of significance for the temperature level. As a rule, a high thermal conductivity is advantageous, because it promotes uniform temperature distribution throughout the piston. Low temperatures not only allow greater loading of the material, but also have a beneficial effect on the process parameters at the piston crown, such as the volumetric efficiency and knock limit.

Static and dynamic strength values describe material behavior under isothermal conditions. Pistons are exposed to severe changes in temperature at times. The transient heat stresses that arise place cyclical loads on the material that can sometimes exceed the elastic limit. Materials must also be resistant to these stresses. Due to the motions and forces that occur at the sliding and sealing surfaces, piston materials must also meet high requirements for seizure resistance, low friction, and wear resistance.

The material pairing of the piston and its sliding counterparts is particularly critical, as are the lubrication conditions. They must be considered as a tribological system. Special surface treatments or coatings improve the properties of the base material.

The requirements for the thermal expansion behavior of the piston material depend on the material pairings of the cylinder and the piston pin. Differences in thermal expansion coefficients should be kept as low as possible in order to minimize changes in clearance between the cold and warm states.

A material with good machining properties supports cost-effective production in large quantities. The manufacture of the raw part should be as near to net shape as possible, and should contribute to high material quality. Suitable processes include gravity die casting and forging. The sliding and sealing surfaces demand high-precision finishing, which requires suitable machinability of the material.

MAHLE GmbH (Ed.), *Pistons and engine testing,* DOI 10.1007/978-3-8348-8662-0_4,

4.2 Aluminum materials

As a light alloy with high thermal conductivity, aluminum is particularly predestined to be used as a piston material. In the unalloyed state, however, its strength and wear resistance are too low. With the discovery of precipitation hardening by Wilm in 1906, aluminum alloys became well suited for technical purposes.

Metals have a mutual solubility that varies with temperature, which is very low for certain metals at low temperatures in the solid state [1]. Phase diagrams, derived from cooling curves from the liquid range, depict these relationships particularly clearly.

As an example, **Figure 4.1** shows the phase diagram of a 2-material (binary) system of aluminum and silicon [2]. Dropping a line through the diagram near 7% silicon, the liquidus line will be crossed at about 620°C during cooling. Below this line, a mixture of primarily precipitated α solid solution and melt is present.

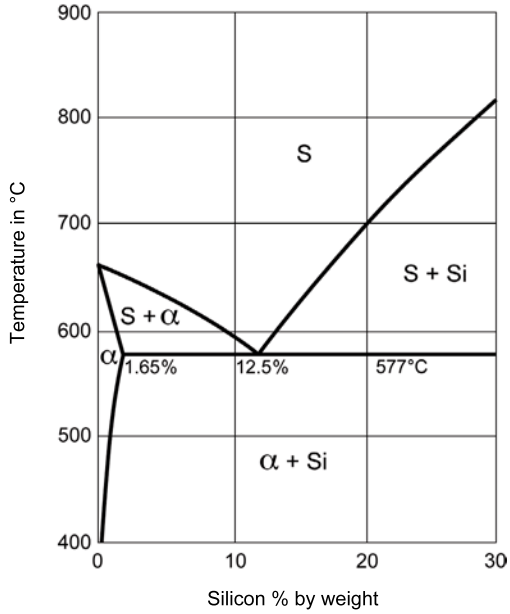

Figure 4.1:
Phase diagram of the 2-material alloy AlSi

The solid solution consists of crystals of the main alloying element (aluminum), with the foreign atoms of the second element (silicon) randomly distributed throughout the matrix. As the temperature drops, the melt becomes more and more rich in silicon, until finally the residual melt solidifies at the so-called eutectic point of 577°C and a content of about 12.5% silicon, forming a eutectic mixture consisting entirely of aluminum α solid solution and silicon

crystals. As the diagram shows, the maximum solubility (1.65%) of the silicon in the aluminum solid solution occurs at 577°C, and drops at lower temperatures. At 200°C, the solubility is only 0.01%.

The microstructure of the solidified alloy consists of the primarily precipitated α solid solution and the AlSi eutectic alloy. The diagram also shows that the percentage of eutectic becomes greater with increasing silicon content, until finally the melt transitions from the liquid to solid eutectic state with no solidification interval at the eutectic point of 12.5% silicon and 577°C.

Alloys with a silicon content of $<12.5\%$ are hypoeutectic, and those with a silicon content of $>12.5\%$ are hypereutectic. It can also be seen in the diagram that the microstructure in the hypereutectic range consists of primarily precipitated silicon crystals and the AlSi eutectic.

Crystallization from the melt is enhanced by nuclei. The number of nuclei and the cooling rate, among others, determine the fineness of the microstructure grains. The crystallites growing from the melt restrict the proportion of liquid metal more and more, and form grain boundaries where their edges run into each other. Intermetallic phases and contaminants arising from the melt are concentrated at these boundaries.

4.2.1 Heat treatment

The temperature function of the solubility of solid solutions is utilized for precipitation hardening. With rapid cooling from the melt or from annealing temperatures of around 500°C (solution annealing), supersaturated solid solution is present at low temperatures. Alloys that are suitable for pistons mainly have aluminum-copper-magnesium and aluminum-magnesium-silicon solid solutions. These alloys, present in supersaturated solid solution, are relatively soft and exhibit minimal volume. Even aging at room temperature causes the supersaturated portions to attempt to reach the state of equilibrium that corresponds to the temperature, which causes stresses in the atomic matrix. This causes no microscopically evident changes to the microstructure.

This process, known as natural aging, leads to significantly greater hardness and strength after hours or days, with a negligible increase in volume. Natural aging, however, can be reversed at relatively low temperatures. It is therefore unsuitable for thermally loaded parts.

So-called artificial aging takes place at temperatures between 100°C and 300°C, and precipitation is microscopically evident. The considerable increase in hardness and strength can lead to undesirable increases in volume for precision parts if the heat treatment process is not performed properly.

The artificial aging curve depends on the exposure time and the temperature level; **Figure 4.2**.

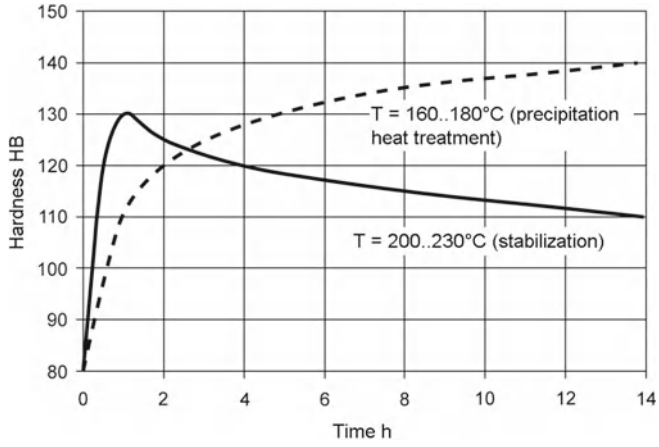

Figure 4.2:
Hardness-time isothermals for artificial aging of aluminum-silicon piston alloys. Initial state: solution-annealed and rapidly cooled

Depending on the temperature of the artificial aging, the hardness-time isothermals pass through a maximum. For stabilizing artificial aging, this maximum is exceeded, which means that some strength is always lost, but adequate volume stability is achieved. The temperature level and the exposure time affect not only the hardness and thus the strength at room temperature, but also the hardness and strength at elevated temperatures, which are of great significance to the operating behavior of the piston material.

Figure 4.3 shows the residual hardness curve for an aluminum-silicon piston alloy, measured on a cooled sample after corresponding temperature exposure. The curves help to evaluate the suitability of alloys with high strength at elevated temperatures. They also allow conclusions to be drawn about the average occurring piston temperatures by measuring the hardness of pistons that have been run.

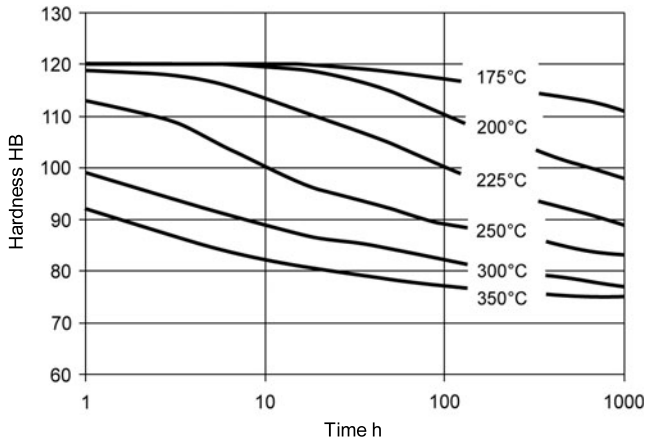

Figure 4.3:
Residual hardness curve of a heat-treated aluminum-silicon piston alloy, by temperature exposure

4.2.2 Piston alloys

Pistons are almost exclusively made of aluminum-silicon alloys of eutectic, and partly hypereutectic composition, which can be cast easily and nearly always can be forged as well. **Table 4.1** shows an overview of the chemical composition of piston alloys used by MAHLE.

The eutectic alloy M124 is the “classic” piston alloy, and has been the basis for the vast majority of pistons in recent decades. Even today it is still a very significant, universally applicable alloy. Pistons made of hypereutectic alloys exhibit even greater wear resistance. From this group, the alloys M138 and M244 are preferred for two-stroke engine pistons, while the M126 alloy is used in the USA for passenger cars gasoline engines.

The alloys M142, M145, and M174+ have been developed only recently. Their common characteristic is the relatively high proportion of the elements copper and nickel. This gives the alloys particularly high strength at elevated temperatures and thermal stability. Despite increasing requirements in terms of casting technology and slight disadvantages due to somewhat greater density and lower thermal conductivity, their high strength at elevated temperatures and thermal stability have led to great market penetration for these alloys in high-performance passenger car and commercial vehicle engines. The eutectic alloy M142 is primarily used in gasoline engines, and the alloy M174+, which is likewise eutectic, is used increasingly in diesel engines. The hypereutectic alloy M145 is used in several gasoline engines.

Aluminum-silicon piston alloys are employed mainly for cast pistons. They can also be forged for special purposes, which leads to somewhat different microstructures and properties. The designation “P” is added to the alloy symbol in order to highlight this distinction.

The alloy M-SP25 is a silicon-free, high-strength aluminum alloy used exclusively for forged pistons and piston components, primarily for racing pistons, but also for skirts of composite pistons in large engines.

Figures 4.4 a–d show examples of characteristic material microstructures. The eutectic alloys M124, M142, and M174+ exhibit a grainy, heterogeneous, eutectic aluminum-silicon mixture with embedded intermetallic phases. In the hypereutectic alloys M126, M138, M145, and M244, the increasing silicon content results in a clearly visible increase in the proportion of primarily precipitated silicon crystals. Small amounts of phosphorus in the aluminum melt act as nuclei for the silicon, resulting in a favorable formation of silicon crystals that promotes machinability. Their edge lengths should not be greater than 100 µm.

Table 4.1: Chemical composition of MAHLE aluminum piston alloys [percent by weight]

	M124	M126	M138	M244
	AlSi12CuMgNi	AlSi16CuMgNi	AlSi18CuMgNi	AlSi25CuMgNi
Si	11.0–13.0	14.8–18.0	17.0–19.0	23.0–26.0
Cu	0.8–1.5	0.8–1.5	0.8–1.5	0.8–1.5
Mg	0.8–1.3	0.8–1.3	0.8–1.3	0.8–1.3
Ni	0.8–1.3	0.8–1.3	0.8–1.3	0.8–1.3
Fe	max. 0.7	max. 0.7	max. 0.7	max. 0.7
Mn	max. 0.3	max. 0.2	max. 0.2	max. 0.2
Ti	max. 0.2	max. 0.2	max. 0.2	max. 0.2
Zn	max. 0.3	max. 0.3	max. 0.3	max. 0.2
Cr	max. 0.05	max. 0.05	max. 0.05	max. 0.6
Al	remainder	remainder	remainder	remainder

	M142	M145	M174+	M-SP25
	AlSi12Cu3Ni2Mg	AlSi15Cu3Ni2Mg	AlSi12Cu4Ni2Mg	AlCu2.5Mg1.5FeNi
Si	11.0–13.0	14.0–16.0	11.0–13.0	max. 0.25
Cu	2.5–4.0	2.5–4.0	3.0–5.0	1.8–2.7
Mg	0.5–1.2	0.5–1.2	0.5–1.2	1.2–1.8
Ni	1.75–3.0	1.75–3.0	1.0–3.0	0.8–1.4
Fe	max. 0.7	max. 0.7	max. 0.7	0.9–1.4
Mn	max. 0.3	max. 0.3	max. 0.3	max. 0.2
Ti	max. 0.2	max. 0.2	max. 0.2	max. 0.2
Zn	max. 0.3	max. 0.3	max. 0.3	max. 0.1
Zr	max. 0.2	max. 0.2	max. 0.2	–
V	max. 0.18	max. 0.18	max. 0.18	–
Cr	max. 0.05	max. 0.05	max. 0.05	–
Al	remainder	remainder	remainder	remainder

The eutectic piston alloy M124 is also used in a refined state (M124V). The eutectic composition between AlSi solid solutions, which develop as dendrites, is made particularly fine by the addition of small amounts of sodium or strontium. Machinability is improved, but resistance to wear is worse than for grainy eutectic structures.

The structures of the forged alloys M124P, M124VP, and the AlCu alloy M-SP25 are also illustrated. The flow structure can be seen in the linear formation of the structure.

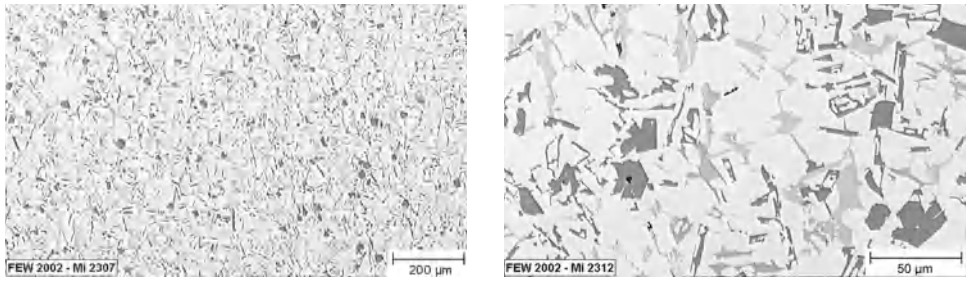

Figure 4.4 a: Eutectic AlSi alloy M142 (representative for M124 and M174+ as well), casting state with grainy structure

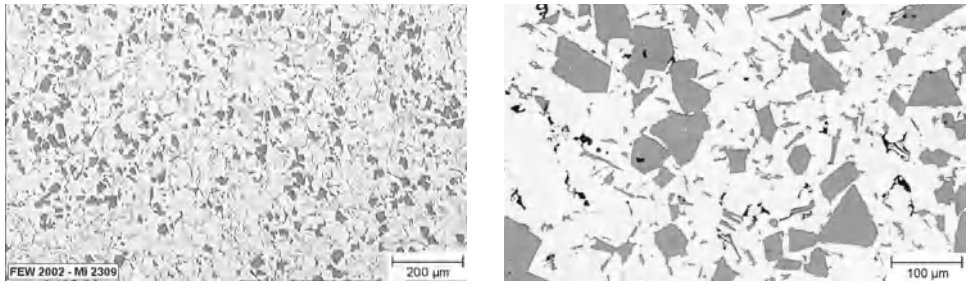

Figure 4.4 b: Hypereutectic AlSi alloys, casting state with grainy structure, left M145 (14–16% Si), right M244 (23–26% Si)

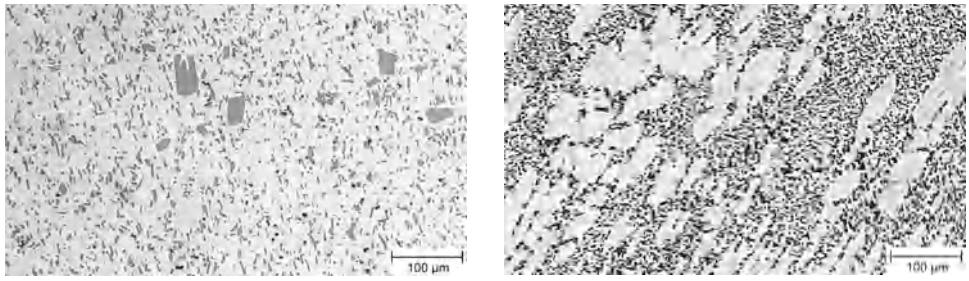

Figure 4.4 c: Al alloys for forged pistons, left M124P with grainy structure, right M124VP with refined structure

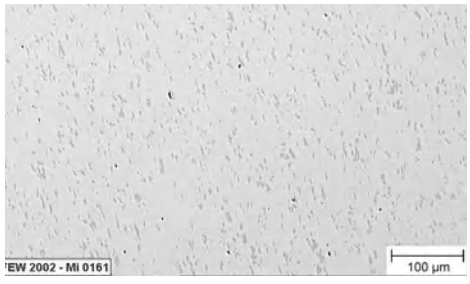

Figure 4.4 d:
Si-free alloy M-SP25

The temperature-dependent physical and mechanical material parameters for cast pistons are summarized in **Table 4.2**. Along with the static characteristics of tensile strength and elastic limit, the dynamic characteristic of alternate strength is also provided for evaluating fatigue resistance [3]. A limit load cycle of 50 x 10^6 was used for determining the alternate strength.

The strength values given here apply to test bars taken from pistons. Prior to testing at elevated temperatures, they were artificially aged at the test temperature for a long period of time. This procedure allows for the current service life of pistons in engine operation, which is significantly longer than the load times that can be produced in materials testing.

The material characteristic values for forged pistons are shown in **Table 4.3**. Compared to the cast state, the material in the forged state exhibits greater strength and greater plastic deformability (greater elongation after fracture). The strength advantage of the forged material structure is greatest in the lower and middle temperature ranges, up to about 250°C, and drops off at high temperatures.

The strength values are based on heat-treated samples taken from pistons and artificially aged at the test temperature.

The wider scatter bands for the strength values as compared to cast alloys, due to differences in heat treatment, account for the use of forged pistons for different durability requirements. The lower limits are representative for production vehicles and large engines, and the higher limits for racing and sports engines.

The wear rates shown–relative to the material M124–are relative values, obtained using a variant of the wear machine according to E. Koch [4]. The practical applicability of values obtained on wear machines, however, is often questionable. Experience has shown that the data determined by MAHLE allow at least a qualitative evaluation of the materials.

Table 4.2: Physical and mechanical properties of cast MAHLE aluminum piston alloys

Description		M124	M126, M138	M142, M145, M174+	M244
Hardness HB10	20°C	90–130	90–130	100–140	90–130
Tensile strength R_m [MPa]	20°C	200–250	180–220	200–280	170–210
	150°C	180–200	170–200	180–240	160–180
	250°C	90–110	80–110	100–120	70–100
	350°C	35–55	35–55	45–65	35–55
Yield strength $R_{p0,2}$ [MPa]	20°C	190–230	170–200	190–260	170–200
	150°C	170–210	150–180	170–220	130–180
	250°C	70–100	70–100	80–110	70–100
	350°C	20–30	20–40	35–60	30–50
Elongation at fracture A_5 [%]	20°C	<1	1	<1	0.1
	150°C	1	1	<1	0.4
	250°C	3	1.5	1.5–2	0.5
	350°C	10	5	7–9	2
Fatigue strength σ_{bw} [MPa]	20°C	90–110	80–100	100–110	70–90
	150°C	75–85	60–75	80–90	55–70
	250°C	45–50	40–50	50–55	40–50
	350°C	20–25	15–25	35–40	15–25
Young's modulus E [MPa]	20°C	80,000	84,000	84,000–85,000	90,000
	150°C	77,000	80,000	79,000–80,000	85,000
	250°C	72,000	75,000	75,000–76,000	81,000
	350°C	65,000	71,000	70,000–71,000	76,000
Thermal conductivity λ [W/mK]	20°C	145	140	130–135	135
	350°C	155	150	140–145	145
Thermal expansion α [10^{-6} m/mK]	20–100°C	19.6	18.6	18.5–19.5	18.3
	20–200°C	20.6	19.5	19.5–20.5	19.3
	20–300°C	21.4	20.2	20.5–21.2	20.0
	20–400°C	22.1	20.8	21.0–21.8	20.7
Density ρ [g/cm^3]	20°C	2.68	2.67	2.75–2.79	2.65
Relative wear rate		1	0.8	0.85–0,9	0.6

Table 4.3: Physical and mechanical properties of forged MAHLE aluminum piston alloys

Description		M124P	M142P	M-SP25
Hardness HB10	20°C	100–125	100–140	120–150
Tensile strength R_m [MPa]	20°C	300–370	300–370	350–450
	150°C	250–300	270–310	350–400
	250°C	80–140	100–140	130–240
	300°C	50–100	60–100	75–150
Yield strength $R_{p0,2}$ [MPa]	20°C	280–340	280–340	320–400
	150°C	220–280	230–280	280–340
	250°C	60–120	70–120	90–230
	300°C	30–70	45–70	50–90
Elongation at fracture A_5 [%]	20°C	<1	1	8
	150°C	4	2	9
	250°C	20	6	12
	300°C	30	20	12
Fatigue strength σ_{bw} [MPa]	20°C	110–140	110–140	120–150
	150°C	90–120	100–125	110–135
	250°C	45–55	50–60	55–75
	300°C	30–40	40–50	40–60
Young's modulus E [MPa]	20°C	80,000	84,000	73,500
	150°C	77,000	79,000	68,500
	250°C	72,000	75,000	64,000
	300°C	69,000	73,000	62,000
Thermal conductivity λ [W/mK]	20°C	155	140	140
	150°C			155
	250°C			165
	300°C	165	150	170
Thermal expansion α [10^{-6} m/mK]	20–100°C	19.6	19.2	22.4
	20–200°C	20.6	20.5	24
	20–300°C	21.4	21.1	24.9
Density ρ [g/cm^3]	20°C	2.68	2.77	2.77
Relative wear rate		1	0.9	1.3

4.2.3 Fiber reinforcement

Ceramic fibers significantly increase the thermal and mechanical load limits of aluminum piston materials. Using pressure-aided casting processes, fiber preforms–short Al_2O_3 fibers with an average fiber diameter of 3 to 4 μm and average fiber length of 50 to 200 μm–are infiltrated with the liquid alloy melt [5]. The structure images in **Figure 4.5** show the distribution and orientation of the ceramic fibers in the metallic matrix. Due to the fiber preform manufacturing process, most fibers are randomly oriented within a plane.

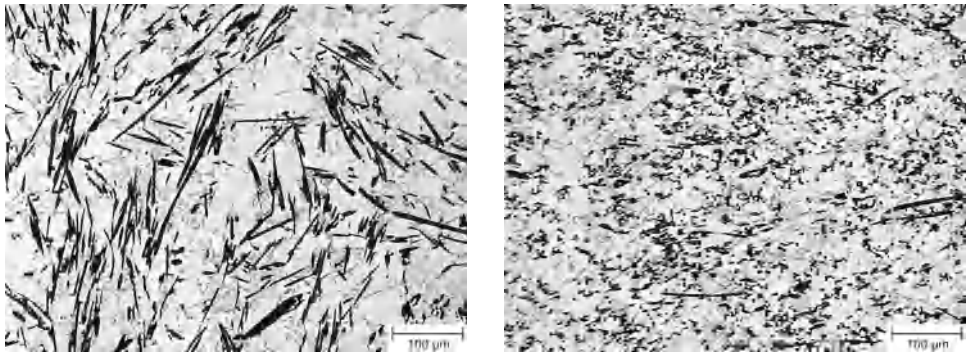

Figure 4.5: Microstructure of the Al piston alloy M124, reinforced with about 15 percent Al_2O_3 fibers by volume, section in the plane, left, and perpendicular to the preferred fiber orientation, right

Slight disadvantages in the form of somewhat greater density and lower thermal conductivity are offset by the many advantages of fiber-reinforced composite materials, such as an increase in Young's modulus and a lower thermal expansion coefficient.

The thermal and mechanical fatigue resistance increases particularly sustainably. For this reason, composite materials are especially well-suited for the local reinforcement of particularly highly stressed zones, such as the combustion bowl in diesel engine pistons. In commercial vehicles, pistons with locally fiber-reinforced combustion chamber bowls have proved their functionality and reliability for many years.

4.3 Ferrous materials

If the strength or wear resistance of aluminum alloys is not sufficient to meet the loads, then ferrous materials are employed. This can begin with local reinforcement (e.g., ring carriers), and extend to parts of composite pistons (e.g., piston crown, bolts), all the way to pistons constructed entirely of cast iron or forged steel.

Carbon is the most important alloying element for iron. The iron-carbon diagram, **Figure 4.6**, enables a thorough assessment of these materials [6]. This diagram differentiates two systems: the metastable or carbidic system, consisting of iron and metastable cementite Fe_3C (solid lines), and the stable or graphite system (dashed lines). In the latter case, the majority of the carbon is embedded in the iron as graphite. In the metastable system, the iron can bind the carbon only as cementite (Fe_3C), up to 6.7%. **Figure 4.6** therefore presents a complete overview (0–100% Fe_3C). Depending on the temperature, carbon atoms can be embedded up to a certain degree in the iron lattice on so-called interstitials. The solubility of carbon in the body-centered cubic α solid solution–also known as α iron or ferrite–is significantly lower (max. 0.02 percent C by weight) than in the face-centered cubic γ solid solution–also known as γ iron or austenite (max. 2.0 percent C by weight).

For carbon contents of less than 4.3%, austenite is primarily precipitated from the melt. At 4.3% C, the melt solidifies eutectically as ledeburite. At greater than 4.3% C, cementite is primarily precipitated from the melt. Below 2.0% C, austenite forms first, and its range of existence drops off with falling temperature to lower concentrations of C, until finally the carbon-rich austenite degrades into low-carbon ferrite and cementite at 723°C. In the range of 0.8% C, the eutectoid perlite is formed, which is a laminar arrangement of ferrite and cementite.

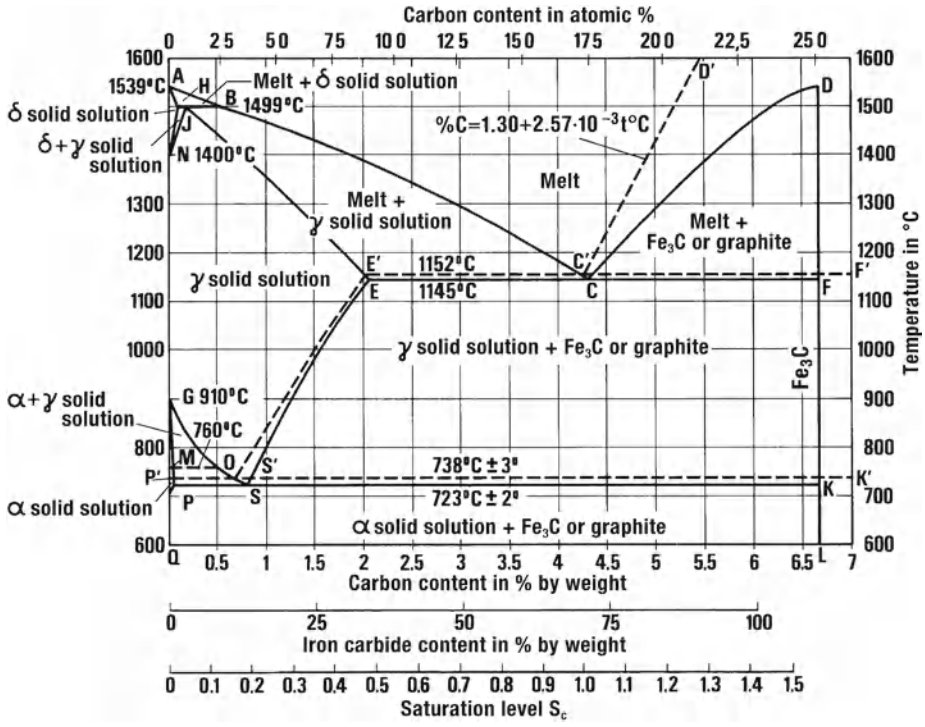

Figure 4.6: Iron-carbon diagram

In the stable system, the processes shown with dashed lines occur at normal cooling speeds only in the presence of additional silicon (>0.5%), because silicon promotes the formation of free carbon (graphite). Fundamentally, the processes are similar to those in the metastable system, except that graphite is formed instead of cementite.

4.3.1 Cast iron materials

Cast iron materials generally have a carbon content of >2%. In these materials, the brittle cementite or graphite can no longer be brought into solution by subsequent heat treatment. They are therefore not suitable for radical hot forming, but their castability can be optimized.

MAHLE uses high-quality cast iron varieties with lamellar and spherolithic graphite for its products. **Table 4.4** contains the composition, physical properties, and strength values of common alloys. The microstructures of these materials are shown in **Figures 4.7 a–c**.

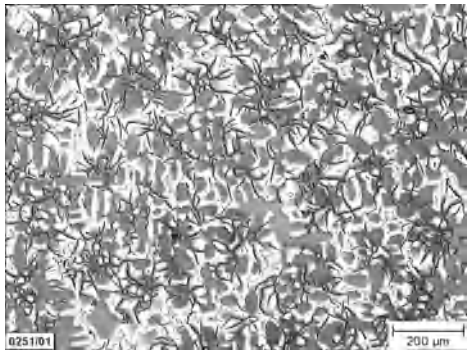

Figure 4.7 a: Microstructure of the MAHLE cast iron material M-H

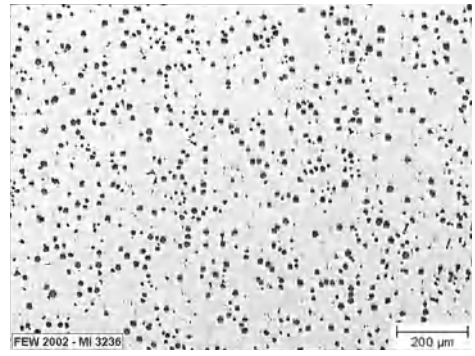

Figure 4.7 b: Microstructure of the MAHLE cast iron material M-K

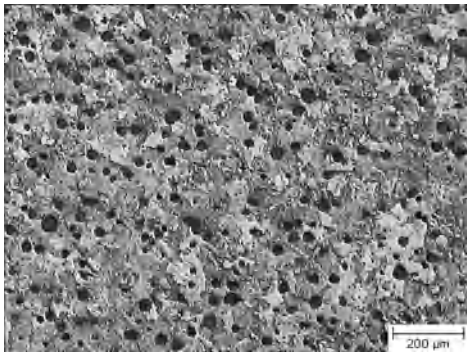

Figure 4.7 c:
Microstructure of the MAHLE cast iron material M-S70

Table 4.4: MAHLE cast iron materials–chemical composition, mechanical and physical properties (guidelines for separately cast sample bars)

Description		Austenitic cast iron for ring carriers		Cast iron with spheroidal graphite for pistons and piston skirts
		M-H (lamellar)	M-K (spherolithic)	M-S70 (EN GJS 700-2)
Alloying elements [Percent by weight]	C	2.4–2.8	2.4–2.8	3.5–4.1
	Si	1.8–2.4	2.9–3.1	2.0–2.4
	Mn	1.0–1.4	0.6–0.8	0.3–0.5
	Ni	13.5–17.0	19.5–20.5	0.6–0.8
	Cr	1.0–1.6	0.9–1.1	–
	Cu	5.0–7.0		<0.1
	Mo			
	Mg		0.03–0.05	0.04–0.06
Brinell hardness HBW 30		120–150	140–180	240–300
Tensile strength R_m [MPa]	20°C	190	380	700
	100°C	170		640
	200°C	160		600
	300°C	160		590
	400°C	150		530
Yield strength $R_{p0,2}$ [MPa]	20°C	150	210	420
	100°C	150		390
	200°C	140		360
	300°C	140		350
	400°C	130		340
Elongation at fracture A_5 [%]	20°C	2	8	2
Fatigue strength σ_{bw} [MPa]	20°C	150		250
Young's modulus E [MPa]	20°C	100,000	120,000	177,000
	200°C			171,000
Thermal conductivity λ [W/mK]	20°C	32	13	27
Thermal expansion α [10^{-6} m/mK]	20–200°C	18	18	12
Density ρ [g/cm^3]	20°C	7.45	7.4	7.2

Due to their relatively high thermal expansion in comparison to cast irons with perlitic or ferritic basic structures, austenitic cast iron materials are of great significance for the production of ring carrier pistons [7]. The alloy M-H, for example, has a thermal expansion coefficient of $\alpha \approx 17.5 \times 10^{-6}$ m/mK, which, compared to $\alpha \approx 10 \times 10^{-6}$ m/mK for normal cast iron, is nearly the same as that of the aluminum piston alloy M124 ($\alpha \approx 21 \times 10^{-6}$ m/mK). For the solidified cast aluminum piston, this means that critical stresses between the piston body and a ring carrier made of austenitic cast iron are much lower than for a ring carrier made of normal cast iron. Most ring carriers are made of austenitic cast iron with lamellar graphite formation M-H. In special cases, the higher-strength austenitic cast iron with spherolithic graphite formation M-K is used. Ring carriers are machined from centrifugally cast tubes. Centrifugal casting produces a dense, consistent casting structure.

For the materials used in piston casting, the basic material of the structure is largely perlitic, due to its good strength and wear properties. Pistons in highly stressed diesel engines and other highly loaded components in engines and machine design are predominantly made of M-S70 spherolithic cast iron. This material is used, for example, for single-piece pistons and piston skirts in composite pistons.

4.3.2 Steels

The iron alloys designated as steels generally have a carbon content of less than 2%. When heated, they transform completely into malleable (suitable for forging) austenite. The iron alloys are therefore excellent for hot forming, such as rolling or forging.

Steels used for components generally have a carbon content of less than 0.8%. If they cool slowly after casting or hot forming, then a ferritic-perlitic structure is formed; **Figure 4.8 b**. In this state, the steel typically has insufficient strength and hardness. The strength of the material is therefore increased by various means.

One technically significant process is tempering, where the steel is cooled rapidly from a temperature of more than 850°C (quenching). The conversion of austenite to perlite and ferrite, as shown in the iron-carbon diagram in **Figure 4.6**, no longer takes place, due to the suddenly limited freedom of motion of the carbon atoms in the iron matrix. The carbon remains forcibly dissolved in the crystal lattice, although it does not have sufficient solubility under equilibrium conditions. This leads to great lattice distortions, which are expressed macroscopically as high hardness and strength, but also brittleness. This hardened structure with a typically acicular appearance is called martensite. Subsequent heating of the material, or tempering, relieves these stresses somewhat and forms a tempered structure; **Figure 4.8 a**. Hardness and strength are reduced somewhat, but toughness is increased [8].

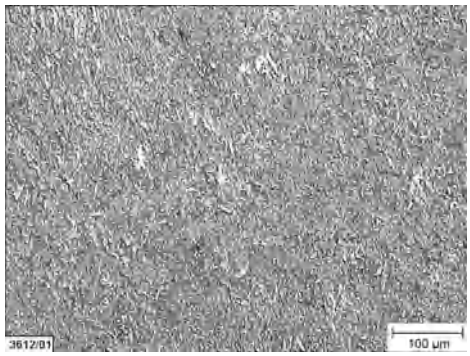

Figure 4.8 a: Tempered structure of steel 42CrMo4

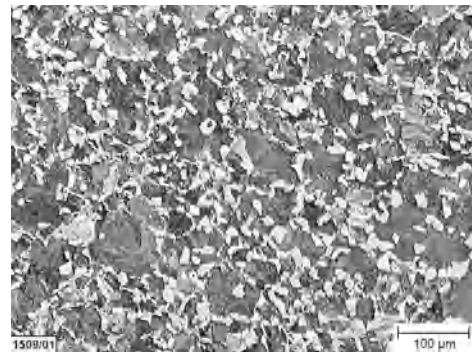

Figure 4.8 b: Ferritic-perlitic structure of AFP steel 38MnVS6

When quenching, the cooling rate decreases from the edge to the core of a component and is ultimately less than the critical cooling rate of the steel, so that the austenite no longer is completely converted to martensite in this area. The material no longer fully hardens. Elements such as manganese, chromium, nickel, or molybdenum increase the hardenability of the alloy by reducing its critical cooling rate. This is particularly important for components with large heat-treatment cross sections, because it can limit the loss of strength toward the core.

For very highly stressed pistons and piston components, the chromium-molybdenum alloy of heat-treated steel 42CrMo4 is used. In addition to improved full hardenability, both alloying elements promote carbide formation, and molybdenum also increases strength at elevated temperatures. However, even for this steel, a decrease in strength toward the core area must be expected for very large heat-treatment cross sections or changes in cross section. The scattering ranges for strength values shown in **Table 4.5** highlight this fact.

Bolts that connect the piston crown of a composite piston to the piston skirt are also generally made of 42CrMo4 heat-treated steel. They must comply with the highest DIN 267 strength classification of 10.9. In special cases, 34CrNiMo6 heat-treated steel is used, which has even greater full hardenability due to the addition of nickel.

Another significant technology for increasing the strength of metallic materials is precipitation hardening. Precipitation-hardened ferritic-perlitic steels, abbreviated as AFP steels, exhibit small amounts of vanadium or niobium added (about 0.1 percent by weight). They are therefore referred to as microalloyed steels [9]. When the material is heated to forging temperatures, these microalloyed elements dissolve completely in the γ solid solution. The forged part is allowed to cool in air at a controlled rate immediately after hot forming. As the austenite converts to ferrite and perlite, the carbides and carbonitrides of these microalloyed elements precipitate in a very fine distribution in the ferrite and increase the strength, particularly the yield point, by preventing dislocation mobility.

Table 4.5: Steels for pistons–chemical composition, mechanical and physical properties

Description		42CrMo4	38MnVS6
State of heat treatment		Heat-treated	Controlled cooling from heat of deformation
Alloying elements [Percent by weight]	C	0.38–0.45	0.34–0.41
	Si	max. 0.40	0.15–0.80
	Mn	0.60–0.90	1.20–1.60
	Cr	0.90–1.20	max. 0.30
	Mo	0.15–0.30	max. 0.08
	P	max. 0.035	max. 0.025
	S	max. 0.035	0.020–0.060
	V		0.08–0.020
	N		0.010–0.020
Brinell hardness HBW 30		265–330	240–310
Tensile strength R_m [MPa]	20°C	920–980	910
	130°C	870–960	860
	300°C	850–930	840
	450°C	630–690	610
Yield strength $R_{p0,2}$ [MPa]	20°C	740–860	610
	130°C	700–800	570
	300°C	680–750	540
	450°C	520–580	450
Elongation at fracture A_5 [%]	20°C	12–15	14
	130°C	8–13	9
	300°C	10–13	11
	450°C	15–16	15
Fatigue strength σ_{bw} [MPa]	20°C	370–440	370
	130°C	350–410	350
	300°C	340–400	320
	450°C	280–340	290
Young's modulus E [MPa]	20°C	212,000	208,000
	130°C	203,000	201,000
	300°C	193,000	189,000
	450°C	180,000	176,000
Thermal conductivity λ [W/mK]	20°C	44	38
	130°C	43	39
	300°C	40	39
	450°C	37	37
Average linear thermal expansion α [10^{-6} m/mK]	20–300°C	13.2	13.1
	20–450°C	13.7	13.7
Density ρ [g/cm^3]	20°C	7.80	7.78

Figure 4.8 b shows a typical AFP structure, using 38MnVS6 as an example. This material is preferably used in steel pistons for commercial vehicle engines and for forged steel skirts in composite pistons. The advantages of this group of materials, compared to heat-treated steels, are improved machinability of the ferritic-perlitic structure and the elimination of costly subsequent heat treatment.

Both steel grades used for manufacturing pistons today, 42CrMo4 heat-treated steel and 38MnVS6 AFP steel, are suitable for use at temperatures of up to 450°C with regard to strength at elevated temperatures and oxidation resistance. When testing new engines, it is partly common to test the service life under overloaded conditions. This can easily involve steel piston temperatures of 500 to 550°C, particularly at the edge of the combustion chamber bowl. In this temperature range, the iron reacts with the excess oxygen of the burning fuel-air mixture, and appreciable scaling occurs. If future engine concepts are going to have similar thermal loads even under normal operating conditions, either antioxidization coatings or other heat-resistant and oxidation-resistant steel grades may be used.

4.4 Copper materials for pin bore bushings

Pin bosses of diesel engine pistons are highly specifically loaded and sometimes have pin bore bushings made of copper materials. The bushings are inserted with interference, i.e., using a shrink fit connection. For aluminum pistons, the pin bore bushing increases fatigue strength of the pin boss. For steel pistons, seizure resistance of the pin boss bearing is the primary emphasis. Besides high strength and good sliding properties, bushing materials should feature these additional properties:

- Similar thermal expansion behavior as the piston material (for constant interference under hot and cold conditions)
- Corrosion resistance against hot, acidified lubricating oil

MAHLE prefers to use solid pin boss bushings. They are machined from drawn tubes, which gets its strength from the deformation process or heat treatment. The range of applications indicated above is covered by two material grades.

Special brass CuZn31Si1 (material 2.1831) per DIN/ISO 4382-2

A nonhardenable material, which obtains its strength from cold forming. It is very resistant to corrosion due to oils and has good sliding properties. The microstructure consists of an α matrix with some proportion of β phase. Alloying silicon improves the wear and corrosion resistance.

Aluminum bronze CuAl10Ni5Fe4

A precipitation-hardened material that is hardened during hot forming. It is characterized by high strength and good corrosion resistance against oils. The microstructure consists of an α matrix with precipitated iron, nickel, and manganese (κ phase). Alloyed aluminum improves the mechanical properties. Nickel increases strength at elevated temperatures, and iron improves fine-graining and strength. The addition of manganese increases corrosion resistance and ductility.

Figures 4.9 a/b display the structures of pin bore bushing materials, and **Table 4.6** shows the composition and properties of the two materials. Due to its very high strength, aluminum bronze CuAl10Ni5Fe4 is preferred for bushings in steel pistons, while the special brass CuZn31Si1 is the preferred bushing material for aluminum pistons, due to its greater thermal expansion coefficient.

Table 4.6: Chemical composition and properties of pin bore bushing materials

		CuZn31Si1	CuAl10Ni5Fe4
Composition [Percent by weight], Reference values	Al	–	8.5–11
	Ni	max. 0.5	4–6
	Fe	max. 0.4	2–5
	Mn	–	0.5–1.5
	Si	0.7–1.3	–
	Pb	0.1–0.3	max. 0.05
	Zn	28.5–33.3	max. 0.5
	other, total	max. 0.5	max. 0.3
	Cu	remainder	remainder
Hardness HB 10	minimal value	150	170
Tensile strength R_m [MPa]	minimal value	540	700
Yield strength $R_{p0,2}$ [MPa]	minimal value	430	460
Elongation at fracture A_5 [%]	minimal value	10	10
Young's modulus E [MPa]		108,000	120,000
Thermal conductivity λ [W/mK]		71	63
Thermal expansion α [10^{-6} m/mK]	300°C	19.2	16.6
Density ρ [g/cm^3]		8.4	7.6

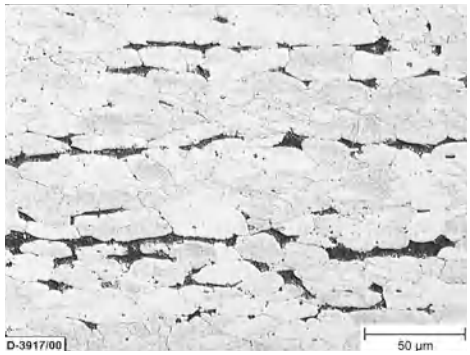

Figure 4.9a: Microstructure of the pin bore bushing material CuZn31Si1

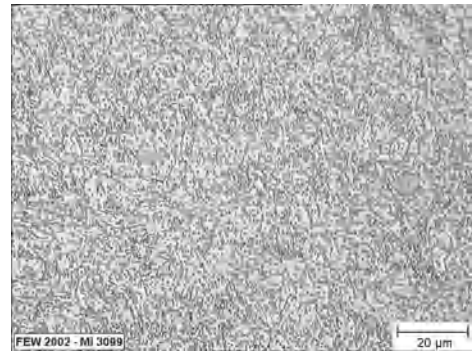

Figure 4.9b: Microstructure of the pin bore bushing material CuAl10Ni5Fe4

4.5 Coatings

4.5.1 Coatings on the piston skirt

Coating of the piston skirt is primarily intended to prevent local welding between the piston and the cylinder, or piston seizing. A wear protective coating is generally not needed in this connection.

Under normal, moderate operating conditions, a piston does not require a skirt coating if its dimensions are designed carefully and correctly. Risk of seizing does exist, however, under extreme operating conditions:

- Lack of local clearance, caused by mechanical and/or thermal deformation of the cylinder
- Insufficient oil supply, such as during cold start
- Insufficient lubrication capability of the engine oil, caused by fuel contamination, extremely high operating temperature, or excessive aging of the oil
- In brand-new condition, when the piston and cylinder have not yet been run in

A coating on the piston skirt provides protection in such extreme situations. It is important that the skirt coating be tribologically matched to the cylinder bore (cast iron or aluminum).

4.5.1.1 GRAFAL® 255 and EvoGlide

The standard coating for the piston skirt is GRAFAL®, for pistons of all sizes and types that are paired with cast iron cylinders.

GRAFAL® is an approximately 20-µm thick sliding lacquer coating with fine graphite particles embedded in a polymer matrix. It withstands temperatures of up to 250°C that can occur at the piston skirt and is resistant to oils and fuels. The film-forming polymer matrix supports the action of the solid graphite lubricant during dry running, with advantageous tribological properties. This provides great seizure resistance for very low clearances and a lack of oil. Under normal loading conditions, the coating does not wear. Under extreme loads, particularly in case of high local surface pressure, it can be partially worn off locally. The resulting greater clearance reduces the tendency to seize. Due to this adaptability and the self-lubricating properties of GRAFAL®, pistons can exhibit very low clearances, which produces favorable acoustic properties with low friction.

Because the lateral forces on the piston skirt are increased when implementing a downsizing concept, the sliding lacquer layer must demonstrate improved wear resistance in the piston/cylinder bore system over the service life of the engine. EvoGlide was developed for this purpose. The addition of certain additives makes the resin matrix more wear-resistant. The ability to wear off locally under extreme stress, however, is retained.

4.5.1.2 Tin

As a soft, deformable material, tin is also suitable as a skirt coating and serves as a run-in aid and preserves boundary lubrication properties, especially for cold starts. The tin coating is 1 to 2 µm thick. The potential for preventing seizing is thus somewhat less than that of a GRAFAL® layer. Tin-plated pistons are paired with gray cast iron or NIKASIL® cylinders, and are preferably installed in passenger car gasoline engines.

4.5.1.3 Ferrostan/FerroTec®

The skirt coatings that have been proven in gray cast iron cylinders, such as tin and GRAFAL®, are not tribologically suited as partners for aluminum running surfaces, because they would lead to rapid seizing and high wear. The Ferrostan coating system and FerroTec® have proved to be excellent for uncoated AlSi cylinders. Both are characterized by a high level of running reliability and low wear. Ferrostan consists of a 10 to 13 µm thick iron coating that is topped with a thin coating of tin as a run-in aid. FerroTec® consists of a pure iron coating that can optionally be tin-plated as well. Ferrostan/FerroTec® pistons are used exclusively in passenger car gasoline engines, because diesel engines typically do not feature AlSi running surfaces.

4.5.1.4 FERROPRINT®

An alternative to the Ferrostan/FerroTec® coating is the FERROPRINT® coating. It also serves to protect the running surfaces for pistons that are paired with high-silicon aluminum cylinders. Similar to GRAFAL®, this layer consists of a highly temperature-resistant polymer in which harder stainless steel particles are embedded as a reinforcement. The layer thickness is about 20 µm. The properties are similar to GRAFAL®.

4.5.1.5 Hard oxide in the first piston ring groove

While the first piston ring groove in a diesel engine piston, or the compression ring groove, is traditionally well-protected against wear by a ring carrier, gasoline engine pistons have not previously required this protection. Recently, however, damage has occurred in the form of disruption and material wear at the groove side faces, particularly at the lower groove side face (microwelding). It presumably occurs due to local microwelds between the piston ring and the groove side face, and particularly on pistons with short top lands, which thus exhibit higher groove temperatures. These higher temperatures presumably arise in conjunction with ring packs that are tuned for extremely low oil consumption. Due to the minimal oil quantity that is available for lubricating the piston rings, microwelds can occur.

One effective means of protection against microwelding is localized hard anodizing of the groove with a coating thickness of about 15 µm. The quasi-ceramic structure of the hard oxide layer eliminates metallic contact between the piston ring groove and the piston ring, and thus prevents microwelding. Although the hard oxide layer is significantly rougher than the finely machined groove side face, there is no problem sealing the piston rings, because the coating surface is quickly smoothed out by the micromotion of the piston rings.

4.5.1.6 Hard oxide on the crown

After longer periods of operation, thermal and mechanical overloads can lead to cracks in the bowl rim and piston crown of passenger car and commercial vehicle diesel engines. In order to prevent such bowl rim cracks, hard oxides are used once more. In this case, however, with a layer thickness of 50 to 80 µm.

The advantageous effect of this coating on the cracking behavior of the piston material can be attributed to bond stresses that reduce the compressive stresses due to thermal and mechanical loading of the piston crown. Because the layer is not applied externally, but results from converting the base material at the surface, high bonding forces arise between the layer and the base material, which resist the severe local loads.

4.5.1.7 Phosphate

Metal phosphates form crystalline or amorphous coatings that stand out for their good oil bonding, high adhesive strength, and good deformability. Phosphate coatings can provide

effective protection against seizing and scuffing between sliding pairs, especially in run-in phases. This effect can also be exploited for pistons, particularly for diesel engine pistons to protect the pin boss.

Relatively thick layers (averaging 5 µm) of manganese-iron mixed phosphates are deposited on steel pistons (MONOTHERM®, FERROTHERM®). They enable direct pairing with hardened steel pins, without the use of pin bore bushings.

Thin (<0.5 µm) aluminum phosphate layers are deposited on aluminum pistons as conversion layers. They also provide limited antiscuffing protection in the pin boss.

4.5.1.8 GRAFAL® 210

Run-in of steel pistons in heavy-duty engines of commercial vehicles is a critical phase with regard to the pin bore/pin tribological system. This requires greater protection, such as is provided by GRAFAL® 210. The layer consists of a highly temperature-resistant polymer matrix, in which graphite particles and molybdenum sulfide pigments–added as a pressure-resistant component–are embedded. The layer thickness is about 8 µm and provides longer antiscuffing/-seizing protection in the pin bore during the run-in phase.

4.5.1.9 Chromium contact surfaces

For composite pistons in large diesel engines, relative motion occurs at the surfaces where the upper part contacts the lower part due to cyclical deformation of the components. Although these relative motions normally amount to less than 100 µm, they can lead to undesired frictional wear at the contact surfaces. For the pairing of an aluminum lower part and steel upper part, the harder steel upper part wears more severely. Dimensional chrome plating of the contact surfaces of the steel upper part with a layer thickness of about 20 µm provides an effective solution.

4.5.1.10 Chromium ring grooves

Heavy fuel oil, used as a fuel for large diesel engines, can contain large quantities of small, hard particles, which can cause severe abrasive wear to the piston rings and piston ring grooves if they enter the combustion chamber. Heavy fuel oil also incidentally contains relatively high concentrations of sulfur compounds, which produce acidic gases during combustion. These condense in the region of the piston ring groove and then cause corrosion damage to the piston rings and piston ring grooves.

Hard chrome plating of the side faces of the compression ring groove, paired with a piston ring with chrome-plated sides, provides highly effective protection against these effects. In order to ensure the very long service life required for these engines, the layer must be appropriately thick, with the standard being at least 200 µm.

4.5.2 Application table

Table 4.7 shows all applications of the various coatings.

Table 4.7: Application table for coatings

	Pistons for passenger cars Gasoline	Pistons for passenger cars Diesel	Pistons for commercial vehicles Steel	Pistons for commercial vehicles Aluminum	Large-bore pistons
GRAFAL®/EvoGlide	X	X	X	X	X
Tin	X			X[1)]	
Ferrostan/FerroTec®	X				
FERROPRINT®	X				
Hard oxide compression ring groove	X				
Hard oxide crown		X		X	
Al phosphate	X	X		X	X[2)]
Fe phosphate			X	X	X[3)]
GRAFAL® 210			X		
Hard chrome					X

[1)] only for old types, [2)] aluminum piston skirts, [3)] gray cast iron piston skirts

5 Piston cooling

As specific power output increases in modern combustion engines, the pistons are subjected to increasing thermal loads. Efficient piston cooling is therefore required more frequently in order to ensure operational safety.

5.1 Thermal loads

The chemical energy stored in the fuel is converted into heat in the cylinder during combustion. The piston, as a moving wall of the combustion chamber, converts part of this heat into mechanical work and drives the crankshaft through the connecting rod. The heat that is not converted into mechanical work is partially dissipated into the exhaust gas. The remainder is transferred, through convection and radiation, to the parts of the engine that are adjacent to the combustion chamber. In addition to mechanical stresses, the elevated temperatures lead to thermal loading of these components.

5.2 Combustion and flame jets

In gasoline engines, the spark plug normally initiates combustion of the fuel-air mixture. The flame front expands evenly in all directions, so that all the surfaces enclosing the combustion chamber are subjected to the gas temperature. This creates a temperature gradient in the piston from the combustion chamber side to the crankcase.

For diesel engines with direct fuel injection, combustion starts in the area of the injection nozzle, because the combustible mixture is first present at that point. After the mixture in this area has self-ignited, several flame fronts in the form of combustion lobes run along the injected streams of fuel toward the surfaces enclosing the combustion chamber, **Figure 5.1**. This generates a nonhomogenous temperature field in the piston, particularly at the rim of the combustion chamber bowl.

MAHLE GmbH (Ed.), *Pistons and engine testing,* DOI 10.1007/978-3-8348-8662-0_5,

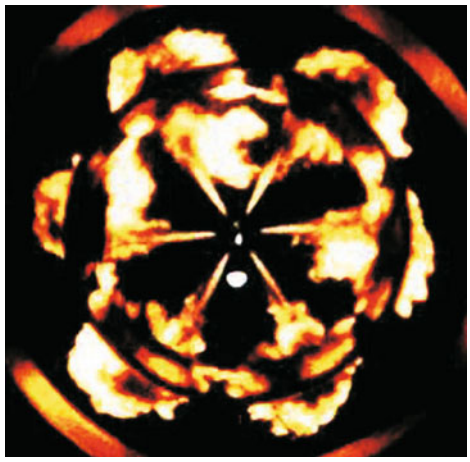

Figure 5.1:
Flame fronts in the diesel process

5.3 Temperature profile at bowl rim

As a result of the nonuniform introduction of heat through the “combustion lobes” described above, a quasi-stationary, wave-shaped temperature profile is established at the bowl rim of the diesel piston. The course of temperature along the bowl rim depicted in **Figure 5.2** shows average stationary temperatures, not considering the additional thermal wave that occurs on the combustion chamber side of the surface of the piston with each combustion cycle. The temperature difference between the locations that are directly in the center of a combustion lobe and the areas in between can be in excess of 40°C.

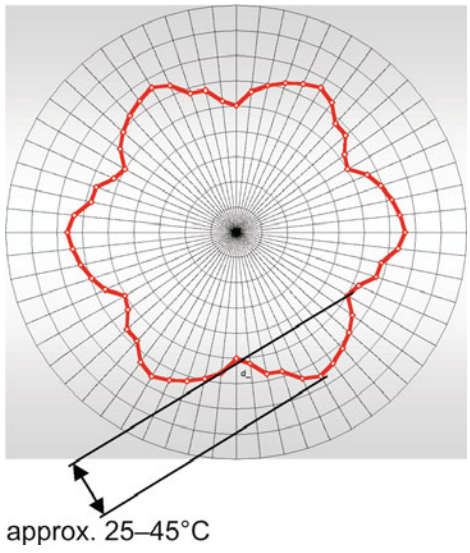

Figure 5.2:
Variance of temperature distribution at the bowl rim

The resulting thermal stresses, combined with additional loads (e.g., mechanical stresses, oxidation, etc.), can cause cracks at the bowl rim.

The temperature profile also shifts toward the exhaust side, due to the influence of the intake and exhaust sides. For passenger car and commercial vehicle engines, additional influences must be considered, such as the cooling water flow between the individual cylinders.

5.4 Piston temperature profile

Due to the various combustion processes and the resulting different piston geometries, diesel and gasoline pistons exhibit different temperature profiles, **Figure 5.3**.

Pistons for gasoline engines typically experience their maximum temperature in the center of the piston crown, but also at the edge of the bowl in the case of direct fuel injection and pronounced combustion bowls. The temperature drops quite evenly toward the top land. For diesel engine pistons, however, the maximum temperature occurs at the locations on the bowl rim that are in the center of the combustion lobes; **Figure 5.2**. The temperature drops evenly toward the center of the bowl and toward the top land. The temperature profile is largely determined by the number and orientation of the injection holes, the injection pressure, the injection time and duration, and the combustion bowl geometry.

Along the piston axis, qualitatively similar temperature profiles arise for diesel and gasoline pistons from the top land past the piston ring set to the pin bore and the end of the piston skirt.

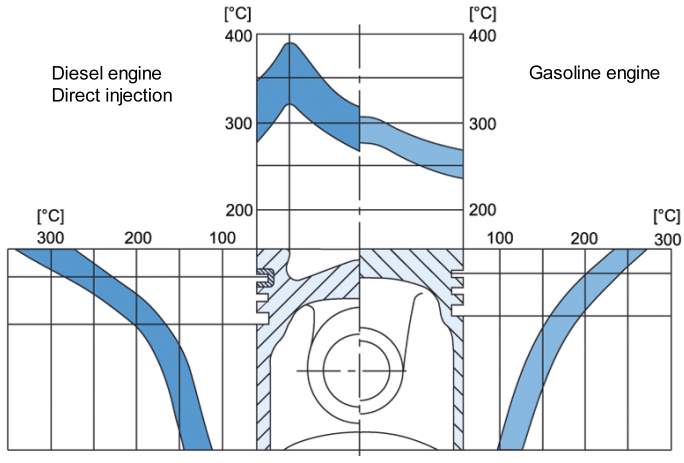

Figure 5.3: Temperature profiles of diesel and gasoline aluminum pistons

5.5 Effects on piston function

The thermal loads on the piston and the resulting temperature profile in the piston, combined with the maximum occurring temperatures, have multiple effects on the piston. In particular, these include deformations, cyclical thermal loads, and the effect on material strength. They affect the piston function and, in extreme cases, lead to component failure and engine damage.

5.5.1 Thermally induced deformation

Thermally induced deformation is a functionally relevant effect on the piston. **Figure 5.4** schematically shows how the piston expands and deforms under the effects of nonhomogenous temperature distribution in a gasoline engine. Pistons in diesel engines show deformation behavior that is similar in principle.

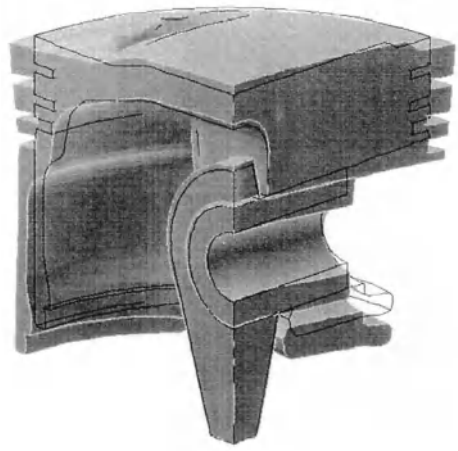

Figure 5.4:
Deformation of a piston under thermal load in a gasoline engine

The extent of the deformation depends on the thermal expansion coefficients and the temperature difference between the cold and warm operating conditions. Radial deformation affects noise, susceptibility to seizure, and frictional loss, and must be compensated for with appropriate clearances, especially in the ring area. The axial deformation must be taken into consideration when designing the clearance at top dead center with respect to the valve lift.

5.5.2 Temperature-dependent material behavior

As shown in **Figure 5.5**, the thermal load and the resulting local component temperatures significantly reduce the fatigue resistance of the piston.

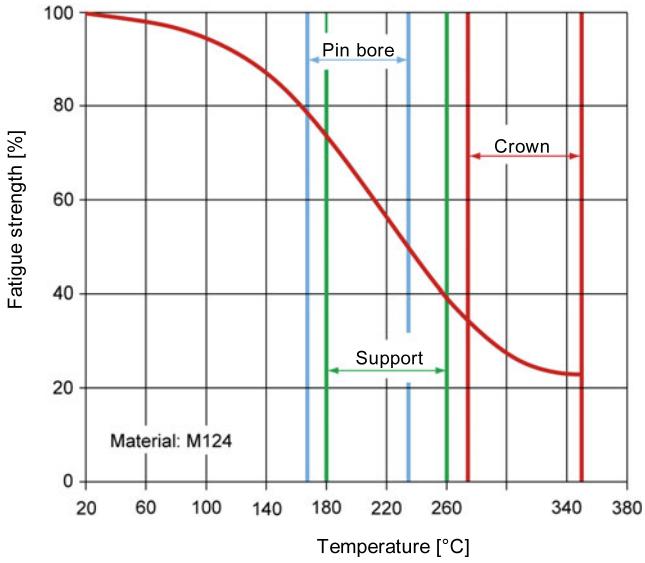

Figure 5.5:
Influence of temperature on the fatigue strength of M124

For the piston alloy M124, for example, this means that the pin bore and support areas, which typically reach a temperature level of 160 to 260°C, exhibit 20 to 60% lower fatigue strength compared to room temperature properties. For the piston crown and bowl rim of diesel pistons, which can reach temperatures of 300 to 400°C, the fatigue resistance drops by as much as 80%. Ferrous materials are significantly less sensitive at temperatures of up to 400°C.

5.5.3 Effects of temperature on the piston rings

If the maximum tolerable temperature of the ring area is exceeded, then plastic deformation and increased wear can occur, particularly in the first piston ring groove. The thermally induced chemical disintegration of the lubricant can additionally cause carbon build-up in the groove root. These residues then act as thermal insulators in the ring groove/piston ring system and reduce the heat transfer from the piston to the cylinder wall. They also obstruct the piston ring movement and can even block them completely. However, the rotation of the piston rings in the piston ring grooves is essential for their proper function. This rotation ensures that the ring gap, through which small amounts of hot combustion gas continuously flow into the crankcase, changes its location. Otherwise, the hot combustion gases that flow through the ring gap can damage both the piston ring groove and the cylinder surface. The lubricating oil film in this area is likewise disturbed, which can result in ring/piston scoring and thus major engine damage.

5.6 Ways to influence piston temperatures

In addition to knowledge of the heat flows at the piston, the maximum temperatures that occur, as well as the resulting effects on the function of the piston, the impact of the engine operating conditions on the piston temperature must be taken into consideration. It includes, for example, the speed, load, ignition timing, or start of injection, and the air, water, and oil temperatures. Examples of temperature changes due to parameter changes for the top ring groove of a gasoline and a diesel piston are given in **Table 7.2.2** (Chapter 7.2).

A comparison of the cooling principles spray jet cooling with a spray jet at the connecting rod end, spray jet cooling with a fixed nozzle on the crankcase, and piston cooling with oil-filled cooling channels indicates that a cooling channel provides the most efficient reduction in temperature. Depending on the design, up to 50°C lower temperatures may be achieved at the first piston ring groove.

5.7 Types of piston cooling

In order to ensure sufficient heat dissipation from the piston and to reduce the temperature in the critical piston zones, various types of cooling are used, depending on the quantity of heat to be dissipated and the combustion process–diesel or gasoline. The cooling medium for all cooling types considered here is engine oil.

5.7.1 Pistons without piston cooling

Pistons without piston cooling are primarily used in gasoline engines because of their lower thermal loading. They are additionally employed in diesel engines with low power output. The temperature profile of these pistons may be more than 20°C higher, depending on the point of measurement, than the same piston with spray jet cooling.

5.7.2 Pistons with spray jet cooling

The simplest way to cool a piston is by means of spray jet cooling, **Figure 5.6**. The interior of the piston is continuously sprayed over as large an area as possible with oil from a cooling oil nozzle. This technology is most common in gasoline engines because the low compression height often leaves no room for cooling channels. For gasoline engines with direct injection, the use of a cooling channel would be easier, due to the bowl-like shape of the piston crown. Spray jet cooling is also used for diesel engines in the lower power output segment.

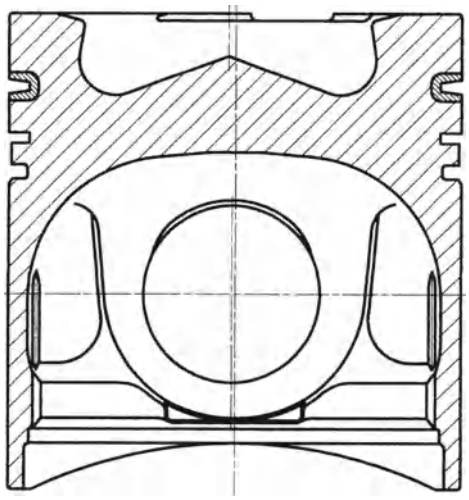

Figure 5.6:
Diesel engine piston with spray jet cooling

5.7.3 Pistons with cooling channels

If the piston temperature is not lowered sufficiently by means of spray jet cooling, then pistons with cooling channels must be used. Cooling oil is continuously run through the cooling channel during operation. One, or occasionally more, oil spray nozzles feed the cooling oil through inlet openings into the cooling channel. The cooling oil exits the cooling channel through one or more drain holes.

Under engine operating conditions, complete filling of the cooling channel is not possible, and the cooling oil moves up and down in the cooling channel with the oscillating motion of the piston. This leads to highly turbulent flow in the cooling channel, with a high heat transfer coefficient.

Depending on the manufacturing process, cooling channels are available as salt core cooling channels, cooled ring carriers, and machined cooling channels.

5.7.3.1 Salt core cooling channel pistons

For pistons with salt core cooling channels, the hollow space in the piston is produced using a salt core, which is placed in the casting die prior to casting. After removing the piston blank, the salt core is dissolved and completely removed, using water under high pressure.

If the inlet and outlet openings are designed as sleeve holes, then they are bored out after rinsing, **Figure 5.7**. Inlet openings with sleeve bores are primarily used with vertically oriented cooling oil nozzles. This design provides the best possible oil supply, and thus the best cooling effect in the cooling channel.

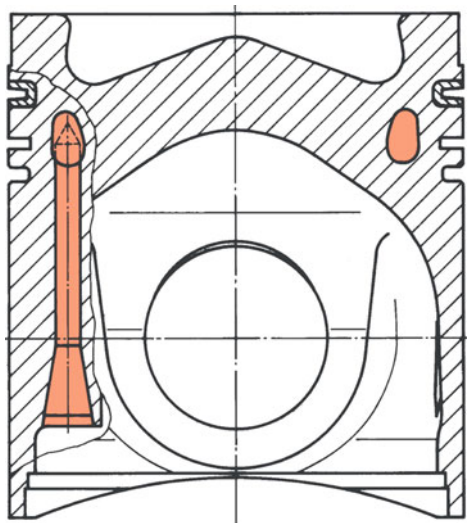

Figure 5.7: Salt core cooling channel piston with sleeve bores

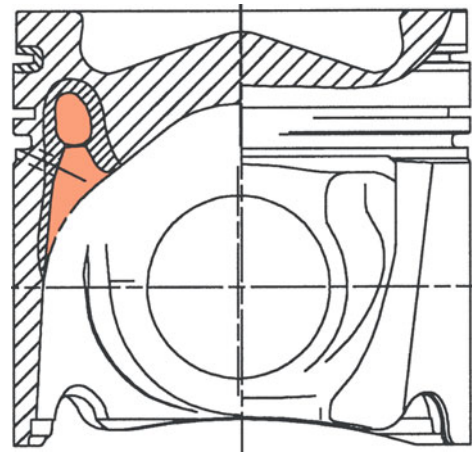

Figure 5.8: Salt core cooling channel piston with funnel inlet

For cooling oil nozzles placed at an angle, a kidney-shaped inlet opening is most often used together with a funnel, **Figure 5.8**, in order to compensate for the changing oil jet in the stream impact point caused by the angled orientation of the nozzle, and thus to provide an uninterrupted flow of oil to the cooling channel. For such a piston design, typically no or very little machining is needed at the inlet and outlet openings.

The salt core cooling channel should be placed as close to the bowl as possible. The mechanical load capacity and castability of the piston, however, place limits in this respect.

The salt core cooling channel reduces the temperature at the bowl rim by up to 20°C, compared to spray jet cooling, **Figure 5.9**. This additional cooling effect amounts to about 10°C at the top land and in the first ring groove.

5.7.3.2 Pistons with cooled ring carrier

For pistons with cooled ring carriers, a sheet metal channel is welded onto the Niresist ring carrier, which creates a closed cooling channel; **Figure 5.10**. Prior to casting the piston, this component is placed into the Alfin bath, inserted into the casting die, and cast into the piston blank. The feed and drain holes are created by drilling through the sheet metal.

For the inlet and outlet areas, the same design criteria apply as for a piston with salt core cooling channels, depending on the spray direction of the cooling oil nozzle.

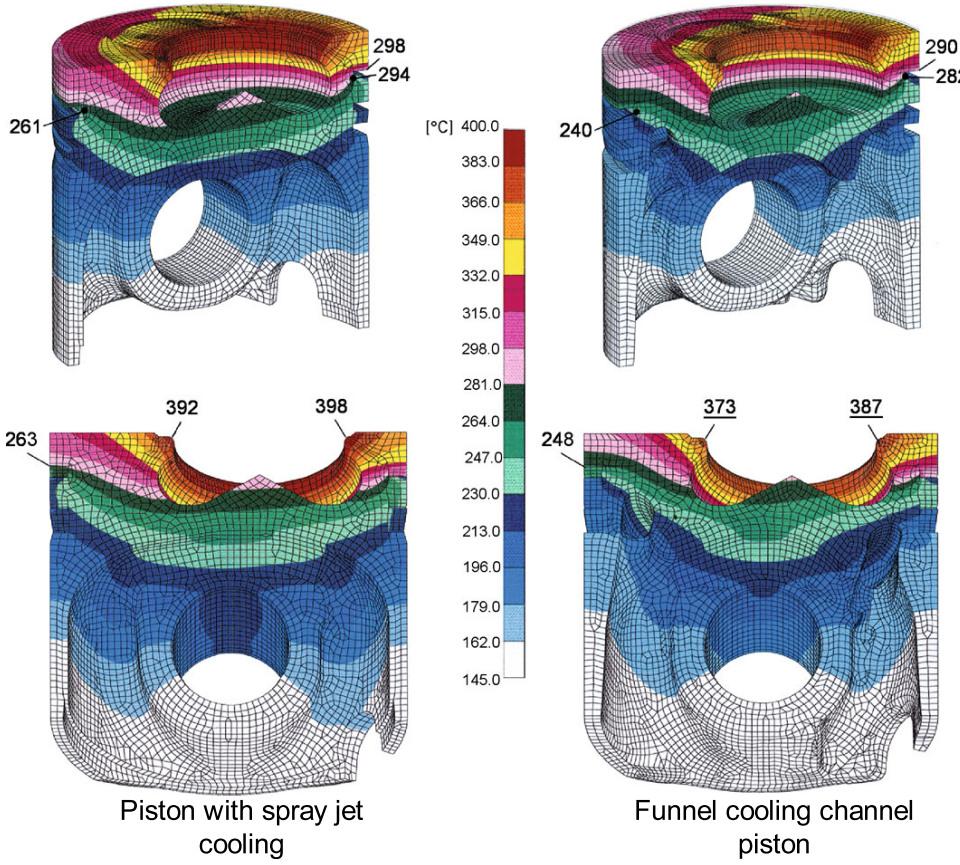

Figure 5.9: Temperature profiles for different types of cooling

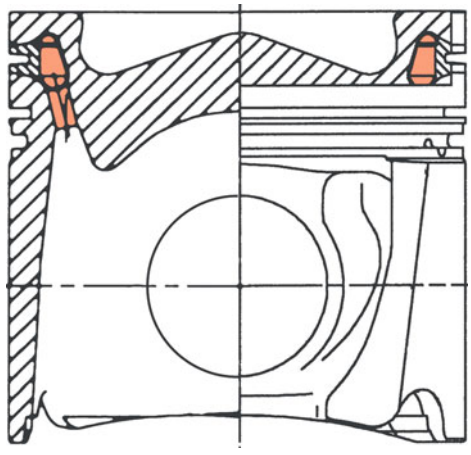

Figure 5.10:
Piston with cooled ring carrier

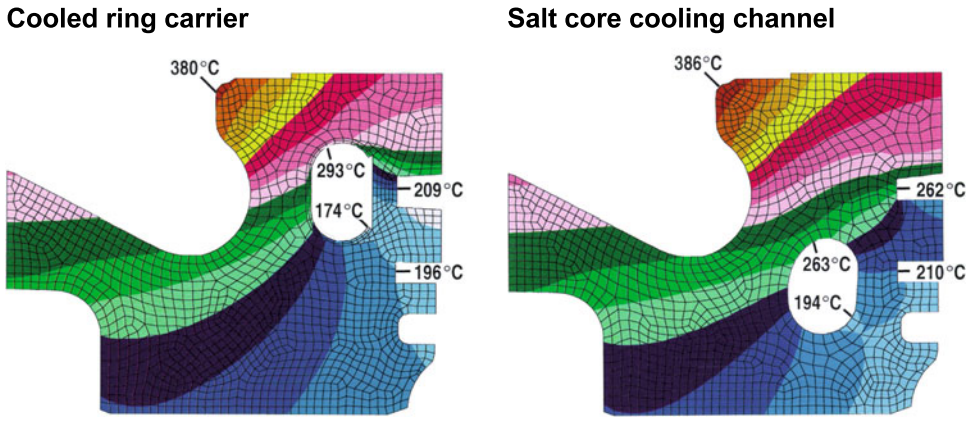

Figure 5.11: Temperature field of a piston with cooled ring carrier and with salt core cooling channel

Cooled ring carriers diminish the temperature at the bowl rim even further, compared to a salt core cooling channel, **Figure 5.11**. A cooled ring carrier helps to reduce the temperature of the first piston ring groove by up to 50°C.

Clearly, the surface temperature in the cooling gallery rises the closer the location of the cooling channel is to the combustion chamber surface. Care must be taken that a maximum temperature of about 250°C is not exceeded. Above this temperature, increased oil aging and disintegration of the cooling oil along with oil carbon deposits are to be expected.

Consideration must be given to the fact that the cooled ring carrier is located in a more highly loaded area of the piston, which presents its challenges to casting technology. With the application of suitable processes, it must be ensured that the cooled ring carrier is functionally secure when cast into the piston.

5.7.3.3 Machined cooling channels

For forged FERROTHERM® and MONOTHERM® steel pistons, the cooling channels cannot be generated with salt cores or in the form of cooled ring carriers. Therefore, the upper part of the cooling channel is machined. For FERROTHERM® pistons, the lower part of the cooling channel is formed by shaker pockets in the articulated skirt, or by a cover plate that closes off the cooling channel toward the bottom. For the single-piece design of the MONOTHERM® piston, only the cover plate is employed, **Figure 5.12**.

The inlet opening for the open FERROTHERM® piston consists of a recess above the cooling oil nozzle in the articulated skirt. The circumferential gap between the shaker pockets and the piston crown serves as an outlet opening. If a cover plate forms the lower part of the cooling channel, then it is fitted with the required inlet and outlet openings.

Figure 5.12:
MONOTHERM® piston with cover plate at the cooling channel

5.7.4 Composite pistons with cooling cavities

In the case of composite pistons, cooling cavities are employed. The multipiece design allows the full machining of these cooling cavities. In addition to the outer cooling gallery behind the ring grooves, composite pistons also feature an inner cooling cavity. The shape and size of the outer cooling gallery is primarily determined by the combustion bowl geometry and the location of the piston rings. The geometry of the inner cooling cavity is significantly influenced by the combustion bowl geometry and the type of bolt connection arrangement of the piston.

For pistons with central bolt connection, the internal cooling cavity is smaller, due to the nut thread that is located there, **Figure 5.13**, and the oil in the cooling cavity flows around the screw.

For pistons with multiple bolt connections, the bolts are placed within the contact surface between the cooling cavities. The inner cooling cavity can therefore be significantly larger, **Figure 5.14**. The outer and inner cooling cavity are connected to each other by multiple scavenging ports or bores.

The cooling oil is typically fed into the outer cooling cavity. Outlet openings are located both in the outer and in the inner cooling cavity. In exceptional cases, the inlet opening is centered in the inner cooling cavity. Outlet openings are then located only in the outer cooling cavity. With the typical flow direction from the outer to the inner cooling cavity, the cooling oil flow in composite pistons is divided by approximately the ratio of the outer outlet to the inner outlet cross section. One part of the oil flow exits the piston after flowing through the outer cooling cavity, while the second partial oil flow enters the inner cooling cavity through the scavenging

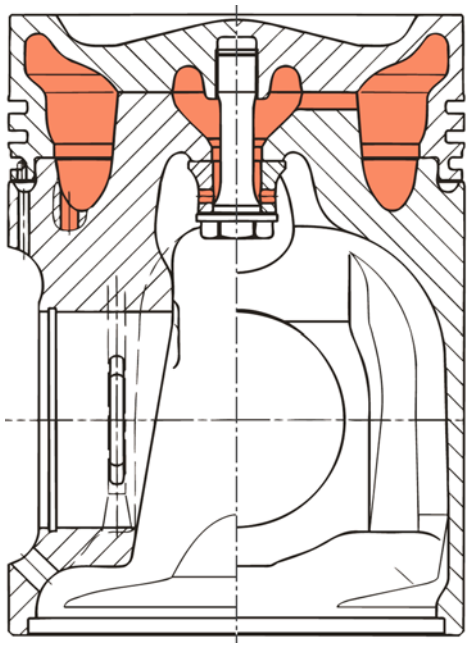

Figure 5.13: Composite piston with central screw connection and shaker cooling

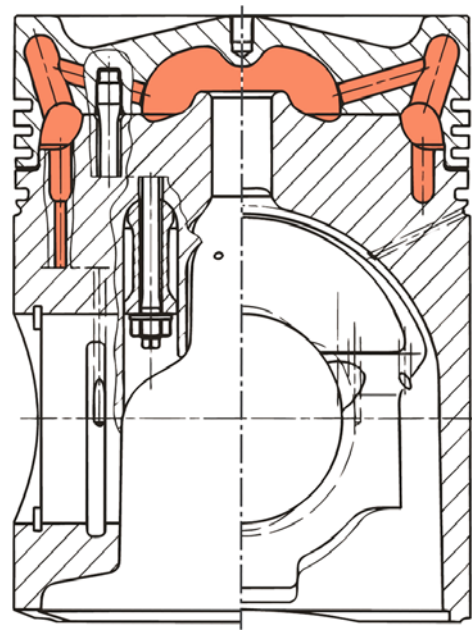

Figure 5.14: Composite piston with multiple screw connection and bore cooling

bores and flows from there back into the crankcase. Depending on the shape of the outer cooling gallery, composite pistons are divided into shaker cooling and bore cooling types.

5.7.4.1 Shaker cooling

In the case of shaker cooling, the outer cooling cavity has a constant, rotation-symmetrical cross section, **Figure 5.13**. The inner cooling cavity is typically connected to the outer one through several milled scavenging ports, which are located at about halfway up the height of the outer cooling cavity.

5.7.4.2 Bore cooling

In the case of bore cooling, the lower part of the outer cooling cavity is likewise rotation-symmetrical. Cooling oil bores run from this side in the direction of the piston crown rim. Some of the cooling oil bores are connected to the inner cooling cavity by means of scavenging bores, **Figure 5.14**.

The advantage of bore cooling, compared to shaker cooling, is the more rigid design of the piston crown. The material between the cooling oil bores can lead to local temperature

maxima on the combustion chamber side. The effort required to machine the cooling cavity and the oil bores is significantly greater than for a shaker cooling design.

5.8 Cooling oil supply

The cooling medium for piston cooling is the engine oil. The cooling oil delivered by the engine oil pump is first filtered, partially cooled, and then distributed via channels in the crankcase. There are essentially two methods for feeding cooling oil to the piston. It can be fed to the cooling channel as a jet, with nozzles mounted in the crankcase; this solution is typical for passenger car and commercial vehicle engines. In the large-bore piston world, the alternative of transporting the oil from the crankshaft through the connecting rod to the piston is applied.

5.8.1 Jet feeding of cooling oil

The cooling oil reaches a nozzle that is fixed to the crankcase through oil channels, and from there it exits as a jet toward the cooling channel inlet bore, **Figure 5.15**.

A pressure regulating valve is typically located between the oil channel in the crankcase and the nozzle, allowing flow of cooling oil to the nozzle only above a predetermined operating pressure. This ensures that all bearing locations are provided with enough lubricating oil

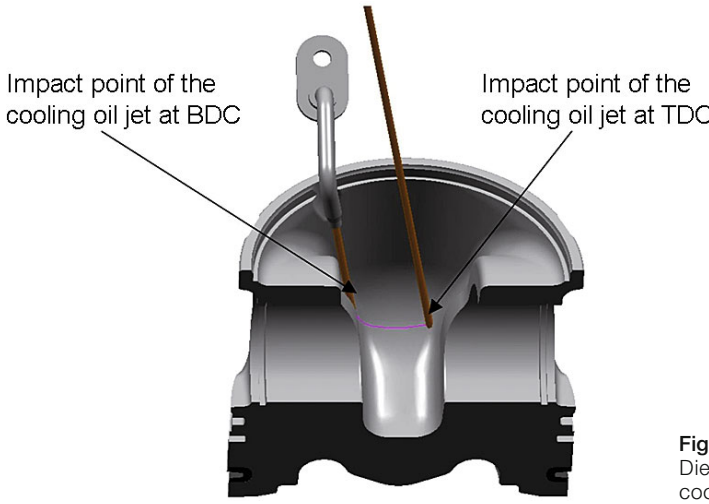

Figure 5.15:
Diesel piston with spray jet cooling of the undercrown

when starting the engine as well as at low speeds. Cooling of the piston is not necessary under these low thermal load operating conditions.

The oil jet expands as it exits the nozzle. The spread angle α depends significantly on the geometry and shape of the cooling oil nozzle.

5.8.1.1 Nozzle designs for spray jet cooling

Cooling oil nozzles for spray jet cooling should generate a wide spread angle of the oil jet in order to extensively supply cooling oil to the inner contour, **Figure 5.16**.

A large spread angle α can be achieved by operating the cooling oil nozzle hypercritically (Reynolds number >2,300), the ratio of the nozzle diameter *d* to the length of the flow-calming section *l* is as large as possible, and the end of the nozzle has no sharp edges (e.g., chamfer). This jet characteristic can also arise unintentionally with an orifice that has been deburred excessively.

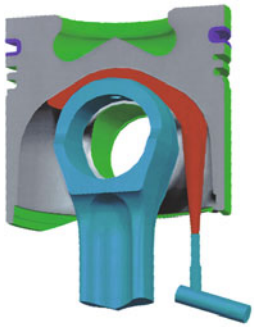

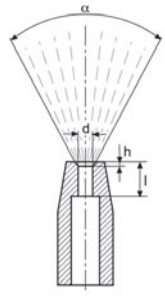

Spray jet cooling

Figure 5.16:
Jet shape for spray jet cooling

5.8.1.2 Nozzle design for supplying cooling channels and cooling cavities

Cooling oil nozzles for cooling channels and cooling cavities should have as small a spread angle as possible, so that the jet reliably hits the inlet opening of the cooling channel and cooling cavity throughout the entire piston stroke, **Figure 5.17**. This bundled jet can be

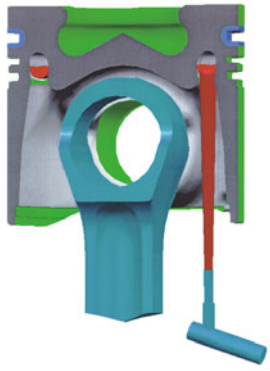

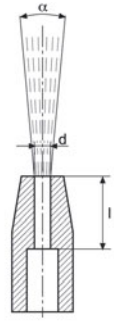

Cooling gallery piston

Figure 5.17:
Jet shape for cooling gallery supply

achieved by operating the cooling oil nozzle subcritically (Reynolds number <2,300), the ratio of the nozzle diameter *d* to the length of the flow-calming section *l* is as small as possible ($l = 4 \ldots 6 \times d$), and the nozzle end is sharp-edged, but free of burrs.

5.8.2 Feeding oil via crankshaft and connecting rod

For this method of feeding the cooling oil, the oil first flows through the main bearing at one end into the bored crankshaft. From here, the oil flows through bores into the crank web, to the conrod bearing journals, onward through side-drilled holes in the crankshaft pin, a groove in the lower rod bearing, and a longitudinal bore in the connecting rod, to the upper connecting rod bore. In this manner, the flowing cooling oil lubricates all the bearing locations of the crankshaft and the rod bearings. There are three different options available for further transport to the cooling channels or cooling cavities.

5.8.2.1 Feeding oil via piston pin and pin bore

The cooling oil flows through a circumferential groove in the upper connecting rod bore and several side-drilled holes distributed about the circumference into the piston pin, which is bored out axially and closed at the ends. From there, it reaches a groove in the pin bore of the piston through additional side-drilled holes in both ends of the piston pin. These grooves are connected to the cooling channel or outer cooling cavity through bore holes.

5.8.2.2 Feeding oil via slide shoe

Cooling oil is fed through a circumferential groove in the bearing of the upper connecting rod bore to a bore hole, through which it enters a slide shoe mounted on the piston side that leads it into the inner cooling cavity of the piston. The cooling oil thus flows through the piston from the inner to the outer cooling cavity. One advantage of this design is that the piston pin is not weakened by through holes.

5.8.2.3 Feeding oil via jet from connecting rod

The third way is a combination of crankshaft, connecting rod, and jet feeding. The cooling oil is once again routed around the piston pin through a circumferential groove. It then leaves the connecting rod bore as a jet through a bore hole that acts as a nozzle. This jet dissipates heat from the inner contour of the piston, similar to spray jet cooling, and simultaneously supplies cooling oil to the inner cooling cavity of the composite piston.

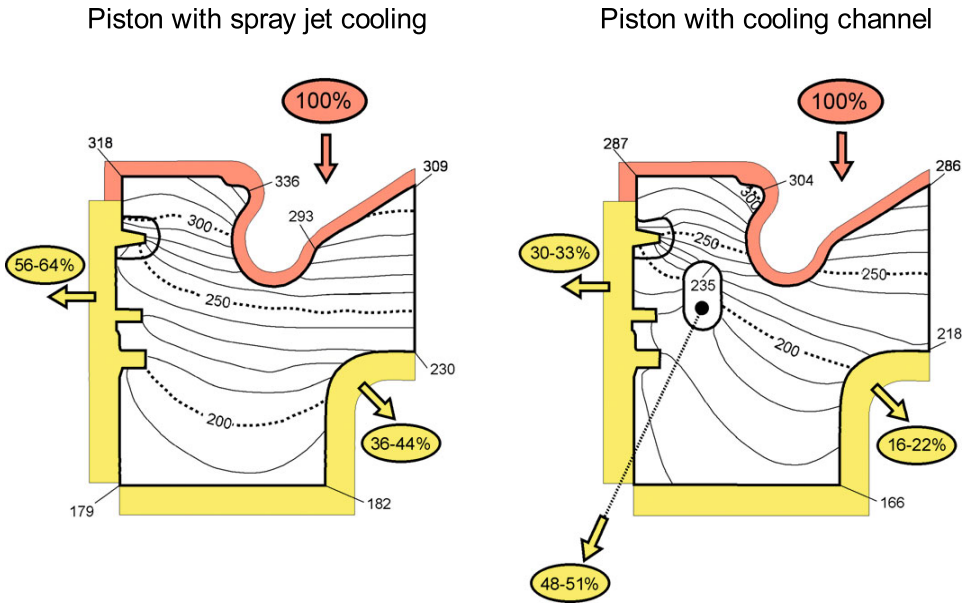

Figure 5.18: Heat flow in the piston depending on the cooling design

5.9 Heat flow in pistons

The heat flow in the piston depends on the type of piston cooling, **Figure 5.18**. The heat flows must comply with the principle of conservation of energy, which states that the total heat flowing into the piston must be equal to the total heat flowing out of the piston.

In a piston with spray jet cooling, about 55 to 65% of the heat flow is transferred through the piston ring set and the associated ring land surfaces on the cylinder wall. The remaining 35 to 45% is dissipated through the inner contour and the cooling oil, as well as through the lower part of the piston skirt, including the pin bore. If cooling channels are used in place of spray jet cooling, **Figure 5.18 right**, the heat flow dissipated through the piston ring set is reduced to 30 to 40%, depending on the position of the cooling channel. The heat flow dissipated through the inner contour and the lower part of the piston skirt is reduced to 15 to 25%. The remaining heat flow of 35 to 55% is dissipated by the cooling oil. Salt core cooling channels are usually positioned in the piston at the level of the oil ring groove, but are often also found below the bottom of the bowl. They reduce the heat flow from the bowl to the piston ring set and to the inner contour to a lesser degree, as compared to a cooled ring carrier. The cooled ring carrier is located in the direct path of the heat flow to the cylinder wall and thus can absorb a significantly greater portion of the heat flow.

Since the absolute quantity of cooling oil depends on the size and power output of the engine, the basis for comparison is the specific quantity of cooling oil. It is the quotient of the

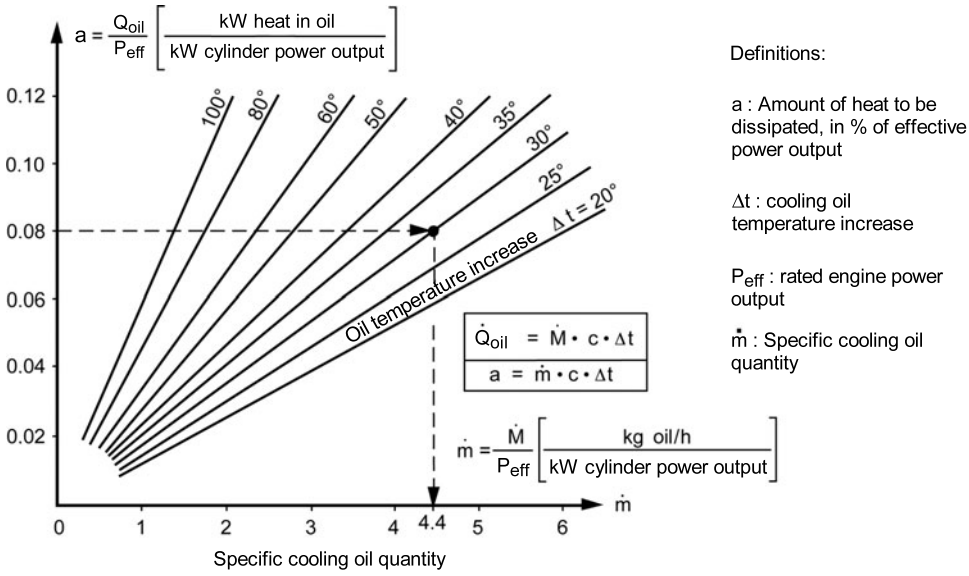

Figure 5.19: Dissipated heat quantity and specific cooling oil quantity

absolute quantity of cooling oil and the engine output, typically specified in kg/kWh. Reference values for the specific cooling oil quantity required at the cooling nozzle are:

- For spray jet cooling: 3–5 kg/kWh
- For jet feeding: 5–7 kg/kWh
- For feeding via crankshaft and connecting rod (large engines): 3–5 kg/kWh

Figure 5.19 shows the relationship between the specific cooling oil quantity, the quantity of heat dissipated by the cooling oil, and the difference between the oil inflow and return flow temperatures. For a quantity of heat to be dissipated of, for example, 8% of the effective power output and a permissible temperature increase of the cooling oil of 30°C, a specific cooling oil quantity of 4.4 kg/kWh is required.

5.10 Determining thermal load

Various methods for determining the piston temperatures and the effects of piston cooling are being used. They exhibit different levels of effort and precision.

The methods are described in detail in Chapter 7.2.

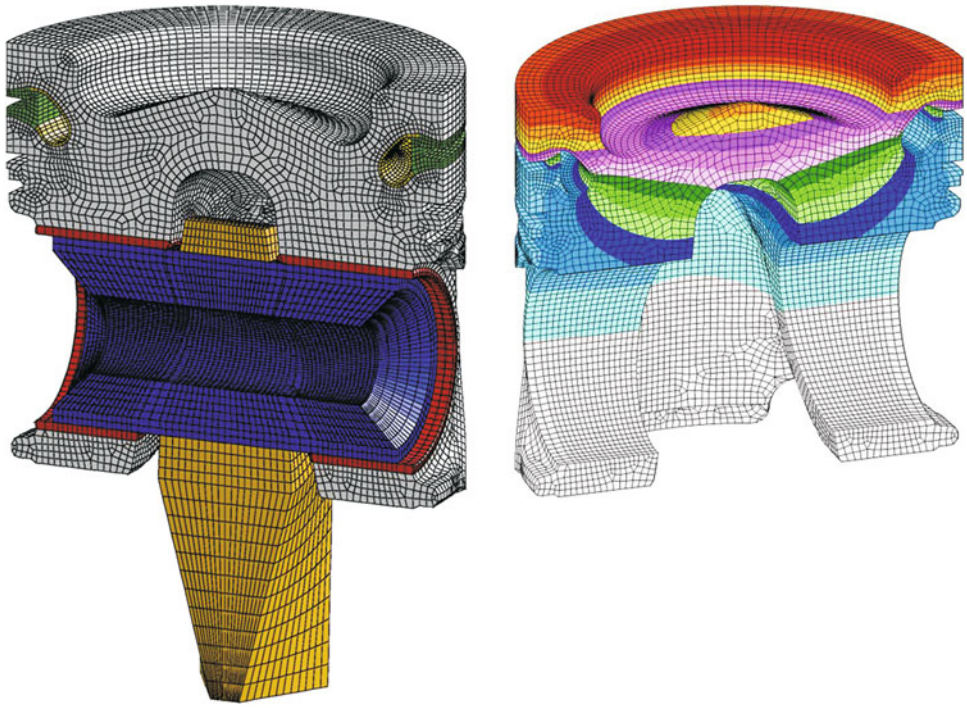

Figure 5.20: FE model and calculated temperature field

5.11 Numerical analysis using the FE method

Measurements taken inside the engine are time-consuming and require actual engines and temperature sensor-equipped pistons. The initial design of new pistons and the comparison of variants is therefore commonly performed using the finite element method (FE); **Figure 5.20**.

The boundary conditions are varied, based on measured temperatures, until the calculated and measured temperatures conform to a sufficient degree. The heat flows can then be determined. If no temperature measurements are available, then the boundary conditions from similar designs can be carried over in order to obtain a first estimate of the expected thermal load.

By varying the piston geometry (e.g., bowl geometry, shape and position of the cooling gallery, position of the ring grooves), its influence on the piston temperature field is determined. Such procedures allow a faster and simpler optimization compared to several engine temperature measurements.

The boundary conditions on which the analysis is based are derived from theoretical considerations, experimental test results, and experience. Regular alignment of the results of the analysis and the temperature measurements is mandatory.

5.12 Laboratory shaker tests

The motion of the cooling oil along the inner contour of the piston and within the cooling channels and cooling cavities has a decisive influence on the achievable heat dissipation. This oil motion cannot be measured during engine operation. Shaker tests provide a substitute. The kinematic and mechanical flow conditions within the engine are simulated on appropriate test rigs. Transparent polymer piston models provide insight into the oil motion when using high-speed video documentation.

5.13 Characteristic quantities

In order to evaluate the feeding and throughput of oil through the cooling channel or cooling cavity when feeding cooling oil through a spray nozzle, the dynamic catching efficiency η_F, **Figure 5.21**, is used. It is defined as:

$$\eta_F = \frac{\dot{V}_{out}}{\dot{V}_{in}}$$

where:

$\dot{V}_{out}$ Volume flow at the drain hole of the cooling channel (on the moving piston model)

$\dot{V}_{in}$ Volume flow through the cooling oil nozzle

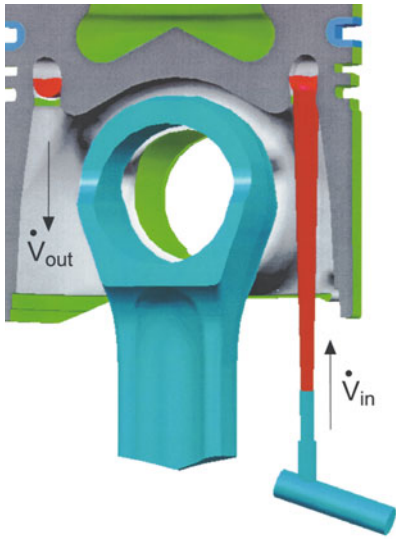

Figure 5.21:
Definition of dynamic catching efficiency

In order to achieve best possible heat dissipation, the cooling oil discharged by the nozzle must enter the cooling channel or cooling cavity as completely as possible, i.e., the highest possible dynamic catching efficiency is required. The dynamic catching efficiency must not be confused with the static catching efficiency used by manufacturers of cooling oil nozzles, which is based on the jet flow rate through a defined orifice.

The filling ratio ψ_F is a dimension for the expected cooling effects due to the shaker effect in a partially filled cooling channel, **Figure 5.22**, and is defined as:

$$\psi_F = \frac{V_{oil}}{V_{cc}} \quad \text{and} \quad \psi_{FA} = \frac{A_{oil}}{A_{cc}} \quad \text{and} \quad \psi_{Fh} = \frac{h_{oil}}{h_{cc}}$$

where:

V_{oil} Volume of the cooling channel filled with oil

V_{cc} Volume of the cooling channel

A_{oil} Cross-sectional area of the cooling channel filled with oil

A_{cc} Cross-sectional area of the cooling channel

h_{oil} Height of the cooling channel filled with oil

h_{cc} Height of the cooling channel

Since the cross-sectional area is proportional to the volume for axisymmetric cooling galleries, the cross-section based filling ratio ψ_{FA} can be used for analysis. For a nearly rectangular cross-sectional area, the height-related filling ratio ψ_{Fh} can be used to further simplify the calculation.

An intensive convective heat transmission arises in the cooling gallery of the moving piston due to the shaker effect, which can be attributed to the highly turbulent mixing motion that

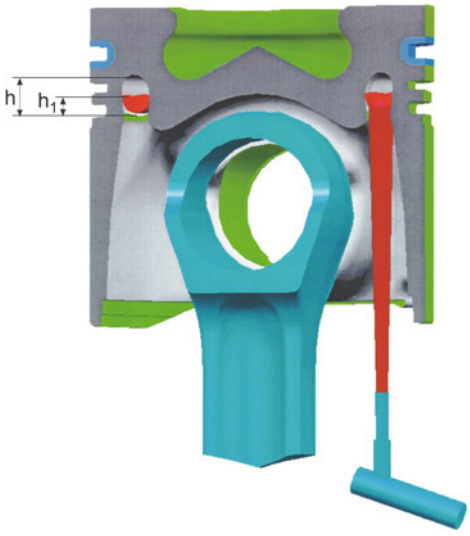

Figure 5.22:
Definition of the filling ratio

enhances energy exchange. A completely filled cooling channel or cooling gallery would exhibit a lower heat transmission coefficient as a result of the lower oil velocities. Basic tests with a heated model show that the filling ratio affects the heat transmission coefficient α, **Figure 5.23**. The optimal filling ratio is 30 to 60%. In this case, the heat transmission coefficient drops off again above a filling ratio of 60%, due to the reduced turbulence in the channel filled to a higher level.

The main variables that affect the catching efficiency and the filling ratio are the engine speed, the quantity of oil available, and the design of the inlet and outlet areas, **Figure 5.24**.

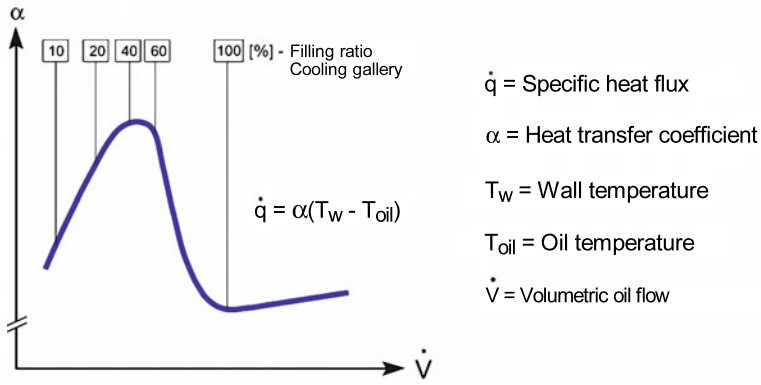

Figure 5.23: Relationship of filling ratio and heat transmission

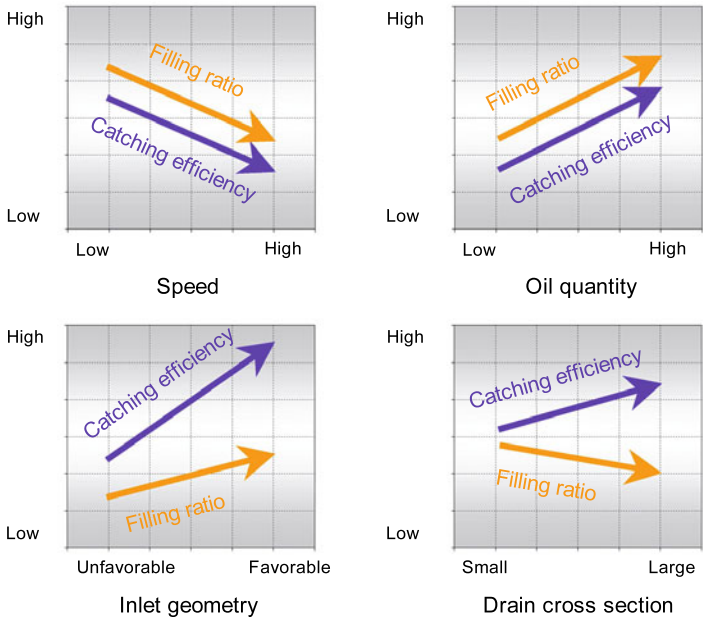

Figure 5.24: Factors affecting the catching efficiency and filling ratio

Both the catching efficiency and the filling ratio decrease with increasing engine speed. This can be attributed to the changing relative velocity between the piston and the oil jet. During the downward stroke, the velocity vectors of the piston and the cooling oil jet point in opposite directions. This results in a high relative velocity between the piston and the cooling oil jet. In this time interval, a great deal of cooling oil enters the cooling channel or cooling cavity at high velocity. In the area of the top and bottom dead center, the piston speed is nearly zero. At these points in time, the cooling oil enters the cooling channel or cooling cavity at the speed of the oil jet. The particularly critical range is the upward stroke, when the velocity vectors of the piston and the cooling oil jet point in the same direction. If the piston speed is greater than the speed of the cooling oil jet, then no cooling oil will enter the cooling channel or cooling cavity for a brief period of time, which can reduce the catching efficiency and filling ratio. This phenomenon can be partially compensated for with a well-designed inlet area. Spindle sleeves, for instance, have a positive effect on the catching efficiency as well as on the filling ratio.

The catching efficiency and filling ratio can be affected significantly by the size of the drain hole. An increasing quantity of oil for a constant nozzle cross section leads to increased catching efficiency and filling ratio.

Another measured variable can be derived from direct measurement of the local heat flow in the shaker test. To this end, heat flow sensors are installed in the piston model to be tested. Their measurement signals are transmitted to the outside by a telemetry system.

5.14 Test equipment

The shaker test rigs are based on kinematics with major dimensions that correspond to the passenger car, commercial vehicle, or large bore engines, and may be driven at variable speed; **Figure 5.25**. The test setup essentially consists of a guided push rod that is connected to the crank mechanism at one end, and to the piston model at the other end. Cooling oil is fed to the model using the original oil spray nozzle. The cooling oil that returns from the piston is guided through tubes, and is captured in a test device in order to determine the catching efficiency. The filling ratio is determined from high-speed video images that are captured at specific crank angles, using computer-aided image processing.

In addition, a nozzle test rig is available that is used to determine the flow characteristic curves and jet patterns in order to evaluate the properties of cooling oil nozzles. These tests form the basis to propose an optimized nozzle design.

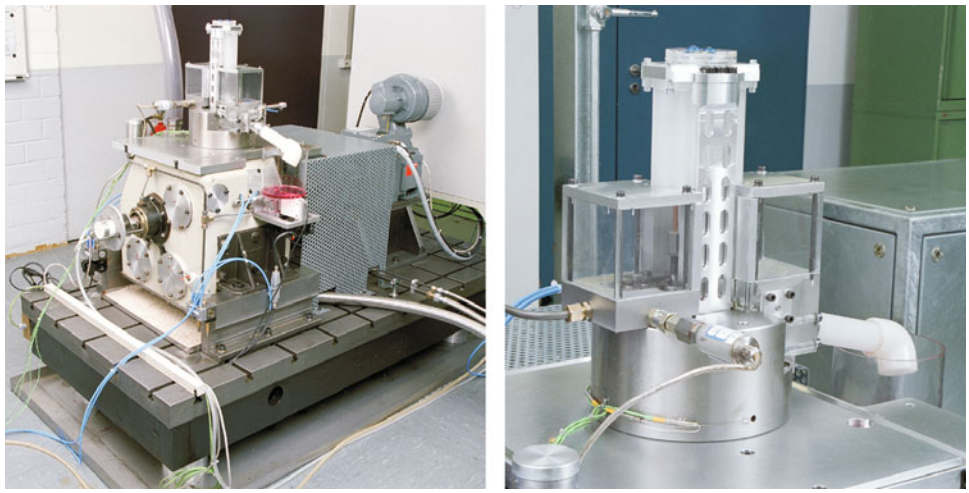

Figure 5.25: Shaker test rig and test setup

5.15 Simulation of oil motion

Another possibility for analyzing the piston cooling is by means of CFD (computational fluid dynamics) simulation of the oil motion, including heat transfer. It is based on modeling approaches from thermo-fluid dynamics, which are converted into mathematic and numerical models for simulation. The theoretical approaches and their mathematic and numerical representation must be confirmed by experimental measurements.

Ongoing development of commercial calculation and simulation programs will allow even more realistic simulation and analysis in the future to describe the oil flow from the nozzle or the connecting rod to the piston, through the cooling channels or cooling cavities, and back to the oil sump. However, both the complex flow characteristics (three-dimensional, turbulent, dynamic, and multiphase) and the heat transfer must be taken into consideration. Realistic simulation of oil motion and validation of the calculation results with experimental data will still require further development activities.

6 Component testing

Component strength of the piston can be ensured in various ways. The finite-element method, strain gage measurement, or dynamic component testing are typically used. In the numerical component analysis, all relevant thermal and mechanical loads, shrink-fit, as well as residual stresses can be analyzed. The basis of the FE model design is the nominal contour as outlined by the CAD data set. The computational and strain gage measurement results are analyzed using temperature-dependent material parameters. These are based on statistically confirmed test results, determined using test specimens taken from pistons and artificially aged at the test temperature prior to testing. This ensures that the least favorable material parameters are taken as a basis.

Strain gage measurements and component fatigue tests are based only on individual load cases, in contrast to FE analysis, but also use real component geometries, tolerances, and, for component fatigue testing, technical influences such as the alloy composition and heat treatment. The results of the three methods thus complement each other. For strain gage measurement as well as for dynamic testing, however, finish machined components are required, while FE analysis is based on the CAD data of the piston design and, hence, does not require physical hardware.

Strain gages are being applied to potentially highly stressed areas. Under static loading in the lab, local stress amplitudes are determined by such strain gage measurements. Dynamic measurements in the engine can provide additional insight about the stresses.

A variety of standardized tests have been devised for strength testing of pistons. Specially adapted loading fixtures are used in individual cases. It is important that the test devices apply the load to the component as realistically as possible. Due to the wide range of load/temperature combinations, a separate test installation must normally be conceived for each load situation. Correct phasing of the combination of several dynamic mechanical loads, however, is difficult to implement for lab testing.

Component testing in the lab is carried out primarily when an absolute conclusion about the strength or wear behavior is expected, or in order to compare different design variations. For engine components, purely static loads generally play a subordinate role. Most experiments, therefore, are durability tests with a high number of cycles. The time required often does not allow a sufficient number of test parts to be tested in order to obtain statistically reliable results. The staircase method is therefore usually applied. Alternatively, accelerated testing at significantly excessive loads is used, but here the applicability of the results to actual engine conditions must be ensured.

MAHLE GmbH (Ed.), *Pistons and engine testing,* DOI 10.1007/978-3-8348-8662-0_6,

6.1 Static component testing

Tear-off or failure load testing, where the component is statically loaded with a continuously increasing load until failure, is among the most commonly used static test methods; **Figure 6.1**. A comparison with empirical values allows the strength reserves of a component to be derived, such as for loading due to inertial forces at high speeds or the critical load in the case of piston seizure.

Strain gage measurement allows to analyze the geometric influences (overall design, local radii and transitions, elasticity, etc.) on the locally measured stress; **Figure 6.2**. The stresses thus derived can be compared to empirical limit values, based on the operating temperature. The test results can also be used to confirm computational results, and thus validate the boundary conditions of the FE analysis.

Using the sectioning method, it is possible to determine the local residual or internal stress state in the component, in order to adequately consider these stresses in a full stress and strength analysis. For measuring local residual stresses, the hole drilling method can also be used.

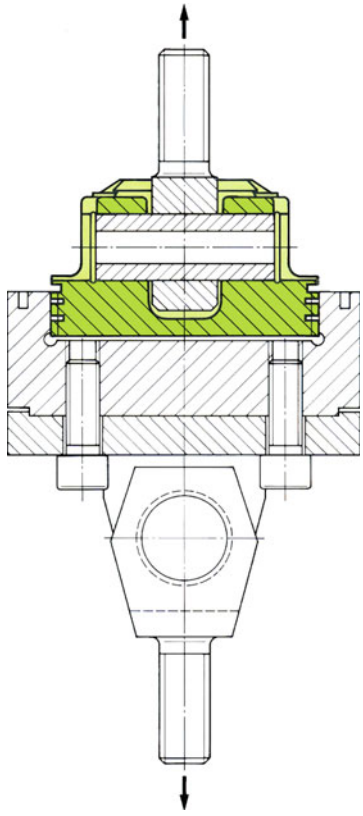

Figure 6.1:
Static tear-off testing on piston

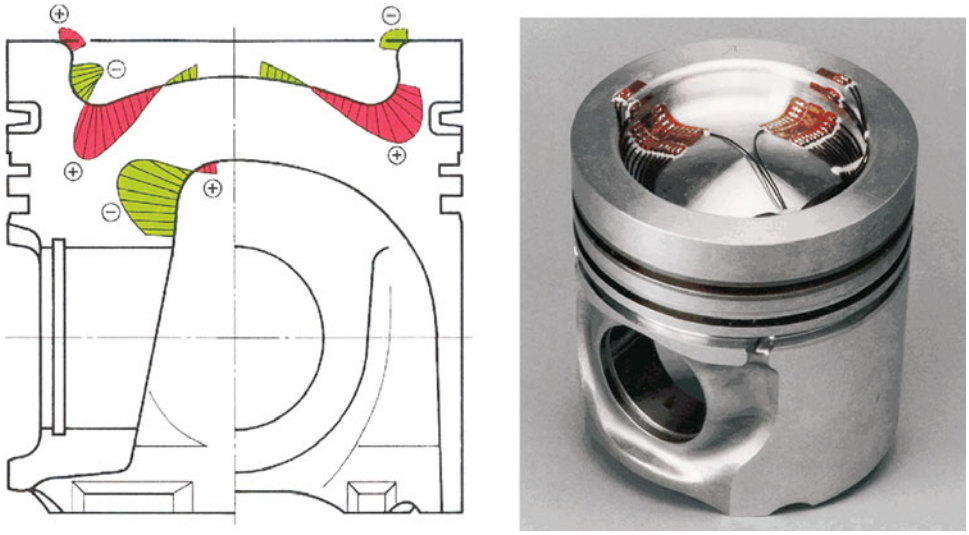

Figure 6.2: Example for strain gage measurements on piston

Other static component tests include deformation and stiffness measurements as well as investigation of pressure distribution between loaded surfaces. For deformation measurements, a defined force is applied to the structure. The deformation is measured at selected locations. The stiffness F/x can be derived from the deformation at the very location where the load is applied.

Pressure distribution in a flange connection, for example, or between the piston skirt and the cylinder is measured with a pressure-sensitive film placed between two surfaces that are in contact with each other. Depending on the local compressive force, a measurement signal or color change is induced; **Figure 6.3**.

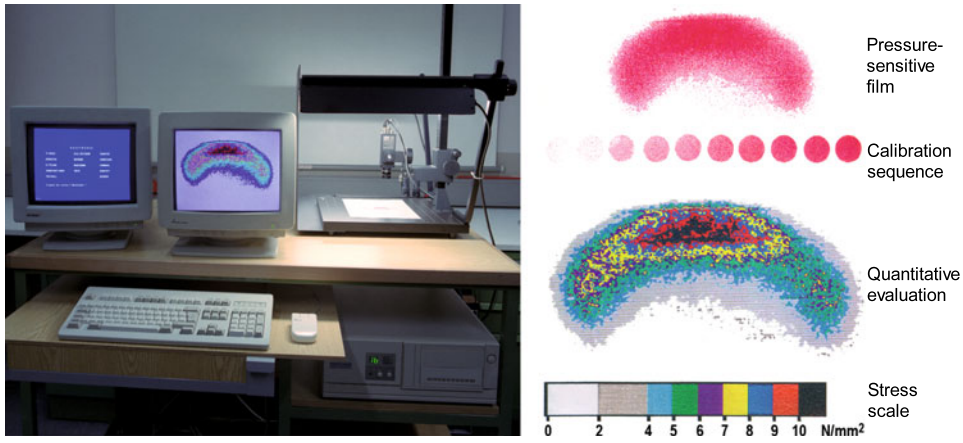

Figure 6.3: Pressure distribution on piston skirt

Creep testing on components is also part of the static test procedures. It is used to determine permanent deformations as a function of load, time, and temperature. For bolted joints, the bolt force may experience a decrease due to relaxation. Other components exhibit settling or creep-related permanent deformation under load and temperature.

6.2 Dynamic component fatigue testing

In the engine, primarily dynamic mechanical loads occur, in addition to variable thermal stresses. Therefore, in order to analyze the actual component behavior, tests with pulsating or alternating loads are most suitable. The variable mechanical load is typically applied by resonant or hydraulic test machines, which also includes the influence of temperature. The temperature gradients found in the piston during actual engine operation, however, cannot be realistically simulated in the laboratory. Tests at a constant component temperature are used as a substitute.

Typical examples of dynamic fatigue tests on the component include:

- Crown fatigue test of pistons
- Skirt fatigue test of pistons in order to simulate normal force loads acting on the piston skirt
- Hydropulsator tests to determine the bore strength and simulation of inertial force; **Figure 6.4**
- Tension-compression fatigue tests on connecting rods with the appropriate load ratio
- Fatigue tests on piston pins, piston rings, and bearings
- Thermal fatigue resistance of combustion chamber bowls
- Tensile fatigue tests on cylinders
- Structural excitation at variable frequencies at defined acceleration, using an electromagnetic shaker system for endurance tests or to determine structural resonances, e.g., for filter modules; **Figure 6.5**

Flame test benches are used to test for thermal fatigue resistance, particularly of combustion chamber bowls for diesel engines. The bowl rim is heated rapidly by a gas-powered burner, similar to the conditions in the engine, and is cooled quickly by water spray after reaching the target temperature (e.g., 350°C). The surface is checked regularly for cracks. Typical test cycle numbers are 500 to 3,000. This test allows to compare different materials and geometries; **Figure 6.6**.

Figure 6.4:
Hydropulsator tests on pistons

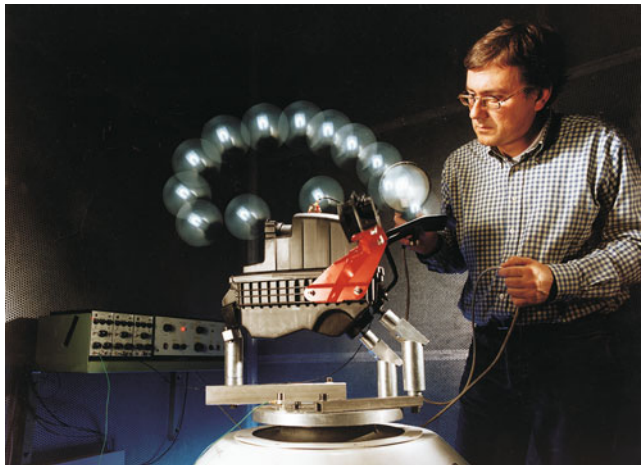

Figure 6.5:
Electrodynamic shaker test of filter assembly

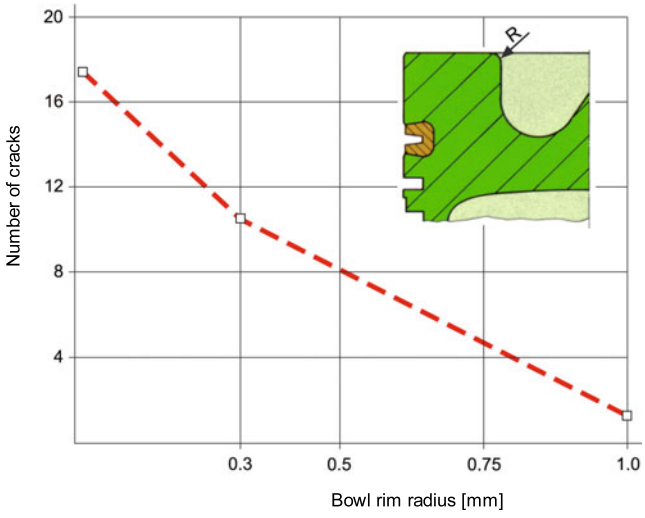

Figure 6.6:
Flame bench test, effect of different bowl rim radii

Various test benches are used to analyze the oil motion in cooled pistons; cf. Chapter 5. Tests are performed for:

- The amount of oil present in the cooling gallery as a function of the oil inflow and speed
- For free jet nozzles, the catching efficiency, i.e., the proportion of oil transported through the cooling gallery relative to the total amount of oil available

The test benches, **Figure 6.7**, are designed as crank mechanisms or on the basis of modified, externally driven one-cylinder assemblies. They simulate the conditions of passenger car, commercial vehicle, and high-speed large engines, respectively. Models can be machined from transparent acrylic resin, in order to be able to determine the instantaneous quantity of oil at a specific location in the cooling gallery, using high-speed video recordings. The test results serve to optimize geometries and oil feed cross sections. Comparisons to temperature measurements in the engine are used to derive the optimum design parameters.

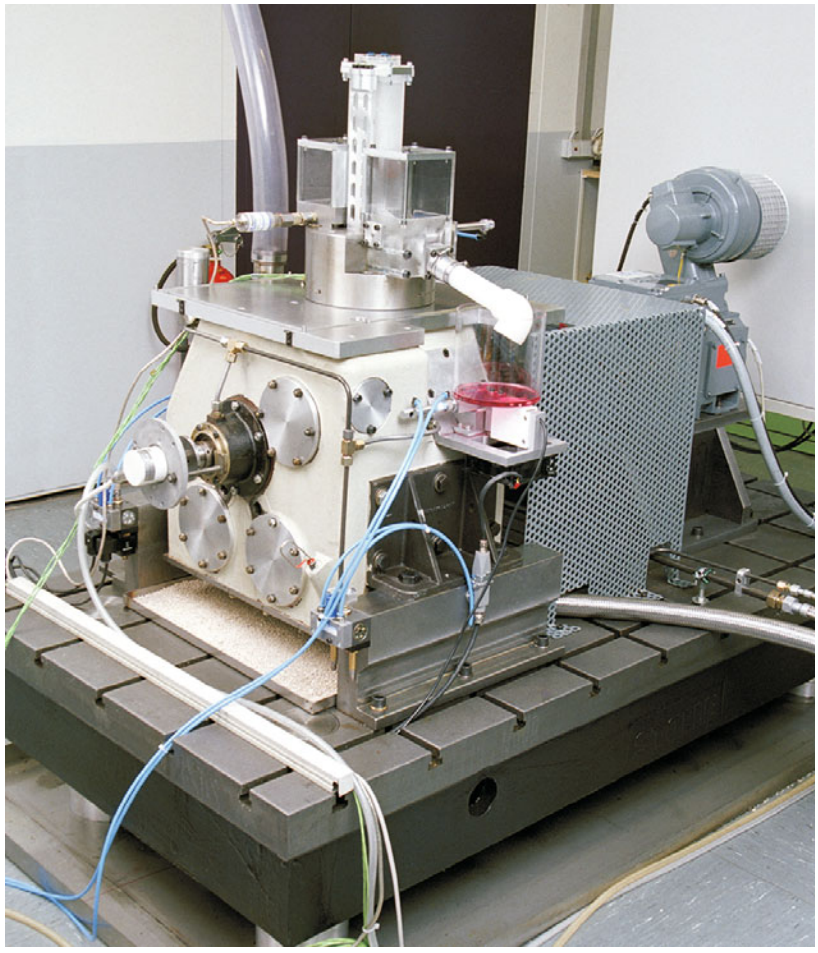

Figure 6.7: Shaker test bench

6.3 Wear testing

Characterization of the wear properties in lab tests is an important means for optimizing surfaces and coatings. Significant factors for wear include the material combination, surface condition, mechanical load, relative speed, lubricant, and possibly the atmosphere and temperature. Therefore, for near-actual test conditions, lab methods using models such as the pin-on-disc, block-on-ring, SRV (vibrational frictional wear), and the like provide results with only limited applicability, particularly if the parts used do not represent the finish or manufacturing process of the real component. Test concepts in the lab use the complete, actual component, or at least parts of it.

In order to characterize the pivoting motion of the connecting rod about the pin bore under pulsating load, MAHLE has conceived a pin/bore test machine; **Figure 6.8**. A sample pin bore moves about a defined pivot angle relative to a fixed, heatable pin bore and is fed with a metered quantity of oil. The axial force drops to nearly zero at the dead center points and reaches a maximum at the time of greatest rotational speed. The surface roughness, dimensional changes, friction torque, optical appearance, and any signs of seizing are evaluated.

Figure 6.8: Pin/bore test machine

The piston skirt or piston ring and cylinder segments are used to characterize the piston/ring/cylinder contact. The effects of piston ring coatings, finish, cylinder material, and honing on the wear or seizing tendency of the system can thus be investigated. In both cases, the test is limited to the simulation of the point of reversal of the piston ring, which undergoes mixed friction, and the local wear at that point. Because the effects of oil additives are not intended to be tested as a priority system parameter, the tests are typically performed

without additional heating. Wear is determined by dimensional or shape measurement, and sometimes by noncontacting analysis of the sample topography using a white-light interferometer; **Figure 6.9**.

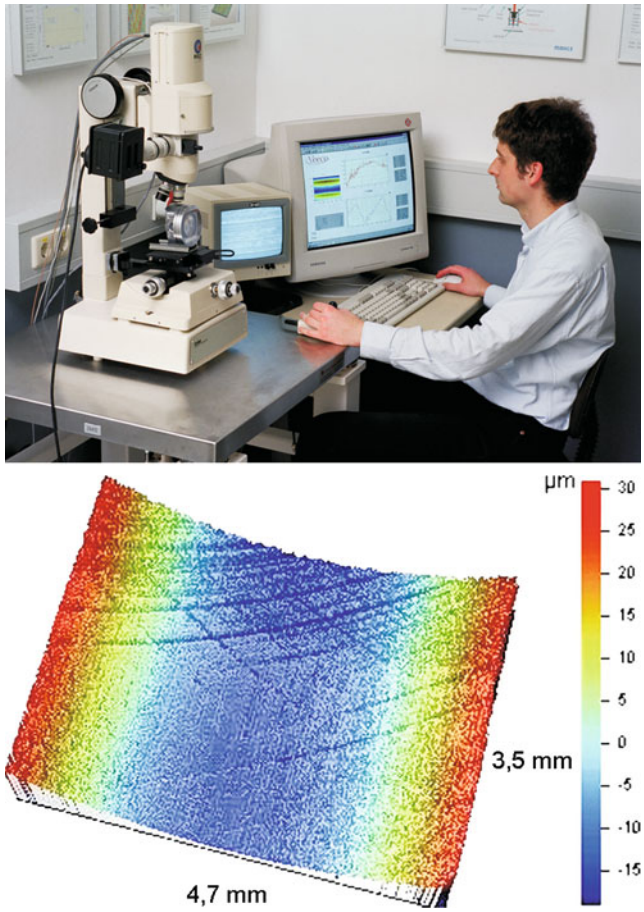

Figure 6.9: White-light interferometer: topography of worn cylinder surface

7 Engine testing

Over the past decade, simulation analysis has taken on greater significance in the development process. The importance of engine testing, however, has in no way been diminished by this trend. It is used not just for direct component development at this point, but also for validating new simulation programs and systematically generating design specifications.

In order to shorten expensive lead times, special measurement techniques are currently being used more extensively in the development of engine mechanics. Without them, mechanisms and backgrounds would no longer be sufficiently understood. Individual engine problems are precisely analyzed, appropriate critical boundary conditions and test programs are defined, and complex measurement and analysis methods are developed and automated, to the extent possible.

Systematic studies of parameters subsequently lead to an extensive array of design and development measures, enabling values to be selected at the initial stages that will be as close as possible to the final series production design. They ultimately allow the number of experimental test bench runs to be reduced during subsequent development phases, thus contributing to savings in development time and costs.

In the course of developing these processes, MAHLE continuously creates new, specific measuring instruments, test programs, and measurement and analysis methods for more effective engine testing. A few selected topics are addressed in this volume.

7.1 Test run programs with examples of results

In order to test engine components, MAHLE uses test run programs for engine testing, which are described in the examples below. They include for every development:

- Full-load curves
- Development tests
- Endurance tests

Special test programs allow the ongoing development of components, particularly with the goal of obtaining specific properties. They include, for instance:

- Cold-start tests for analyzing cold-friction resistance of piston coatings
- Burning mark tests for evaluating scuffing resistance of piston ring surfaces

MAHLE GmbH (Ed.), *Pistons and engine testing,* DOI 10.1007/978-3-8348-8662-0_7,

The MAHLE engine test laboratories are thus able to perform all of the tests that customers require for series production development. In addition, in the course of product development, we constantly develop new test methods and equipment to meet new requirements.

7.1.1 Standard test run programs

7.1.1.1 Full-load curve

The performance settings of the engine are tested using the full-load curve. The relevant operating parameters are determined for various speeds under full load. Depending on the engine type, these may include:

- Power output
- Torque
- Fuel consumption
- Lambda value
- Smoke emission value
- Intake air temperature
- Charge air temperature
- Charge air pressure
- Exhaust temperature
- Exhaust back pressure
- Peak cylinder pressure
- Blow-by value

Figure 7.1 represents selected operating values for a combustion engine under full load, as a function of engine speed.

7.1.1.2 Blow-by characteristic

The characteristic of the blow-by value as a function of engine load and speed is shown in **Figure 7.2** This is the quantity of gas that flows from the combustion chamber past the piston, piston rings, and cylinder into the crankcase. These gases are stripped of oil and fed back into the intake manifold for combustion. Typically, the amount of gas is determined at defined points over the entire speed range of the engine, for example, at zero, partial, and full load.

7.1.1.3 Seizure test

The seizure test checks the seizure resistance of the piston, piston rings, and cylinders under extreme engine running conditions; **Figure 7.3**.

The engine is run at full load and rated speed, with elevated coolant and oil temperatures. The installation clearance of the pistons can also be reduced and a run-in phase can be

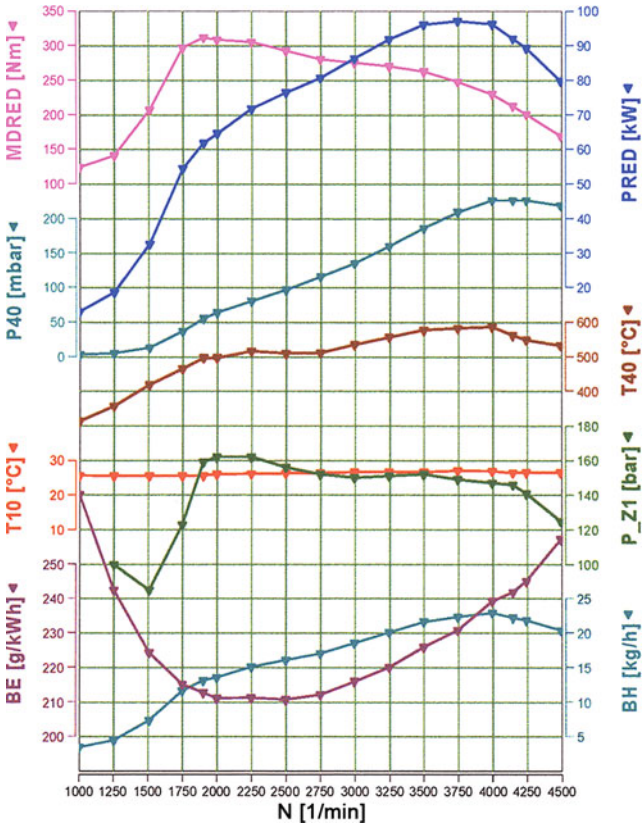

Figure 7.1:
Full-load curve for a combustion engine, with corresponding operating values

MDRED	Normalized torque
P40	Exhaust back pressure after turbocharger
T10	Intake air temperature
BE	Specific fuel consumption
PRED	Normalized power output
T40	Exhaust temperature after turbocharger
P_Z1	Peak cylinder pressure, cylinder 1
BH	Fuel consumption per hour
N	Engine speed

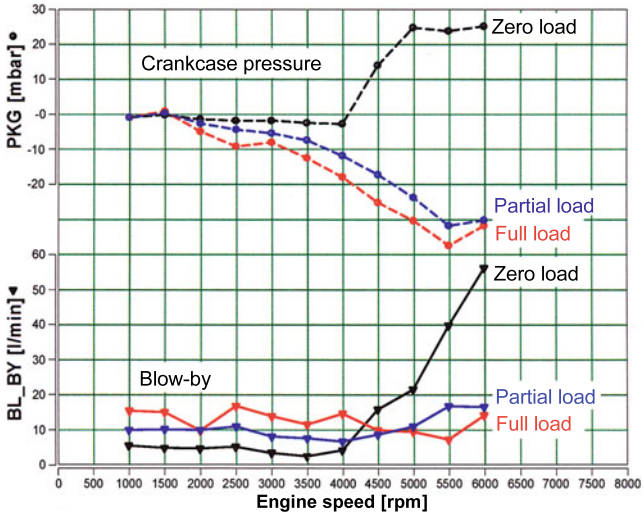

Figure 7.2:
Blow-by characteristic of a gasoline engine

PKG	Crankcase pressure
BL_BY	Blow-by value
N	Engine speed

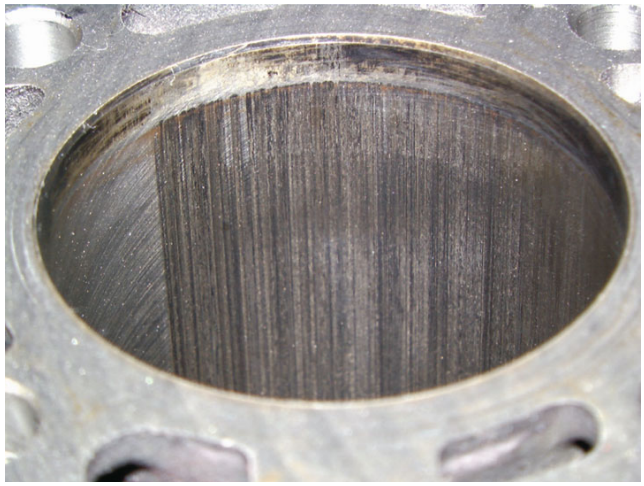

Figure 7.3:
Visible seizure damage to cylinder bore

skipped, in order to make the test more severe. The engine is run under full load and at rated speed immediately after starting.

Running times for seizure tests are typically between 0.5 and 5 hours.

7.1.1.4 Development test

In the development test, the piston, piston rings, and cylinder are tested for the following characteristics:

- Blow-by
- Oil consumption

Additional development focal points include:

- Wear patterns on pistons and piston rings
- Carbon build-up on the top land and in the ring belt area, and related cylinder polishing effect

Running times for development tests are typically 50 to 100 hours.

The programs generally include a high proportion of full-load points at rated speed as well as points of maximum torque. Depending on the development goal, additional points can also be included in testing, such as partial-load and zero-load points; **Figure 7.4**.

In order to achieve the test goals listed above, mainly geometric alterations are made to the components. They essentially pertain to high-precision optimization of forms and clearances. For the piston, this means alteration of clearances at the piston crown and skirt, as well as tuning of chamfers in the ring belt area. The axial groove clearances must be tuned along with the piston rings, because it is important both to ensure sufficient sealing against blow-by and oil pumping, and to provide resistance against piston ring sticking due to carbon

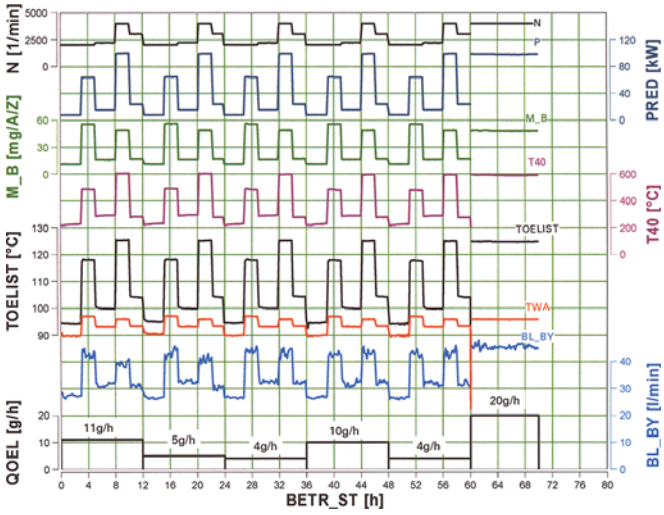

Figure 7.4:
Test run diagram for a sample development test

M_B	Fuel consumption per combustion cycle and cylinder
TOELIST	Oil temperature
QOEL	Oil consumption
BETR_ST	Operating hours

build-up–particularly in diesel engines. Other optimization points include the oil drainage in the oil ring groove.

The potential factors of influence in piston rings extend to the various parameters of ring geometry, including ring height and width, running surface shape, and internal bevels.

The design of the cylinder or engine block can affect distortions, and therefore blow-by and oil consumption. Oil consumption can also be affected by the type of honing and the resulting surface roughness.

7.1.2 Long-term test run programs

7.1.2.1 Standard endurance test

Endurance tests take anywhere from 1,000 hours for passenger car engines to 3,000 hours for commercial vehicle applications. The high costs associated with these tests means that they are run only at the end of the development of the appropriate components. Endurance tests document the effectiveness of the design measures that were developed in the previous shorter development tests.

The goals of the endurance tests are to obtain proof of

- unlimited long-term functionality of the engine components, with regard to low oil consumption and blow-by, low wear, and
- service life of the developed components.

Passing the endurance test is often the basis for a series production release of the tested components.

7.1.2.2 Hot-cold endurance test

One variant of the standard endurance test is the hot-cold endurance test. Extreme changes in the temperature of the cooling water cause great changes in material stresses due to thermal expansion. Affected by this can be components such as the pistons, piston rings, cylinder head, and cylinder head gasket. In the worst case, cracks can form, as shown here on a piston ring running surface; **Figure 7.5**.

Figure 7.6 shows an example of such a hot-cold cycle, with a cycle time of about 10 minutes.

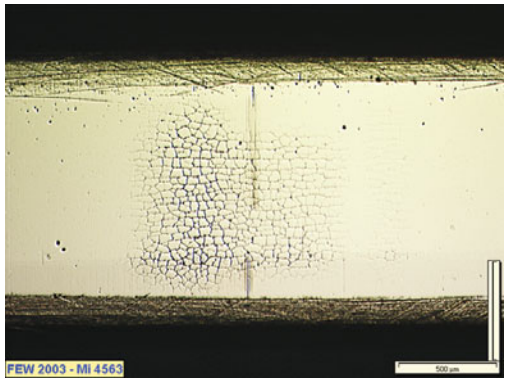

Figure 7.5:
Network of cracks in the piston ring running surface

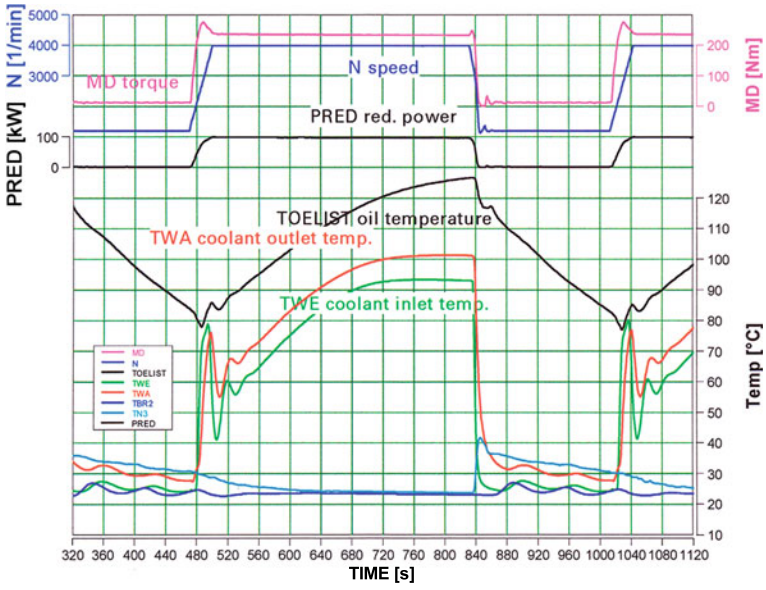

Figure 7.6: Temperature change cycle for hot-cold endurance test

N	Engine speed	TOELIST	Oil temperature
MD	Torque	TWA	Cooling water temperature at engine outlet
PRED	Normalized power output	TWE	Cooling water temperature at engine inlet

7.1.3 Special test run programs

7.1.3.1 Cold-start test

The cold-start test is designed to examine piston coatings, in order to prevent so-called cold-start scuffing, which can occur in gasoline engines if the increased fuel injection in a cold engine washes off the lubricating film of the cylinder bore. Uncoated pistons that can develop such cold-start scuffing are used first, as a basis for the cold-start test. Various coatings are then tested in direct comparison.

The engine can be run without load for the cold-start test. Prior to actual testing, the engine runs at room temperature, in order to ensure uniform distribution of the oil in the engine. The engine, including the oil and coolant, is then cooled to −25°C in a cold chamber. **Figure 7.7** shows details of such a cycle as an example.

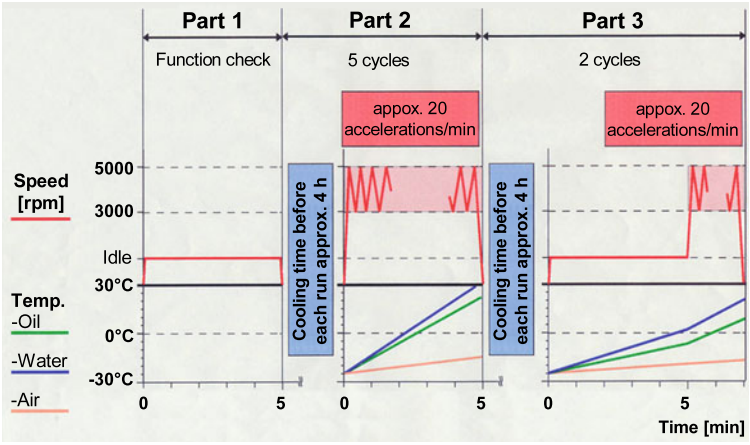

Figure 7.7: Speed and temperature course in cold-start testing

7.1.3.2 Microwelding test

Microwelding, or groove side damage, refers to a local process of destruction on the bottom side of the piston ring groove in an aluminum piston; **Figure 7.8**. It occurs primarily in the 1st piston ring groove of gasoline engine pistons. Some cases of microwelding in the 2nd piston ring groove are also known for aluminum pistons in diesel engines, because this groove is typically not protected against wear by a ring carrier, as is the case for the 1st piston ring groove.

In microwelding, the material is locally torn out of the stressed side of the 1st piston ring groove, then deposited onto the 1st piston ring, and pressed into the groove side again at another location.

Because microwelding can be detected after only a short period of operation, such as after run-in or audit testing of the engine, the running time of the test program developed for this

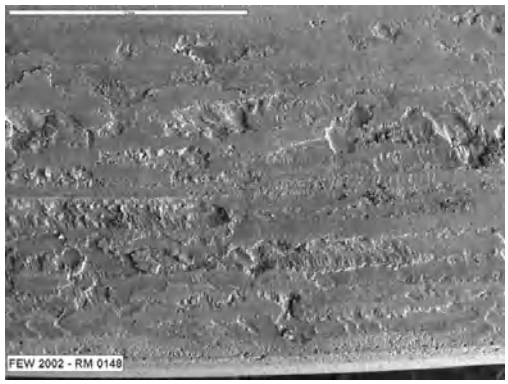

Figure 7.8:
Microwelding damage on the bottom side of the 1st piston ring groove of a piston without ring carrier

condition is only 23 hours. This includes run-in, full-load curves, and the actual microwelding cycle, which takes 3 hours and is repeated several times. In this cycle, the maximum torque, rated power, and governed speed are run in an alternating sequence. Visual assessment of the damage is carried out after the test. For less severe damage, optimization of the piston ring may be sufficient. This could entail, for example, rounding off the edges of the ring (tumbling), fine finishing of the bottom side to increase the bearing surface, or coating the bottom side of the ring. Hard-anodizing of the 1st piston ring groove is a remedial measure for severe microwelding.

7.1.3.3 Fretting test

Fretting refers to vibrational frictional wear and occurs primarily in highly stressed heavy duty diesel engines, on the bottom side of the 1st piston ring groove and the 1st piston ring.

In a manner similar to microwelding, material is torn out of the piston and piston ring locally and is deposited at another location, partly in combination with hard carbon residues. At first, only slight surface damage of a few µm is visible, but as the test progresses, local cavities of up to several tenths of a millimeter can occur; **Figures 7.9** and **7.10**.

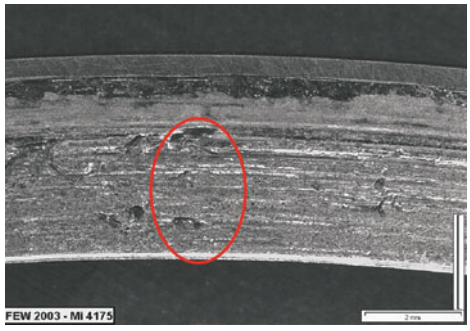

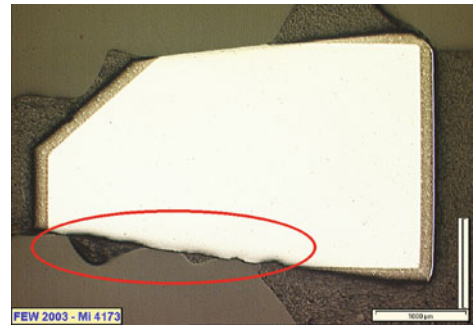

Figures 7.9 and **7.10:** Fretting damage to the bottom side of a 1st piston ring

A full-load program is used to test surface modifications or coatings on the piston groove or the ring side face. The running time is 100 hours. This gives a good initial estimate of the capability of the measures applied to the piston or ring. Further tests are then performed as part of the standard endurance tests. Depending on the running time and the appraisal of the damage, measures such as full-nitriding of the entire cross section of the ring or chrome-plating of the lower ring side face may be applied.

7.1.3.4 Burning mark test

The burning mark test is used in the development of piston rings. Burning marks occur on the piston ring running face under high thermal loads. It is a kind of damage where larger cracks and spalling can occur in the ring running face; **Figure 7.11**.

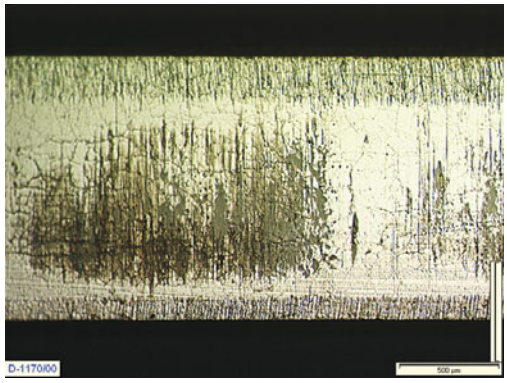

Figure 7.11:
Burning marks on the piston ring running face

In advanced stages, the burning marks become so severe that the running surface of the piston ring starts to disintegrate. This, in turn, leads to damage to the cylinder surface. Ultimately, this damage can cause seizing in the affected cylinder, and therefore may result in complete engine failure. In order to prevent such damage, piston ring materials and coatings that are highly resistant to the formation of burning marks must be developed.

One important step in this development is the ability to assess burning markr resistance under severe conditions, directly in the engine. Tribometer testing cannot sufficiently simulate the total complexity of stresses in a real engine. Therefore, a special test procedure, known as the burning mark test, had to be developed for this purpose. Although the piston rings in diesel and gasoline engines must fulfill comparable tasks in the engine, there are actually significant differences in geometry and material selection. This has made it necessary to develop dedicated test procedures for each of the two kinds of engines. The test conditions for a burning mark test are significantly more severe than typical test run programs; an example for diesel engines is shown in **Figure 7.12**.

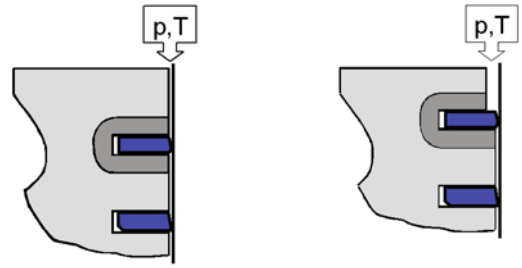

Type of test	Standard	Burning mark test
Piston type	Cooling channel	Spray jet cooling
Cooling oil supply	Large	Small
Top land width	Large	Small
Top land clearance	Small	Large
Gap clearance, 1st ring	Small	Large
Axial clearance, groove 1	Small	Large
Axial clearance, groove 2	Small	Large
Coolant	50% water / 50% antifreeze	100% antifreeze
Coolant temperature	90°C	100, 110, 120, 130°C
Oil temperature	130°C	150°C
Charge air temperature	50°C	90°C
Test run program	Customer-defined	10 h at rated power

Figure 7.12: List of intensified test conditions for diesel engine burning mark test

The unique feature of the burning mark test, unlike tribometer tests or any other external test procedures, is the ability to analyze and classify the burning mark resistance of ring surface materials, particularly ring coatings, under true operating conditions.

In order to determine the burning mark limit of a piston ring material, a new test setup is used each time (new engine block, new piston rings), and the coolant temperature is increased by 10°C each time, over the range of 100, 110, 120, and 130°C. In order to assess burning mark resistance, four classifications of the severity of the burning marks are carried out within the coolant temperature level reached in the burning mark test. These four assessment levels are assigned the colors white, light gray, dark gray, and black. This simplifies the visual representation of the data in tables and charts. The entire circumference of the ring is used for the assessment.

- "White" classification ☐ no burning marks
  In the best case, the ring running faces exhibit no burning marks or other changes whatsoever. Individual scratches are permissible.
- "Light gray" classification ▭ slight burning marks
  This level allows individual, slight burning marks.

- "Dark gray" classification severe burning marks
  The burning marks extend over a larger area of the ring running face and are significantly more widespread than in the "light gray" class. Significant, visible stripes or even slight seizure marks are evident on the affected cylinder surface at the same time.
- "Black" classification seizure marks over a wide area of the circumference
  This assessment is assigned if the burning marks affect nearly the entire circumference of the ring running surface and have already caused some disintegration of the surface. The associated cylinder typically has severe seizure marks across wide areas of the circumference.

After performing such an evaluation of the running face, the result can be depicted simply in the form of a chart. **Figure 7.13** shows an example of burning mark limits determined for various ring running surface materials in diesel engine applications.

As a summary of all the tests, an estimate can be made as to which ring running surface material is most suitable for which engine type, based on burning mark resistance and classified by specific power output. An example of this overview for diesel engines is shown in **Figure 7.14**.

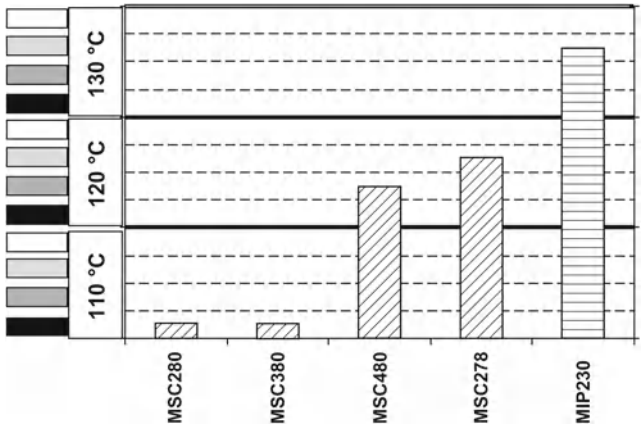

Figure 7.13:
Burning mark resistance of thermal spray coatings (MSC280, MSC380, MSC480, MSC278) compared to PVD coating (MIP230)

	Ring running surface material	Application range for diesel engines
Burning mark resistance +	**PVD coatings:** MIP230	Engines with very high specific power output
	Galvanic chrome coatings: MCR236, MCR256 **Thermal spray coatings:** MSC480, MSC278	Engines with medium to high specific power output
Burning mark resistance −	**Thermal spray coatings:** MSC280, MSC380	Engines with low to medium specific power output

Figure 7.14: Burning mark resistance of different ring running surface materials

7.2 Measurement methods used for determining piston temperature

Engine combustion is inevitably linked to tremendous increases in pressure and temperature in the combustion chamber, which places severe mechanical and thermal stresses on the piston.

Mechanical stresses on the piston are primarily caused by the gas pressure acting on the piston crown, the movable part of the combustion chamber, inertia force, and side load.

Thermal stress starts with the exposure of the combustion chamber side of the piston crown to hot combustion gases. Heat then flows from the combustion chamber through the piston crown into the piston material. A large portion of the heat flowing into the piston material is dissipated via the piston rings, particularly the 1st piston ring, to the cylinder wall, and from there to the surrounding coolant. Another portion of the arising heat is carried off by the engine oil, in engines with piston cooling.

A specific temperature field arises from these heat flows, as shown in the example in **Figure 7.15** for a passenger car diesel engine.

The permissible stresses for the aluminum alloys (AlSi) typically used as piston materials are greatly dependent on the temperature. At first, however, the engine data provided by the engine manufacturer are used to estimate the stress field and temperature field and to calculate the safety factors for the highly stressed areas of the piston, relative to the required load spectrum.

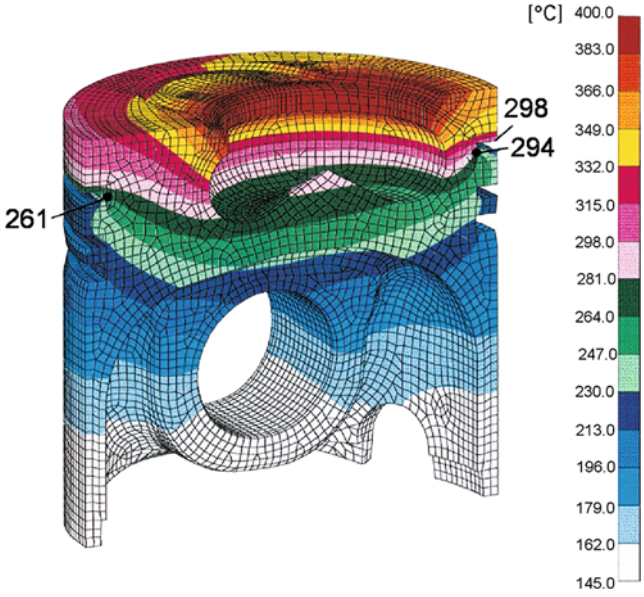

Figure 7.15:
Temperature field, using the example of a diesel engine passenger car ring carrier piston with an eccentric combustion chamber

If these safety factors are not sufficient, despite further optimization steps, then suitable means can be proposed as a consequence of piston temperature measurements, in order to obtain sufficient safety factors by lowering the component temperatures (such as by modifying the engine calibration).

Temperatures measured at various positions on the piston are needed as initial values for the FE computation of the temperature field. Particularly when developing pistons for highly stressed passenger car diesel engines, measuring the piston temperature is an important and common step.

7.2.1 Methods for measuring piston temperature

Measurement methods are classified as thermomechanical (fusible plugs and templugs) or thermoelectrical (NTC thermistors and thermocouples).

7.2.1.1 Thermomechanical methods for measuring piston temperature

7.2.1.1.1 Use of fusible plugs

Fusible plugs help to determine the temperature of the piston during steady state engine operation. The method is based on the use of several, typically three, small metal plugs made of suitable alloys, with melting points spaced apart over a range of 10 to 15°C. The plugs are inserted into the measurement locations on the piston. The melting points of the plugs are selected so that they cover the expected temperature range.

After the measurement run at steady state conditions, the fusible plugs are checked to see if they have started to melt. The temperature at the measurement location can thus be estimated, because it must lie within the interval of melting points between a melted plug and one that has not started to melt.

Advantages:
- Little equipment and measuring instruments required
- Short prep and measurement time

Disadvantages:
- Expected temperature must be estimated in advance
- Low measurement precision due to intervals in temperature between the melting points
- Can measure only one operating point per measurement run

The fusible plug method has largely been supplanted by the more suitable method of using templugs.

7.2.1.1.2 Use of templugs

Templugs are small, hardened pins made of a special metal alloy; **Figure 7.16**. After performing a measurement run at the desired operating point under constant conditions, the average temperature during the measurement run is determined on the basis of the decrease of hardness of the templug.

A single type of alloy is sufficient for the required temperature range for pistons. Templugs are available in various sizes.

The temperature to which the templug has been exposed is derived, after the plug has been removed from the piston, as a function of the decrease of hardness and the duration of the measurement run.

Advantages:

- Little preparation, equipment, and measuring instruments required
- Relatively high measurement precision
- A large number of measurement locations can be used on each piston, due to the small size of the plugs

Disadvantages:

- Loss of time due to external analysis
- Can measure only one operating point per measurement run
- Duration of a measurement run is typical 10 hours

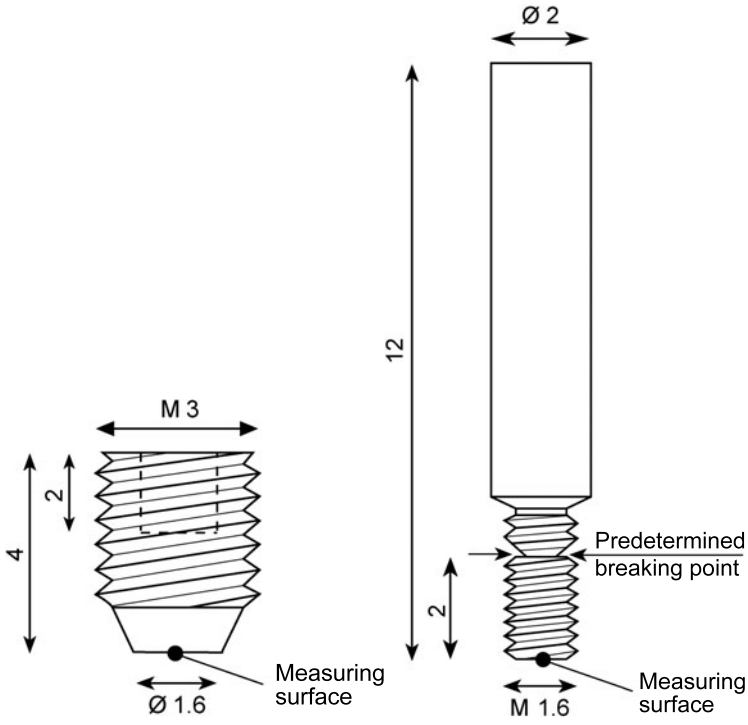

Figure 7.16: Templug dimensions; left: standard templug with Allen socket; right: templug with predetermined breaking point

7.2.1.2 Thermoelectrical methods for measuring piston temperature

7.2.1.2.1 Use of NTC resistors

NTC resistors (NTC = Negative Temperature Coefficient) are used as transducers whose electrical resistance changes as a function of temperature; **Figure 7.17**.

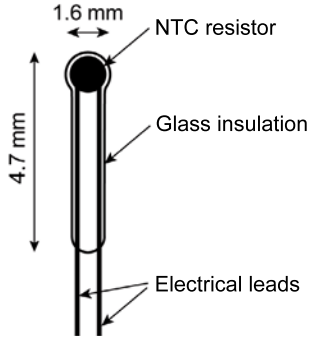

Figure 7.17:
Example of dimensions of an NTC resistor with glass insulation

The measurement value is transferred without contact by means of inductive coupling of two oscillating circuits at the bottom dead center of the piston. Ring coils are used on the piston, and pin coils are used on the engine block. **Figure 7.18** shows an example of a measurement piston equipped with NTC resistors.

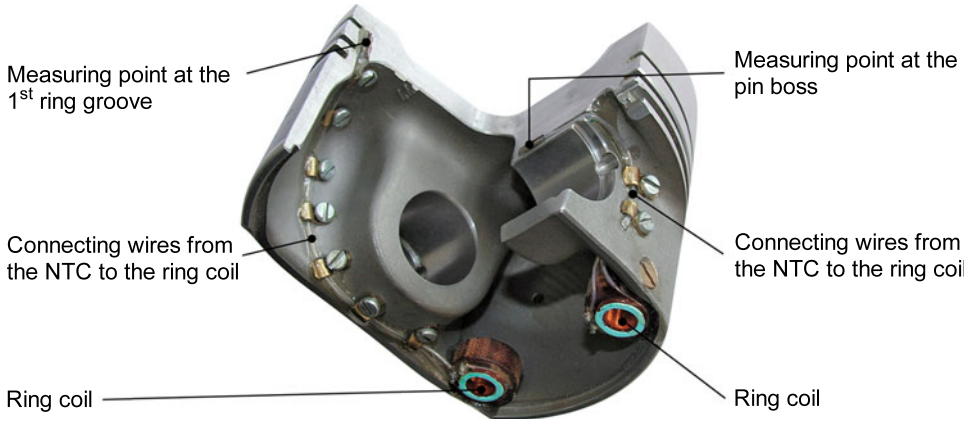

Figure 7.18: Measurement piston fitted with NTC resistors

Advantages:

- Proven, standard measurement method
- Well-suited for high speeds

Disadvantages:

- Physical and mechanical stability of the sensor is insufficient
- Measurement range limited to 400°C, due to adhesives used in the application
- Sensitive to interference signals and impact on inductive coupling from metal near the transmitters, due to the oscillating circuit principle of measurement using amplitude modulation
- Depending on spatial conditions (piston diameter), a maximum of three sensors can be used
- It may be impossible to mount only one ring coil on a piston with a very small diameter
- Depending on the measurement locations and the temperature loads to be expected for the piston, suitable sensors must be used

7.2.1.2.2 Use of NiCr-Ni thermocouples

Unlike NTC thermistors, NiCr-Ni thermocouples can be used universally, i.e., over the entire temperature range that can occur in a combustion engine. **Figure 7.19** shows an application example of such a thermocouple.

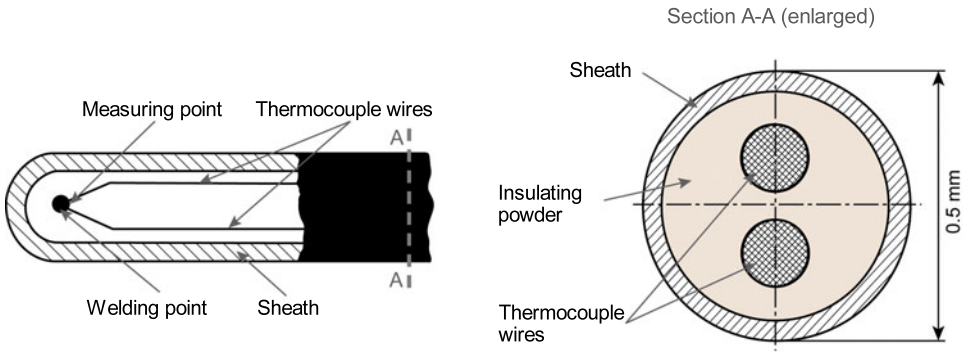

Figure 7.19: Schematic configuration of a NiCr-Ni sheath thermocouple

Advantages:

- Due to the small diameter of the thermocouple, sensor positions can be selected almost without restriction
- The measurement range is typically between −200°C and +1,150°C; for measuring the piston temperature, however, they are typically calibrated only up to 650°C
- Very well-suited for measuring large temperature amplitudes in transient test run programs

7.2.1.3 Transmitting measured values from thermocouples

7.2.1.3.1 Transmitting measured values from thermocouples with measurement leads supported by linkages

The measured values are transmitted out from the thermocouple in the piston through measuring lines supported by a linkage construction; **Figure 7.20**. The linkage is supported movably on the piston pin or the lower side of the pin boss at one end, and on the crankcase at the other end.

Using the type of measured value transmission described above, the number and type of NiCr-Ni thermocouples can be selected without restriction.

Advantages:

- The number of measurement locations is limited only by the geometric conditions
- Rapid changes in temperature can be captured (including resolution by degrees of crank angle)
- Well-suited for steady state and transient measurements
- Required power supply can be provided by lines supported by linkage system, so that no battery is needed

Disadvantages:

- High level of design effort and mechanical modifications to the engine
- Ability to install a linkage system in individual cylinders is limited by engine design
- Can usually be installed on only one cylinder, due to design constraints
- Maximum measuring speed is limited by the mechanical design of the linkage system
- Measurement duration is generally limited to a few hours, due to extreme stresses on the measuring lines

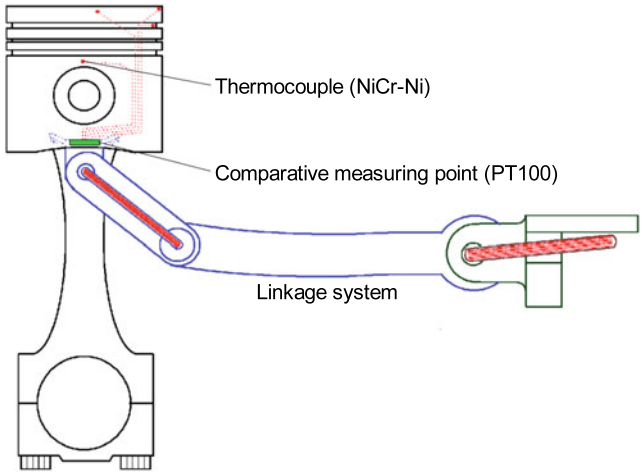

Figure 7.20:
Principle of signal transmission using measuring lines supported by linkage system

7.2.1.3.2 Transmitting measured values from thermocouples through telemetry

Measured values are transmitted from thermocouples in the piston by means of an RTM measurement system (Real-time Telemetry Temperature Measurement), newly developed by MAHLE. The integrated sensor signal amplifier, **Figure 7.21**, receives the power it needs through inductive coupling.

The measured values are transmitted once per revolution in the area of the bottom dead center. The minimum coupling time per revolution is 0.8 ms.

Advantages:

- Technical effort is less than for measured value transmission using measuring lines supported by linkage system, for the same quality of results
- There is no limitation on engine speed for series production applications
- Changes in temperatures can be captured quickly (data is transmitted per revolution of the crankshaft)
- Low level of modification to the engine block
- Up to seven temperatures can be measured on each piston, and this number can be increased by using several sensor signal amplifiers in one piston
- The sensor signal amplifiers used are stable at temperatures up to 175°C
- Service life is much greater, compared to measurements using linkage systems or measurements using NTC sensors
- The temperature-compensated sensor signals are already digitized and therefore can be transmitted to the evaluation unit without interference
- With real-time visualization, the RTM system is well-suited, particularly for optimizing combustion parameters

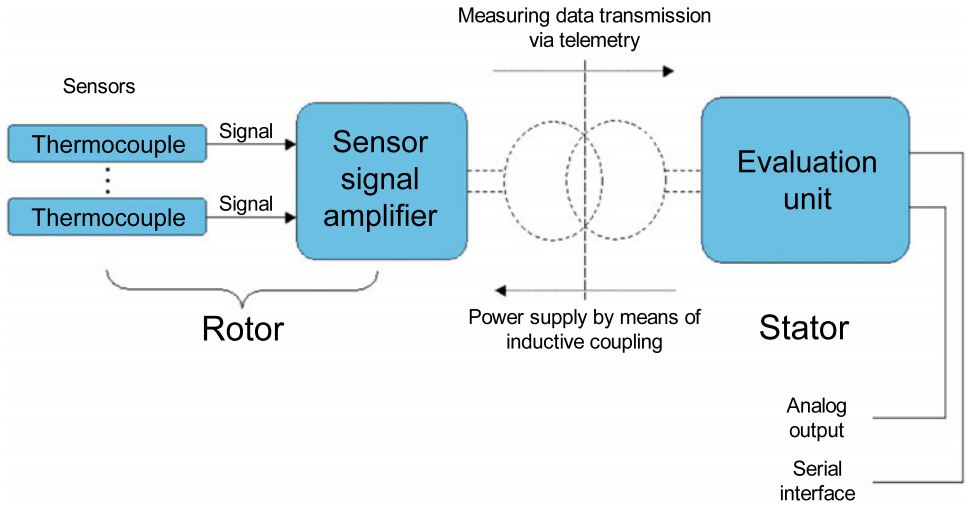

Figure 7.21: Schematic diagram of the measurement principle and measuring data transmission using telemetry (RTM system)

Disadvantages:

- Relatively high effort in applying the measuring equipment to the piston
- High financial cost for electronic components (sensor signal amplifiers)

7.2.1.4 Assessment of the methods used at MAHLE for measuring piston temperatures

The selection of the right method depends on the application requirements. If information is needed only for one defined operating point (e.g., the rated power point), then templugs can be used. If, however, a large number of measurements in the characteristic map or real-time visualization is needed, then the use of sheath thermocouples and telemetry is recommended, i.e., the RTM system described above. **Table 7.1** shows corresponding options, considering the preferred parameters in each case.

Table 7.1: Methods used at MAHLE for measuring piston temperatures

Measurement method		Templug	NTC	NiCr-Ni	NiCr-Ni
Transmission method			Inductive coupling	Linkage system	Telemetry
Classification of methods		Thermo mechanical	Thermoelectric		
		Steady state	Transient		
Operating points per measurement run		1	No limit		
Typical number of measurement points per piston	Passenger car application	8	2–3	10–20	7
	Commercial vehicle application	15	4		
Robustness	of the sensor	high	low	high	high
	of the measured value transmisssion	–	medium	low	high
Suitability for high engine speeds		high	high	low	medium
Precision		medium	high	high	high
Requirements for test lab equipment		low	medium	high	high
Project running time		50%	70%	100–200%	100%

7.2.2 Piston temperatures in gasoline and diesel engines

When measuring the piston temperature, very specific positions are preferred for the sensor locations. They are shown in **Figure 7.22**, using the example of a passenger car diesel piston.

The criteria for selecting these measurement points are:

- The bowl rim and bowl floor are highly stressed, both thermally and mechanically, and cracks can occur here in case of overload.
- The temperature in the 1st piston ring groove is essential to the function of the piston rings (resistance to burning marks on the ring running face). Build-up of residues in the 1st piston ring groove is also affected, and therefore the susceptibility to ring sticking.
- The pin boss transmits the entire gas force to the piston pin and is highly mechanically stressed. This can lead to the occurrence of pin boss cracks.

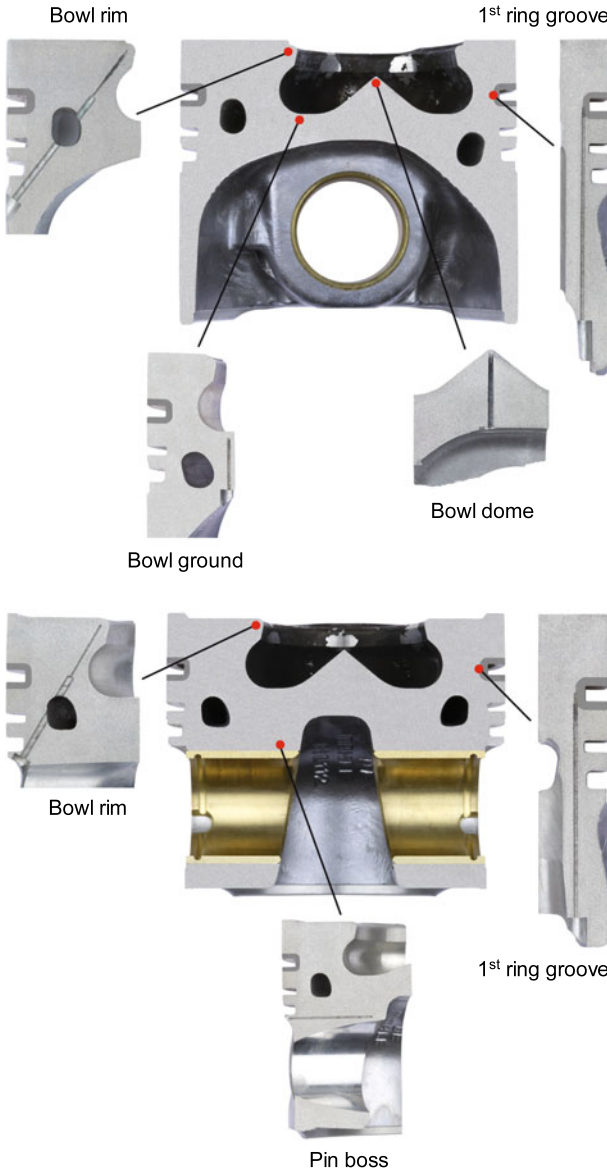

Figure 7.22:
Examples for equipping a passenger car diesel piston with sensors for measuring piston temperature

7.2.2.1 Typical temperature maxima on the piston

It is not possible to define maximum permissible temperatures at various positions on the piston as a definitive limit, because the load spectrums specified by the engine manufacturer, or expected during operation, are very different. The full-load portion in the range of the rated speed will thus be much lower, over the life of the engine, for a high-performance sports car than for a small truck with an economy engine model.

Furthermore, due to design boundary conditions, such as the location of the combustion bowl and the valve pockets, conrod design, etc., and the maximum gas pressure, different stresses can arise. The safety factors can therefore vary at the same temperature. The maximum permissible temperatures are therefore, of necessity, dependent on the application.

The values shown in **Table 7.2** are not a recommendation for limit values, but are simply orientation points for maximum measured values in current, highly stressed engines.

Table 7.2: Measured maximum temperatures on the piston for different applications

Measurement point	Application			
	Commercial vehicle application		Passenger car application	
	Al piston	Steel piston	Diesel engine	Gasoline engine
Bowl rim	340°C	470°C	380°C	–
Piston crown	–	–	–	290°C
1st piston ring groove	260°C	260°C	300°C	270°C
Pin boss	190°C	180°C	235°C	240°C

7.2.2.2 Effects of various operating parameters on piston temperature

When measuring temperatures with templugs, due to the limitation to one operating point that is inherent to the principle, the rated power point under standard operating conditions is typically selected. In nearly all cases, the highest temperatures can also be expected at this point.

For methods that allow several operating points, the full-load curve under standard operating conditions is used first to obtain base data. The result provides the actual maximum temperatures at the various measurement points, which are then entered into the simulation calculation as input variables. The temperature differentials between individual cylinders and the engine speed, at which the maximum temperature occurs, can also be determined.

If needed, the effects of various engine operating conditions of interest on the piston temperature, while keeping the other parameters constant, can be determined as part of a measurement program.

Table 7.3 shows the average effect of some important operating parameters on the temperature in the 1st piston ring groove.

Table 7.3: Effect of various operating parameters on the temperature in the 1st piston ring groove

Operating parameters	Change in engine conditions	Change in temperature in the 1st piston ring groove
Coolant temperature	10°C	4–6°C
Water cooling	50% antifreeze	5°C
Lubricating oil temperature (without piston cooling)	10°C	1–2°C
Charge air temperature	10°C	1.5–3°C
Piston cooling with oil	Spray nozzle at conrod big end	–8°C to –15°C on one side
	Stationary nozzle	–10°C to –30°C
	Salt-core cooling channel	–25°C to –50°C
	Cooled ring carrier	–50°C (additional reduction in temperature, relative to the salt-core cooling channel)
Cooling oil temperature	10°C	4–7°C
Brake mean effective pressure p_{me} (n = const.)	1 bar	4–8°C
Speed n (p_{me} = const.)	100 rpm	2–4°C
Ignition angle, injection timing	1°CA	1.5–3°C
Air/fuel ratio λ	Range of variation λ = 0.8–1.0	< 10°C

The effect of the knock control characteristic in gasoline engines and that of pre-injection in diesel engines is also of interest, for example. Such a typical measurement program is often supplemented with a measurement under "worst case" conditions. The coolant, engine oil, and intake or charge air temperatures are set to maximum levels, such as would occur in desert testing, for example.

The result of a variation of the air/fuel ratio λ for a passenger car gasoline engine is shown as an example in **Figure 7.23**. It is evident that the maximum piston temperatures occur at approximately the same air/fuel ratioλ as the maximum power output.

The lowest specific fuel consumption is seen at approximately $\lambda = 1$. However, the highest exhaust gas temperatures occur at this point. Due to the maximum permissible exhaust gas temperatures at the exhaust treatment system inlet (such as a catalytic converter), or at the turbocharger inlet in a turbocharged engine, this "lean" range may be limited.

The lowest piston temperatures, and simultaneously the lowest exhaust gas temperatures, occur in the "rich" range, such as at $\lambda = 0.8$ or less. The specific fuel consumption, however, increases drastically at this point.

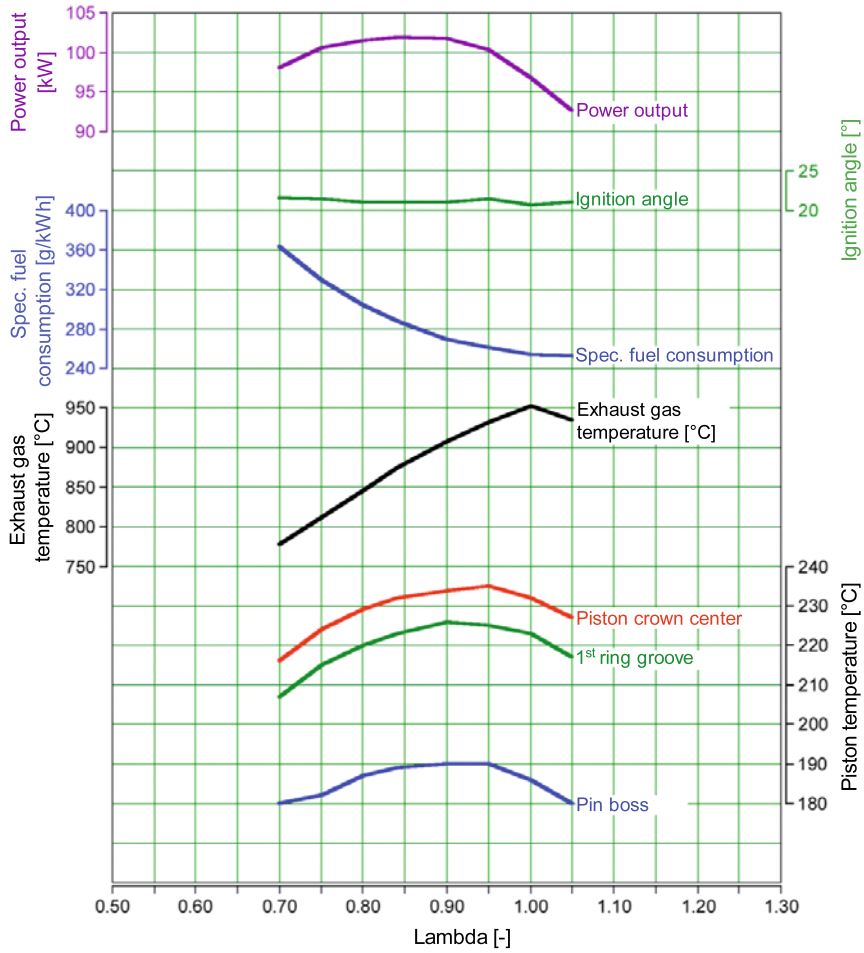

Figure 7.23: Relationship of engine operating values to air/fuel ratio lambda λ in a gasoline engine

The best possible compromise must be found for engine calibration, considering the various boundary conditions. Varying other parameters, such as the ignition angle or start of injection, also can lead to such conflicting goals due to different requirements for the operating values.

7.2.2.3 Effect of cooling oil quantity on the piston temperature

For engines equipped with piston cooling, the optimal amount of cooling oil is often the subject of discussion. Engine manufacturers always tend toward lower values. The goal is to reduce the required oil pump power and oil foaming.

From the piston manufacturer's point of view, on the other hand, a large amount of cooling oil is desirable for optimal piston cooling. This must be ensured even for engines with long

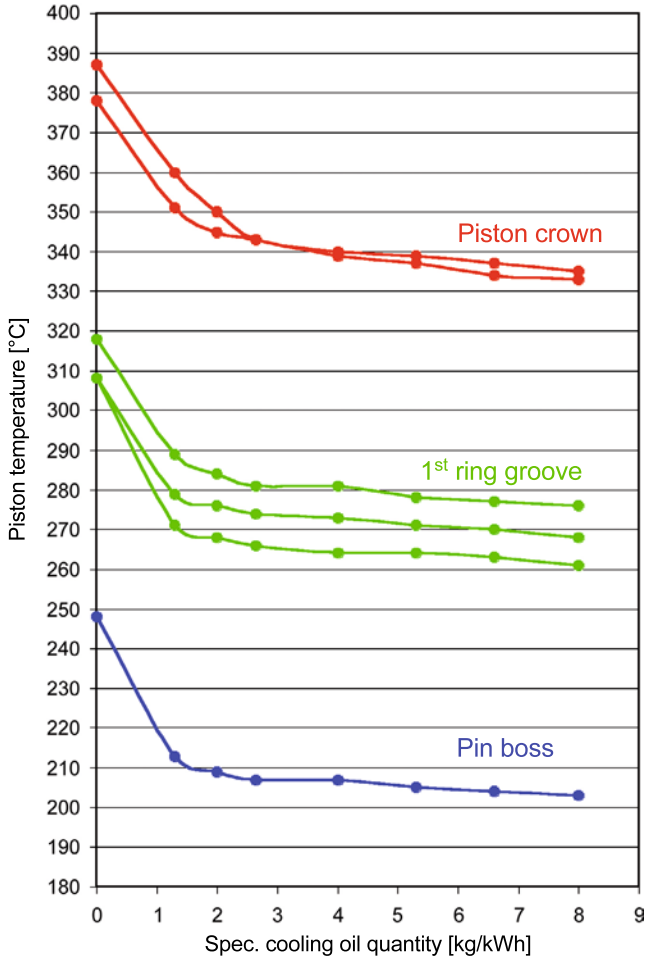

Figure 7.24:
Effects of specific cooling oil quantity on piston temperature (six measurement points) in a passenger car piston with cooling channel

service life and low oil pressure associated with advanced bearing wear. As is shown as an example in **Figure 7.24**, the specific cooling oil quantity should not fall below 3 kg/kWh.

The optimum point can be determined using appropriate piston temperature measurements and variable quantities of cooling oil.

The ratio of the cooling oil mass flow to the effective power output is known as the specific cooling oil quantity. The recommendation according to **Table 7.4** for special cooling oil quantities is based on the operating oil pressure at rated speed and the engine oil temperature specified for the same point.

Table 7.4: Recommended specific cooling oil quantities

	Spray jet cooling (passenger cars)	Cooling channel piston (aluminum, passenger cars and commercial vehicles)	Cooling channel piston (steel, commercial vehicles)
Recommended specific cooling oil quantity	3 kg/kWh	5 kg/kWh	5–7 kg/kWh

TIn addition, the cooling oil nozzles must meet specific requirements with regard to jet formation and the function of the pressure retention valve. It is therefore important to calibrate the cooling oil nozzles, including the pressure retention valves, on a suitable test bench prior to measurement of piston temperatures.

The opening and closing pressures of the cooling oil nozzles are controlled either by central valves (in a separate oil supply channel) or internal nozzle pressure retention valves, and must be tuned to the boundary conditions of the engine. Using this type of valve, the minimum oil pressure needed for the bearings is ensured at low rpm, such as at idle speed.

Extensive piston temperature measurements are needed to optimize systems with controlled piston cooling. The cooling oil nozzles are then supplied with oil only in those engine characteristic ranges where it has been shown that a drop in piston temperature is needed. Reducing the oil pump power, and therefore fuel consumption, is the advantageous associated effect.

7.2.2.4 Piston temperature measurement in transient programs

Figure 7.25 shows a cross section of a commercial vehicle diesel piston. Pistons of this type were used in an engine that was the subject of a so-called thermoshock run.

The engine is first run under overload conditions–increased injection quantity, higher peak cylinder pressure, increased coolant temperature. In a thermoshock run, a sudden change is then made from full load to no load, while switching from a hot coolant flow to a cold coolant flow.

The diagram shows the time trace of the temperatures at prescribed measurement points during the thermoshock cycle, using the piston mentioned above as an example. One of the results that is evident here is that the bowl rim has the greatest temperature change stress, with a temperature amplitude of about 240°C. Together with the temperature gradients that occur, stresses on the piston can be calculated and used to determine service life.

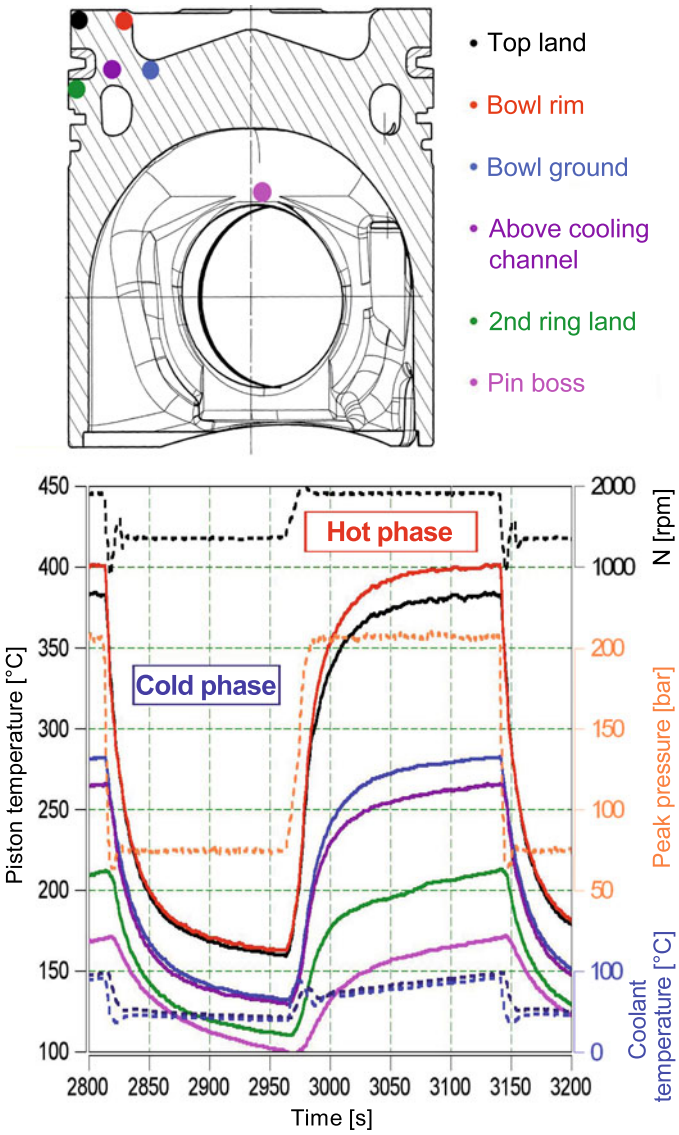

Figure 7.25: Section view of a commercial vehicle diesel piston with six temperature measurement points, and associated results of measurements made during a transient thermoshock cycle. Piston temperatures were measured using the RTM system.

7.3 Measurement of friction losses on a fired engine

Continuously rising crude oil prices and the declared goal of reducing environmental impact by minimizing emissions of toxic exhaust gas components as well as carbon dioxide have lead to the demand for drastically reducing fuel consumption in combustion engines.

In addition to downsizing with turbocharging, the development of new combustion processes, and dethrottling of the intake system, the reduction of mechanical losses is an important approach for reducing fuel consumption. It is important to understand the association of mechanical losses to various components. Loss distributions have long been discussed in literature, but are mostly based on motored engines.

Figure 7.26 shows an example of the distribution of mechanical losses in gasoline engines, as determined back in 1984 by motored engine testing.

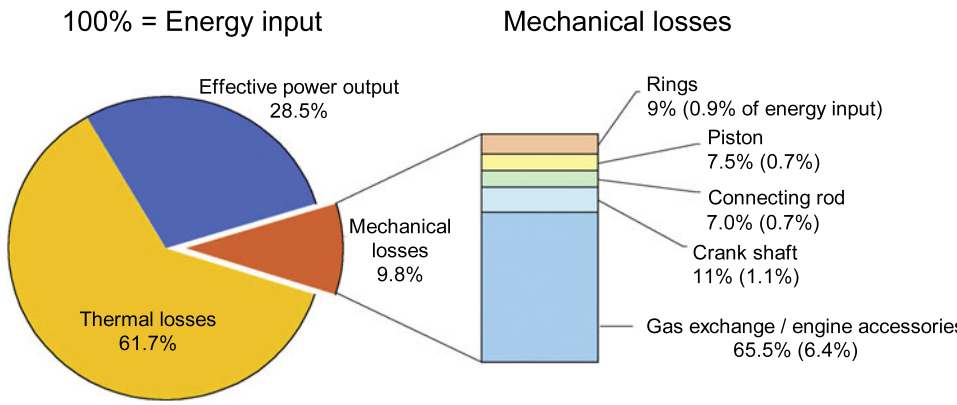

Figure 7.26: Loss distribution (averages of three different 2.0-liter gasoline engines at 5,000 rpm, motored operation, as of 1984)

The proportions of mechanical losses shown on the right in **Figure 7.26**, obtained from motored engine tests, are small relative to the thermal losses in a fired engine, on the left in the figure. It can be assumed, however, that the actual distribution of mechanical losses changes significantly in a fired engine. The piston group, in particular, takes on a greater share of the mechanical losses with increasing engine load. It therefore makes complete sense to determine and optimize the frictional loss under load of this assembly, known as the power cell unit (PCU). The PCU includes the following components:

- Piston
- Piston rings
- Piston pin
- Piston pin circlips
- Connecting rod with bearings
- Cylinder liner

The prerequisites for sensible optimization are very precise and reproducible measurements of the frictional losses under real engine operation, using a suitable method of measurement and analysis.

7.3.1 Measurement methods for determining the friction mean effective pressure

A few measurement methods are described below that serve to determine the friction mean effective pressure, but which vary greatly in precision and in the technical effort required.

7.3.1.1 Willans line method

This method is based on a measurement of fuel consumption per combustion cycle, at a constant engine speed, with varying brake mean effective pressure.

In order to determine the friction mean effective pressure, a tangent is drawn from the linear portion of the consumption curve, which is extrapolated to the axis of the brake mean effective pressure (x-axis). The intersection yields the value of the friction mean effective pressure of the engine (negative brake mean effective pressure); **Figure 7.27**.

This graphical method is a simple way to estimate the friction mean effective pressure of an entire engine. Due to the extrapolation, however, only an approximate trend forecast can be made for comparing different engine types.

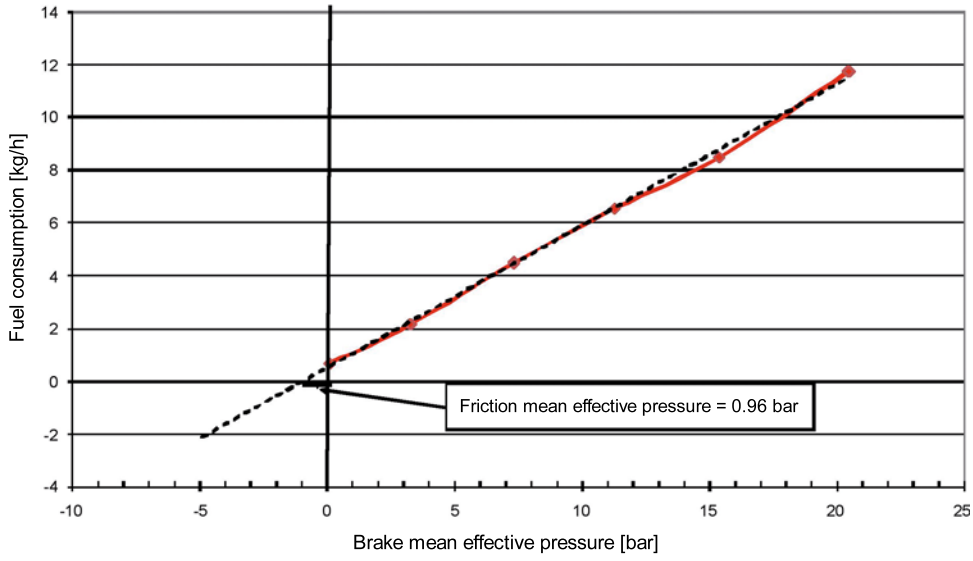

Figure 7.27: Willans line–4-cylinder diesel engine at 1,500 rpm

7.3.1.2 Motoring and tear down methods

When motored, the combustion engine is driven by an electric motor and the ignition and fuel supply are switched off to prevent combustion. The temperatures of coolant and oil are maintained at operating temperature by means of external conditioning units. The friction mean effective pressure of the engine, including charge exchange losses, can then be derived from the driving power consumed by the electric motor.

One special form of motoring is known as the tear down method. The engine is motored and disassembled, or stripped, step by step. In this manner, friction losses can be determined for each individual engine component.

General disadvantages of motoring, relative to measurements on a fired engine, include:

- The loads on the affected components are very low due to the absence of gas pressure.
- The operational and component temperatures are lower, and the operating clearance conditions are significantly different.
- Charge exchange losses are assigned to friction.
- The high-pressure loop of the 4-stroke engine does not do any work. Due to leakage and wall heat transfers, the brake mean effective pressure has a negative sign, which is interpreted as friction.

7.3.1.3 Cylinder deactivation

In order to determine the friction mean effective pressure, the power output from the engine is measured, and then one cylinder of a multicylinder engine is shut off by interrupting the flow of fuel. The power that is then output by the engine is measured as well. By comparing the two power output levels, the friction mean effective pressure of the engine can be determined.

The disadvantages described above for motoring also apply to cylinder deactivation.

7.3.1.4 Coast down test

In order to calculate the friction mean effective pressure using this method, the decrease in speed level (change in speed as a function of time) is measured, which yields the internal friction in an unbraked, coasting motor. If the inertial torque of the engine is known, then the drop in speed level can be used to calculate the loss of engine torque, from which the friction mean effective pressure can be determined.

7.3.1.5 Floating liner method

In the floating liner method, the frictional forces caused by the piston assembly are measured directly. The level of design and technical effort required is very high, which is why this method is used only on single-cylinder units. The cylinder liner is supported such that it floats with very low friction, and the lower end is supported on load sensors. This makes

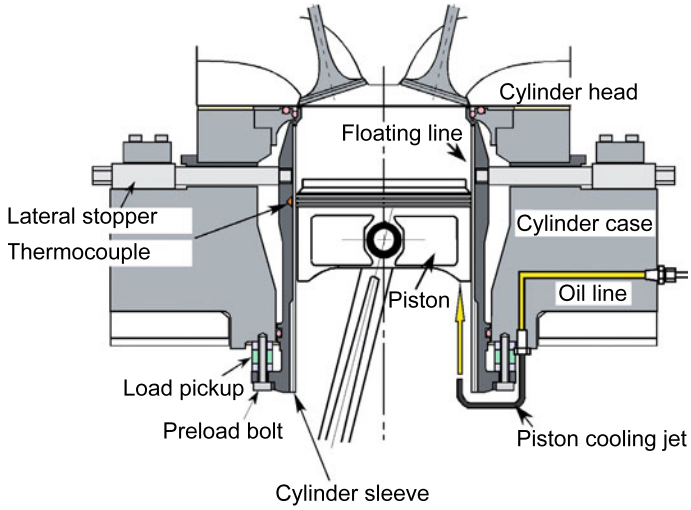

Figure 7.28:
Floating liner system [10]

it possible to represent the friction force curve in the stroke direction over one combustion cycle. **Figure 7.28** describes the principle construction of a floating liner system.

The results, tracked against the crank angle, are very helpful for validating numerical calculations and for interpreting mechanisms of action. The friction mean effective pressure can then be derived from the measured friction force curve.

A disadvantage of this measurement method is that the maximum achievable engine speeds and loads are severely constrained by the design. In addition, due to the floating support of the cylinder liner, the cylindrical distortions that arise are not representative of those for actual complete engines.

7.3.1.6 Indication method

The indicated mean effective pressure (*IMEP*) in the combustion chamber is determined using pressure sensors. High-precision measurement of the output torque at the flywheel can be used to derive the brake mean effective pressure (*BMEP*). The friction mean effective pressure (*FMEP*) is the difference between these two values:

$$FMEP = IMEP - BMEP$$

The principle behind the derivation of the friction mean effective pressure is seemingly quite simple. The greatest challenge, however, is the very high measurement accuracy and reproducibility required for *IMEP* and *BMEP*, because they are very close in value and are subtracted to get the result.

Unlike the other measurement methods, this principle enables friction mean effective pressure to be measured during real engine operation. The ranges of speed, load and temperature

are not limited. Operating temperatures, and thus the local operating clearances and distortions, correspond to the actual conditions.

7.3.2 Friction mapping using the indication method

7.3.2.1 Requirements

The friction power test bench is a development tool that can be used throughout the entire engine operating map to examine parameters for the following engine components and frictional pairs:

- Crank mechanism and bearing
  - Piston and cylinder bore
  - Rings and cylinder bore
  - Rings and piston grooves
  - Pin boss bearing in piston and connecting rod
  - Big end bore and crankshaft
  - Main crankshaft bearing
- Valve train
  - Camshaft and bearing
  - Cams and rocker arms
- Engine accessories
  - Water pump
  - Oil pump
  - Generator
  - Vacuum pump
- Timing chains (belts) and drive chains (belts)
  - Crankshaft/camshaft connection
  - Connection to engine accessories
- Effect of operating media and temperatures

The results of measurements of the power cell unit based on Chapter 7.3 are discussed as an example in Chapter 7.3.3. The main focus of attention is the crank mechanism and its bearing, and here in particular the piston friction, piston ring friction, and piston pin friction.

Parameters such as installation clearance, piston pin offset, piston shape, as well as skirt roughness and coating are of particular interest for piston friction.

In relation to the ring pack, the parameters of ring width and tangential load, as well as bore coating and geometry, are of great interest.

For friction in the piston pin bearing, parameters such as coating and installation clearance are critical.

Parameter investigations should be feasible on all engine types and concepts.

The engines should be able to be measured under the following conditions, whether motored or fired:

- Fired operation is possible up to a maximum rated power of 200 kW.
- Motored operation should also be possible with external loading (max. combustion chamber pressure can be set continuously, up to over 200 bar).
- Basic prerequisites for obtaining reproducible results are precise conditioning and adjustability of the engine operating media.

The operating values for the engine, including the cylinder pressure curves, must be extensively documented in order to have sufficient input data for the numerical calculation.

7.3.2.2 Friction power test bench for passenger car engines

Figure 7.29 shows the schematic construction of the frictional loss test bench. It shows the engine being operated without its own engine accessories.

The oil and water pumps are replaced by external conditioning systems. An external high-pressure pump is used to generate pressure in the fuel rail.

The use of external systems ensures that reproducible operating conditions can be set up. Using the indication method, the frictional losses in the engine accessories would also be included in the friction mean effective pressure calculation for the entire motor. Any fluctuations within these engine accessories would therefore cause significant errors in the derivation of the friction mean effective pressure. The use of external conditioning systems and drives can minimize this error potential.

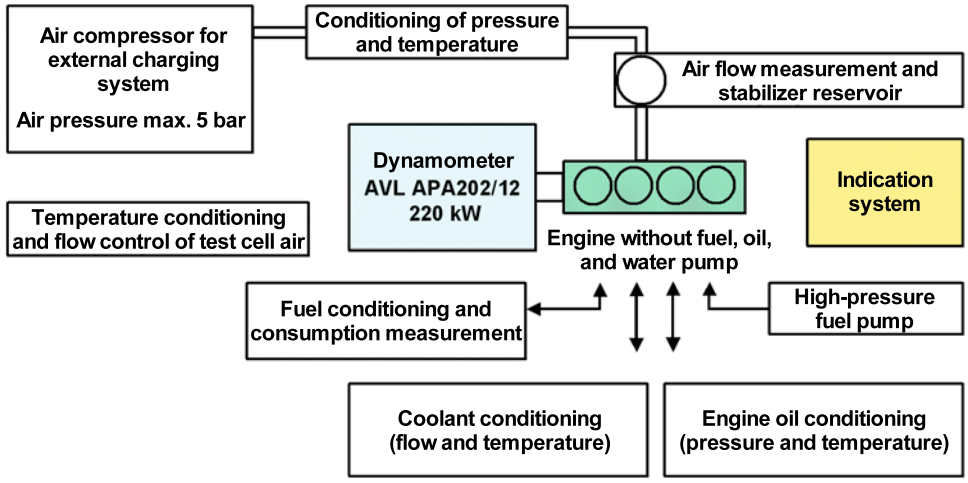

Figure 7.29: Schematic construction of the friction power test bench

An indication system with water-cooled pressure sensors is used to determine *IMEP* with a high level of precision. Precise association of the cylinder pressure to the crank angle over time is critically important. The crank angle sensor used must therefore have the highest angular precision possible. The top dead center is determined dynamically with a capacitative sensor in the cylinder head.

A high-precision dynamometer is used to determine *BMEP*, which is calculated from the torque. Precise observance and reproducibility of the boundary conditions are indispensable for accurately determining the friction losses. In addition to the engine operating media of coolant, oil, and fuel, the ambient air temperature must also be precisely and reproducibly controlled. One external conditioning unit each is available for conditioning the engine oil and coolant. They replace the pumps and controllers on the engine; **Figure 7.30**. The fuel is also externally conditioned.

In motored operation, the engine can be run by means of an external charging system with a defined cylinder pressure (load). The pressure of the intake air in the intake system can be increased accordingly. The greater charge density in the combustion chamber that results after "close intake" can reach peak cylinder pressures of over 200 bar due to compression in so-called "motored externally charged" mode.

Figure 7.31 shows the setup of the test bench, with test engine and dynamometer.

The key data for the friction power test bench are compiled in **Table 7.5**.

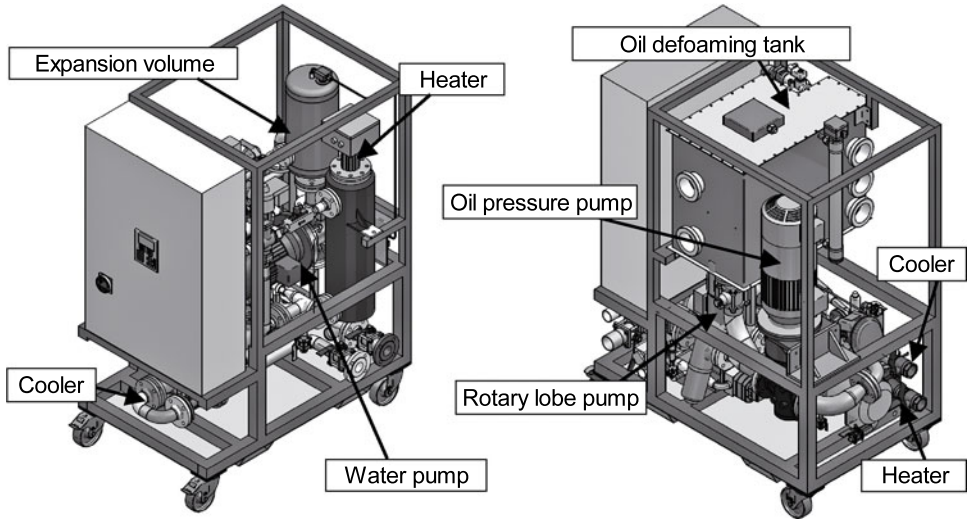

Figure 7.30: Conditioning systems for coolant circuit (left) and oil circuit (right)

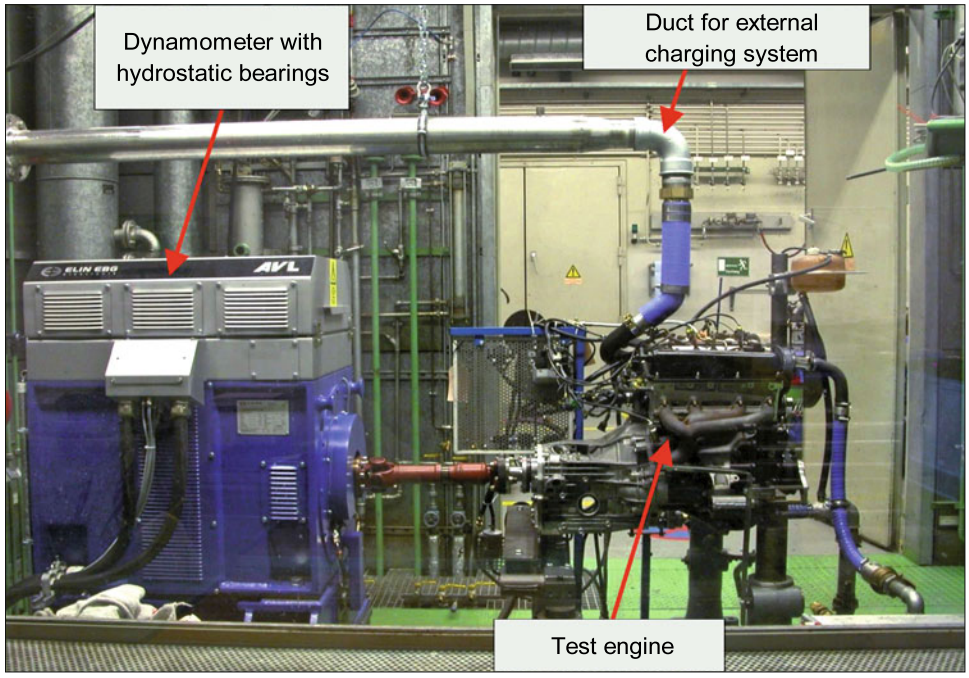

Figure 7.31: Test engine with external charging system connected

Dynamometer	
Speed	max. 12,000 rpm
Torque	max. 525 Nm ± 0.3 Nm
Coolant conditioning system	
Temperature setting	40–120°C ± 1 K
Flow rate	50–200 l/min ± 5 l/min
Engine oil conditioning system	
Temperature setting	40–120°C ± 1 K
Oil pressure	1–10 bar ± 0.05 bar
Allows engine to be operated with dry sump lubrication	
External charging system	
Air flow rate	max. 25 m^3/min
Air pressure	max. 5 bar
Air temperature	25°C ± 1 K
Fuel conditioning and consumption measurement	
Temperature stability	+ 0.1 K
Flow rate	max. 125 kg/h ± 0.15 kg/h
Ambient air temperature controller	
Air temperature	25°C ± 2 K

Table 7.5:
Technical data of the friction power test bench

7.3.2.3 Measurement and analysis methods

In order to determine the effects of PCU design parameters on the friction mean effective pressure, different variants are analyzed. The measurement program includes measurement of the friction mean effective pressure during the run-in phase, over full-load curves, and for the engine operating map for each variant. Engine operating map measurements are made both in fired mode and in motored externally charged mode.

The operating maps, for which the effects of the parameters of load, speed, and engine temperature on the friction mean effective pressure of a combustion engine are to be determined, are created using a statistical test planning method, design of experiments (DoE). The core of this approach is the definition of a multidimensional experiment space and the optimal distribution of the measuring points in this space.

The advantages of DoE are that the results can be displayed as a function of all the selected parameters, and the test time required can be significantly reduced.

Figure 7.32 shows the variation parameters and desired response parameters selected for the DoE analysis, as well as the set boundary conditions and the relationships between the individual parameters.

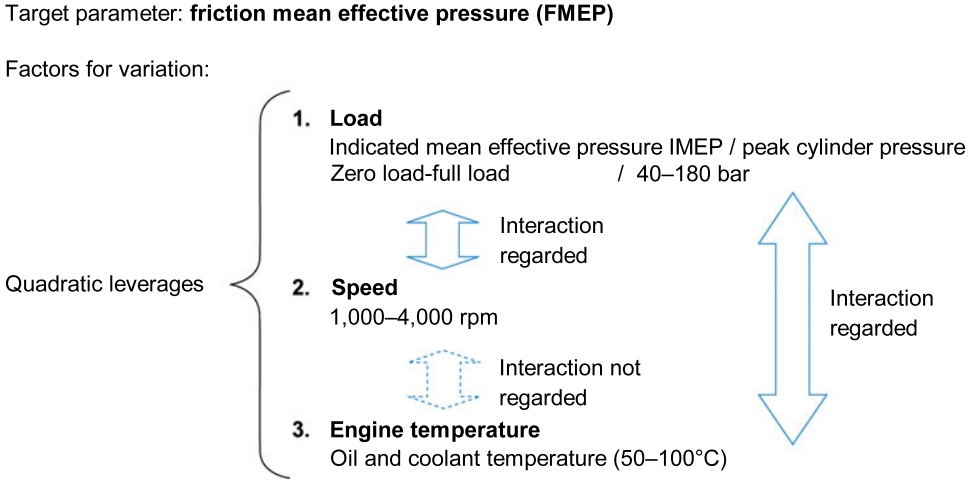

Figure 7.32: Variation parameters and response variables for compiling a DoE test plan

Figure 7.33 shows two friction mean effective pressure maps at different engine temperatures, 50°C and 100°C, which were compiled using a mathematical approximation from the DoE program. The friction mean effective pressure is shown as a function of the engine speed and load (indicated mean effective pressure). In this case, engine temperature means the same value for coolant temperature and oil temperature.

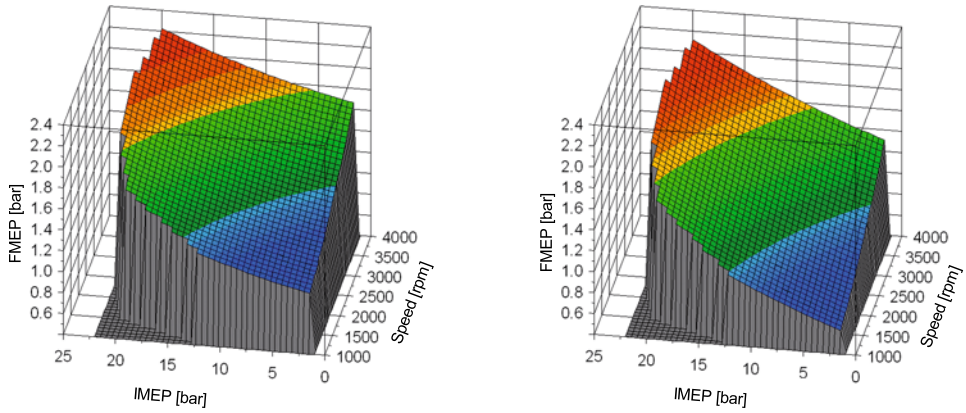

Figure 7.33: *FMEP* maps at different engine temperatures; variant A: 50°C engine temperature (left), variant B: 100°C engine temperature (right)

A comparison of the two maps shows that engine friction depends on the engine temperature. The higher the operating fluid temperatures, the lower the friction mean effective pressure. It can also be seen that the friction mean effective pressure increases with rising rpm, and that the friction mean effective pressure is significantly dependent on the load.

A detailed interpretation by visually comparing the friction mean effective pressure maps is difficult, because the differences are very slight. If the difference between the two is considered, however, even small differences can be displayed clearly. A positive difference indicates the potential for reducing friction mean effective pressure in variant B; **Figure 7.34**.

A comparison of the different engine temperatures with the aid of the friction mean effective pressure difference map, **Figure 7.34**, shows no significant dependence on speed, but a strong dependence on load.

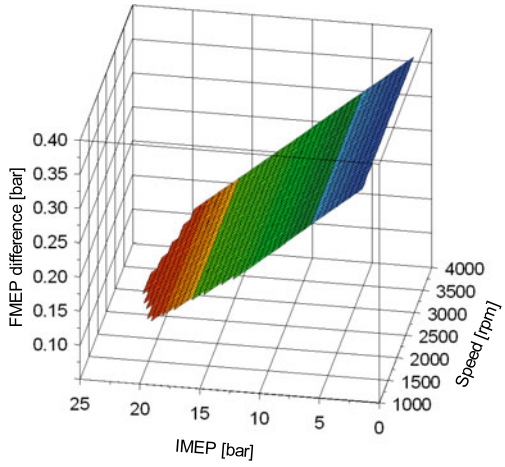

Figure 7.34:
Friction mean effective pressure difference map, calculated from the friction mean effective pressure operating maps of variants A and B. The differential can here be attributed to a difference in engine temperature of 50°C.

The interpretation of such friction mean effective pressure difference maps allows fundamental statements about the influences of the parameter changes made on the characteristic curve of the friction mean effective pressure in the operating map.

7.3.3 Selected results

The following results were obtained from a turbocharged 4-cylinder passenger car diesel engine with a gray cast iron block.

The friction mean effective pressure values obtained are shown for an engine operating temperature of 100°C. The friction mean effective pressure difference map for the motored externally charged mode is compared to that of the fired mode in each case.

7.3.3.1 Piston installation clearance

If two extremely different installation clearances are run under identical external boundary conditions, then the result is the friction mean effective pressure difference maps shown below; **Figure 7.35**.

The variant with the greatest installation clearance, as expected, shows a lower friction mean effective pressure in both operating modes. This is evident in the positive friction mean effective pressure difference.

A significant dependence on speed can be seen in the friction mean effective pressure difference map for the motored externally charged mode, but only a very slight dependence on load is detected.

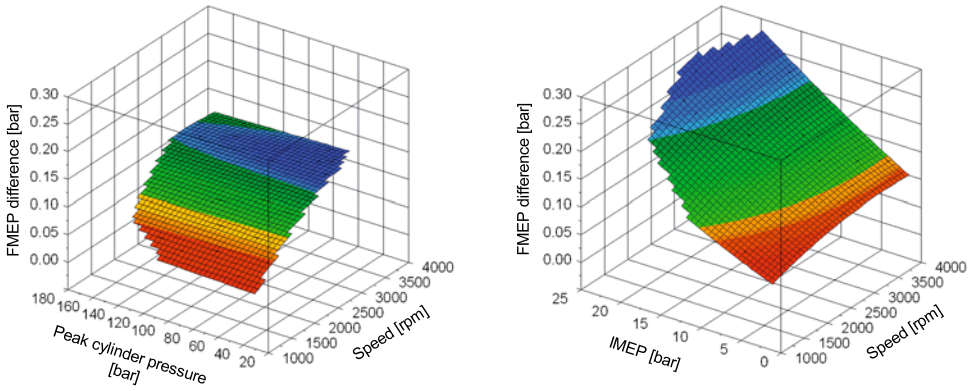

Figure 7.35: Friction mean effective pressure difference maps, different piston installation clearance (17 µm compared to 101 µm), motored externally charged (left) and fired mode (right), engine temperature 100°C

By contrast, a very significant dependence on load is present in the fired mode. With increasing load, i.e., increasing indicated mean effective pressure, increasingly greater advantages are seen for the variant with greater installation clearance.

This difference in the characteristic, especially for increasing load, can be attributed to the fact that the motored externally charged mode has excluded the component temperature from the net effect of the gas pressure on friction, because the piston temperature increases only slightly at peak pressure; **Figure 7.36**. In fired mode, in contrast, this effect due to the gas pressure also has a thermal effect superimposed on it. This is evident in **Figure 7.36** in the significantly greater increase in the piston temperature with increasing load. Therefore, the pistons have different operating clearances at the same peak cylinder pressure in the two different engine operating modes. For the piston with the smaller installation clearance, under increasing load in fired operation, the operating clearance is used up sooner than that of the piston with the greater installation clearance. This leads to the severe increase in friction mean effective pressure difference in fired operation; **Figure 7.35, right**. In the motored externally charged operating mode, this increase does not occur, due to the lesser increase in component temperature; **Figure 7.35, left**.

For the reasons just listed, a motored externally charged friction mean effective pressure difference map is of only limited use in engine optimization for actual driving operation. However, because it can be compared to fired operation, it contributes significantly to the understanding of friction mechanisms, especially for detecting thermal influences. Friction

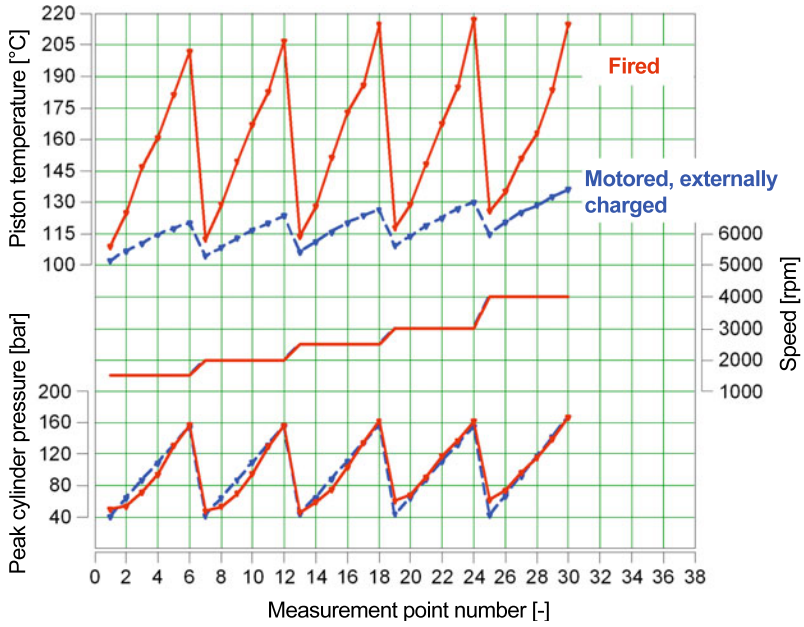

Figure 7.36: Measured piston temperatures (pin boss) for motored externally charged and fired engine operation, with equal peak cylinder pressures

mean effective pressure difference maps for fired operation can be used unconditionally for determining the potential of a change to a parameter in real driving operations.

7.3.3.2 Surface roughness of the piston skirt

In order to test the effect of surface roughness, pistons without skirt coatings were used. This allowed precise adjustment of defined surface parameters. For the piston with a smooth skirt surface, an average roughness of *Ra* = 0.2 µm was selected, and for pistons with a rough skirt surface, it was *Ra* = 2.1 µm. In order to exclude any potential run-in effects, the values indicated were measured after the run.

An increase in the friction mean effective pressure difference, i.e., an improvement in friction mean effective pressure, occurred under increasing load for the variant with the smooth skirt surface; **Figure 7.37**. The cause for this is that a hydrodynamic lubricating film can form more easily on the piston with the smooth skirt surface. This positive effect is more extensive in fired operation, due to the tighter operating clearances caused by the different thermal loading.

Roughness measurements on the skirt surfaces before and after the test show clear run-in effects of the rough piston. The roughness peaks are severely worn away, which give the piston the opportunity to adapt its wear to the distortions in the individual cylinder. For the smooth piston, this effect is definitely lessened, or even undetectable.

For current production pistons with relatively tight installation clearance, the two described effects can be combined by using GRAFAL®. Coating a relatively rough piston skirt with GRAFAL® allows the piston shape to be adapted to the cylinder distortions by wearing off the remaining roughness. At the same time, the supporting area on the shaft smoothes out after just a short run-in period, leading to low frictional losses. In engines with greater clearance design, smoothing coating wear during run-in is undesired. For this reason, the parts,

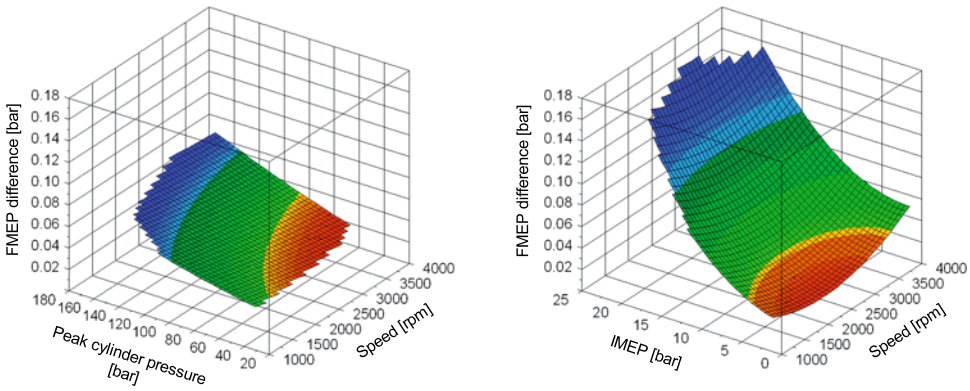

Figure 7.37: Friction mean effective pressure difference maps, different surface roughness of the piston skirt (*Ra* = 2.1 µm compared to *Ra* = 0.2 µm), motored externally charged (left) and fired mode (right), engine temperature 100°C

whose surface is less rough, are applied with a more resistant coating, such as EvoGlide. This is the case in particular for frictional loss optimized engines with reduced cylinder distortions.

7.3.3.3 Piston pin offset

A piston pin offset can be used to affect the secondary movement of the piston, and therefore the formation of a lubricant film on the piston skirt. For this reason, a parameter study was performed with a stepwise change in the offset, from a value of 0.5 mm toward the antithrust side (ATS) to 0.5 mm toward the thrust side (TS).

The results of the comparison of offsets, from 0.5 mm toward the antithrust side and 0.5 mm toward the thrust side, are described below. The *FMEP* difference maps for fired and motored externally charged operation, **Figure 7.38**, yield very different curves. This leads to the conclusion that the piston pin offset is a parameter that is strongly dependent on the component temperature.

In motored externally charged operation, **Figure 7.38 left**, there is a strong dependence of the friction mean effective pressure difference on the peak cylinder pressure at lower speeds. The load dependency decreases as speed increases. The greatest apparent advantage of offsetting in the direction toward the thrust side is seen at low speed and high load.

In actual fired operation, however, **Figure 7.38 right**, a clear dependence on speed can be seen for low loading. The dependence on speed drops off clearly as the load increases. The greatest potential of the thrust-side offset for reducing friction mean effective pressure can be detected at low load and high speed.

Figure 7.39 shows the frictional losses of the four offset variants that were tested, comparing different speeds. The variant with an offset of 0.5 mm toward the thrust side always exhibits

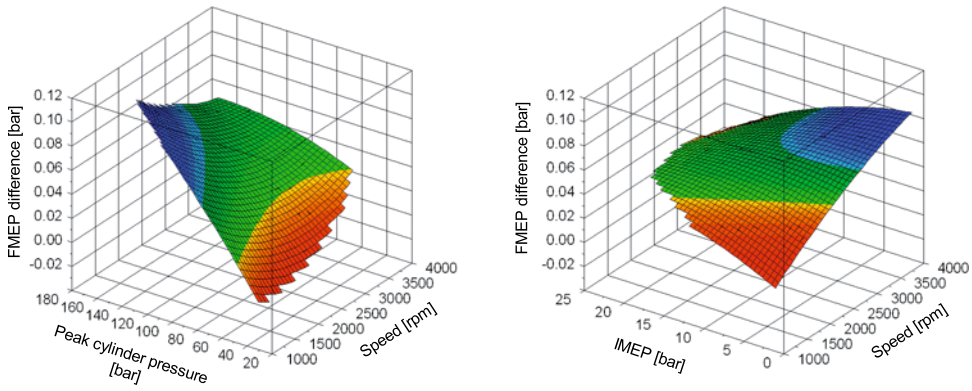

Figure 7.38: Friction mean effective pressure difference maps, different piston pin offset (0.5 mm toward the antithrust side compared to 0.5 mm toward the thrust side), motored externally charged (left) and fired mode (right), engine temperature 100°C

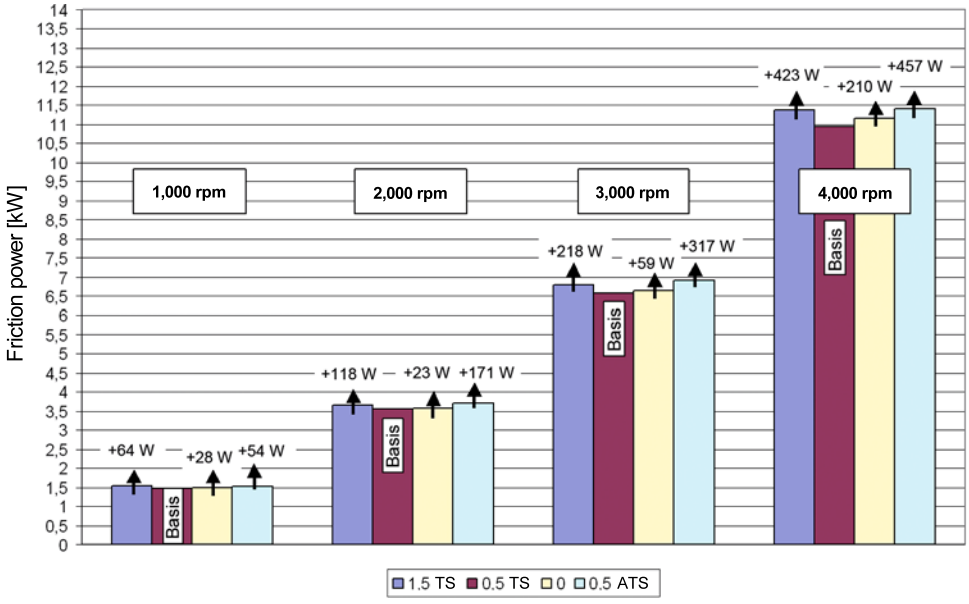

Figure 7.39: Frictional losses for four different offsets, at different speeds and pmi = 10 bar, engine temperature 100°C

the least frictional loss, regardless of the speed. A change in the offset in the direction of the thrust side, or in direction of the antithrust side, causes an increase in frictional loss.

7.3.3.4 Width of the piston ring in groove 1

In order to determine the effect of the width of the compression ring in groove 1 on the friction mean effective pressure, tests were run with piston rings having widths of 1.75 mm and 3.0 mm.

Due to design boundary conditions, the 3.0 mm high ring also had the tangential load increased by 11 N per ring (44 N for the entire engine). This means that these two parameter changes are superimposed in the friction mean effective pressure difference map.

The friction mean effective pressure difference maps, **Figure 7.40**, show an advantage for the 1.75 mm high compression ring, both for motored externally charged operation and for fired engine operation, across all speeds and loads.

The increase in potential savings with increasing speed, even at low loads or maximum pressures, can be attributed to the change in tangential force and was also detected in purely motored experiments.

The load-dependent portion of the friction mean effective pressure difference comes from the increased surface pressure in the contact surface between the ring and the cylinder wall. This increase for the 3.0 mm high compression ring results from the greater inner surface

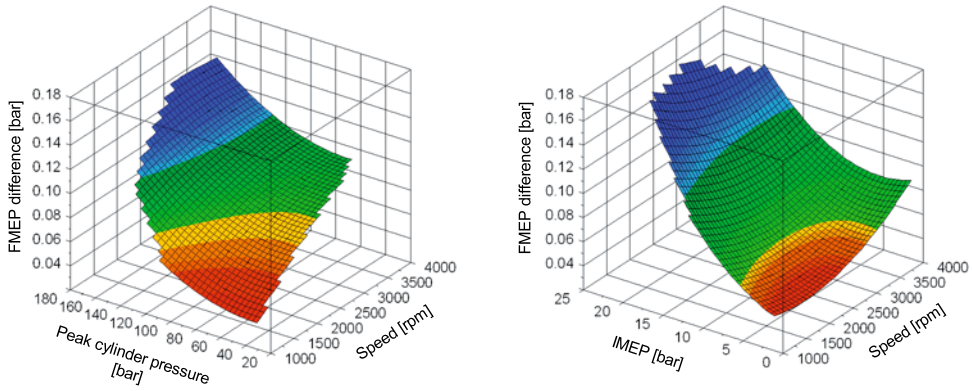

Figure 7.40: Friction mean effective pressure difference maps, different compression ring widths (3.0 mm compared to 1.75 mm), motored externally charged (left) and fired mode (right), engine temperature 100°C

area of the ring at the same gas pressure load behind the ring, compared the 1.75 mm high compression ring, and thus the increasing contact pressure.

Due to this increase in surface pressure, the mixed friction component of the 3.0 mm high compression ring increases under combustion loading. This results in the friction mean effective pressure becoming worse with increasing load.

It is notable that in this variant, the friction mean effective pressure difference maps for motored externally charged operation and for fired operation are very similar in terms of values and curves. This indicates a subordinate effect of the component temperatures–in contrast to the changes to the piston.

In **Figure 7.41**, the difference in friction losses for fired operation at a speed of 2,500 rpm is divided into a portion for the compression ring width and a portion for the tangential load. Measurements with different tangential loads were performed in advance.

7.3.3.5 Tangential load of the oil control ring

Preliminary experiments clarified that if the tangential load is reduced by 18 N per ring (72 N for the entire engine), the engine boundary conditions, such as oil consumption or blow-by, are not significantly affected.

An increase in the friction mean effective pressure difference with increasing speed can be observed for both the motored externally charged mode and the fired operation; **Figure 7.42**. A slight increase in the difference with increasing load is evident only for fired operation.

This characteristic leads to the conclusion that the mechanical load, i.e., the peak cylinder pressure, only slightly affects the potential savings in friction mean effective pressure

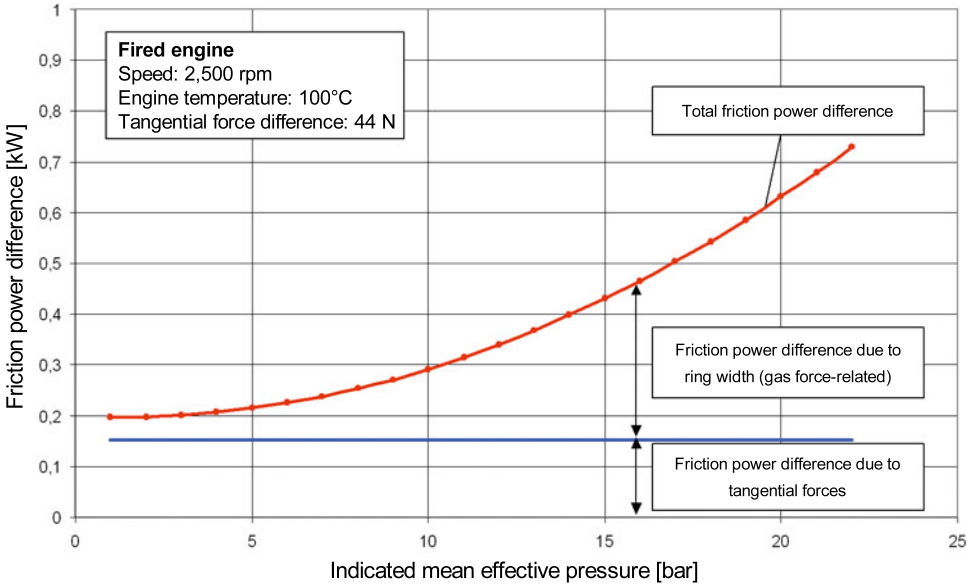

Figure 7.41: Division of the measured friction loss difference into components for ring width and for tangential load for a compression ring, fired engine operation, engine temperature 100°C

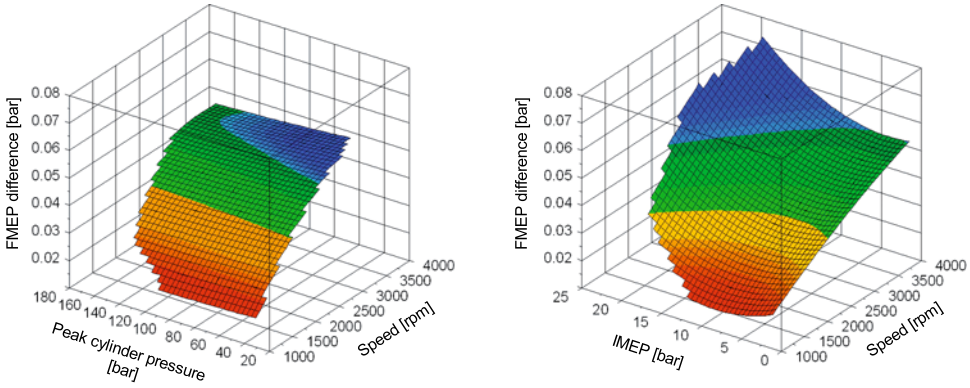

Figure 7.42: Friction mean effective pressure difference maps, reduction in tangential load of the oil control ring by 18 N, motored externally charged operation (left) and fired operation (right), engine temperature 100°C

obtained by reducing the tangential load on the oil control ring. Thermal effects, such as the reduction in operating clearance under increasing load, also exhibit only a subordinate influence. The comparison of the fired friction loss difference map to the results of an approximation formula derived from motored measurements confirms both the value and the nature of this characteristic; **Figure 7.43**.

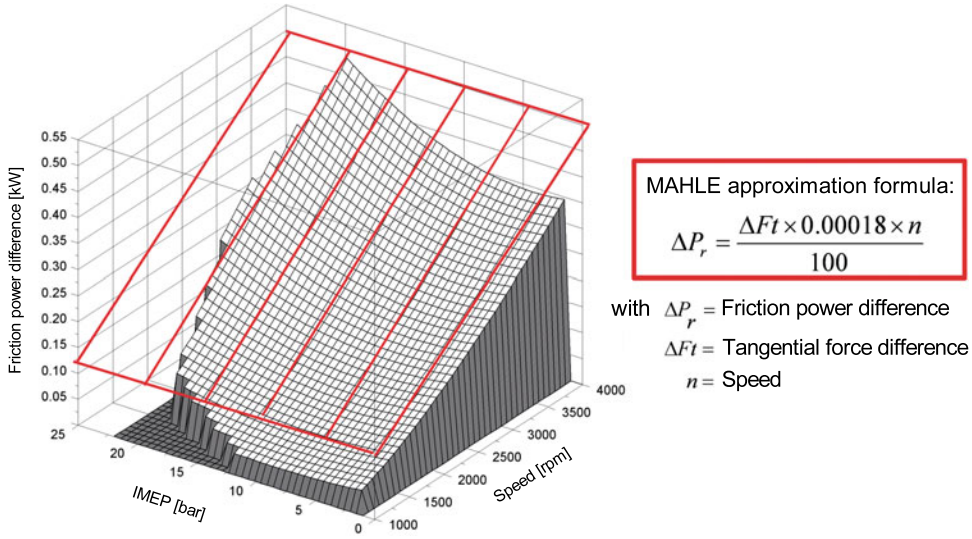

Figure 7.43: Comparison of the friction loss difference map measured in fired mode (black) to the results of the MAHLE approximation formula (red). The tested tangential load difference for the four oil control rings is 72 N for the entire engine, engine temperature 100°C

7.3.3.6 Coating of the piston pin

In **Figure 7.44**, it is interesting to note that the response of the friction mean effective pressure differences relative to increased load is quite different between the motored externally charged mode and fired operation. While the greatest potential is seen at low loads in fired operation, in motored externally charged operation it is found at high peak pressures, i.e., at high loads.

This characteristic indicates that the varying parameter is strongly dependent on the thermal loading of the engine. As is known from the piston temperature measurements, **Figure 7.36**, component temperatures, particularly the piston temperature, increase only slightly with increasing peak pressure in motored externally charged operation. This means that the operating clearance in the pin boss bearing does not change significantly, despite the different thermal expansion coefficients of the piston and pin materials. In fired operation, however, the operating clearance in the boss increases with increasing load. This difference in operating clearance appears to lead to various mixed-friction components, while the superior dry coefficient of friction for DLC can have a greater effect in motored externally charged operation under high loads.

7.3.3.7 Engine oil viscosity

In order to determine the effect of oil viscosity on friction losses, experiments were performed using typical commercial oils of the viscosity classes 10W60 and 5W30.

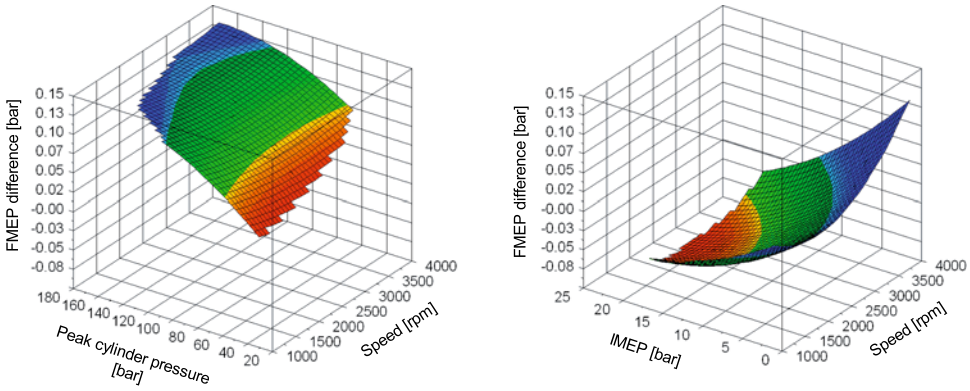

Figure 7.44: Friction mean effective pressure difference maps, piston pin coating (steel compared to DLC), motored externally charged (left) and fired mode (right), engine temperature 100°C

When interpreting the results of experiments with different oils, care must be taken that the oil type is changed not only around the piston group, but throughout all the relevant friction sources in the engine, such as the main bearings and valve train. The changes in the friction mean effective pressure due to changing the oil type, therefore, must not be assigned to only one friction pair.

Low-viscosity oil has a fundamental advantage with regard to frictional loss. This can be seen in that the friction mean effective pressure difference maps, **Figure 7.45**, have a similar advantage in friction mean effective pressure for both motored externally charged operation and fired operation. However, this is expressed quite differently in the characteristic in the operating map. In motored externally charged operation, the greatest advantage of

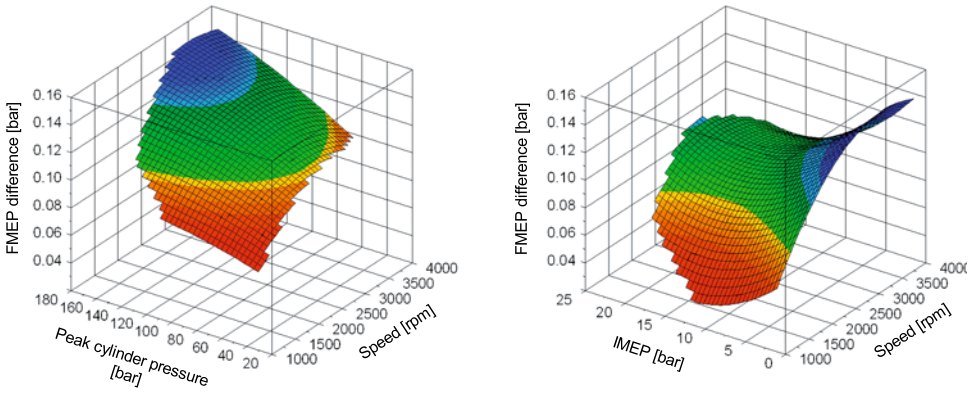

Figure 7.45: Friction mean effective pressure difference maps, different engine oil viscosities, motored externally charged (left) and fired mode (right), engine temperature 100°C

the low-viscosity oil is at high speed and high peak pressure, while in fired operation it is at very low loads. This difference in operating maps may again reflect the effect of the different component temperatures. In fired operation, the operating clearances between the piston and cylinder get smaller and smaller with increasing load, and the load-bearing oil film thickness gets thinner and thinner. The advantage of low-viscosity, thinner oil thus becomes less significant as the load increases; **Figure 7.45**.

These results again show that only experiments under actual engine operating temperatures provide the information that is necessary for optimizing the frictional losses in actual driving operation.

7.3.4 Comparison of results and outlook

The maximum values of the friction mean effective pressure differences to be measured indicate the potential for the parameter change being investigated. A summary of these maximum potentials that can be achieved in the operating map is shown in **Figure 7.46** for some of the investigated parameters. It is evident that the parameters of installation clearance, skirt roughness, piston pin offset, and piston form have, in decreasing order, potential for improving the piston. In the ring pack, the tangential load and the top ring width are influence variables. The oil viscosity also has great potential due to its effects throughout the engine.

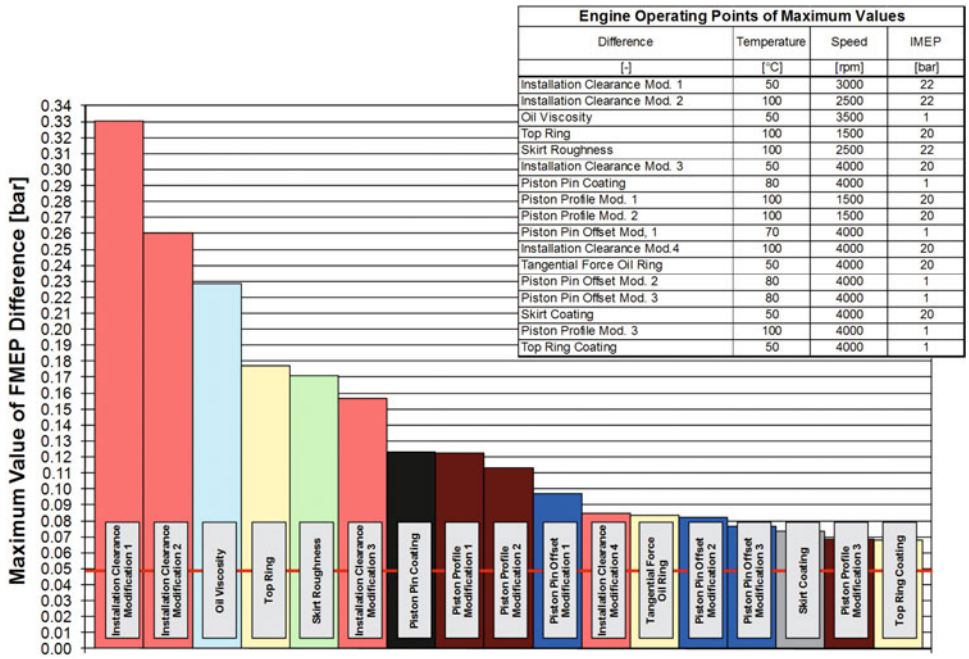

Engine Operating Points of Maximum Values

Difference	Temperature	Speed	IMEP
[-]	[°C]	[rpm]	[bar]
Installation Clearance Mod. 1	50	3000	22
Installation Clearance Mod. 2	100	2500	22
Oil Viscosity	50	3500	1
Top Ring	100	1500	20
Skirt Roughness	100	2500	22
Installation Clearance Mod. 3	50	4000	20
Piston Pin Coating	80	4000	1
Piston Profile Mod. 1	100	1500	20
Piston Profile Mod. 2	100	1500	20
Piston Pin Offset Mod. 1	70	4000	1
Installation Clearance Mod.4	100	4000	20
Tangential Force Oil Ring	50	4000	20
Piston Pin Offset Mod. 2	80	4000	1
Piston Pin Offset Mod. 3	80	4000	1
Skirt Coating	50	4000	20
Piston Profile Mod. 3	100	4000	1
Top Ring Coating	50	4000	1

Figure 7.46: Friction mean effective pressure potential due to varying different design parameters for the piston group of the tested 2.0-liter four-cylinder diesel engine

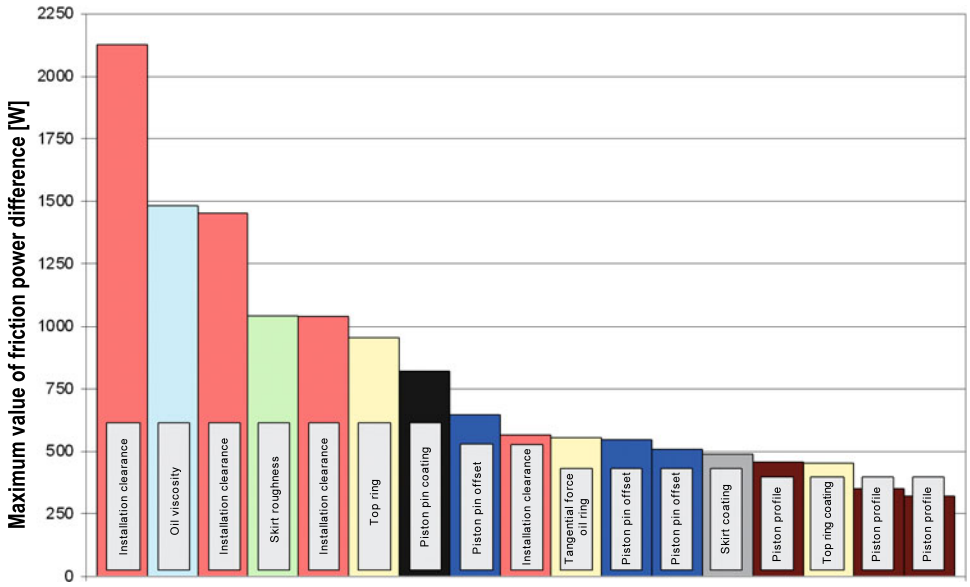

Figure 7.47: Frictional loss potentials due to varying different design parameters of the piston group of the tested 2.0-liter, four-cylinder diesel engine (n = 4,000 rpm, various loads, various temperatures)

Converting the friction mean effective pressure differences into frictional loss differences yields the ranking shown in **Figure 7.47**. Because there are interactions between different variants, the superposition of individual measures is only somewhat accurate. In order to obtain an estimate of the entire frictional loss potential for the piston group, this must be taken into consideration. In the four-cylinder diesel engine used here, for a speed of 4,000 rpm and power output of about 100 kW, the findings indicate that there is a potential for improving the piston group to save about 3,500 watts.

In order to allow the measures for various engine concepts and load spectrums to be assigned and optimally combined, the engine operating map is divided into four quadrants, each of which has typical operating conditions for various engine concepts. An internal ranking of the measures is generated for each quadrant; **Figure 7.48**.

For low loads, the oil viscosity is the dominant influence factor. The piston installation clearance, however, is the most significant design measure. The effects of skirt roughness, piston pin offset, tangential load of the oil ring, and measures for the top ring are considered to be about equal.

In the high-load range, the oil viscosity loses significance. Installation clearance, however, is still the most critical design parameter here. Optimization measures on the top ring and the skirt surface also increase in significance at higher loads.

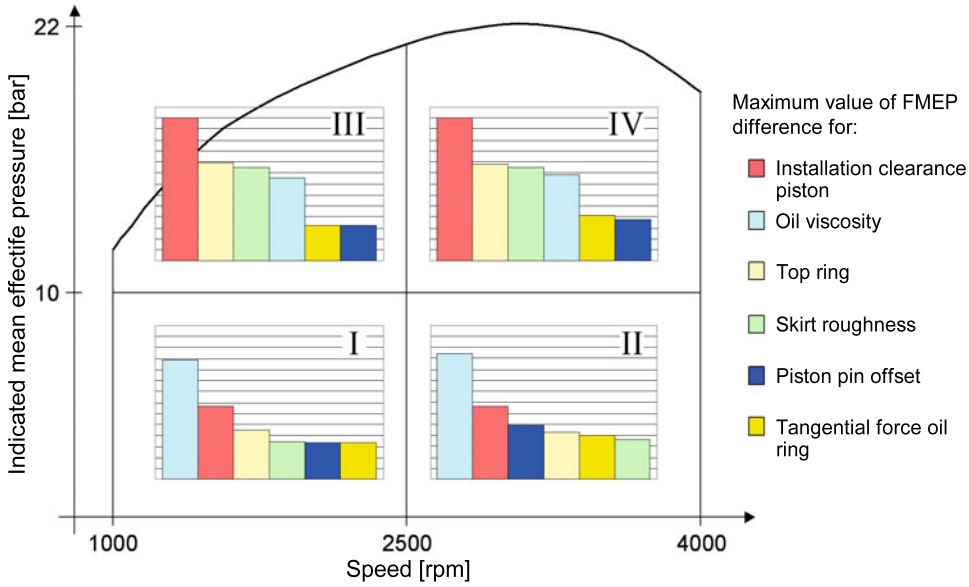

Figure 7.48: Quadrant ranking of the frictional loss results obtained (fired), where
Diagram I: relevant to the cycle,
Diagram II: representative for gasoline engines,
Diagram III: representative for commercial vehicle diesel engines,
Diagram IV: representative for passenger car diesel engines.

In motored externally charged operation, the effects of peak cylinder pressure can be investigated without the overlay of thermal influences. **Figure 7.49** shows the corresponding quadrant rankings for motored externally charged operation. It is evident that the sequence of the individual parameters has changed in comparison to fired operation. Oil viscosity is the dominant influence factor for all operating ranges in motored externally charged operation. Pin bore offset increases in significance across all operating map areas, while piston installation clearance decreases. This change in the rankings can be attributed to the lack of heat input and the related increase in piston operating clearances.

The test bench and systematic investigations of individual design parameters, as shown, allow an extensive array of measures for minimizing friction to be developed. Together with an evaluation of the specific operating ranges, they allow the minimization of friction losses to be targeted to a specific engine concept.

The ultimate evaluation of the individual potentials, however, will only be possible with the use of a driving cycle computational program and the derived friction mean effective pressure difference maps. They can be used to make a future statement about the probable fuel savings that can be achieved in the driving cycle for the investigated parameters; **Figure 7.50**.

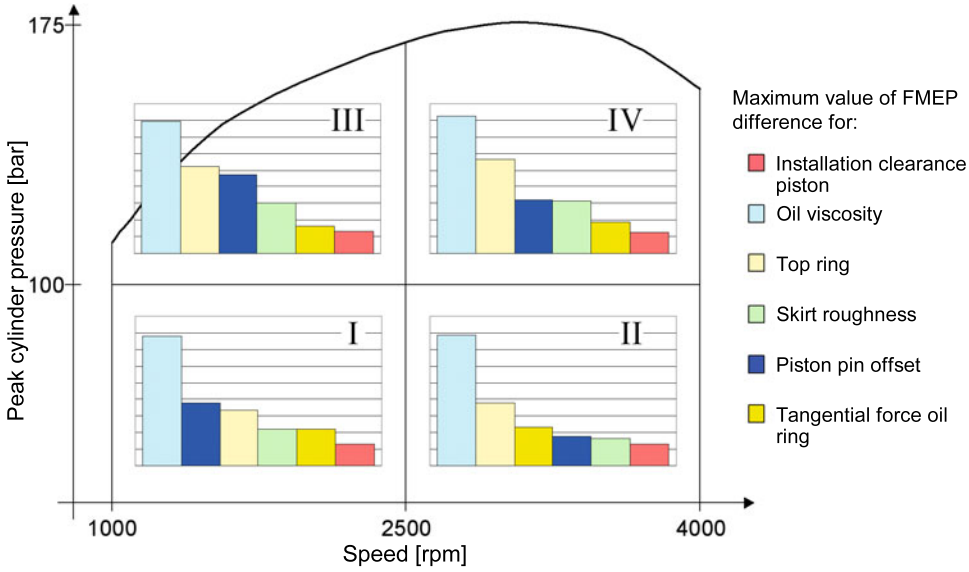

Figure 7.49: Quadrant ranking of the frictional loss results obtained (motored externally charged), where
Diagram I: relevant to the cycle,
Diagram II: representative for gasoline engines,
Diagram III: representative for commercial vehicle diesel engines,
Diagram IV: representative for passenger car diesel engines.

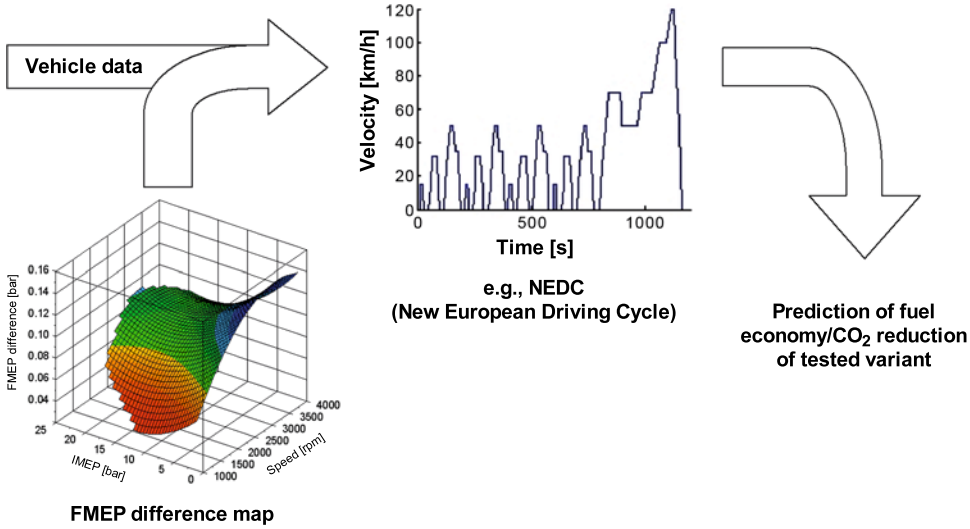

Figure 7.50: Calculating fuel savings and reduction in CO_2 in a driving cycle, using a friction mean effective pressure difference map

7.4 Wear testing of the piston group

This article addresses wear in the context of the piston group. The affected components are:

- Pistons
- Piston rings
- Piston pins
- Locking rings
- Cylinder surfaces

7.4.1 Piston skirt

7.4.1.1 Skirt collapse and coating wear

In order to be able to detect skirt collapse and wear of a piston skirt coating (such as GRAFAL®) that may occur during operation, the shape of the generating line of the piston is charted.

Figure 7.51 shows a passenger car diesel piston that has been run, with the surface of the skirt being coated with GRAFAL®. **Figure 7.52** shows the result of the measurement of the generating line of a new, unused piston, where the second ring land is set back so far that it does not appear in this view. The smaller diameter of the first ring land in the pin axis is due to the specified ovality of the piston shape.

At the level of the diameters D_N and D_1, the measured curve for the unused piston shows the recesses in the GRAFAL® coating on the skirt. The base piston material can be accessed at these locations in order to take the measurements. These windows can also be seen on the used piston in **Figure 7.51**. The thickness of the GRAFAL® coating is about 20 µm radially in the new condition. **Figure 7.53** shows the result of measuring the generating line of the used piston.

Figure 7.51:
Piston with GRAFAL® coating, with recesses for measuring the skirt profile

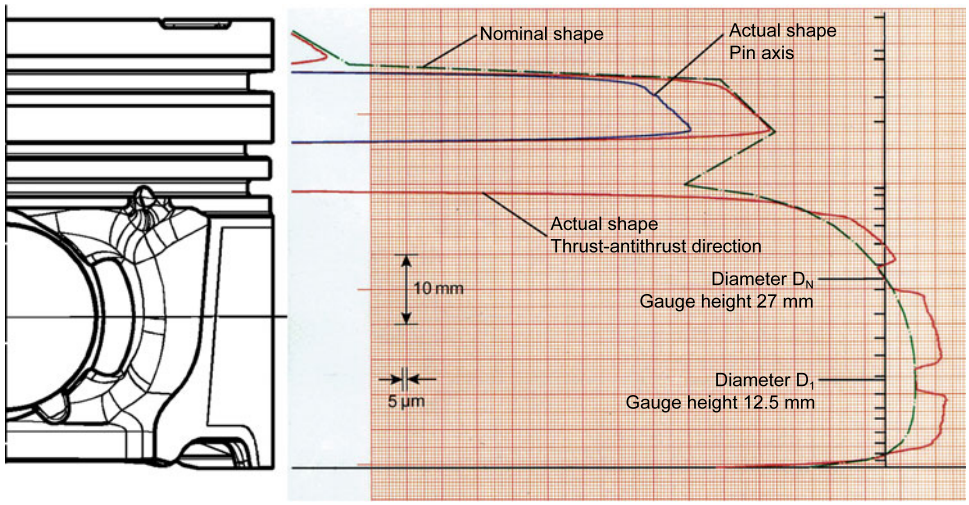

Figure 7.52: Results of measuring a new, unused piston. Measurement results apply diametrically.
D_N: Nominal piston diameter
D_1: Largest diameter of the piston
Green: Nominal shape of the generating line in the thrust-antithrust direction
Red: Measured curve in the thrust-antithrust direction
Blue: Measured curve in the pin axis

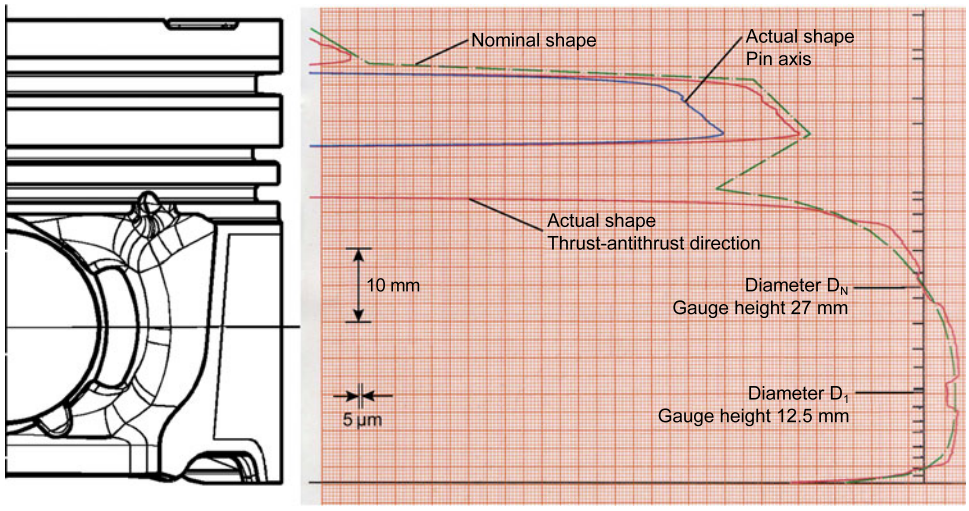

Figure 7.53: Results of measuring a used piston. Measurement results apply diametrically.
D_N: Nominal piston diameter
D_1: Largest diameter of the piston
Green: Nominal shape of the generating line in the thrust-antithrust direction
Red: Measured curve in the thrust-antithrust direction
Blue: Measured curve in the pin axis

According to this example, the skirt collapse is approximately 10 µm diametrically at the level of the diameter D_1. This cannot be attributed to wear at this location, because the measuring point is within the GRAFAL® window and therefore is not exposed to wear. At the same time, the GRAFAL® coating at this location has been ablated by 20 µm diametrically, or 10 µm radially.

7.4.1.2 Ovality

Another way to show and evaluate potential deformation of the piston skirt and potential coating wear is to record the ovality at prescribed heights on the skirt, according to **Figure 7.54**. This allows the circumferential deviations of the real piston shape from the nominal shape to be evaluated (ovality and shape distortion).

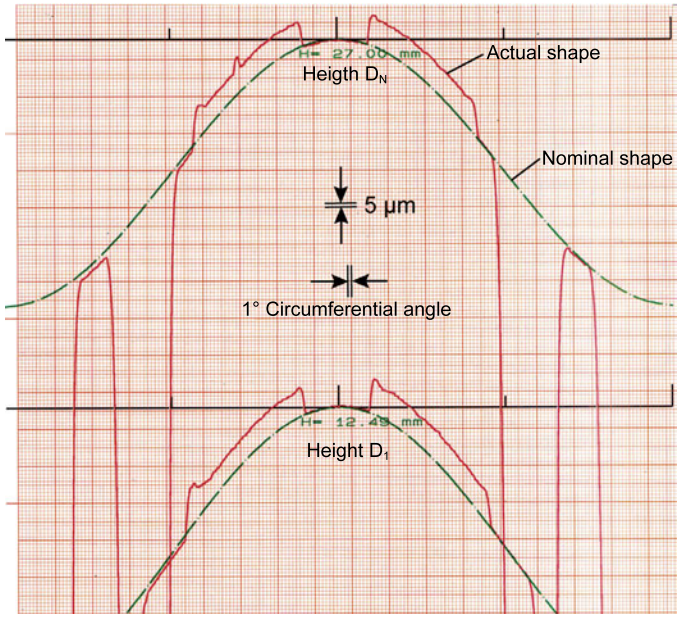

Figure 7.54: Ovality record around the circumference of the piston in new, unused condition

The values of diameters D_N and D_1 serve as reference dimensions for such ovality records, shown as a flat projection.

Similar to the representation of the generating lines, here again the skirt collapse can be measured as 10 µm diametrically at the level of diameter D_1, and the thickness of the GRAFAL® coating as about 10 µm radially.

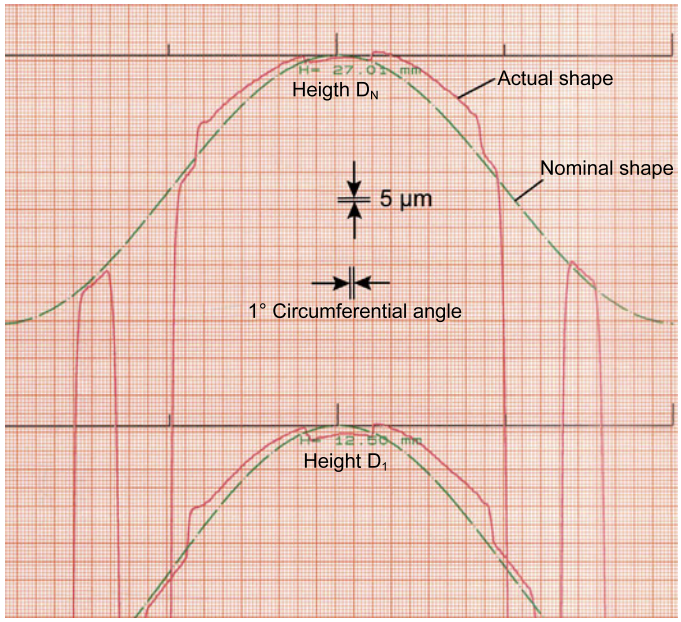

Figure 7.55:
Ovality record around the circumference of the piston in used condition in order to determine deformation and wear of coating

7.4.2 Piston ring and cylinder surface

7.4.2.1 Piston ring running surface

In order to fulfill its function, the piston ring exerts a defined radial force on the cylinder surface, acting perpendicular to it. To define it, a band encompassing the piston ring is contracted so far that the prescribed gap clearance is achieved. The necessary force to contract the band–called tangential load–is measured. The tangential load of the piston rings is directly related to friction and wear.

The gas pressure also acts on the back side of the compression rings and presses them against the cylinder surface. Due to the high gas pressure load under load conditions, the 1st piston ring is most affected. This increase in radial force leads to severe loading of the running surface of the compression rings, particularly in the top dead center (TDC) area. Another difficulty is that the piston briefly stops moving at the dead center point, causing the hydrodynamic pressure in the lubrication wedge between the two wear partners to drop and leading to metallic contact.

Figure 7.56 shows the profile of the piston ring in its new, unused condition (top), after a period of running (center), and both in direct comparison (bottom). Wear can be clearly detected in

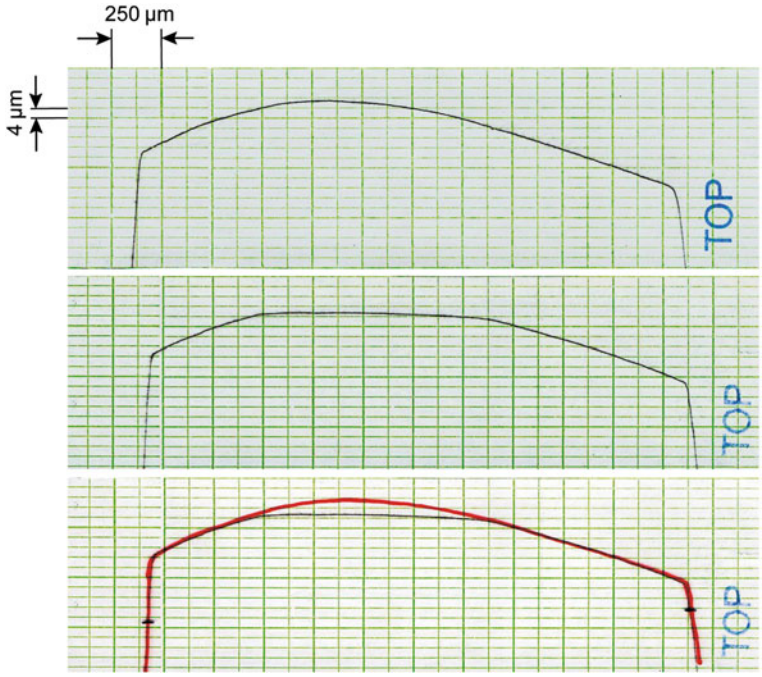

Figure 7.56: Shape measurement of 1st piston ring with an asymmetrical, barrel-shaped running surface
Top: New, unused condition
Center: Used condition
Bottom: Direct comparison

the area of the greatest barrel shape. This wear can also be verified by measuring the radial wall thickness of the piston ring and is typically in the range of a few microns, depending on the running period. The consequences of such wear are increased gap clearance and a reduction in the tangential load of the piston ring. There is a direct relationship between the increase in gap clearance and the decrease in radial wall thickness, **Figure 7.57**.

If the radial wall thickness of the piston ring is reduced, it will result in the ring gap being opened up. Because this causes the ring to relax, the tangential load also decreases. The type of wear described here can therefore also change the engine operating parameters, such as blow-by and oil consumption.

For compression rings that do not exhibit extensive barrel shape, chamfering, or other measures that define a contact point of the running surface on the cylinder, this can lead to so-called “double contact.” This results in two different running levels at different heights on the ring running surface, due in part to the twisting of the ring and in part to the flat contact under peak cylinder pressure. In the interest of good sealing and oil control, however, a defined running level is generally aimed at.

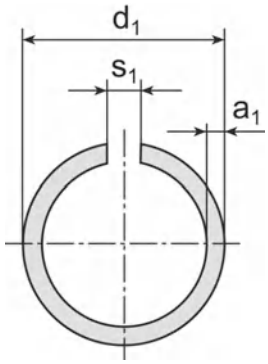

Figure 7.57: Dimensioning of a piston ring according to DIN ISO 6621 Part 1
s_1 = gap clearance
a_1 = radial wall thickness
d_1 = nominal diameter of the piston ring

7.4.2.2 Cylinder surface

The greatest wear on the cylinder surface caused by the piston ring occurs in the running area around the top dead center (TDC). This wear pattern, which is evident from the cylinder measurement as a locally limited area with an above-average increase in diameter at the reversal point of the 1st piston ring, is known as top dead center wear. **Figure 7.58** shows the shape record of the cylinder opposite the pin axis, clearly showing the top dead center wear.

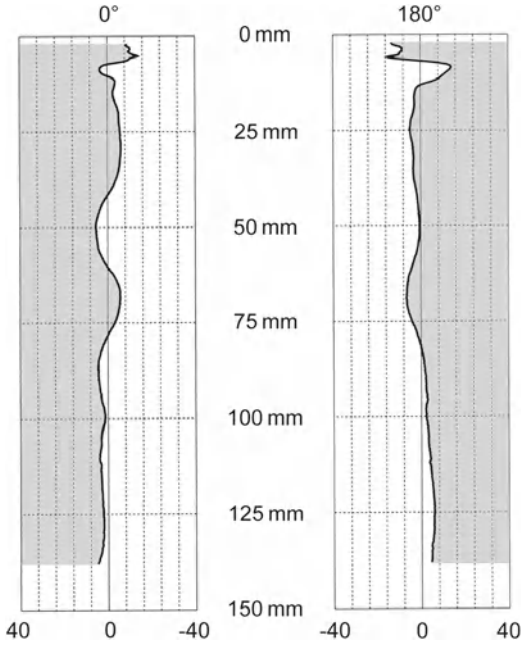

Figure 7.58:
Measurement record of vertical cylinder generating lines in the pin axis. The shape of the cylinder surface is shown greatly exaggerated due to magnification.

7.4.2.3 Coil springs

Coil springs are used to support so-called two-piece oil control rings. After long running periods, it is possible for the ends of the oil control ring to dig into the coil-supported oil control ring; **Figure 7.59**.

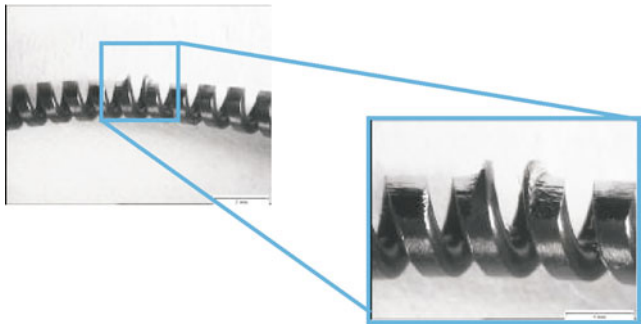

Figure 7.59:
So-called burial in the coil-supported oil control ring, caused by the ends of the oil control ring

7.4.2.4 Abnormal wear patterns

Figure 7.60 shows an example of a piston ring with extreme wear on the running surface, where the radial wall thickness has been partially severely reduced diametrically opposite the ring gap. The oil control rings shown in **Figure 7.61** also exhibit extreme wear on the running surface. The uppermost ring has no scraping edge left at all.

Abnormal wear rates, as shown here, can typically be attributed to abrasive particles in the intake air, due to a missing air filter element, for example. The associated running surfaces of the cylinder liners have a matte gray appearance in such cases, typically with many fine grooves in the direction of the stroke.

Figure 7.60:
Example of extreme single-sided wear of 1st piston ring

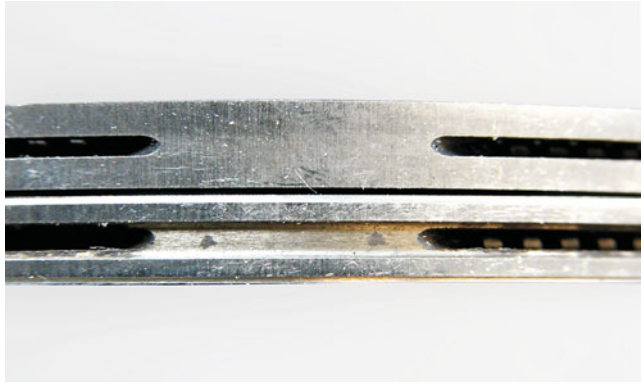

Figure 7.61:
Example of extreme wear of two oil control rings

7.4.3 Piston ring side face and piston ring groove

Similar to the wear on the running surface, the relative motion between the piston ring and the piston can cause a loss of material, both at the side faces of the piston rings and at those of the 1st piston ring groove.

7.4.3.1 Side faces of the 1st piston ring

Wear occurs particularly at the bottom side of the piston ring. **Figure 7.62** shows the shape record of the top and bottom sides of the 1st piston ring in new condition. The slight roof-like slope of the ring side faces indicates that this piston ring has a slight negative twist.

Figure 7.63 shows the shape record of the 1st piston ring shown above, after its use in an engine. A clear wear zone has formed on the bottom side of the piston ring, on the side facing the running surface of the cylinder liner. The depth of this burial is typically in the range of a few microns.

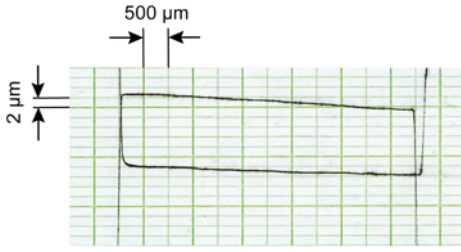

Figure 7.62: Shape record of the top and bottom sides of 1st piston ring in new condition (under tension). The vertical spacing of the two records is arbitrary and does not represent the actual ring height.

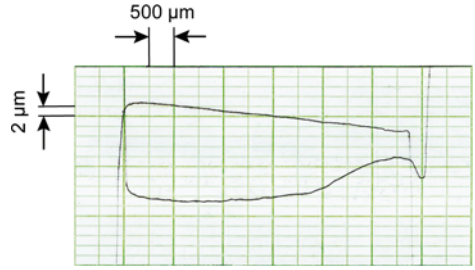

Figure 7.63: Wear on the bottom side of used 1st piston ring (under tension). The vertical spacing of the two records is arbitrary and does not represent the actual ring height.

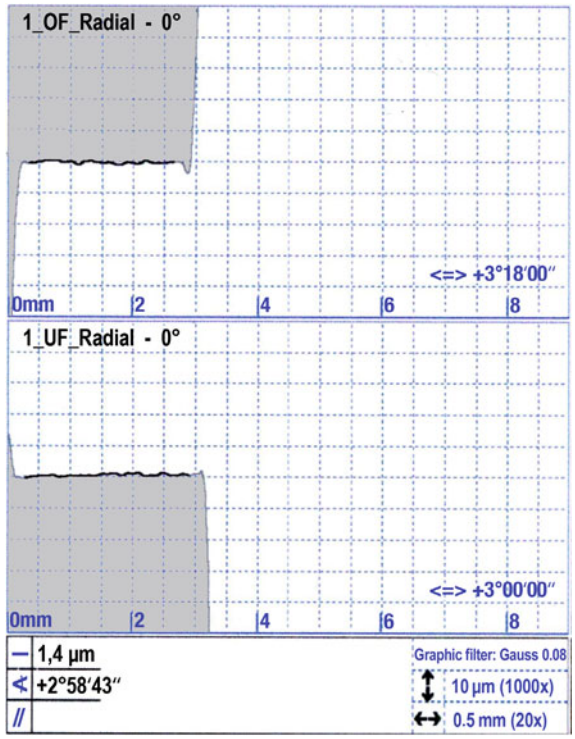

Figure 7.64:
Measurement record of the side faces of a keystone groove in new condition. The nominal angle that is preset for measurement probing is noted on the measurement sheet.

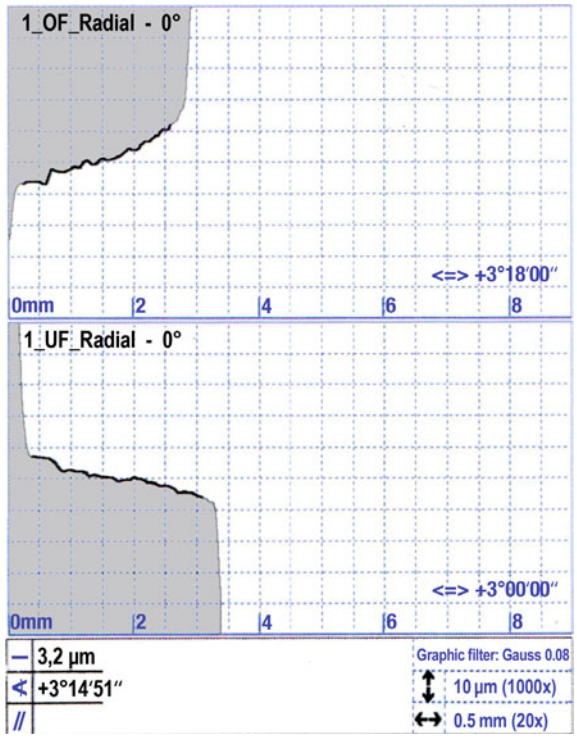

Figure 7.65:
Measurement record of the side faces of a keystone groove in used condition. The nominal angle that is preset for measurement probing is noted on the measurement sheet.

7.4.3.2 Side faces of the 1st piston ring groove

The bottom side of the 1st piston ring groove is particularly highly stressed. The results of a test on a piston with keystone ring are shown here as an example.

Figure 7.64 shows the result of a measurement of the side faces of the keystone groove in new condition. In order to capture the measurement record, the groove side faces are tilted by the nominal angle, so that the shape record of the groove side faces does not deviate from the horizontal on the measurement sheet if the inclination is correct.

Figure 7.65 shows the profile of the groove side faces in used condition. The deviations due to wear are once again in the range of a few microns.

7.4.4 Piston pin and pin boss

7.4.4.1 Piston pin

The piston pin transmits the force due to the combustion chamber pressure from the piston to the connecting rod, and thus enables the necessary relative motion between piston and small end bore due to the movement of the connecting rod. According to the effective forces, the piston pin is deformed within its elastic range by bending and ovalization. Wear also occurs at the affected contact surfaces due to relative motion, though this wear is typically low.

A corresponding measurement result for the piston pin is shown in **Figure 7.66**. The orientation of the degree scale is arbitrary. There is no reference to the installed orientation of the pin in the boss, because the pin typically rotates during operation.

In new condition, piston pins are nearly perfectly round and cylindrical. As is evident in the measurement record, the piston pin shows permanent ovalization in the used condition.

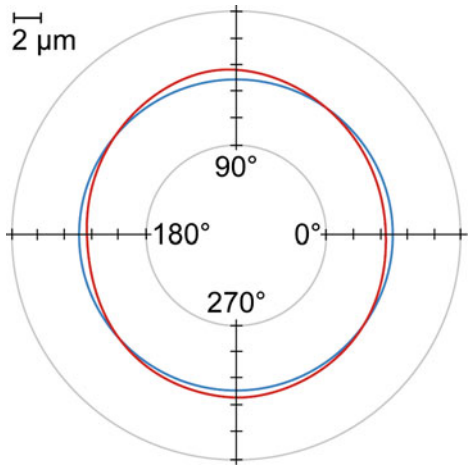

Figure 7.66:
Measurement results of roundness of piston pin in used condition.
Blue: target form
Red: actual form

Residual bending, in turn, is evident from the generation line measurements in **Figure 7.67** and **Figure 7.68**. Also evident in the area of the generating line at 180° is a significantly different wear pattern than with the other measured generating lines. This shows, without a doubt, that the pin was no longer turning for some time prior to being removed. The wear pattern would otherwise have the same structure at every point around the circumference.

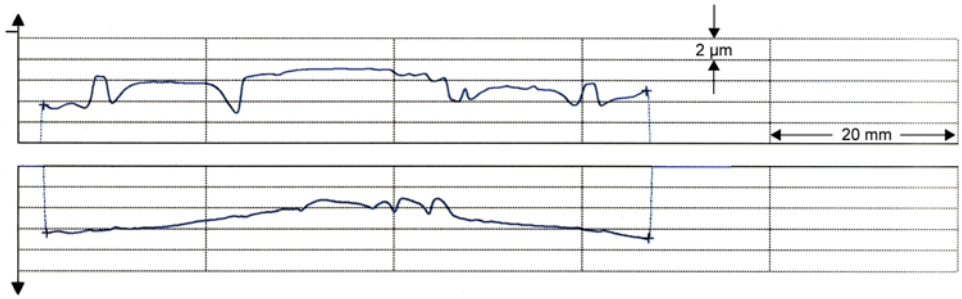

Figure 7.67: Measurement results of the generating line measurement of a piston pin in used condition, in the direction of 0°–180°
Above: Generating line at 180°
Below: Generating line at 0°

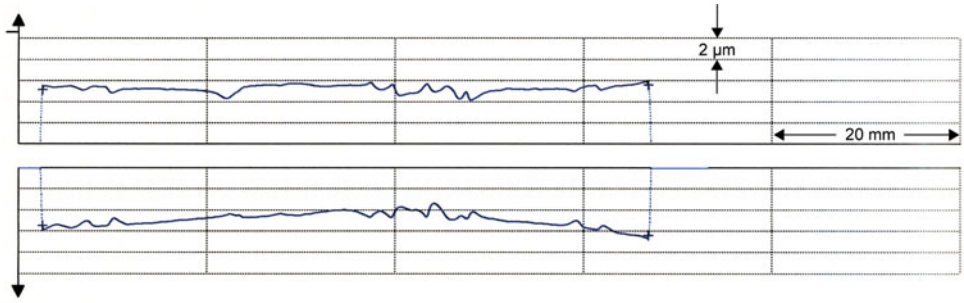

Figure 7.68: Measurement results of the generating line measurement of a piston pin in used condition, in the direction of 90°–270°
Above: Generating line at 270°
Below: Generating line at 90°

The individual contact zones on the pin can be seen in **Figure 7.69**. The engagement area of the small end of the connecting rod is located in the center. A narrow range with no contact can be seen to the right and left. The brownish circumferential stripes are due to oil varnish build-up. The two ends of the pin are located in the pin boss.

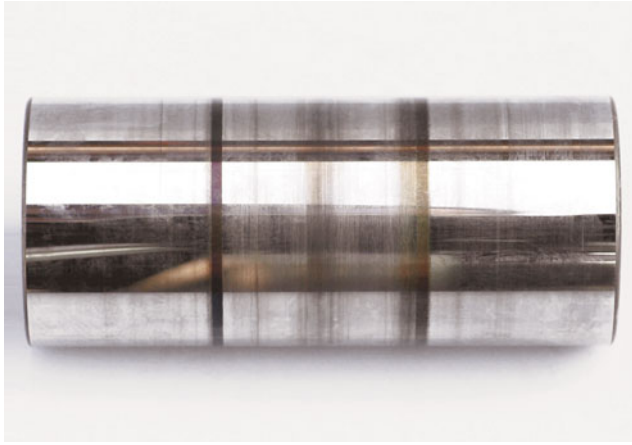

Figure 7.69:
Photo of used piston pin

7.4.4.2 Pin boss

The dynamic deformation of the piston and the bending of the pin that occur at peak cylinder pressure change the shape and the alignment of the pin bore. For this reason, pin bores are often designed as so-called shaped pin bores. They deliberately deviate from a precise cylindrical shape and extend the diameter toward the ends of the bore (crowning). This can be done both internally and externally on the pin bore, in order to prevent an increase in local wear. **Figure 7.70** shows the dimensions of the support points of such a shaped pin bore.

The values B and C indicated in **Figure 7.70** define the important node points for manufacturing and measuring the crown.

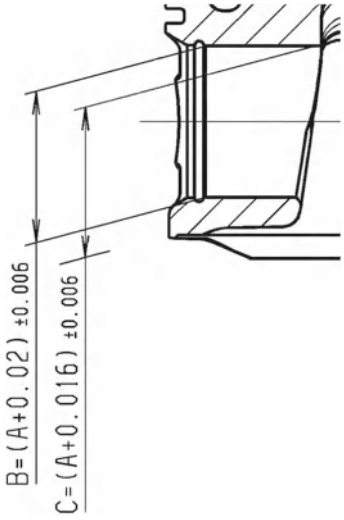

Figure 7.70:
Dimensions of support points of a shaped pin bore with crowning

A: Nominal diameter of the crowned pin bore
B: Definition of the support dimension of the pin bore in the indicated area, important for machining
C: Definition of the support dimension of the pin bore at the inner extension of the pin bore, important for machining

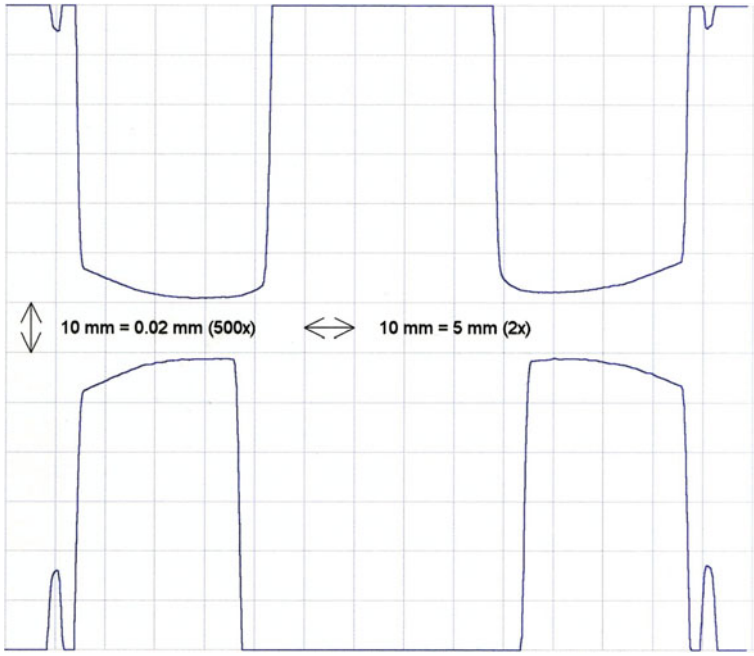

Figure 7.71: Measurement of the form bore of a pin boss in new condition

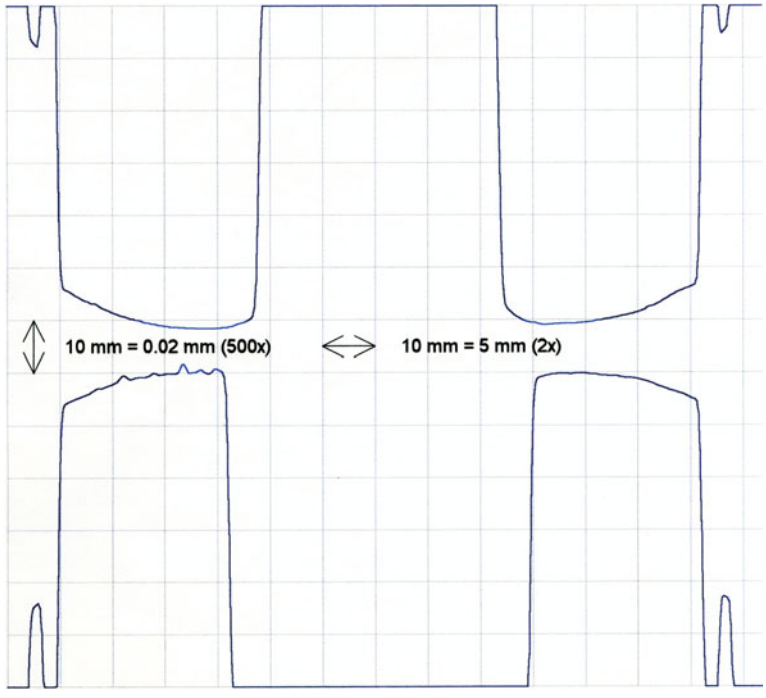

Figure 7.72: Measurement of the form bore of a pin boss in used condition

Figure 7.71 shows the measurement of the shape of the pin bore of an unused piston. The inner and outer areas of the bores exhibit a defined crown.

The measurement of a pin bore of a used piston in **Figure 7.72** shows that the bore shape has not changed significantly, even after a long running period.

7.4.5 Locking ring and locking ring groove

The task of the locking ring is to limit the motion of the piston pin in the axial direction in the piston. Theoretically, there are no axial forces acting on the piston pin in a symmetrically designed crank mechanism. Any type of asymmetry, however, such as a tilt in the orientation of the piston bore or the connecting rod end, or due to shifting of the conrod shaft, can give rise to an axial force component. The associated motion behavior of the connecting rod in the longitudinal axis of the engine can lead to what is known as pin displacement. In some cases, wear and even damage can occur in the area of the locking ring groove.

Figure 7.73 shows the dimensions of a locking ring groove in an excerpt from a piston drawing.

In the simplest case, the associated locking ring consists of an annular, bent spring steel wire with a round cross section and a diameter that is slightly less than the groove width.

Figure 7.74 shows a cross section through the locking ring groove according to **Figure 7.73**, which is widened significantly due to the axial forces acting on the piston pin. The dashed-line

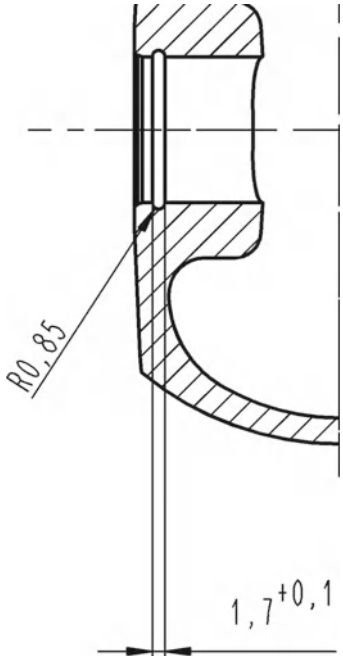

Figure 7.73:
Dimensions of locking ring groove

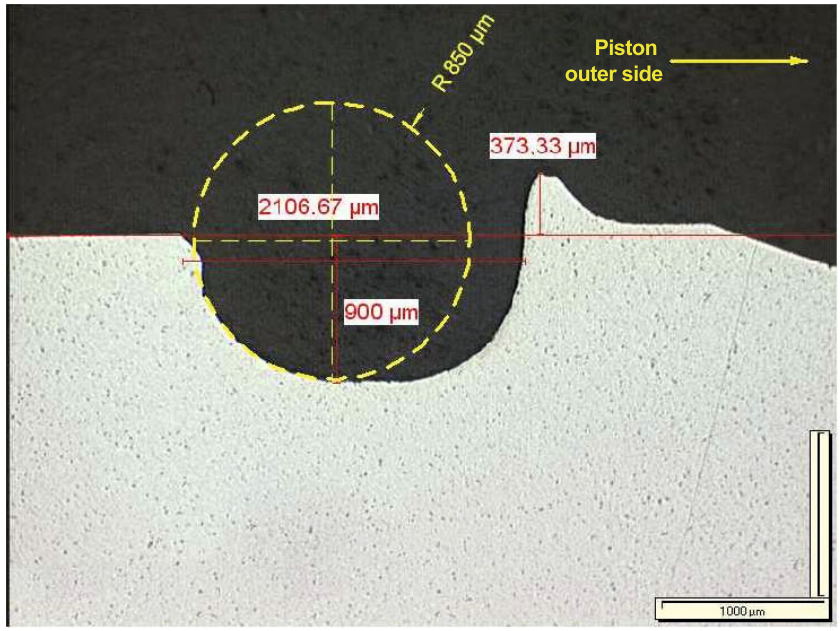

Figure 7.74: Cross section through locking ring groove

circle shows the original machining radius and location. The locking ring groove is plastically deformed in the outward piston direction by the locking ring, which is under load, to a width of over 2 mm. The deformation can also be seen in the material that is built up above the right side face.

7.4.6 Carbon build-up and cylinder polishing

Under unfavorable operating conditions, hard and abrasive carbon can build up on the top land of the piston. **Figure 7.75** shows the top land of a piston, with hard carbon in a locally limited area.

The influence of this local carbon build-up on the associated cylinder surface is shown in **Figure 7.76**. The cylinder surface has already been damaged by the carbon in this case. In the area of the top dead center (TDC) of the top land, the honing has been partially worn off. Directly below that, within the running range of the piston rings, another so-called polish site can be detected.

The task of the honing, which is to retain lubricating oil and to ensure lubrication between the piston ring and cylinder surface, particularly at TDC, can no longer be ensured at these locations. The consequences are local disturbances in the tribological system of the piston

Figure 7.75: Carbon build-up on the top land of a commercial vehicle piston

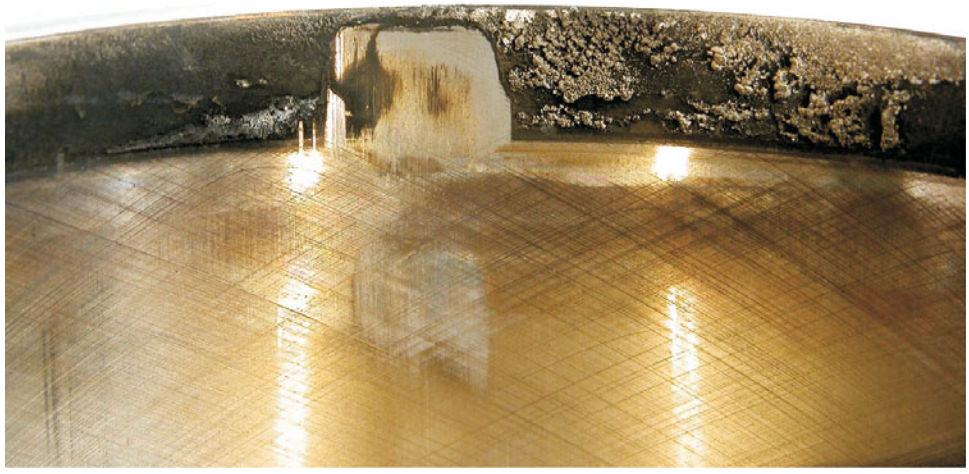

Figure 7.76: Cylinder area polished by the build-up of carbon on the top land

ring and cylinder surface. This causes a risk of burning marks on the piston ring running surfaces, and therefore also a risk of piston ring seizure.

With suitable design measures, the build-up of carbon on the top land, and thus the occurrence of such cylinder polishing, can be specifically prevented.

7.5 Piston stress due to knocking combustion

In the context of more severe exhaust gas legislation, with simultaneous demand for improved fuel consumption, modern gasoline engines increasingly reach the limits of thermal and mechanical load capacity. Downsizing, greater compression, and optimized combustion lead to higher stress. The components in the combustion chamber are particularly affected.

Specific power output, also an indicator of engine stress, has increased significantly in recent years. **Figure 7.77** shows trends in the development of gasoline engines over the last 30 years.

The use of exhaust gas turbochargers is unavoidable in the development of downsizing engines. There is also a trend toward increasing compression ratios and charge-air pressures in turbocharged engines. The level of compression in gasoline engines is limited by the occurrence of knocking combustion. In knocking combustion, the unburned residual mixture after regular combustion self-ignites due to the increase in pressure and high local temperatures. This unburned residual mixture combusts explosively in the local area, i.e., at a very high velocity. The resulting rapid local pressure increase causes pressure waves that propagate through the combustion chamber at sound velocity. This overlapping gas pressure load can cause mechanical damage to the components that bound the combustion chamber.

A high compression ratio enables optimized consumption values in the partial-load range, but requires additional measures in the full-load range, such as dynamic retardation of the

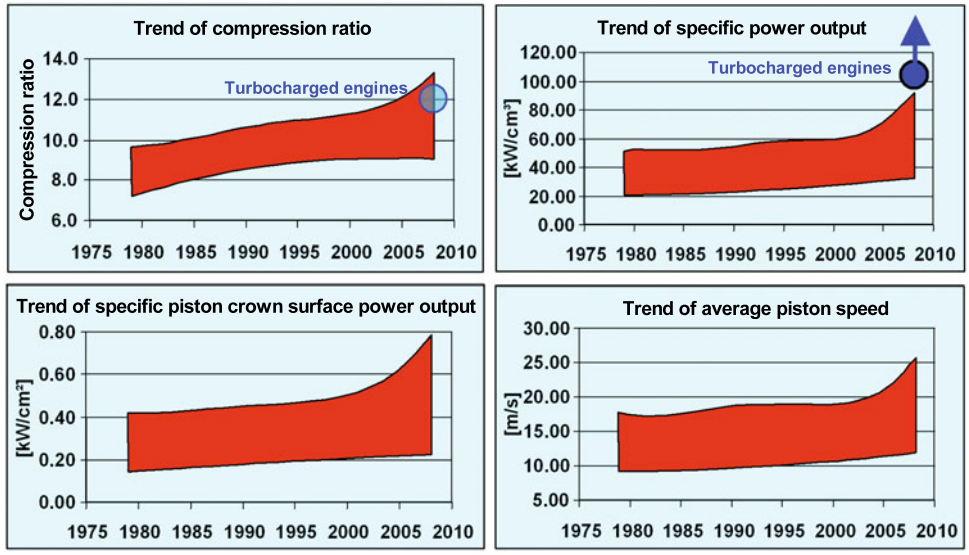

Figure 7.77: Trends of engine key parameters for gasoline engines

ignition angle through knock control systems. Modern gauging methods, such as the MAHLE KI meter [11], can help with tuning these systems.

7.5.1 Knock damage and damage evaluation

Figure 7.78 shows knock damage on the top land and in the 1st piston ring groove. The erosion damage on the top land shows that knocking combustion has occurred here over a long period of time.

The shape measurement of the 1st piston ring groove, shown in flat projection, shows significant local wear on the top and bottom sides. This is known as “pound out” of the piston ring groove. During knocking combustion, the 1st piston ring is excited by the high pressure amplitudes such that plastic deformation of the piston material occurs at the top and bottom sides.

The greatest widening of the groove often exhibits areas of outward deformation as well, which can make contact with the cylinder wall. This pound out of the groove due to knocking combustion is also sometimes seen without the erosion damage to the top land that is typical of knocking. It can occur over a relative short running period due to singular high knock amplitudes. This damage is mechanical in nature. The component temperatures are in an uncritical range, according to measurements. The fact that this damage is of mechanical

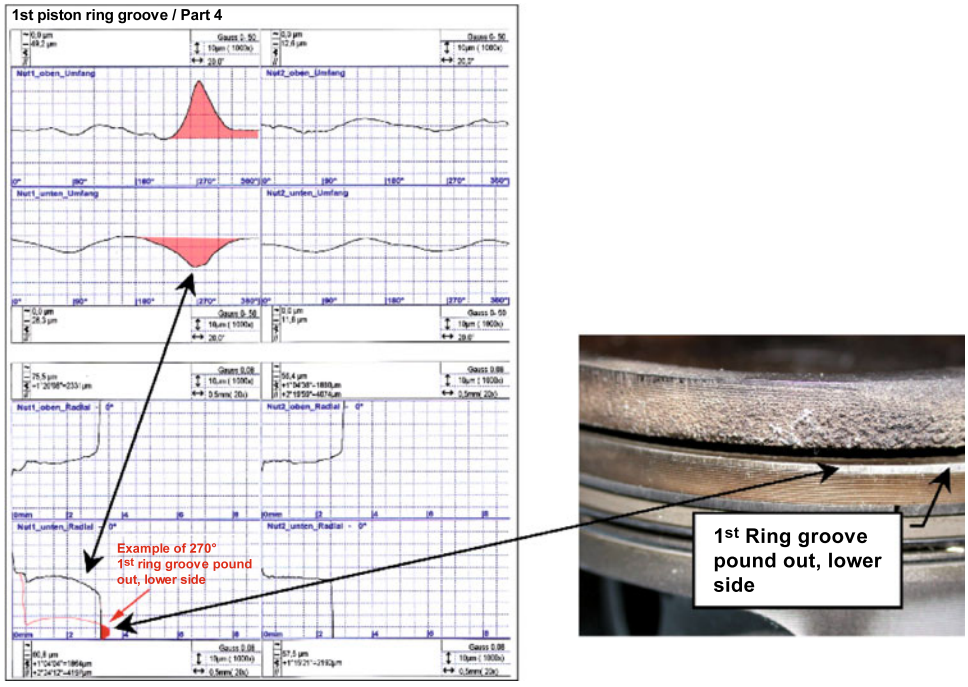

Figure 7.78: Deformation and wear of the 1st piston ring groove due to knocking combustion

nature is demonstrated by a test, in which the area of damage is bounded. A relief groove, 1 mm deep, was made in a piston at the lower area of the top land.

Figure 7.79 shows the pistons after 105 h of long-term knocking under full load. Both pistons were operated under continuous knocking, with maximum knock amplitudes of about 25 bar.

The piston on the left exhibits knock damage that extends to the lower edge of the top land. The damage to the piston on the right extends only as far as the relief groove. No knock damage is detected below the relief groove. The pressure wave is dissipated in the relief groove, so that no damage can occur below the relief groove.

This measure for limiting the damage is restricted by the design of modern gasoline engine pistons with short top land width. The relief groove also looses effectiveness in normal operation if it is clogged by oil carbon.

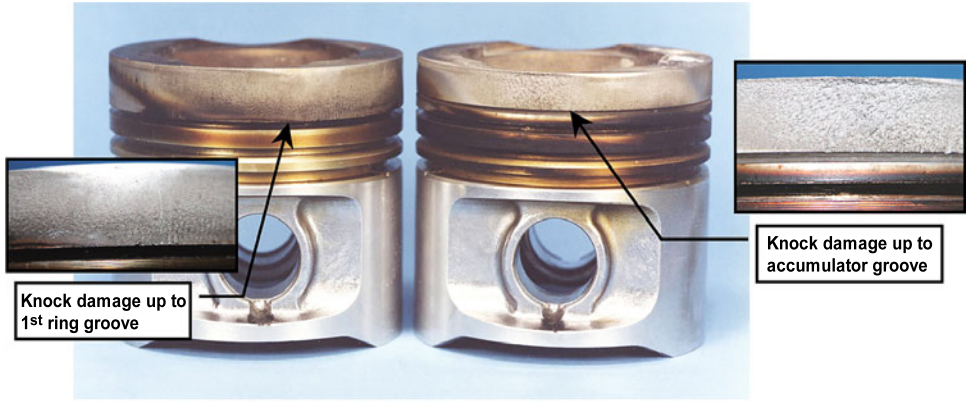

	Top land without accumulator groove	Top land with accumulator groove
Knock damage	Knock damage over a large area, up to the upper side of the 1st piston ring groove (without groove flank protection)	Knock damage on the top land, only above the accumulator groove (without groove flank protection)

Figure 7.79: Knock damage on the top land, with and without relief groove

The damage shown thus far is relatively easy to identify as knock damage. It is more problematic to evaluate damage that occurs due to individual knocks of very high amplitude, which does not leave the erosion damage that is typical of knocking.

Figure 7.80 shows four pistons from an engine with ring land fractures. In all four pistons, the fracture area is opposite the spark plug, in the direction of the exhaust valve. Appropriate

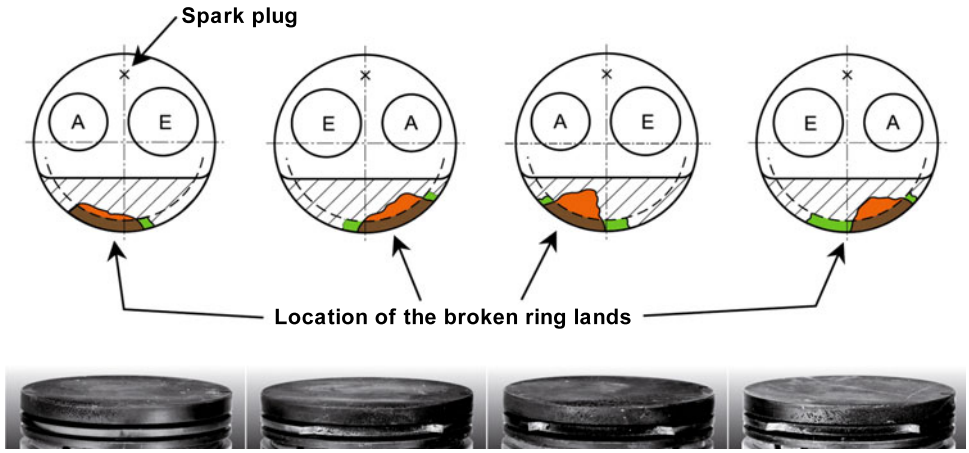

Figure 7.80: Ring land fractures due to knocking combustion

measurements show that the very high knock amplitudes of over 100 bar are superposed over the normal cylinder pressure. A single one of these high knock amplitudes can be sufficient to cause such damage.

Figure 7.81 shows two pistons with fractures at the 1st and 2nd ring land after only a brief period of engine operation. The load on the 2nd ring land was so high that it could not withstand the stress. The support for the 3rd piston ring also broke off of one piston. This was caused by individual, extremely high knock amplitudes. Other typical signs of knocking damage are therefore not evident on the piston.

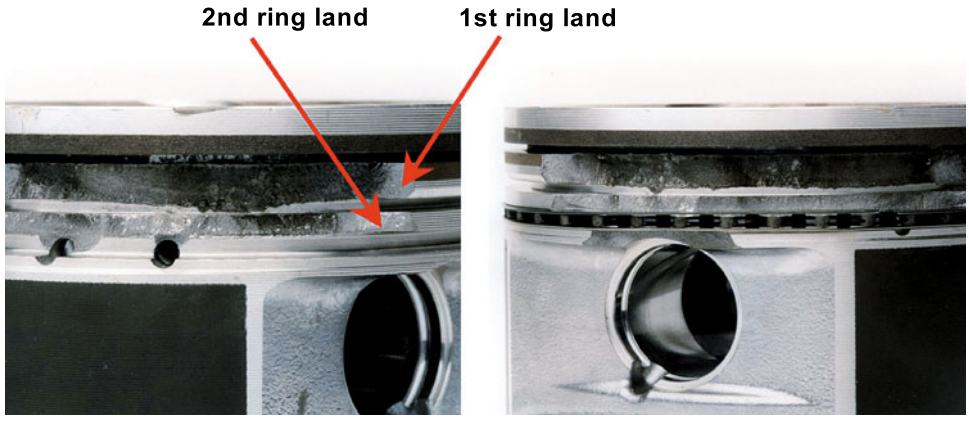

Figure 7.81: Ring land fracture at 1st ring land and 2nd ring land–caused by severe knocking combustion

7.5.2 Knock measurement hardware and the MAHLE KI meter

It was our objective to develop a measurement method for the quantitative evaluation of the knock severity. Knocking occurs rather stochastically. The measurement method must thus be able to capture a large number of combustion cycles, evaluate them statistically, and make them available in real time. The maximum, positively superimposed knock amplitude is derived as an indicator of damage; **Figure 7.84**. The KI meter (KI = Knock Intensity), developed by MAHLE, fulfills these requirements.

Precise indication signals are needed in order to determine the exact knock amplitude level. A prerequisite for precise indexing is the correct positioning of the pressure sensors in the combustion chamber; **Figure 7.82**. It is particularly critical that they are properly bonded to the combustion chamber, in order to prevent connection channels. They would corrupt the signal with pipe oscillations, so that high knock amplitudes, in particular, would not be recorded at the correct level.

The KI meter, **Figure 7.83**, is capable of displaying measured signals for each combustion cycle for up to eight cylinders, in real time. The measurement system can capture the ignition angle for each cylinder separately for each combustion cycle, without needing to access the standard electronic control unit (ECU). Further signals can be captured on two additional

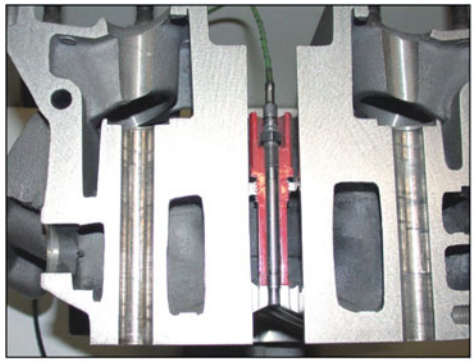

Kistler 6001 or 601 pressure sensor, noncooled, installed flush with combustion chamber

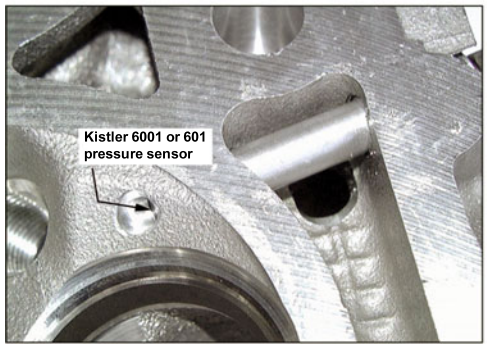

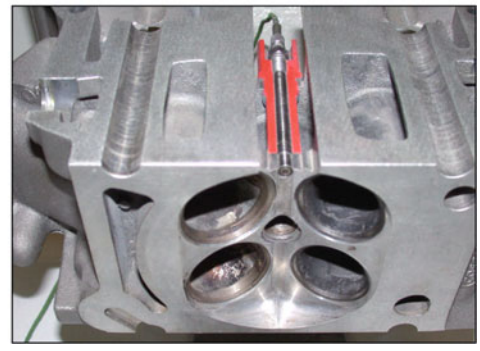

Figure 7.82: Pressure sensors in the cylinder head–installation examples

	Cyl. 1 max.		Cyl. 2 max.	
Classes [bar]	detected	not detected	detected	not detected
0 - 1	0	135	0	522
1 - 2	0	1210	1	1245
2 - 3	2	547	4	208
3 - 4	0	87	1	12
4 - 5	2	8	1	1
5 - 6	1	0	0	0
6 - 7	1	0	0	0
7 - 8	1	0	0	0
8 - 9	1	0	0	0
9 - 10	0	0	0	0
10 - 12	0	0	0	0
12 - 14	0	0	0	0
14 - 16	0	0	0	0
16 - 18	0	0	0	0
18 - 20	0	0	0	0
20 - 24	0	0	0	
24 - 28	0	0	0	
28 - 32	0	0	0	
32 - 36	0	0	0	
36 - 40	0	0	0	
40 - 44	0	0	0	

Figure 7.83: The MAHLE KI meter [12] and statistical analysis of the knocking combustion cycles detected and not detected by the knock control system

channels per cylinder (e.g., acceleration signals), which can be displayed precisely relative to the combustion cycle.

Automatic analysis allows this information to be used to determine for each combustion cycle whether a measured knock amplitude was detected by the knock control system and whether the ignition angle was reduced; **Figure 7.84**. After a measurement, it is thus possible to capture the knock amplitudes that were and were not detected by the knock control system in tabular form.

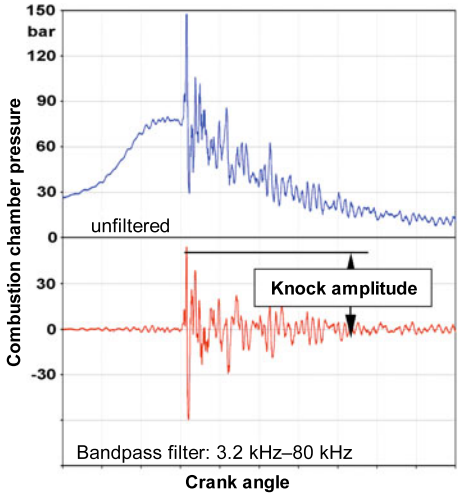

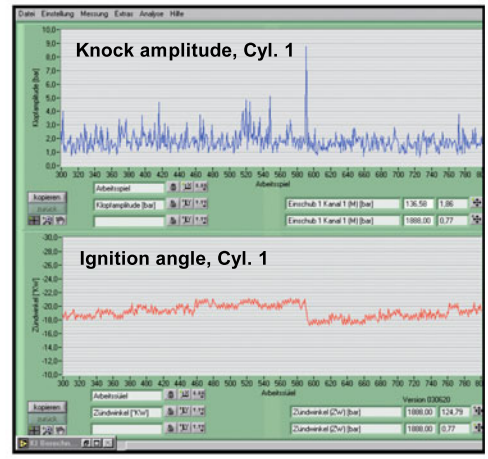

Figure 7.84: Analysis of positively superimposed knock amplitudes and control process of the knock control system, in online mode

In order to analyze the quantitative knock intensity, a value must be created that reflects the quantity and level of knock amplitudes. A knock intensity (KI) factor is defined for this purpose.

The calculation of the knock intensity factor KI uses the summation formula shown in **Table 7.6** for a predetermined number of four-stroke cycles to be measured. The example shows the knock amplitudes measured with increasing advanced ignition and the calculated KI factor.

Table 7.6: Calculation of the MAHLE knock intensity factor KI
Window position: 0 degrees Speed: 5,000 rpm, full load
Window width: 150 degrees Load cycles: 200

			Variation in ignition angle [°CA]					
			22°	23°	25°	27°	30°	35°
Class	Analysis factor	Pressure range [bar]	Number of four-stroke cycles					
0	0	0–2	199	199	190	145	82	9
1	0.5	2–4	1	1	10	48	69	15
2	1	4–8	0	0	0	7	41	70
3	2	8–12	0	0	0	0	6	49
4	3	12–16	0	0	0	0	2	25
5	4	16–20	0	0	0	0	0	9
6	5	20–24	0	0	0	0	0	8
7	6	24–28	0	0	0	0	0	5
8	7	28–32	0	0	0	0	0	4
9	8	32–36	0	0	0	0	0	4
10	9	36–40	0	0	0	0	0	0
11	10	40–44	0	0	0	0	0	0
12	11	44–48	0	0	0	0	0	2
13	12	48–52	0	0	0	0	0	0
14	13	52–56	0	0	0	0	0	0
15	14	56–60	0	0	0	0	0	0
16	15	60–64	0	0	0	0	0	0
Overrun		> 64	0	0	0	0	0	0
Knock intensity factor KI			0.05	0.05	0.5	3.1	9.35	43.85

$$KI = N \cdot \frac{\sum_{k=0}^{m} (n_k \cdot f_k)}{c}$$

KI: Knock intensity factor
k: Class number
m: Maximum number of classes
n_k: Number of cycles with pressure amplitudes in a class
f_k: Weighting factor of a class
c: Number of four-stroke cycles measured
N: Standardization constant

Using the functions of the KI meter as described above, it is possible, for example, to run a performance check on the knock controller. This can expose errors in the control strategy or show a level of detection sensitivity for each cylinder.

Using an automated analysis system, the knocking behavior of each individual combustion cycle can be monitored during an endurance test and displayed graphically in real time. For example, individual severe knocking events that occur very rarely (mega-knocks) can be detected. In addition, the system shown can perform systematic investigations of knocking behavior, such as the effect of knocking combustion on the piston temperature or the effect of the air-fuel mixture on the knock limit.

7.5.3 Examples of measurement results

Figure 7.85 shows an example of the result of an analysis using the measurement method described, together with a piston temperature measurement. As is evident the KI factors for cylinders 2 and 3 increase relative to the ignition angle much earlier and more quickly than for cylinders 1 and 4. At this operating point, the tested engine has a nonuniform mixture distribution between the inner (cylinders 2 & 3) and outer (cylinders 1 & 4) cylinders. Cylinders 2 and 3 are running a relatively lean mixture, so that knocking occurs more intensely under high loads.

From **Figure 7.85**, it can also be seen that the increase in piston temperatures rises linearly up to the knock limit, at about 2.5°C/°CA. A disproportional increase in piston temperature is evident only after severe knocking has occurred.

In another series of tests, the effect of the air-fuel mixture (lambda) on the piston temperature and knock limit was determined.

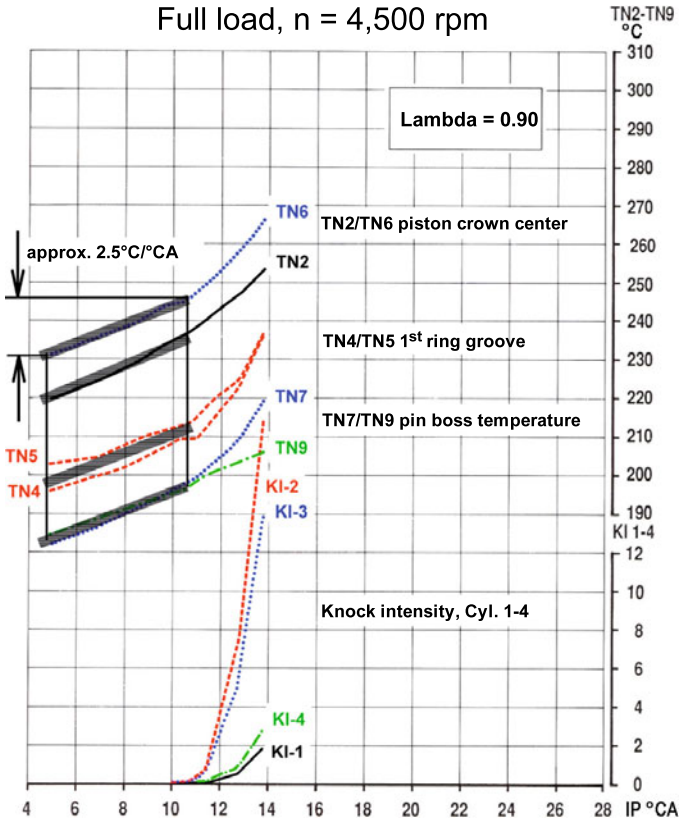

Figure 7.85: Piston temperatures and knock intensity as a function of the ignition angle (comparison of all four cylinders) for a 2.0-liter, four-valve, naturally aspirated engine

Operating conditions:
Full load, n = 4,500 rpm
T_{oil} = 100°C
T_{wa} = 90°C
Fuel: Reference fuel SUPER ROZ 96

Temperature descriptions:
TN2 Center of combustion bowl, piston 1,
TN4 1st piston ring groove, ATS, piston 2
TN5 1st piston ring groove, TS, piston 2
TN6 Center of piston crown, piston 3
TN7 Vent side pin boss, piston 3
TN9 Flywheel side pin boss, piston 4

Figure 7.86 shows a shift in the knock limit for a rich mixture of about 3°CA in the direction of an advanced ignition angle. The piston temperature is lower for the rich mixture, but the temperature at the knock limit (now 3°CA earlier) is greater than for the lean mixture.

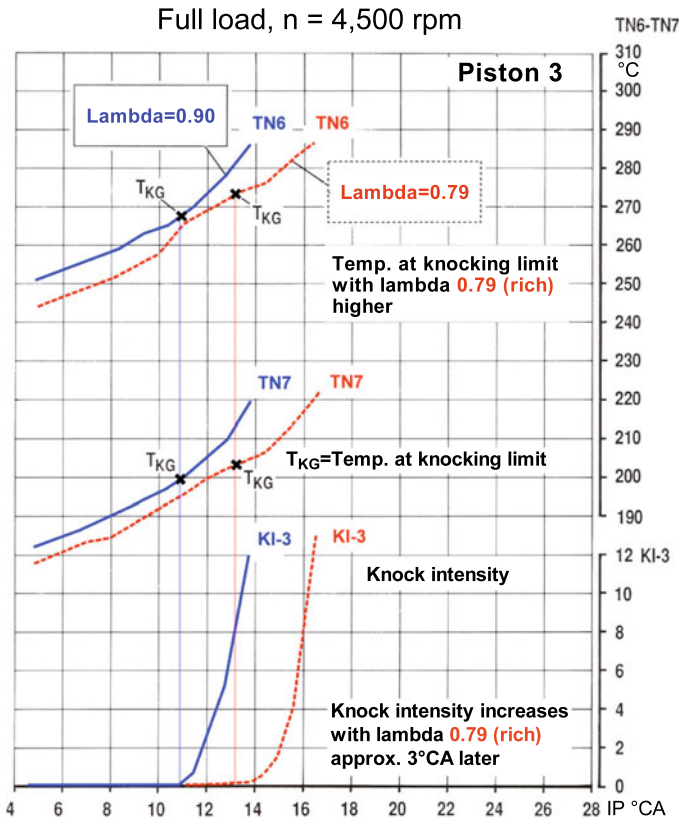

Figure 7.86: Piston temperatures and knock intensity as a function of the ignition angle, at λ = 0.90 (lean) und λ = 0.79 (rich)

Operating conditions:
Full load, n = 4,500 rpm
T_{oil} = 100°C
T_{wa} = 90°C
Fuel: Reference fuel SUPER ROZ 96

Temperature descriptions:
TN6 Temperature at center of piston crown, piston 3
TN7 Temperature at vent side pin boss, piston 1
T_{KG} Temperature at knock limit

Both figures show that the ignition angle (IA) fundamentally has a significant effect on component temperatures, even without knocking. An additional increase in temperature due to knocking combustion, in contrast, is evident only at very high knock intensities.

7.5.4 Detection quality of knock control systems

Knock damage, such as axial pound out of the 1st piston ring groove, **Figure 7.78**, can be attributed to deficient knock-detecting functionality of the knock control system, among other factors. It was demonstrated that even relatively slight increases in knock amplitudes can cause such damage.

Such knocking behavior is shown in **Figure 7.87**. For each combustion cycle, these are the maximum knock amplitudes and the cylinder-specific retardation angle of the knock control system for cylinder 1. For the ROZ 95 fuel that was used, a control depth of the knock control system of about 3°CA was determined.

Knocking amplitudes of up to 25 bar were measured in cylinder 1. With this knock controller setting and ROZ 95 fuel quality, the knock damage indicated above was caused in a full-load endurance test. With a fuel quality of ROZ 99, in contrast, comparable full-load endurance testing showed no knocking damage; **Figure 7.88**. The maximum knock amplitudes dropped to about 5 to 6 bar, and the control depth of the knock control system is much lower.

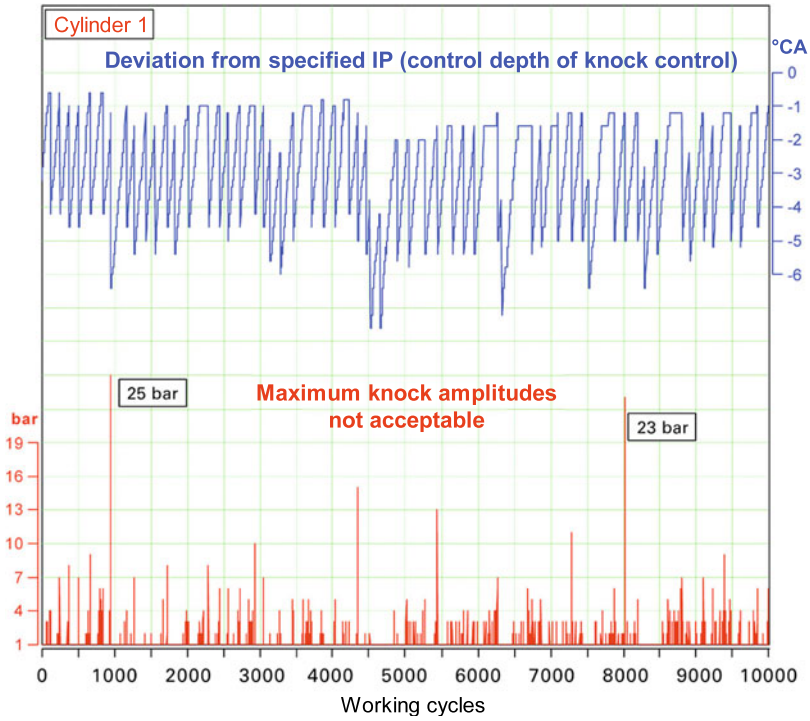

Figure 7.87: Maximum knock amplitude and associated change in ignition angle for 10,000 combustion cycles, full load, 5,600 rpm, with ROZ 95, 1.8-liter turbocharged engine

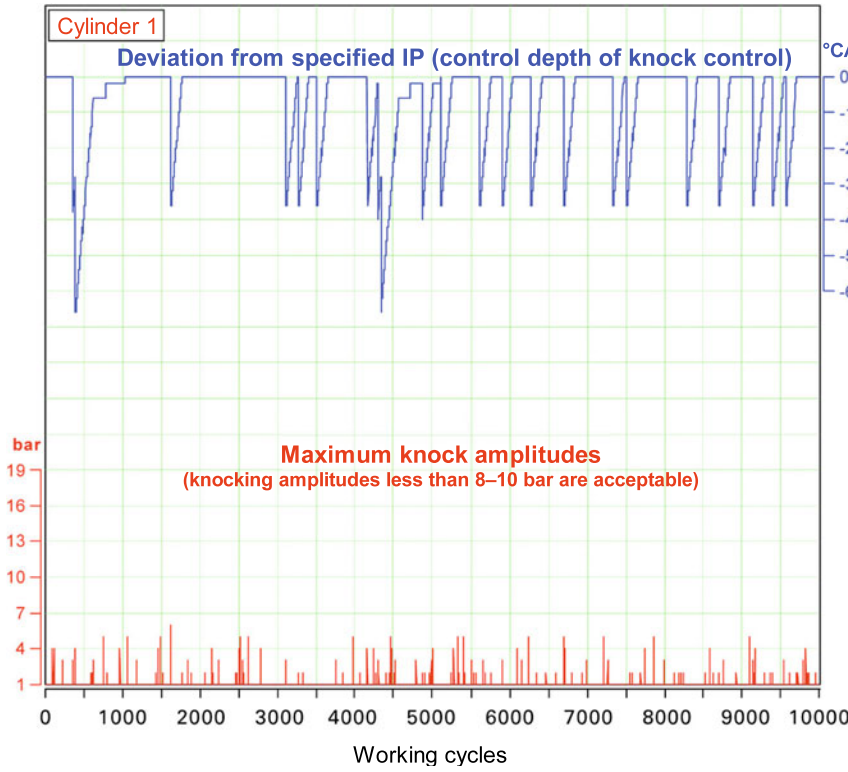

Figure 7.88: Maximum knock amplitude and associated change in ignition angle for 10,000 combustion cycles, full load, 5,600 rpm, with ROZ 99, 1.8-liter turbocharged engine

The level and quantity of the maximum permissible knock amplitudes cannot be generalized, but must be determined by endurance testing for each application. Knock amplitudes of greater than 8 to 10 bar have already caused problems in a wide range of cases and should be avoided.

It is evident from **Figure 7.89** that the previous example is a cylinder-specific problem. The measured maximum knock amplitudes for all engine cylinders are summarized in a table.

Knock amplitudes that were and were not detected by the knock control system are differentiated. The left part of the figure (results with ROZ 95 fuel quality) shows that the problem indicated earlier affects only cylinder 1. The detection quality of the knock control system is not satisfactory for this cylinder. It failed to detect knock amplitudes of 8 to 9 bar. The poor detection quality for cylinder 1 was evident for ROZ 99 fuel quality as well.

Deficient detection quality can have many causes. The causes often cannot be addressed by design changes, because the engine development has already progressed too far. Software applications can provide a remedy in this connection.

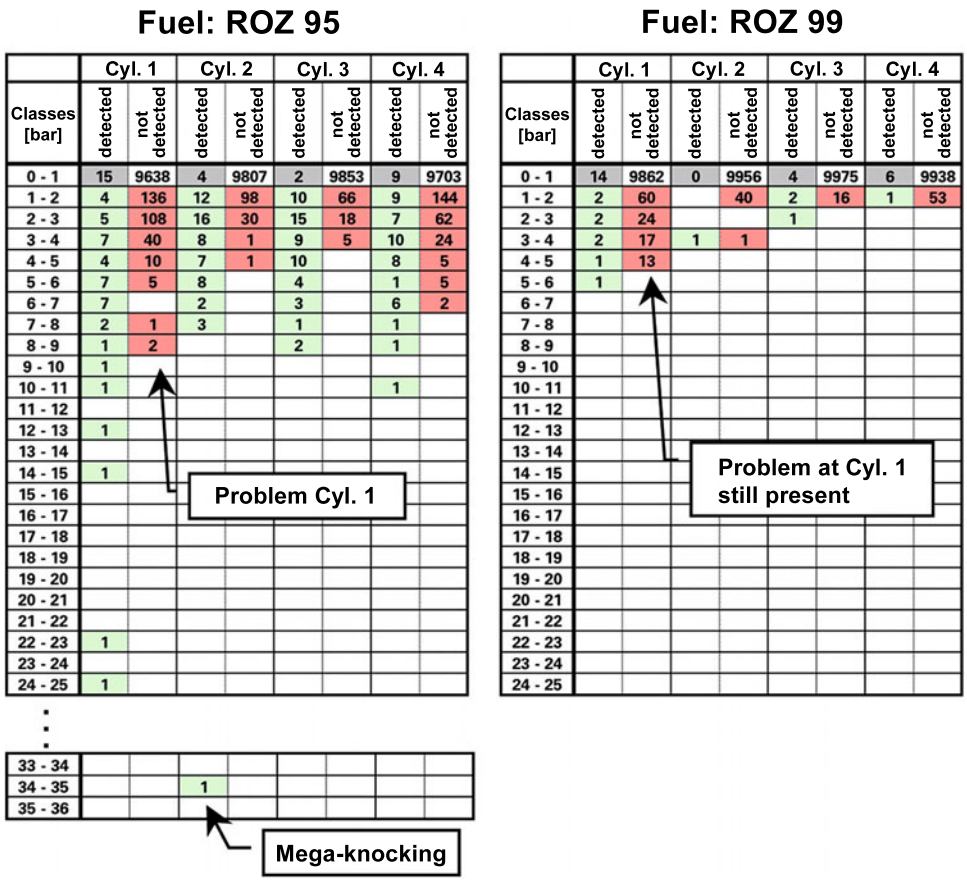

Classes [bar]	Cyl. 1		Cyl. 2		Cyl. 3		Cyl. 4	
	detected	not detected	detected	not detected	detected	not detected	detected	not detected
0 - 1	15	9638	4	9807	2	9853	9	9703
1 - 2	4	136	12	98	10	66	9	144
2 - 3	5	108	16	30	15	18	7	62
3 - 4	7	40	8	1	9	5	10	24
4 - 5	4	10	7	1	10		8	5
5 - 6	7	5	8		4		1	5
6 - 7	7		2		3		6	2
7 - 8	2	1	3		1		1	
8 - 9	1	2			2		1	
9 - 10	1							
10 - 11	1						1	
11 - 12								
12 - 13	1							
13 - 14								
14 - 15	1							
15 - 16								
16 - 17								
17 - 18								
18 - 19								
19 - 20								
20 - 21								
21 - 22								
22 - 23	1							
23 - 24								
24 - 25	1							
⋮								
33 - 34								
34 - 35			1					
35 - 36								

Classes [bar]	Cyl. 1		Cyl. 2		Cyl. 3		Cyl. 4	
	detected	not detected	detected	not detected	detected	not detected	detected	not detected
0 - 1	14	9862	0	9956	4	9975	6	9938
1 - 2	2	60		40	2	16	1	53
2 - 3	2	24			1			
3 - 4	2	17	1	1				
4 - 5	1	13						
5 - 6	1							
6 - 7								
7 - 8								
8 - 9								
9 - 10								
10 - 11								
11 - 12								
12 - 13								
13 - 14								
14 - 15								
15 - 16								
16 - 17								
17 - 18								
18 - 19								
19 - 20								
20 - 21								
21 - 22								
22 - 23								
23 - 24								
24 - 25								

Figure 7.89: Statistical analysis of the measured knock amplitudes, comparing ROZ 95 to ROZ 99, 10,000 combustion cycles, full load, 5,600 rpm, 1.8-liter turbocharged engine

One method is to back off the ignition angle values in the characteristic map, thus moving away from the knock limit and reducing the control drop of the knock control system. Typically, this can only be implemented for all cylinders at once. The result, however, is a degradation in engine efficiency, even in operating ranges where the knock limit is not reached.

7.5.5 The mega-knocking phenomenon

A mega-knocking is an extremely high knock amplitude that can be up to 100 bar or greater, which occurs very rarely. As shown in Chapter 7.5, one single knock amplitude at this level can destroy the top land or the ring land.

Figure 7.90 shows a typical mega-knocking detected in an eight-cylinder naturally aspirated engine in full load/partial load operation. The maximum knock amplitude and ignition angle trace for cylinder 1 are shown for 10,000 combustion cycles, as well as the engine load at

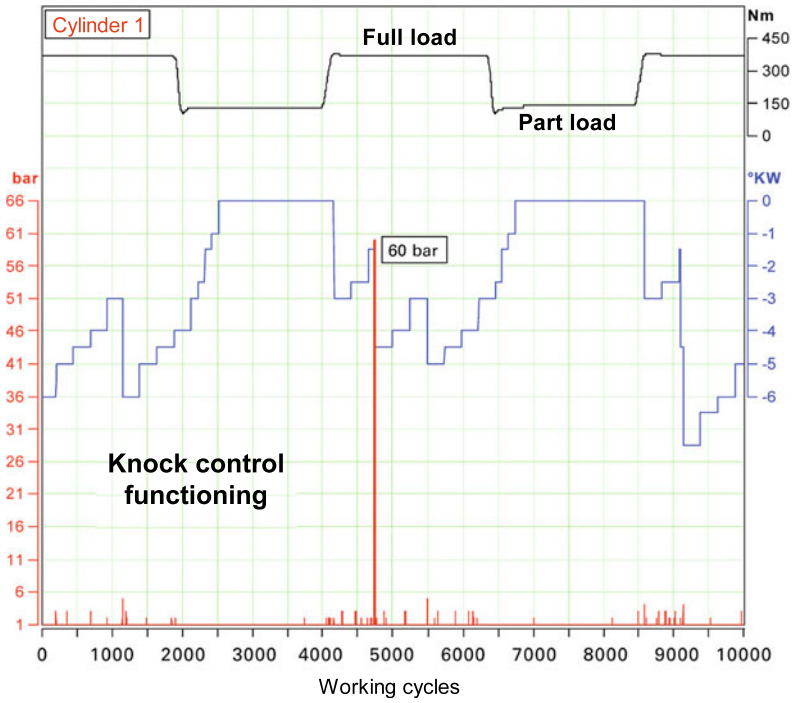

Figure 7.90: Mega-knocking in cylinder 1, full load/part load operation at n = 6,000 rpm, ROZ 95 fuel, eight-cylinder naturally aspirated engine

a constant speed of n = 6,000 rpm. The knock control system works perfectly under these operating conditions. In combustion cycle no. 4747, an extreme knocking combustion event took place, with a maximum knock amplitude of 60 bar.

This combustion cycle was recorded online and is shown in **Figure 7.91**. At the start of the pressure curve, normal combustion is evident, which then leads to an extreme knocking event, without any apparent cause.

The table with the data from all eight cylinders shows nothing else unusual. The mega-knocks do not occur only in cylinder 1 in this engine. No particular cylinder seems to be preferred. The running program–alternating load in this case–was likewise not a determining factor. It was established, however, that the mega-knocking occurred only at high speeds and under full load.

Potential defects of the ignition can be ruled out by monitoring the ignition signal.

Mega-knocking is known not only in naturally aspirated engines, but also in turbocharged engines with indirect and direct injection. In most cases, the main initiator of such mega-knocking seems to be a nonhomogenous mixture control in the combustion chamber. Hotspots can form in which the air-fuel mixture leads to severely knocking combustion [13].

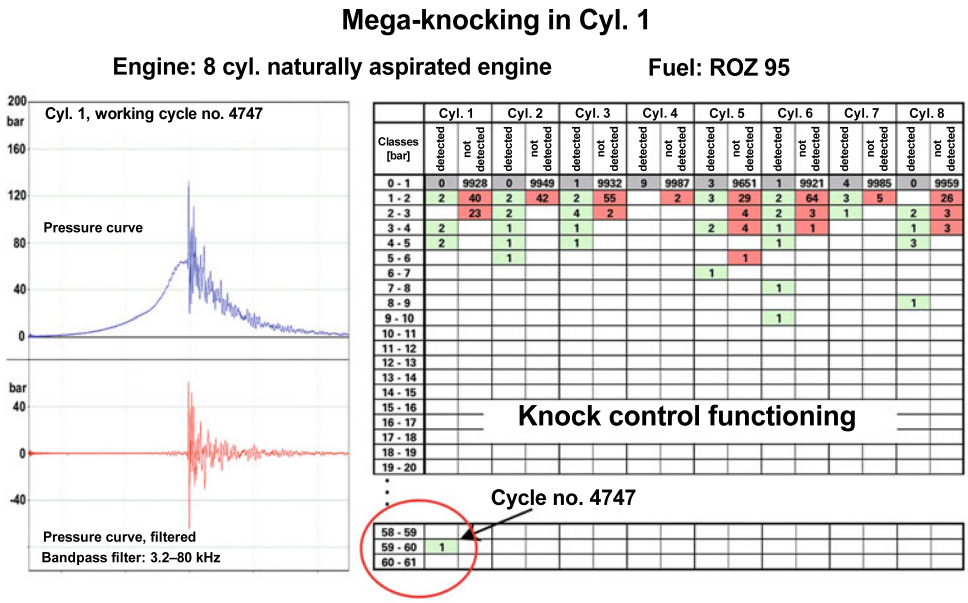

Classes [bar]	Cyl. 1		Cyl. 2		Cyl. 3		Cyl. 4		Cyl. 5		Cyl. 6		Cyl. 7		Cyl. 8	
	detected	not detected	detected	not detected	detected	not detected	detected	not detected	detected	not detected	detected	not detected	detected	not detected	detected	not detected
0 - 1	0	9928	0	9949	1	9932	9	9987	3	9651	1	9921	4	9985	0	9959
1 - 2	2	40	2	42	2	55		2	3	29	2	64	3	5		26
2 - 3		23	2		4	2				4	2	3	1		2	3
3 - 4	2		1		1				2	4	1	1			1	3
4 - 5	2		1		1						1				3	
5 - 6			1							1						
6 - 7									1							
7 - 8											1					
8 - 9															1	
9 - 10											1					
10 - 11																
11 - 12																
12 - 13																
13 - 14																
14 - 15																
15 - 16																
16 - 17																
17 - 18																
18 - 19																
19 - 20																
58 - 59																
59 - 60	1															
60 - 61																

Figure 7.91: Measurement of 10,000 combustion cycles, with mega-knocking in cylinder 1

The mega-knocking phenomenon should not be confused with that of premature ignition. Premature ignition occurs occasionally in the development of highly stressed turbocharged engines. In this case, the air-fuel mixture ignites prior to actual induced ignition by the spark plug [14]. Premature ignition is caused by an extreme increase in the peak cylinder pressure in the compression phase. This greatly increased pressure curve can also be superimposed with additional knock amplitudes. Cylinder pressures of greater than 300 bar have been measured.

These phenomena, mega-knocking and premature ignition, cannot be seen in conjunction with the function of the knock control system.

7.6 Piston noise and piston transverse motion

7.6.1 Procedure for systematically minimizing piston noise

In order to optimize the acoustics of a combustion engine, the individual sources of sound and their contribution to the overall engine noise must be identified as precisely as possible. This is the only way to demonstrate which combination of measures will have the best effect, with the minimum number of engine tests.

One of the mechanisms that generates noise in a reciprocating piston engine is the motion of the piston, due to its clearance perpendicular to its normal running direction. Under the effects of the gas and inertial forces, referred to hereafter as inertia forces, the connecting rod angle and the necessary installation clearance inevitably cause transverse motion of the piston. When the piston contacts the cylinder wall, it causes impacts that excite structure-borne noise in the engine structure. This is the cause of piston noise.

Piston noise contributes a significant component of the mechanically caused crankshaft drive noise. It is therefore important to optimize piston transverse motion in order to minimize engine noise in the summation of the sound level, but also in the degree of subjective unpleasantness.

The following boundary conditions should be met in order to quickly and successfully achieve this optimization:

- An occurring piston noise should be clearly identifiable and assessable as such, at least for gasoline engines.
  This prevents expensive changes to components or clearances without any detectable improvement in the auditory impression.
- Each individual type of piston noise should be objectively quantifiable.
  This allows a quantitative analysis of the effects on noise generation of changes made to the piston.
- For each individual type of piston noise, the characteristic motion sequence of the piston must be known.
  Visualization of the piston transverse motion measured on a loud piston shows the mechanism of the motion that must be prevented for the particular piston noise.
- The effects of various piston design measures on transverse piston motion must be precisely identified.
  Systematic parameter studies assist in acquiring the appropriate expert knowledge in order to keep the number of engine tests to a minimum.

In order to meet these requirements, the assessment and systematic minimization of piston noise follows four different principle approaches, as listed in **Figure 7.92**. These four approaches to the investigation of piston noise and its causes require completely different

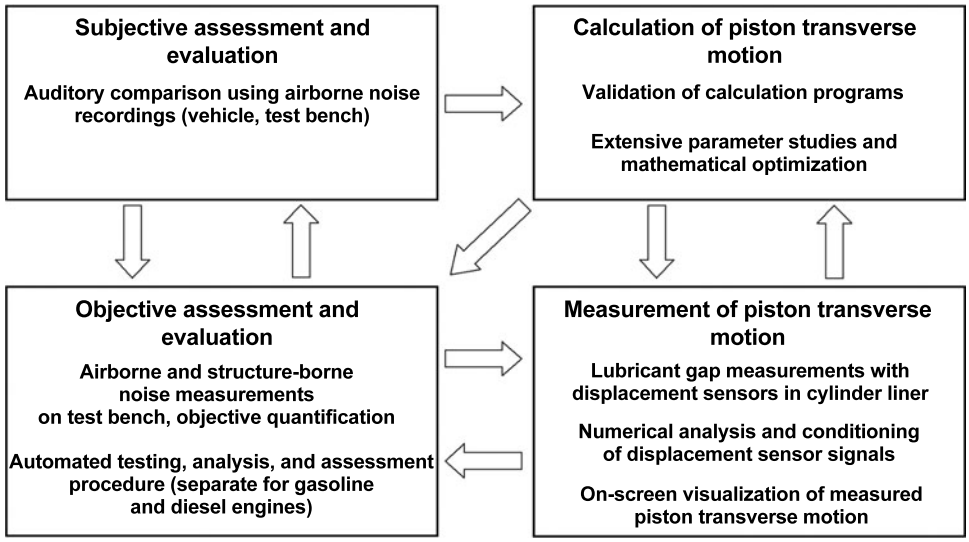

Figure 7.92: Procedure for systematically minimizing piston noises

levels of time and resources. Depending on the problem, task definition, and objective, they are pursued at different intensity levels and combined as needed. Common to all procedures is the overall goal of systematically expanding knowledge and insight in order to be able to perform future optimization efforts more quickly and reliably.

Subjective assessment and evaluation of engine noise must be considered a necessary step at the start and finish of every optimization process. At the start of optimization, the auditory impression provides an initial diagnosis and helps to qualitatively evaluate the initial state as quickly as possible. A defined airborne noise recording allows subsequent auditory comparisons. After completing the optimization, subjective assessments and a direct comparison to the initial state serves as verification that the improvements made have brought about a subjectively improved auditory impression. Such subjective assessment of engine noise can be performed either in the vehicle or on a test bench.

If subjective assessments and specifically prepared auditory comparisons are not sufficient as diagnostic tools, which is frequently the case with diesel engines, then reproducible airborne and structure-borne noise measurements must be taken on the test bench. The analysis of signals measured with different pistons, comparing them to each other, can provide an objective quantification of the piston noise. Standardization and partial automation of the analysis process allows the necessary experimental variations to be performed quickly.

A significant goal of systematic test planning is to minimize the number of variations of experiments, and therefore the number of engine test runs, while obtaining as much information as possible. The existing wealth of experience and the ability to make predictive computations contribute greatly to this goal.

Using numerical simulations of piston transverse motion, not only can the acoustically objectionable piston motions be recorded and analyzed, but the appropriate solution alternatives can also be qualitatively assessed, thereby reducing the time needed to implement them. This assumes that appropriate parameter studies have been completed.

In order to validate simulation programs and in support of basic development work, additional measurements of piston transverse motion are carried out. The effort needed to equip an engine is considerable, in terms of both time and resources. It is more economical to prepare a few typical representatives as test carriers for such experiments–for example, a conventional gasoline engine, one with direct injection, IDI and DI diesel engines, and commercial vehicle diesel engines. Using a measurement method with displacement sensors mounted on the cylinder liner [15], a number of critical parameters and their effects on piston transverse motion can be investigated on these engines with little retooling effort. The analysis and visualization procedures are largely automated. The valuable results support the targeted selection of test variants and the preparation of measures catalogs.

7.6.2 Piston noise in gasoline engines

7.6.2.1 Subjective noise assessment

In gasoline engines, piston noise can be identified as such based on the subjective auditory impression. Several different types of noise can even be distinguished this way. A practiced listener can determine the actual excitation mechanism in the engine based on the sound pattern and the operating conditions.

The individual types of piston noise are classified by cause, location of excitation on the piston or cylinder, crank angle, as well as range of engine speed, load, and temperature. Based on the auditory impressions, “sound-rich” descriptions have been developed over time for these various types of excitation, a list of which is shown in **Figure 7.93**, without making a claim as to its completeness.

Several recordings of auditory examples are now available to experienced development engineers, which can be used as comparative examples for assessing the acoustics of an engine. In many cases, the cause of a noise can be diagnosed right away in the first subjective assessment. This means that the best possible test variants can be proposed early in the process for any subsequent engine testing.

A grading scale from 1 to 10 is typically used in the automotive industry for subjectively assessing engine noise, as documented in **Figure 7.94**.

If several piston variants are run in comparison during acoustic optimization, then this type of subjective assessment is often not sufficient for precise quantification. An objective noise analysis and quantification of the noises must then be performed.

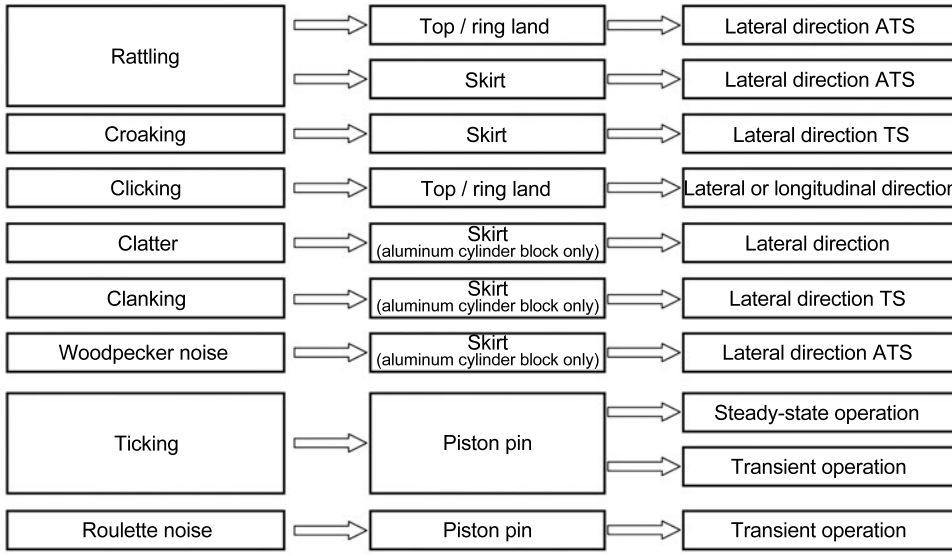

Figure 7.93: Piston noises in gasoline engines

Grade	Evaluation	Description	Comments
10	Excellent	Cannot be detected, even by practiced evaluators	Marketable
9	Very good	Can only be detected by practiced evaluators	
8	Good	Can only be detected by critical customers	
7	Satisfactory	Can be detected by all customers	
6	Acceptable	Considered disturbing by some customers	
5	Unsatisfactory	Considered disturbing by all customers	Not marketable
4	Deficient	Considered defective by all customers	
3	Insufficient	Claimed as a severe defekt by all customers	
2	Poor	Only conditionally functional	
1	Very poor	No longer functional	

Figure 7.94: Grading scale for subjective assessment of piston noises

7.6.2.2 Objective noise assessment and quantification

The most common piston noises in a gasoline engine are:

- So-called "rattling"–impact of the piston crown or, depending on the piston geometry, the rigid upper part of the piston skirt against the antithrust side in the crank angle range immediately prior to or at the ignition top dead center ITDC (TDC in the combustion cycle). The excitation mechanism is based on an inertia-induced traverse of the clearance, from the thrust side to the antithrust side, superimposed by a rotary motion component of the piston crown toward the antithrust side.
- So-called "croaking"–the impact and deformation of the elastic piston skirt on the thrust side of the cylinder, in the crank angle range after ITDC. The excitation mechanism is based on a rotary motion, induced by the gas pressure, about a center of rotation in the lower skirt area.

The motion mechanisms described here are shown schematically in **Figure 7.95**. The most critical geometric parameters that can affect piston noise behavior with a reasonable amount of effort are piston pin offset, piston crown offset, cylinder distortion, piston shaping (contour and ovality), and clearance. Note that the minimum permissible installation clearance is largely determined by the shape of the piston skirt.

Both noises are very typical of gasoline engines and occur almost exclusively in a cold engine under low to medium load.

"Croaking," similar to the dark tone of a frog's call, mostly occurs at low engine speeds of less than 2,000 rpm. The brighter, sharp "crown rattling," on the other hand, is generally observed at speeds of greater than 3,000 rpm. If "skirt rattling" occurs due to the piston geometry, then it may be observed at lower speeds of around 2,500 rpm.

The gasoline engine operating map in **Figure 7.96** shows the operating ranges in which the piston noises can occur in principle.

If an engine is to be checked for the piston noises of "croaking" and "rattling" using measurement technology, then continuous measurement of the airborne and structure-borne noises should be applied during an increase in engine speed, under a constant, low load. The standard measurement program suggested for two different load cases in a cooled engine (coolant and oil temperature near –20°C) is indicated by the dashed line arrows in **Figure 7.96**.

Figure 7.97 shows an example of the spectral distribution of the airborne noise signal measured during a run-up. As would be expected from the subjective auditory impression, the "croaking" and "rattling" piston noises have very different frequency distributions. The "croaking" caused by the piston skirt shows up as a relatively narrow band in the frequency range between 1 and 2 kHz. "Rattling," meanwhile, occurs due to the high rigidity of the impacting components and is seen as a wide-band excitation. Depending on the impact intensity and the engine structure, it can propagate in the range from 2 to well over 5 kHz.

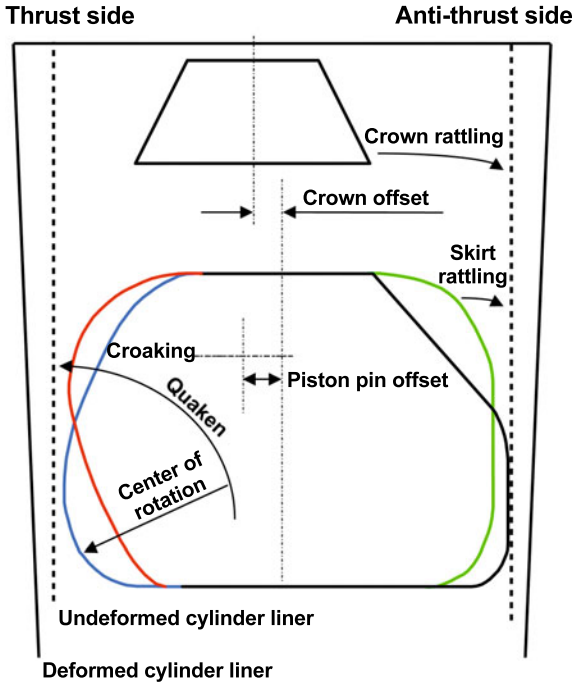

Figure 7.95: Relationship between piston design and piston noise in gasoline engines

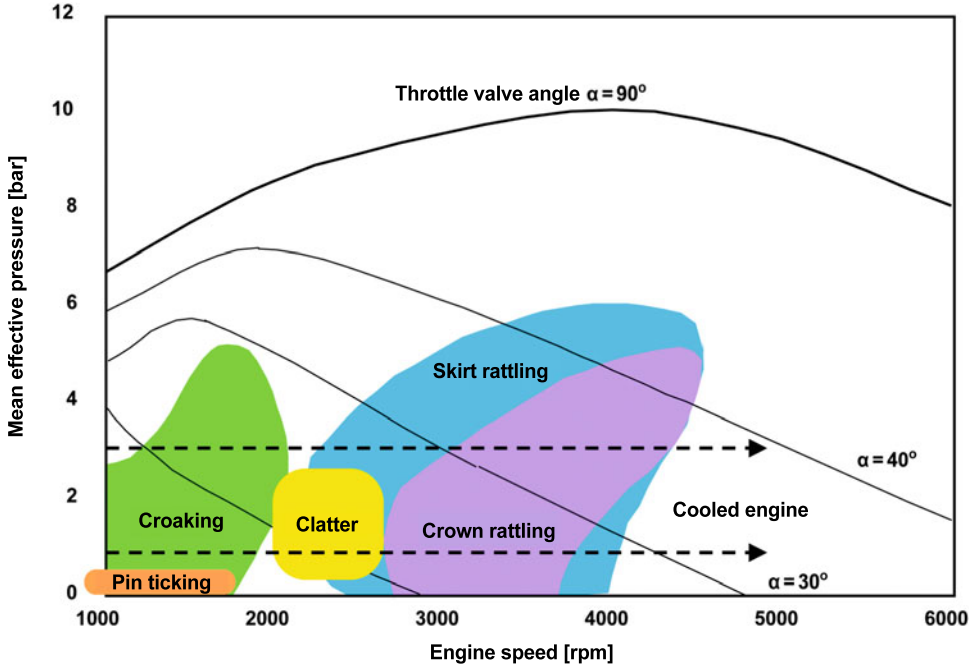

Figure 7.96: Gasoline engine operating map with typical operating ranges for piston noises and recommended measurement program

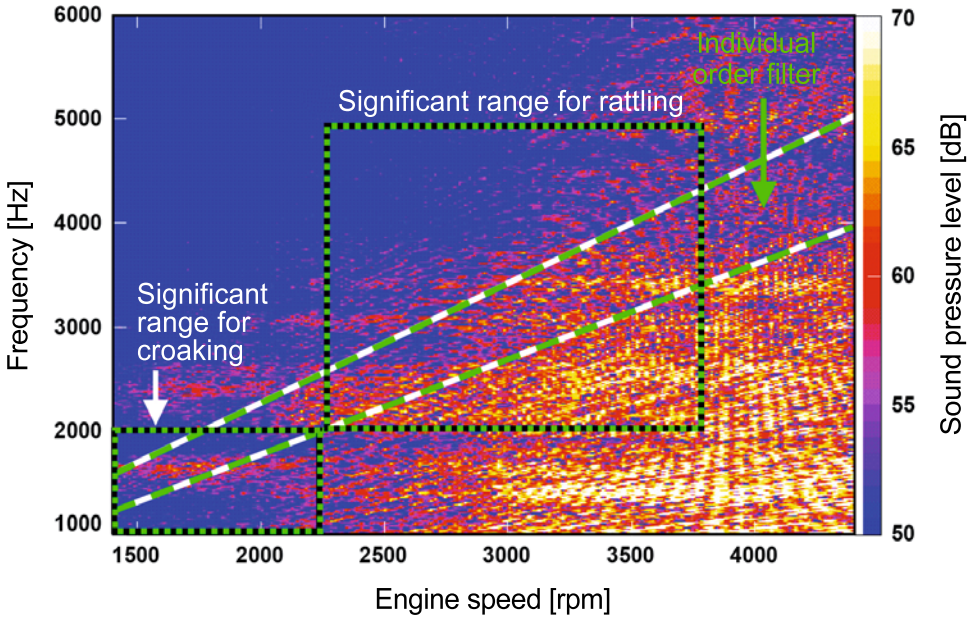

Figure 7.97: Spectral distribution of the airborne noise measured during a run-up in engine speed, showing “croaking” and “rattling”

In addition to engine speed, another important aspect for using measurement technology to differentiate the two types of noise has thus been identified. Both criteria together allow selective assessment of the signals, using defined frequency-speed windows, as shown in **Figure 7.97**.

In order to ensure as part of such a procedure that the objectionable noises lie within the selected frequency-speed windows, a comparison of the measurement data with and without the piston noise should be performed at all times. An estimate of the potential, comparing a piston version that has been deliberately designed to be acoustically problematic to one that has been acoustically optimized with very little installation clearance, can be helpful in this regard. Often, no optimized piston is available and the engine is not allowed to be reconfigured, so measurements from cold- and hot-engine operation can be compared instead. Because not all of the differences detected in the airborne noise spectrum can be attributed to piston noise, however, the ranges with the piston as the predominant cause of excitation must be verified using structure-borne noise signals.

This is done by analyzing simultaneous measurements of the accelerations on the cylinder block, which represent the piston noise to a large degree. **Figure 7.98** shows a comparison of airborne and structure-borne noise spectra for a cold engine (with “croaking”) and a hot engine (no “croaking”).

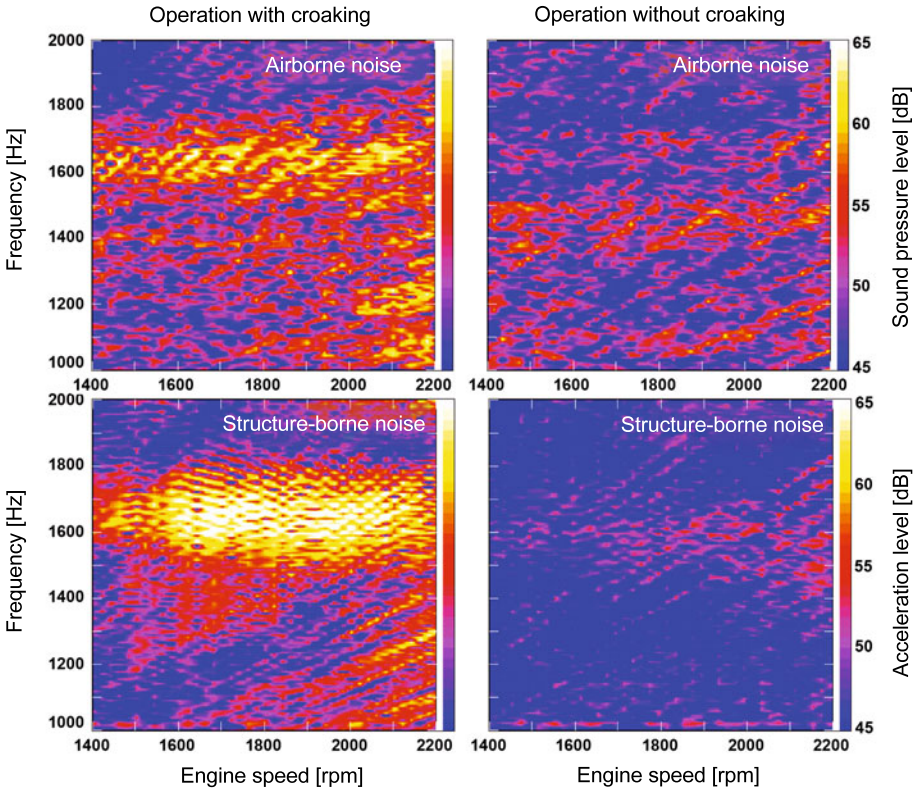

Figure 7.98: Partial airborne noise spectra (far field, thrust side) and structure-borne noise spectra (cylinder block, thrust side) for operation with and without "croaking"

The airborne and structure-borne noise spectra in **Figure 7.99** indicate that this type of representation also can visualize wide-band "rattling" and that the point of impact (crown or skirt) can also be differentiated in the frequency range. It is notable that the excitations that occur at a higher speed also affect a higher frequency range. This is due in part to the rigidity of the components undergoing impact, and in part to the rising gas pressure and inertia forces at higher speeds.

Depending on the location of the piston noises identified within the frequency-speed windows, an individual filter band can be defined as a function of the speed. This band covers the ranges of interest for piston analysis and masks the less informative ranges. A simple narrow order filter, as is indicated in **Figure 7.97**, can often be used for this purpose as well. If the level of only that portion of the signal within the filter band is calculated, the piston noises present in the range are indicated by significant peaks. **Figure 7.100** shows the curves of these order levels in comparison to the calculated overall level of the airborne noise, as measured for cold- and hot-engine operation.

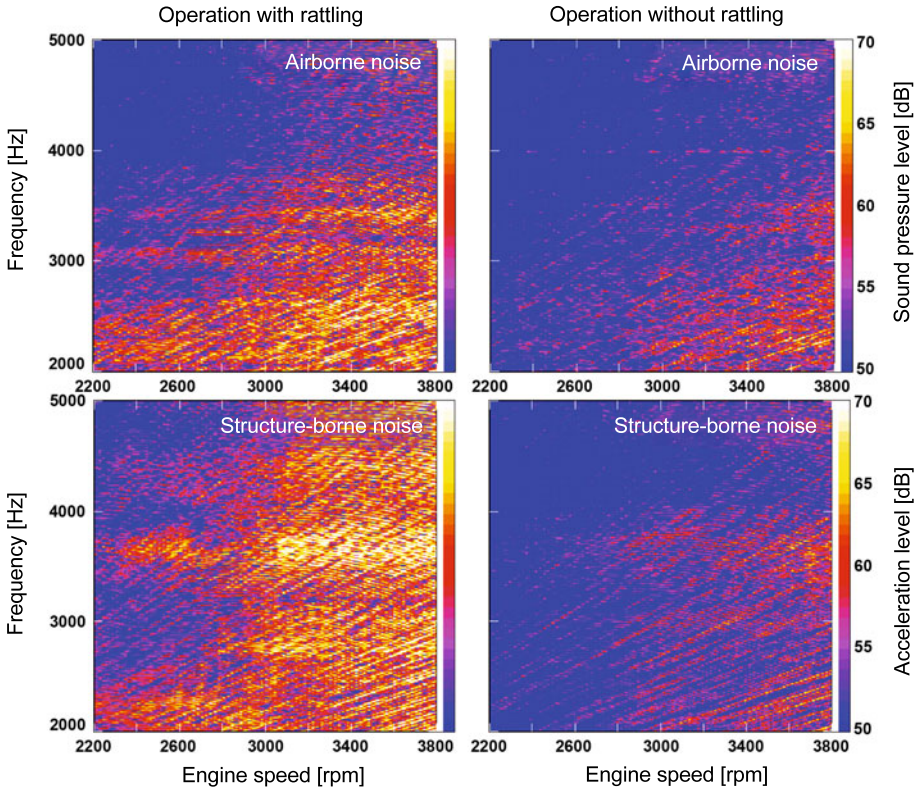

Figure 7.99: Partial airborne noise spectra (far field, antithrust side) and structure-borne noise spectra (cylinder block, antithrust side) for operation with and without "rattling"

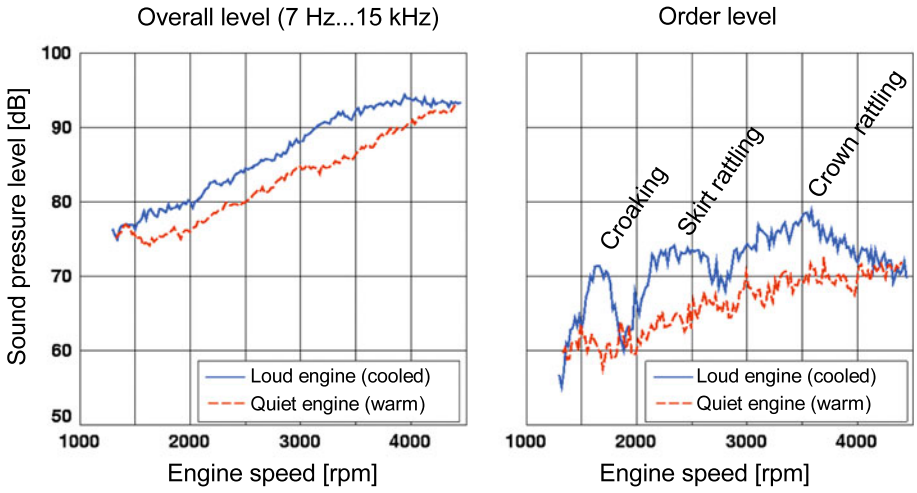

Figure 7.100: Overall levels and order levels as functions of engine speed, calculated from identical airborne noise signals

If different piston variants are run under essentially identical operating conditions during the optimization process, then the differences in sound levels can be used to quantitatively analyze the individual piston noises. An analogous procedure can also be used for the measured structure-borne noise signals, allowing additional cylinder-specific analysis, depending on the location and number of the measurement points.

7.6.2.3 Piston transverse motion and influence parameters in gasoline engines

The impact excitation caused by the piston can be minimized only by optimizing the piston transverse motion. The overall goal should therefore be to "model" the piston transverse motion for all operating points such that only a minimum amount of the impact energy is transmitted to the engine structure upon contact alteration.

In order to change the motion mechanism of the piston at the point in time that contact is made with the cylinder wall, the preceding phase of motion must be targeted. Precise knowledge of the motion behavior of the piston, as a function of the speed, load, and temperature, is therefore just as critical as the knowledge of the effects of individual design parameters on piston transverse motion.

Measuring the piston transverse motion is therefore an indispensible means for obtaining basic knowledge, and also serves to validate simulation models for computations and parameter identification.

When applying a measurement method with displacement sensors [15] mounted in the cylinder liner, a moving measurement linkage is not needed for data transmission. The advantage of this method is a quick and simple changeout of the test variants, without requiring setup of the measurement equipment on the piston. A disadvantage is the increased programming effort for the numerical analysis of the individual lubricant gap signals measured between the piston and the cylinder wall. The tilt angle curve for the piston axis and the translational displacement of the piston pin must be calculated from the usable individual segments of such lubricant gap curves as shown in **Figure 7.101**. Signals caused by the piston rings must be ignored. The signal range that can be interpreted may be limited to the crank angle range about the top dead center and depends on the piston skirt length and the application to the cylinder.

In order to reduce the effort for setup, in terms of both time and resources, a few typical engine variants have been prepared as test carriers. A number of critical parameters and their effects on piston transverse motion and structure-borne noise excitation can be investigated using these setups.

Selected examples will clarify the motion mechanisms that are associated with the noises known as "croaking" and "rattling." A few typical displacement signals for the motion curves are observed, along with the accelerations measured simultaneously at the cylinder.

Figure 7.102 (left side) shows the typical signal curves for operation with "croaking".

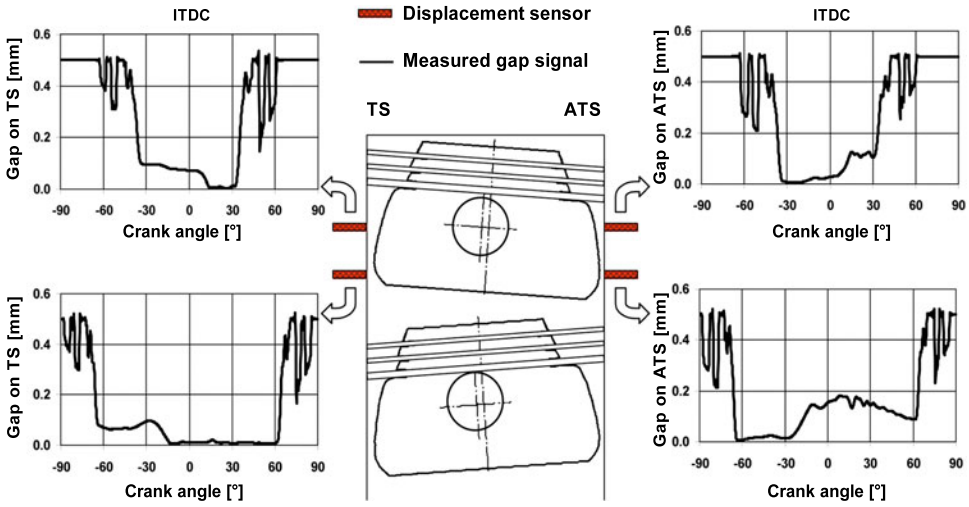

Figure 7.101: Measured lubricant gap signals between the piston surface and cylinder wall

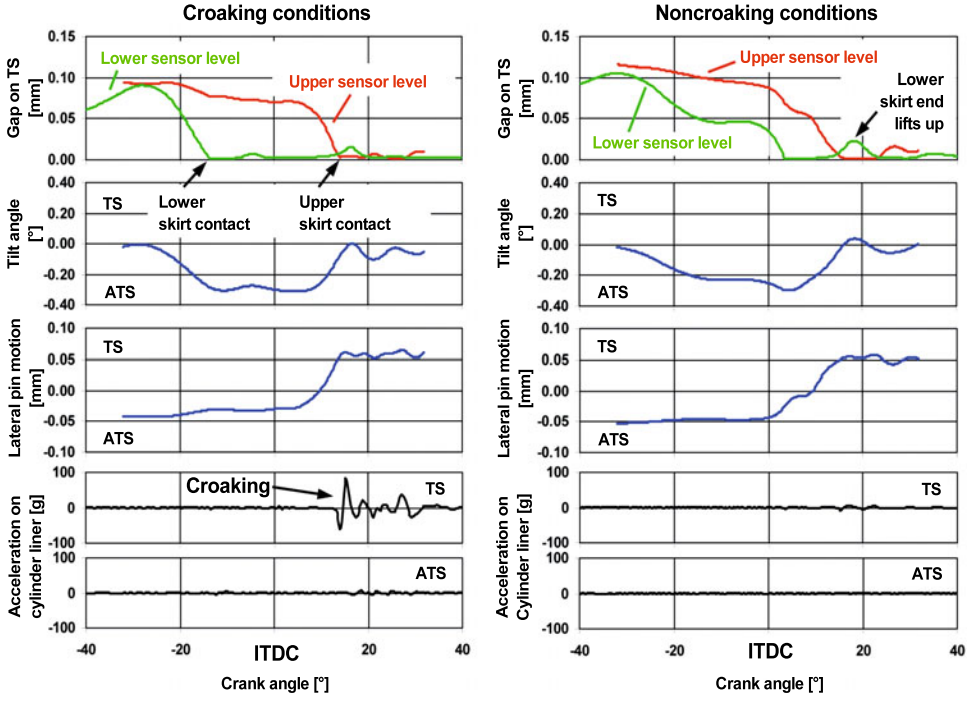

Figure 7.102: Relationship between measured lubricant gap, piston axis motion, and structure-borne noise excitation during operation with “croaking” (left, low speed, low load) and without “croaking” (right, low speed, no load)

At lower speeds, the gas pressure is predominant, even in the early compression phase, thereby inducing contact on the antithrust side as the piston is thrust upward. Not until the crank angle range of 30° to 10° before ITDC does the bottom end of the skirt change contact from the antithrust side to the thrust side. The associated impact of the skirt, which is very elastic at this height, generally does not lead to any significant structure-borne noise excitation. The resulting diagonal orientation remains until after ITDC. Under the influence of gas pressure, the piston then straightens out, and the more rigid upper skirt area strikes the thrust side of the cylinder liner. The piston skirt is deformed over a large area, so the bottom end of the skirt lifts only slightly off the cylinder wall. The thrust-side structure-borne noise excitation generally occurs in the crank angle range between 10° and 25° after ITDC.

Measures with a positive effect include:
- Greater barrel shape of the piston contour
- Greater tapering of the lower end of the skirt
- Greater rigidity in the middle of the skirt
- Greater piston pin offset toward the thrust side
- Reduced installation clearance

A piston transverse motion under similar operating conditions, but without measurable piston noise, can serve as a model for an optimized, “quiet” sequence of motion. Direct comparison of such data often reveals the cause for the structure-borne noise excitation. The diagrams on the right side in **Figure 7.102** show that “croaking” does not occur for measurements at lower gas pressure, and thus lower lateral force, despite similar behavior of the transverse piston motion. In the present case, this indicates insufficient skirt rigidity as the cause of the “croaking.”

An optimized shape and rigidity of the piston skirt reduces the severity of the skirt deformation under load. The improved shape stability promotes continuous rolling of the piston skirt on the thrust side, thus preventing the impacts that lead to “croaking,” as has already been determined for operation with lower lateral force loads. A characteristic of improved rolling motion is a more obvious lifting of the bottom end of the skirt at the point of the maximum tilt angle.

Figure 7.103 shows the typical signal curves for operation with “rattling.” At high speeds, the piston is located on the thrust side during the upward stroke, due to the effect of inertia force. The increasing effect of the gas pressure causes the piston crown to move from the thrust side to the antithrust side well before ITDC. If the top land or the first ring land of the piston crown strikes the antithrust side, this is known as crown rattling. If the impact occurs at the rigid upper skirt area, then this is logically known as skirt clatter. The antithrust-side structure-borne noise excitation takes place between 15° and 5° after ITDC.

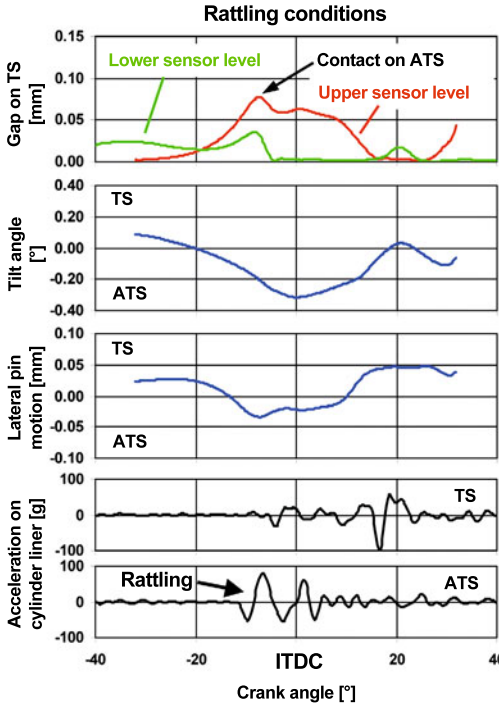

Figure 7.103:
Relationship between measured lubricant gap, piston axis motion, and structure-borne noise excitation during operation with "rattling" (high speed, low load)

Measures with a positive effect include:

- Crown offset toward the thrust side
- Greater tapering of the upper end of the skirt
- Adapted top land and ring land clearances
- Lesser piston pin offset toward the thrust side
- Reduced installation clearance
- Reduced cylinder distortion

Due to the diagonal piston orientation arising in the region of the ignition top dead center, the sequence of motion described above for "croaking" typically follows this effect. A second structure-borne noise excitation on the opposite thrust side, as can be seen in **Figure 7.103**, is therefore often detected, but is not subjectively perceived as additional "croaking" at the higher speed.

As an adjunct to manual analysis and interpretation of the individual diagrams, the measured displacement signals can be used as input variables for computer animation of the transverse piston motion. Only a clear visualization and comparison of a number of suitable test variants can provide the insight that the engineer needs for quick and reliable development.

7.6.3 Piston noise in diesel engines

7.6.3.1 Subjective noise assessment

The acceptance of the diesel engine as a comfortable vehicle drive has increased greatly since the introduction of the high-torque direct-injection passenger car engine. For this reason, the acoustic optimization of diesel engine combustion is considered by vehicle manufacturers to be one of the most critical future tasks, besides the reduction of consumption and exhaust gas emissions.

Modern injection systems, which allow pre-injection based on the operating point, or modeling of the injection sequence, contribute greatly to this end. This and the current pump concepts with reduced hydraulic noise lead to a reduction in noise level, which has caused mechanically induced noise to play a more prominent role again. Systematic minimization of piston noise is therefore more and more important in diesel engines as well.

In contrast to the gasoline engine [16, 17], diesel engines [18] have no typical types of piston noise that can be identified by their sound alone. The physical boundary conditions that prevail in diesel engines, however, do not support the conclusion that less piston noise should be expected than in gasoline engines. Higher gas pressures, more rigid pistons with greater mass, and greater installation clearances indicate that greater structure-borne noise excitation is more likely.

Nevertheless, for many drivers, the degree of sensitivity to piston noise appears to be less and the general tolerance of mechanically induced noises to be greater. Both tendencies are certainly due to the dominant combustion noise that is common in diesel engines.

The acoustic similarity of the combustion noise and piston noise often makes a subjective assessment of piston noise difficult. A direct comparison of recorded signals, however, allows the human ear to detect even slight differences very well. When variants are compared, however, because these differences are attributed to the change in the running characteristic of the piston, scrupulous attention must be paid to the fact that in such a comparison the combustion sequence remains unchanged and must not appear here as a second parameter. In order to ensure this, the combustion chamber pressure curve must be recorded and appropriately controlled, even in the case of signal recording for subjective noise assessment.

In order to determine the subjective, acoustically relevant operating ranges in the diesel engine, an estimate of potential is helpful. The engine noises are compared between a selected loud piston (piston A: without piston pin offset, with acoustically unfavorable piston shape, and large installation clearance) and a piston designed specifically to be quiet (piston B: with computationally optimized piston pin offset, acoustically favorable piston shape, and very small installation clearance). The most important results of such a comparative, subjective noise assessment are shown in **Figure 7.104**.

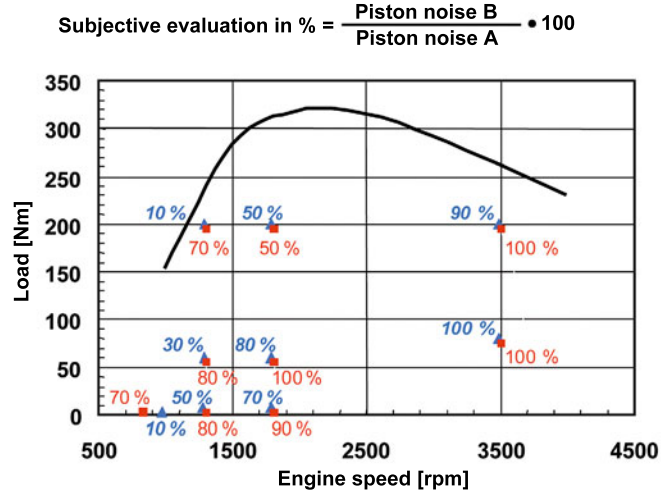

Operating point	Idle 0 Nm	1300 rpm 0 Nm	1300 rpm 60 Nm	1300 rpm 200 Nm
Warm ■				
Piston A	100 %	100 %	100 %	100 %
Piston B	70 %	80 %	80 %	70 %
Cooled ▲				
Piston A	***100 %***	***100 %***	***100 %***	***100 %***
Piston B	***10 %***	***50 %***	***30 %***	***10 %***

Figure 7.104: Engine operating map of a DI passenger car diesel engine, with subjective assessment of the piston noise of two different pistons, assessed in direct listening comparison

Piston A is defined as 100% for each operating point. The result for the piston noise detected from the quiet piston B is therefore a lower value.

While the subjectively perceived difference is very low at high speeds–although this is precisely where a high proportion of mechanical noise is present–a significant effect on the overall noise by the piston excitation can be detected at low speeds. This applies particularly to speeds of less than 2,000 rpm, at very low or high loads. In the lower part load range, where combustion causes high pressure rise values, however, the combustion noise is dominant, so that the piston noise that must surely also be present in this range plays a secondary role.

The effect of piston design on the piston noise is fundamentally greater in a cold engine than in a hot engine. Nevertheless, an improvement can be perceived subjectively, even in a hot operating state.

Therefore, it is proposed that a measurement program be standardized that includes both the cooled (symbol Δ, water and oil temperature around −20°C) and hot (symbol □) engine. **Figure 7.105** again shows the operating map of a diesel engine, now with the measurement program resulting from the above conclusions, consisting of run-up curves above the load at low speed and for different engine temperatures (symbolized by the vertical arrow), and a few selected stable measurement points from the ranges that are particularly relevant from an acoustical standpoint. Previous experience has shown that these operating conditions are not only representative of subjective assessments, but are also very well-suited for computational optimization processes and as measuring points for objective noise assessment.

In the crank angle range around the ITDC, the contact side of the piston in the cylinder changes from the antithrust side to the thrust side. For pistons with no piston pin offset or with an offset toward the antithrust side, this is a largely translational motion sequence with small tilt angles about the piston axis. This can give rise to a free motion phase for the piston, which causes the piston to accelerate toward the thrust side. The piston then strikes the thrust-side cylinder wall, causing structure-borne noise excitation in the engine structure.

If the piston is offset toward the thrust side, however, then the contact alteration starts with the bottom end of the skirt, at an earlier crank angle, and the motion of the piston crown toward the thrust side is slowed. The result is greater tilt angles of the piston axis and a temporary diagonal orientation in the cylinder. Due to the supporting lateral forces and the greater deformations of the piston skirt, the structural sound excitation can be reduced [19]. In current DI engines, the optimum piston pin offset is generally between 0.3 and 0.6 mm

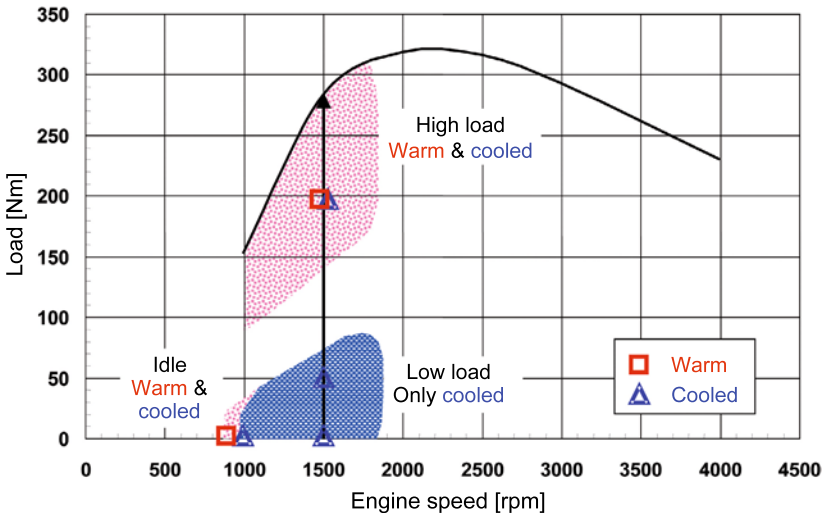

Figure 7.105: Noise operating map of a DI passenger car diesel engine and recommended measurement program, based on subjective auditory impression, for subjective and objective noise assessment

toward the thrust side. Therefore, a starting value of 0.5 mm is suggested for the experimental development phase.

Seizure resistance must be considered in the optimization of the barrel-shaped, oval piston form. Because this has a direct interrelationship with the installation clearance, only an overall analysis makes sense. This circumstance can be clarified with the help of two piston skirt profiles; **Figure 7.106**.

If a piston has less deviation in the upper skirt area (piston profile A)–indicated here as height D2, according to the piston drawings–then the guidance of the piston in the cylinder appears to be better, and less structure-borne noise excitation is to be expected. If, however, the reduction in seizure resistance is taken into consideration, then the piston must be installed with a nominal installation clearance that is greater by this amount; **Figure 7.106**, lower diagram. In this case, piston B appears to provide better guidance in the cylinder, and therefore less structure-borne noise excitation. The two influence parameters, piston shape and installation clearance, can be clarified by a fast and rough projection to determine which design will tend to lead to a running characteristic that is more favorable from an acoustical standpoint.

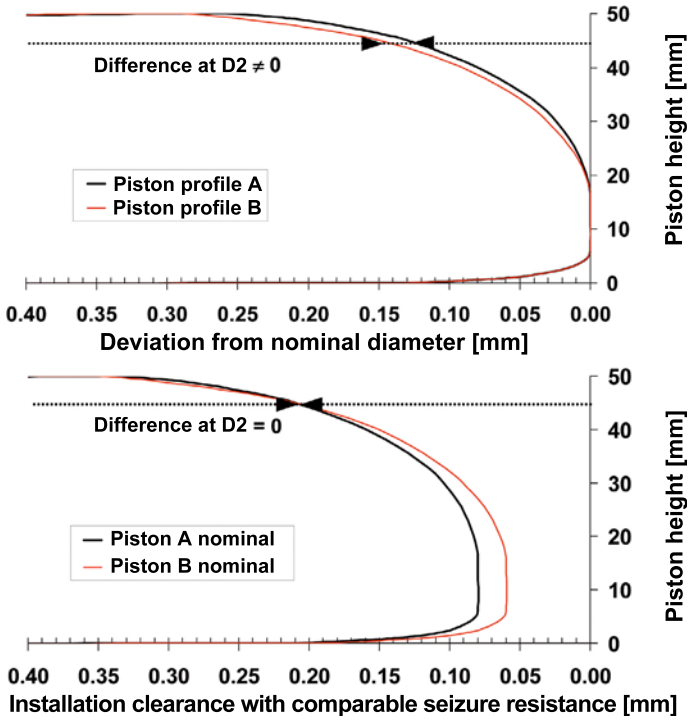

Figure 7.106: Interrelationship between the piston profile, installation clearance, and seizure resistance
D2: Piston diameter at a fixed piston height in the upper skirt area

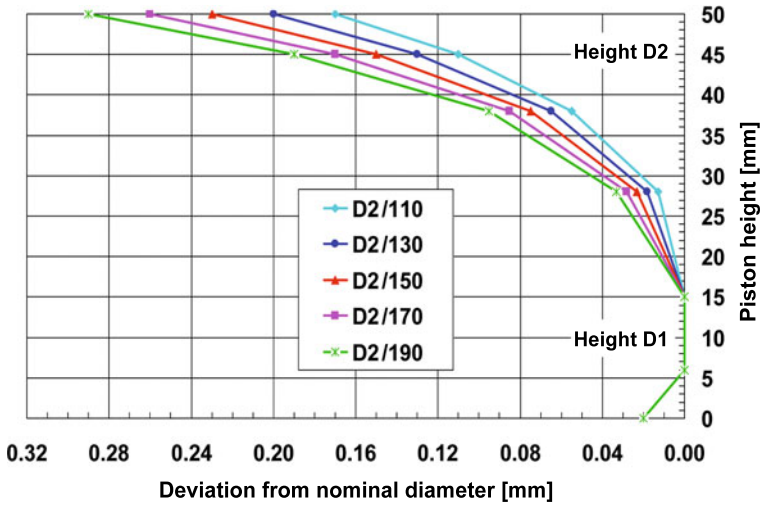

Figure 7.107: Piston skirt geometries used for calculations, with different implementations of seizure resistance
Height D1: Piston height at which the piston has the greatest diameter D1

The key parameters for five piston skirt profiles are sketched in **Figure 7.107**, differentiating the upper skirt taper at height D2 between 110 and 190 µm in steps of 20 µm. The lower skirt taper remains unchanged. The analysis of the piston transverse motion is made for different assumptions of installation clearance, such as the steps of 20 µm.

If the maximum contact force that occurs on the thrust side is again taken as an approximate criterion for structure-borne noise excitation, then the result is the lines drawn in **Figure 7.108** for the individual piston profiles, which indicate smaller installation clearances, as expected. Also, as assumed, pistons with increasingly greater upper skirt taper cause a shift toward greater maximum forces.

If points with identical running clearance at height D2 (deviation of the piston geometry at height D2 plus installation clearance) are connected to each other, then the result is the connection line, as a line of comparable seizure resistance. This is additionally shown in **Figure 7.108**, using the example of 190 µm. Its progression shows clearly that for such engines with comparable seizure resistance, the least possible installation clearance with the correspondingly necessary large upper skirt taper provides the best acoustic solution.

This potential for improving the acoustics often justifies the implementation of small installation clearances, using a graphite coating on the piston skirt to increase seizure resistance. The positive influence of reducing the installation clearance and the negative effect of the greater upper skirt taper cancel each other out only for large installation clearances greater than 60 µm.

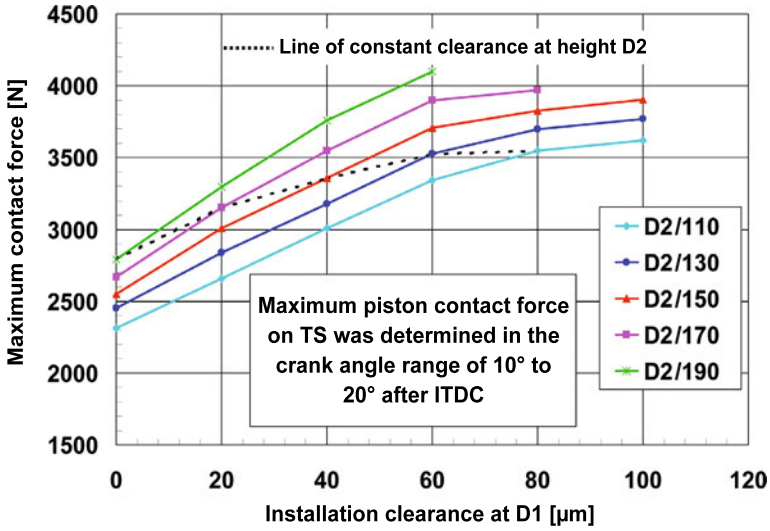

Figure 7.108: Maximum contact force as a function of piston shape and installation clearance, calculated for low speed and low load

Due to the high rigidity of the skirt in diesel engine pistons, compared to gasoline engine pistons, the typical ovality values in series production diesel pistons are considerably less dispersed. A computational pre-estimate is therefore not absolutely necessary for a first test. The final ovality values arise largely from the optimization of the contact pattern on a piston that has been run. Particularly for pistons with optimized profiles and small installation clearances, the acoustic effect of the ovality of the piston skirt is of secondary importance.

7.6.3.2 Objective noise assessment and quantification

Noise analyses and a subsequent objective noise assessment have the goal of identifying an existing piston noise as such and quantifying it, so that piston variants can be made objectively comparable.

In order to determine the absolute value of the noise component caused by the piston, a systematic partial sound source analysis must be performed with the goal of quantitatively separating the noise excitation from combustion, the injection system, the valve train, the crankshaft drive, and various auxiliary systems. Such extensive tests are primarily suited for basic research work, but not for the regular optimization work leading up to series production.

A method is used, therefore, that allows piston variants to be objectively compared to each other with relatively little effort. The portion identified as piston noise, however, can be quantified only relative to other piston variants. An initial basis for such an A/B comparison is often

the potential estimate suggested previously, with selected loud and quiet piston designs. Every other test variant can be arranged between them. The improvement that has been achieved between the initial state and the optimized piston can then be documented, as shown in the following example.

If a noise excitation due to piston impact occurs in a diesel engine, then it can be assumed that this mechanical impact excitation will be found to be much stronger in a structural noise signal measured in the upper area of the cylinder block, due to the dominant external structural noise conductance path, than in a signal measured at the main bearing cover of the associated cylinder [21]. The force excitation due to combustion and the impact excitation of the crankshaft in the bearing, on the other hand, are greater in the area of the main bearing than at the exterior of the crankcase. The internal structural sound conductance path is dominant.

If such structure-borne noise measurements are performed with piston variants that are very different acoustically and the signal levels measured at the main bearing do not significantly deviate from each other, then the difference that can be measured in the upper crankcase area and in the airborne noise can only be attributed to excitation by the piston. A prerequisite, however, is that each measured operating point has been checked using the combustion chamber pressure curves captured at the same time, to determine whether operation with both piston variants and identical combustion has taken place.

Figure 7.109 shows such a measurement result, using overall levels (up to 10 kHz) over the load, derived for the sound pressure at a distance of 140 cm from the engine, for the structure-borne noise on the thrust side of the crankcase (centered on the selected cylinder), and for the structure-borne noise at an associated bolt for the main-bearing cover.

The acoustically optimized piston B differs from the acoustically objectionable piston A by a piston pin offset optimized by computation and experimentation, by a modified skirt profile having greater upper skirt taper, and by minimized installation clearance. The skirt ovality and the piston ring and top land clearances are adapted to the modified running characteristic with the help of visual inspection of the pistons that have been run. All prescribed seizure tests have been passed previously.

The reduction in sound level achieved by these measures can be as much as 5 dB. The significant reduction in the structure-borne noise level on the thrust side is effective only at very low loads and high loads–as is sketched schematically in **Figure 7.104**. The accelerations measured at the main bearing cover do not exhibit these blatant differences. It can be assumed, therefore, that the difference in noise excitation in this case can be attributed solely to the piston.

In the lower partial-load range, in contrast (cf. load range from 50 to 100 Nm), the dominant excitation is due to very rapidly advancing combustion caused by the considerable ignition lag, especially in the cooled engine. In this load range, the combustion noise determines the

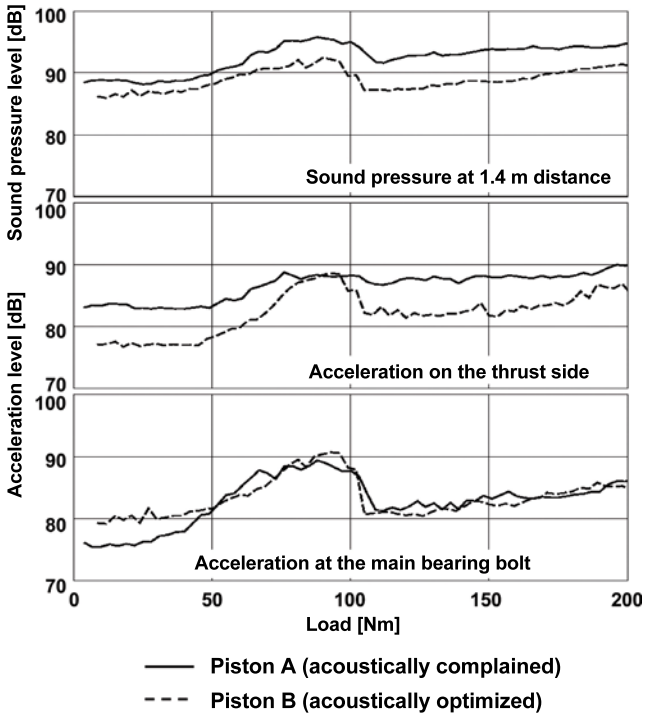

Figure 7.109:
Sound pressure and acceleration level as a function of the load, measured on a DI passenger car diesel engine, engine speed 1,500 rpm, cooled engine (total level over 0–10,000 Hz)

sound level. In the lower partial-load range, therefore, neither subjective nor objective assessment of the piston noise is recommended.

The airborne and structure-borne noise levels depicted in **Figure 7.109** are analyzed more closely in order to quantify the noise components caused by the piston. The comparison of the two Campbell diagrams for airborne noise shown in **Figure 7.110** demonstrates clearly that the frequency range around 1,850 Hz is emitted more strongly with the acoustically objectionable piston over the entire load range.

The spectral representation of the accelerations measured on the thrust side, shown in **Figure 7.111**, confirms that the piston is the cause of this partial increase in sound level. The accelerations measured at the main bearing, in contrast, would not show this increased excitation in the case of piston impact, which is also evident in **Figure 7.112**.

The frequency content of an impact excitation caused by the piston has been empirically found to have a broader band than is evident in the diagrams in **Figure 7.110** and **Figure 7.111**. The intense increase in just a narrow range is surely not attributable to the excitation characteristic, rather, it is due to the operational vibration behavior of this special engine structure. In many diesel engines, however, this has been observed in a similar manner when piston impact occurs. The bandpass levels measured in the narrow raised frequency range,

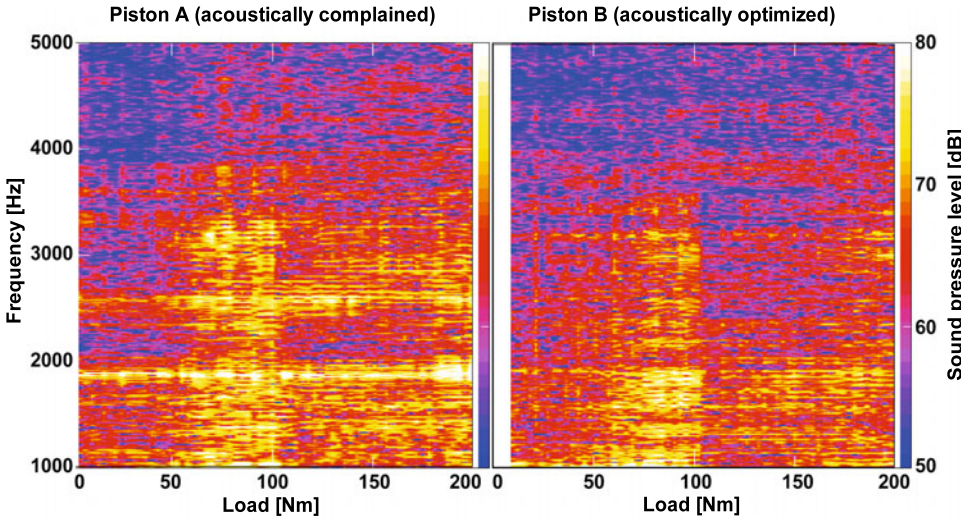

Figure 7.110: Sound pressure spectra as a function of load, measured on a DI passenger car diesel engine, engine speed 1,500 rpm, cooled engine

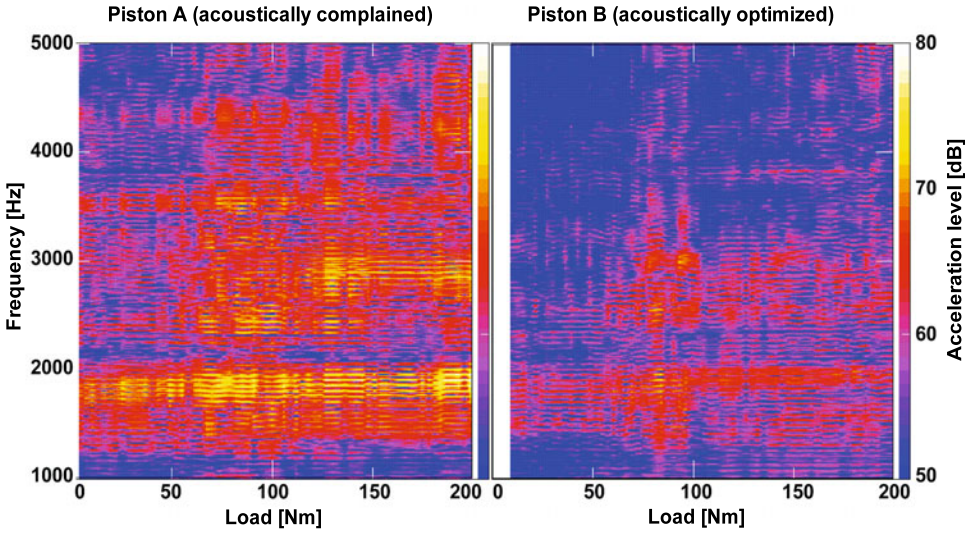

Figure 7.111: Acceleration spectra (thrust side) as a function of load, measured on a DI passenger car diesel engine, engine speed 1,500 rpm, cooled engine

as shown in **Figure 7.113**, can be used as a comparative criterion for objective analysis of the individual piston variants. The acceleration measured on the thrust side of the engine block represents the effect of the piston on the noise excitation much more specifically than the airborne noise signal measured at a distance from the engine and is therefore also more appropriate for such a quantitative analysis in most cases.

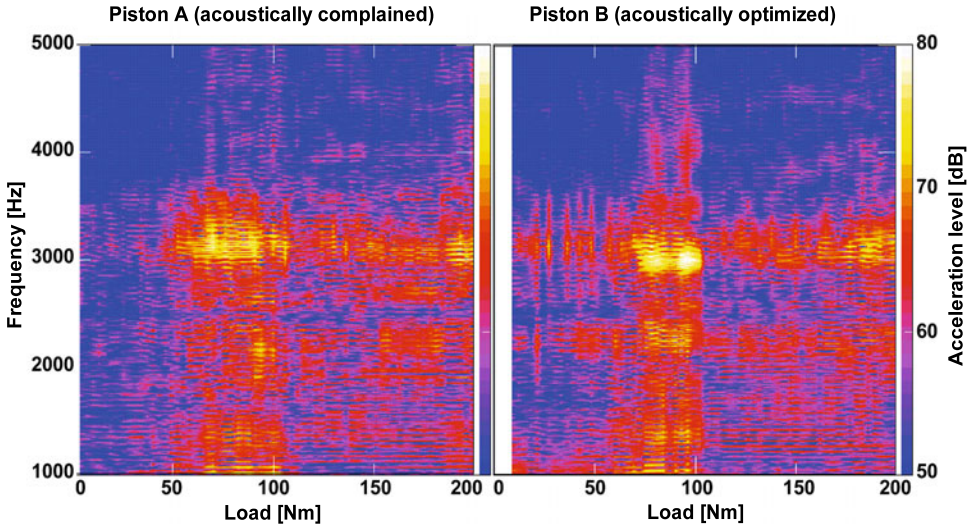

Figure 7.112: Acceleration spectra (main bearing cover bolt) as a function of load, measured on a DI passenger car diesel engine, engine speed 1,500 rpm, cooled engine

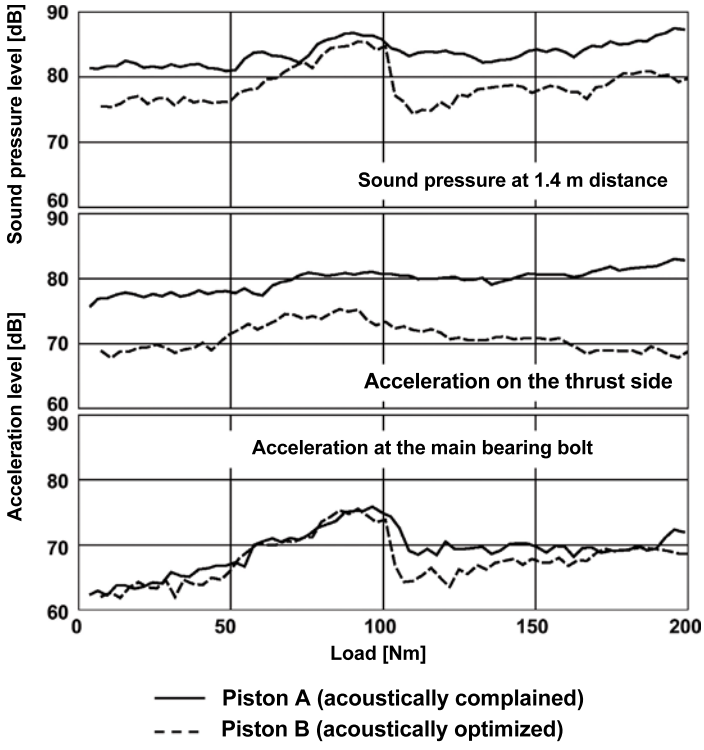

Figure 7.113: Sound pressure and acceleration level as a function of the load, measured on a DI passenger car diesel engine, engine speed 1,500 rpm, cooled engine (bandpass filter frequency 1,750–1,950 Hz)

7.6.3.3 Piston transverse motion and influence parameters in diesel engines

Analogous to the procedure for gasoline engines, a characteristic behavior of the piston transverse motion is to be depicted for the diesel engine. **Figure 7.114** shows an analysis of such superimposed signals together with the pressure curve measured simultaneously in the combustion chamber and the structure-borne noise measured at the cylinder liner.

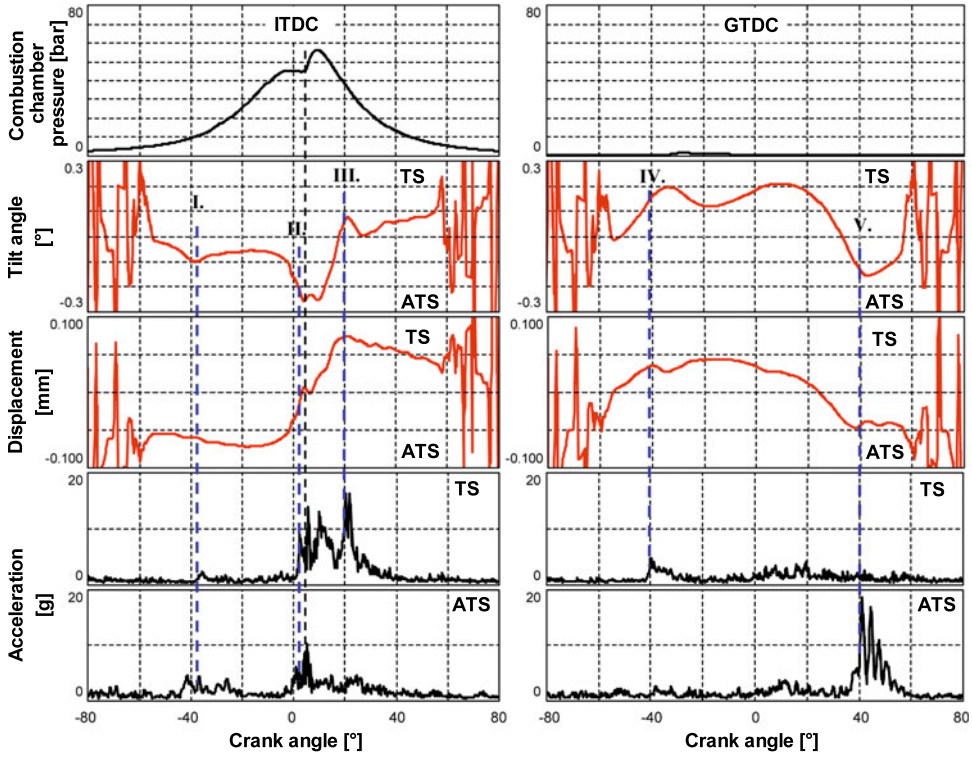

Figure 7.114: Mechanisms for structure-borne noise excitation in diesel engines

The example shown is typical of the sequence of motion of a diesel piston with a slight offset toward the thrust side, immediately after cold start. Due to the very large installation clearance selected for this measurement, five excitation mechanisms that may occur in the diesel engine can be depicted for using a single operating point. Assigning the translational and rotational piston transverse motion to the corresponding structure-borne noise excitation, in terms of both time and location, defines the mode of action of mechanisms I through V unambiguously.

If a piston noise is identified as such in the diesel engine, and if a known mechanism of motion can be determined as the cause based on experience, then the number of engine tests needed for optimization depends only on the correct decision of how many test variants to run.

In order to increase the understanding of concrete motion sequences and of the measures to be taken, measured motion information is prepared so that the entire piston transverse motion, including the deformations of the piston skirt, can be visualized quickly and easily. This makes it easier for the engineer to find a solution in a quick and precise manner.

Using the insight drawn from several DI passenger car diesel engines, a few helpful tips can be formulated for the design of an acoustically favorable diesel piston:

- The distinct barrel shape of the upper area of the skirt, together with sufficient rigidity in the middle area of the skirt, supports rolling of the piston against the cylinder wall, thus helping to reduce impact excitations.
- The skirt end taper with a hydrodynamically optimized design should act over a circumferential angle of about 60 degrees, in order to ensure seizure resistance even at low installation clearances.
- The installation clearance, to be defined in the lower skirt area, should be as small as possible. In case of insufficient seizure resistance in the area of the thrust-side or antithrust-side generating line of the piston skirt, the upper shaft taper should without fail be increased before increasing the installation clearance. The use of a graphite coating on the piston skirt can provide a double enhancement in this case.
- The ovality of the skirt can be used exclusively for optimizing the width of the contact pattern and helps to ensure the necessary seizure resistance in the more rigid side areas of the piston skirt as well. The direct effect of skirt ovality on the acoustic behavior is of secondary importance in a piston design that has been optimized in all other aspects.
- For diesel pistons, a small piston pin offset of 0.3 to 0.6 mm toward the thrust side is preferred over a design with no offset. A potential increase in oil carbon buildup, which can lead to “bore polishing” under certain circumstances and thus to increased oil consumption, can be counteracted with suitable measures, such as an offset of the piston crown or adaptation of the conicity and clearance at the top land or ring land.

7.7 Piston pin noise

7.7.1 Causes of noise

As has been described in Chapter 7.6, the subjectively objectionable noises that can be attributed to the piston and its periphery in a gasoline engine have sound characteristics that are very different from each other. In addition to the piston noises that have already been analyzed, in some cases a harsh, metallic, impulse noise can occur erratically at idle speed or increased speed (up to about 2,000 rpm) and only at zero load. It is subjectively perceived to be very objectionable.

This noise, known as “pin ticking,” is induced as the pin impacts against the bore wall after passing through the clearance of the piston pin in the pin bore. Noise induced by the pin in the small conrod eye, which can also cause a comparable ticking noise, and is therefore also sometimes called pin ticking, is not the subject of this discussion. As has been shown by experience, however, the procedure described for measuring and analyzing the pin noise in the boss is also suitable for quantifying the excitation caused in the small conrod eye.

Complaints due to pin noises are unknown for the diesel engine, as these experience completely different pressure ratios in the compression phase. All further considerations, therefore, deal with gasoline engines exclusively.

In a gasoline engine, in the affected operating ranges, the cylinder is under vacuum in the early compression phase. Combined with the arising inertia forces, this forces the pin to make contact in the lower boss area. As the compression pressure increases, the sign of the resultant vector for the gas and inertia forces changes in a crank angle range well before ITDC. At the point when this resultant force changes sign, the contact of the piston pin changes from the pin bore ground to the pin bore zenith. If this change occurs along a more or less direct path to the opposite wall rather than as a rolling or sliding motion along the pin bore, then this can cause noise excitation after passing through the clearance [22].

While the piston noises of croaking and rattling are generally audible at low engine temperatures, and decrease as the engine warms up, piston pin noises in the pin bore occur predominantly during the warm-up phase or in a warm engine. One reason for this phenomenon is the difference in thermal expansion coefficients between the aluminum piston and the steel pin. Particularly during the warm-up phase, but also in the warm operating condition, the thermally induced running clearance between the pin and piston can increase relative to the installation clearance, which is measured at 20°C. This promotes the excitation of this noise.

7.7.2 Structure-borne noise transmission paths and measurement program

If a pin noise is to be objectively analyzed, then the best and simplest way to clarify it with measuring equipment must first be determined. **Figure 7.115** shows the locations of structure-borne noise excitation for the piston noises of croaking and rattling, as well as for pin ticking. For the first two noises, the cylinder wall is excited directly by the piston on the thrust side (TS) or antithrust side (ATS). Following the outer structure-borne noise transmission path, the acceleration measurement is applied directly to the surface of the block. For the pin noise, the structure-borne noise primarily takes the inner transmission path, via the connecting rod, the crank pin, and the crankshaft, into the main crankshaft bearing. The main crankshaft bearing cover, or one of the two mounting bolts for the cover, is thus ideal as a measurement position for an acceleration sensor [23].

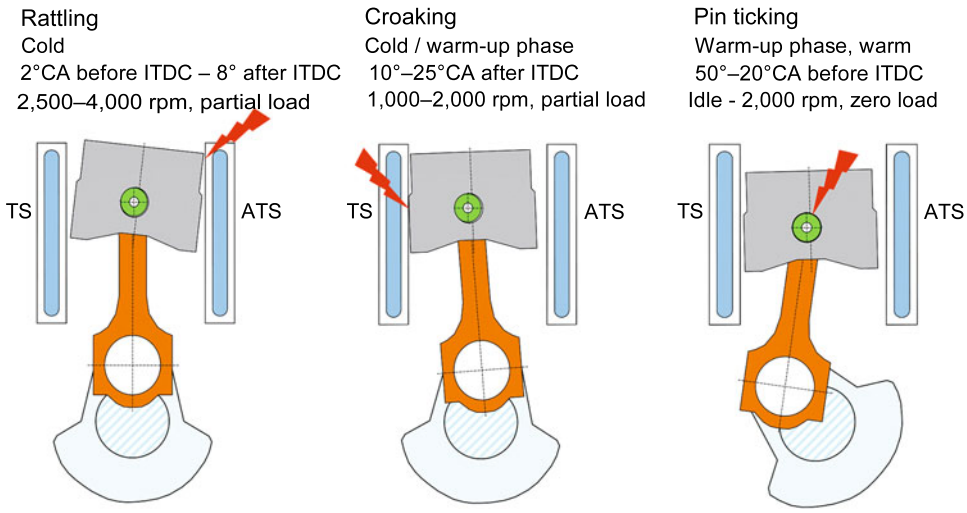

Figure 7.115: Locations of structure-borne noise excitation for typical piston and piston pin noises in a gasoline engine

Figure 7.116 shows the time signal sequences of various acceleration sensors and a microphone at an operating point with a clearly audible pin noise. Five working cycles are shown. A piston with an oversized pin bore diameter is installed only in the test cylinder, resulting in oversized pin clearance. All the other cylinders in the four-cylinder engine are equipped with pistons that allow pin clearance at the lower tolerance limit, and therefore verifiably do not cause any piston pin noises.

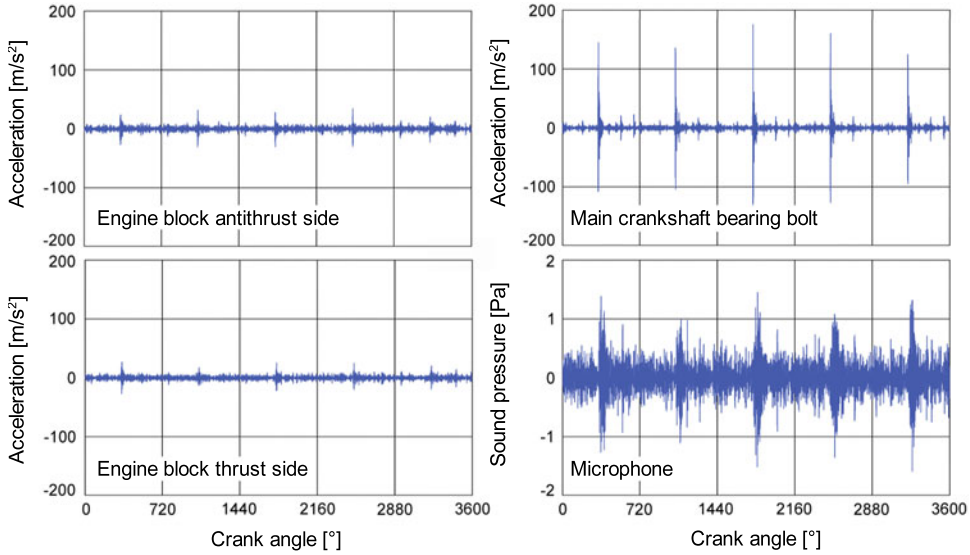

Figure 7.116: Typical time signal sequences for a given piston pin noise

The structure-borne noise excitation by the piston pin can also be detected in the signals from the sensors on the thrust and antithrust sides of the engine block surface, but significantly greater distinction between the useful signal and the background noise can be obtained at the bolt location on the main crankshaft bearing cover. Therefore, this measurement position is ideal for a sensitive assessment of the different variants that affect the piston pin noise. The microphone position is selected at the location where the noise of interest is subjectively most clearly audible.

The pin noise behavior of different engines will normally vary greatly. Therefore, a standardized measurement program has been developed, which allows the detection of any piston pin noises. It consists of various running programs at constant speed, and dynamic run-ups followed by run-downs. The water temperature is varied through the range from 30 to 100°C for each run. The most acoustically noticeable temperature range is then measured more precisely at a constant water temperature using dynamic variations in engine speed.

The measurements are carried out continuously over the entire rise in temperature. A large amount of data is produced, because the measurement period lasts for several minutes. In order to extract the important information from the measurement signals, the method described in the next section is used. The structure-borne noise at a main bearing cover bolt, which corresponds very well to the airborne noise, is used exclusively for this evaluation.

7.7.3 Evaluation procedure in the time domain

The amplitude of the excitation determines the intensity of the perceived piston pin noise. Therefore, only the maximum acceleration amplitude that is excited by the piston pin at the structure-borne noise measurement point on the main-bearing cover bolt is used. If the structure-borne noise excitation is as dominant as in the example in **Figure 7.116**, the maxima can simply be sought out in the individual working cycles. For less distinctive piston pin noises, and if other noise sources are also present, as is often the case, then the results can easily be misinterpreted. Therefore, the maxima should be sought out only in the crank angle range in which piston pin noises might occur. In this example (see **Figure 7.117**), a crank angle range from 50° to 20° before ITDC was selected for a maxima search. All working cycles accumulated during the measurement are analyzed for maximum amplitude in the indicated crank angle range. These maximal amplitudes are then plotted against temperature and time.

In this example, no irregularities can be seen during the temperature run-up at idle speed. The test engine used does not have any piston pin noise in this operating state, despite its large pin clearance. Experience shows, however, that other engines can generate clearly audible piston pin noises at idle speed. At first, when measured at a constant speed of 1,500 rpm, pin excitation still cannot be detected. Above a water temperature of approximately 83°C, however, a significant increase in the amplitude height becomes evident. The temperature run-up with dynamic increase in speed, from idle speed to 2,000 rpm, shows a similar behavior. Here the first signs of noise excitation by the piston pin can already be detected at a low

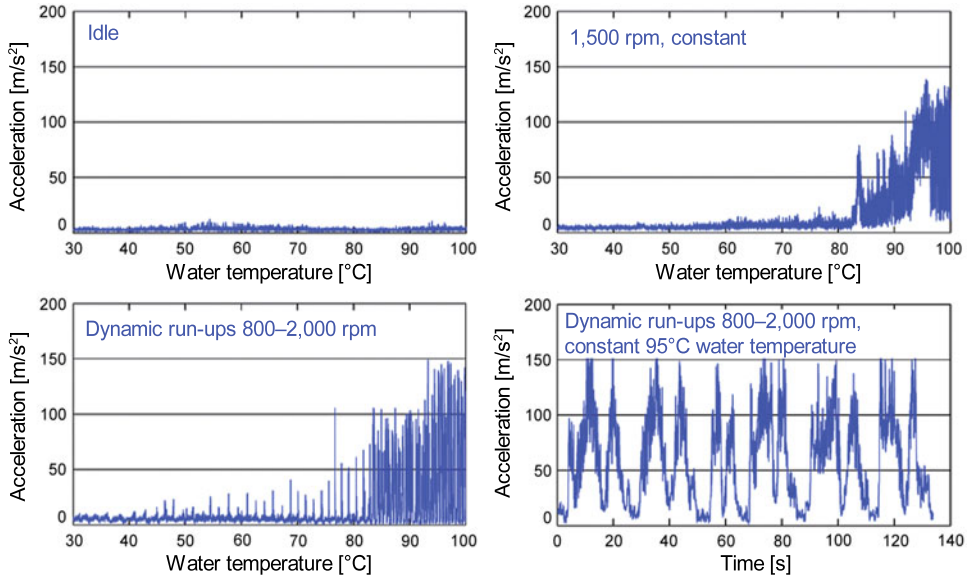

Figure 7.117: Effects of various operating conditions on piston pin noise using the standardized measurement program

temperature. The greatest amplitudes occur at a water temperature of about 95°C. For this reason, the measurement at constant water temperature with a dynamic speed increase will also be run at 95°C. This measurement shows the very characteristic behavior of the piston pin noise in the test engine, and, after further refinement of the analysis method, helps to evaluate various parameters that affect the pin noise.

The speed, the maximum acceleration amplitudes determined for a crank angle window prior to ITDC, and the crank angle at which the individual amplitudes occur are all plotted against the measurement time in **Figure 7.118**.

At both rising and falling speeds, the greatest amplitudes are observed in the range between 1,600 and 1,800 rpm. The crank angle values at which the maximum amplitudes occur are between 35° and 20° crank angle before ITDC.

In order to reliably evaluate and classify the results in a parameter study, a large number of such dynamic acceleration and deceleration runs must be incorporated in the analysis. Using a special type of averaging, reproducible and significant results can be obtained. Examples are included in the following section, using concrete parameter studies. Including a sufficiently high number of run-ups used for averaging provides sufficiently stable results.

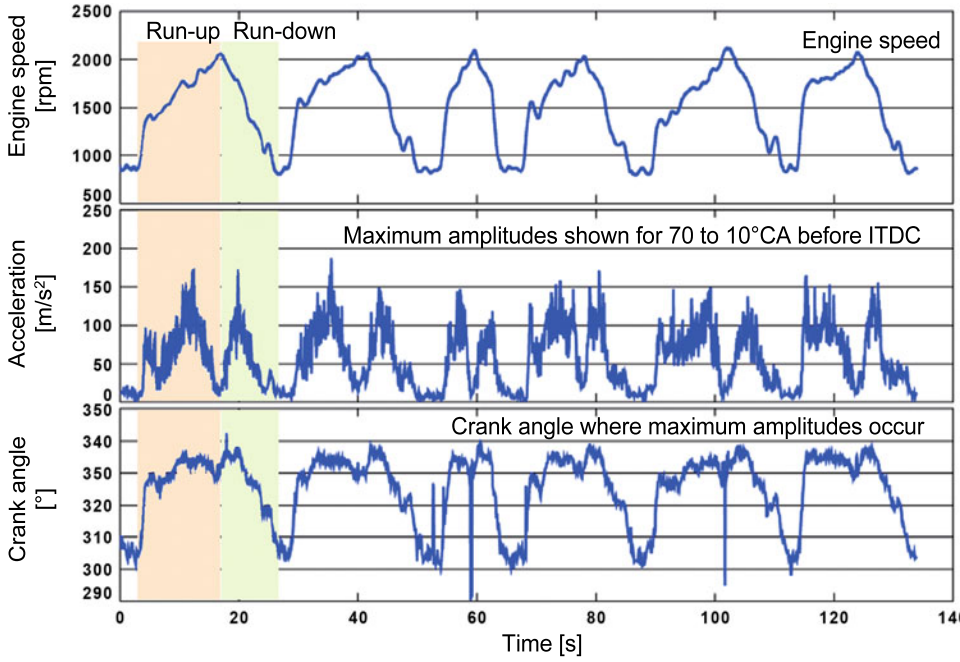

Figure 7.118: Maximum amplitudes, measured at the main bearing cover bolt and corresponding crank angle, at varying engine speed

7.7.4 Results from parameter studies

7.7.4.1 Influence of piston pin clearance

One parameter that has a great influence on piston pin noise is the piston pin clearance in the pin boss. With a floating pin design, the typical design clearance is between 2 and 12 µm. These values refer to a cold engine. During the warm-up phase, and in the warm condition, the operating clearance is greater due to the thermal expansion coefficient of the aluminum piston material, which is nearly double that of the steel used for the pin.

Figure 7.119 shows the effect of different pin installation clearances on the maximum structure-borne noise excitation, from 50° to 20° crank angle before ITDC, measured at the main bearing cover bolt. Pin clearances were varied over a range from 5 µm to 24 µm. As expected, increasing pin clearance is associated with a steady increase in the maximum accelerations. In order to evaluate the amplitude above which the structure-borne noise measured at the main bearing can be heard as airborne noise, and therefore perceived as objectionable, the results of a subjective auditory impression are used. The variations in clearances differ clearly not only in the intensity of the piston pin noise, but also in the speed range at which a piston pin noise first becomes audible. While no piston pin noise can be heard at 5 µm and 8 µm clearance, an audible noise occurs at 12 µm clearance between 1,600 and 1,800 rpm. At 24 µm clearance, the speed range with audible pin ticking starts just above idle speed, at about 900 rpm, and again ends at about 1,800 rpm.

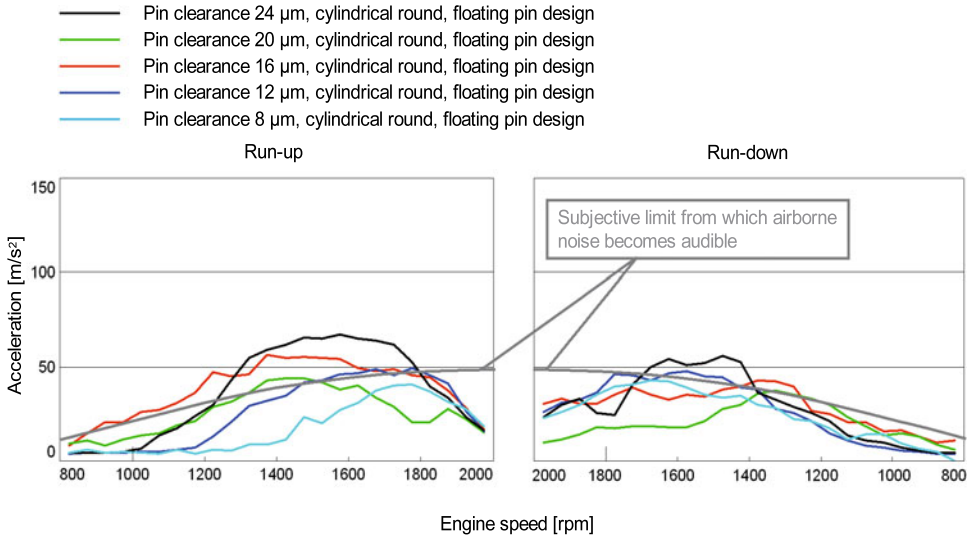

Figure 7.119: Influence of piston pin clearance on the structure-borne noise excitation in a cylindrical round pin bore

Based on this observation, the diagram in **Figure 7.119** for speed increases and decreases includes a curve showing the level at which the structure-borne noise becomes audible as objectionable airborne noise. This audible limit is included in all the other diagrams without further explanation.

7.7.4.2 Influence of pin boss geometry

There are many common versions of pin boss geometry designs. Intentional deviations from the cylindrical round pin boss shape, however, are typically not related to the acoustic behavior of the engine; rather, they are intended to reduce local component stresses, thereby increasing service life. Other measures have the goal of improving lubrication in the boss, thus reducing wear and the risk of seizing.

7.7.4.2.1 Oil pockets and circumferential lubrication groove

The oil pockets (slots) are continuous recesses running along the pin bore, which improve the oil supply (see sketch in **Figure 7.120**). Circumferential lubrication grooves running perpendicular to the pin bore serve the same purpose.

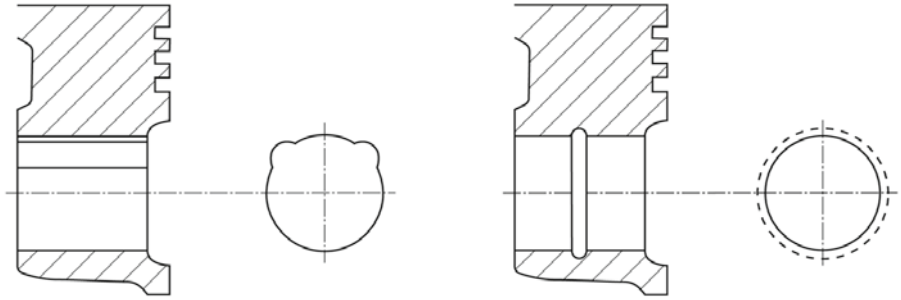

Figure 7.120: Schematic diagram of a pin bore with oil pockets (slots, left) and circumferential lubrication groove (right)

Both measures improve lubrication in the boss and reduce the structure-borne noise excitation considerably below an acoustically critical level; **Figure 7.121**. For the variant with a cylindrical round boss combined with a circumferential lubrication groove, even pin clearances of up to 24 µm were implemented without any acoustical concerns.

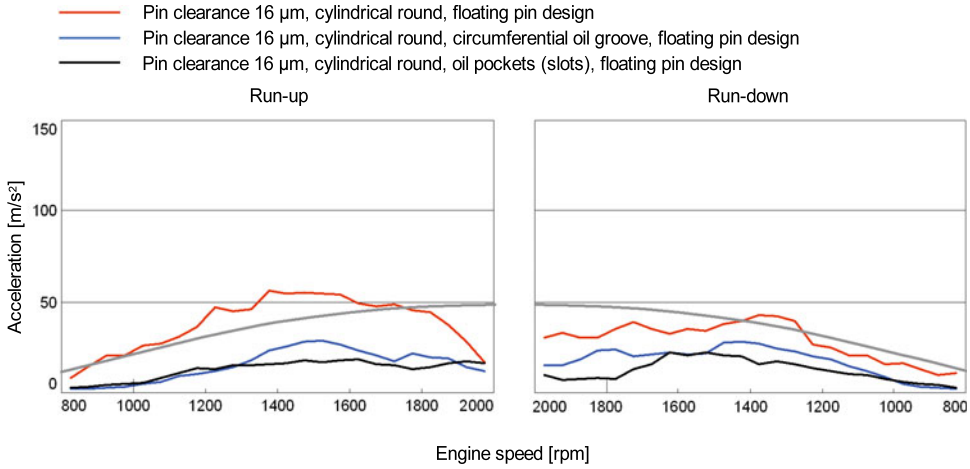

Figure 7.121: Influence of oil pockets and circumferential lubrication groove on the structure-borne noise excitation

7.7.4.2.2 Horizontal oval pin bore and side reliefs

Both measures help to reduce stresses in the pin boss support for piston pins that deform into an oval shape under high gas pressures. For designs, see sketches in **Figure 7.122**.

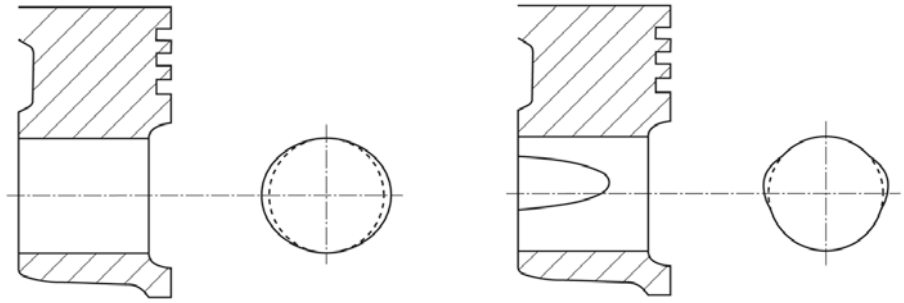

Figure 7.122: Schematic diagram of a horizontal oval pin bore (left) and a round pin bore with side reliefs (right)

Figure 7.123 shows a comparison between round and horizontal oval pin bore designs, as well as pin bores with side reliefs, with 16 µm basic installation clearance for each pin. Both measures reduce the structure-borne noise excitation by the piston pin. The version with side reliefs, however, is near the audible limit. The horizontal oval pin bore achieves a significant improvement in comparison with the cylindrical round pin bore. It has significantly lower acceleration values, which do not cause any audible piston pin noise. With horizontal pin

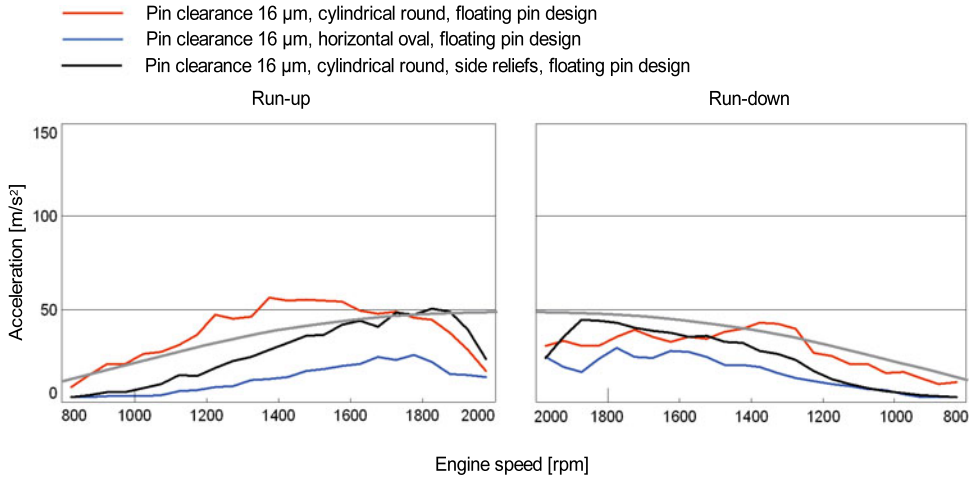

Figure 7.123: Influence of horizontal oval pin bore and side reliefs on the structure-borne noise excitation

boss geometry, even a very large basic fitting clearance can be implemented without causing perceptible noise. The horizontal oval design of the pin bore thus represents a very effective measure to reduce piston pin noises.

7.7.4.2.3 Single-sided vertical oval pin bore

In very highly stressed gasoline engines, the high gas pressures induce large bending moments in the piston about the longitudinal axis of the pin. This is often associated with high stresses on the surface of the piston, which bounds the combustion chamber in the transverse direction of the engine. The vertical oval design of the upper half of the pin bore helps to reduce these stresses significantly; **Figure 7.124**. This measure, intended to increase service life, is also accompanied by an increased pin clearance in the vertical direction.

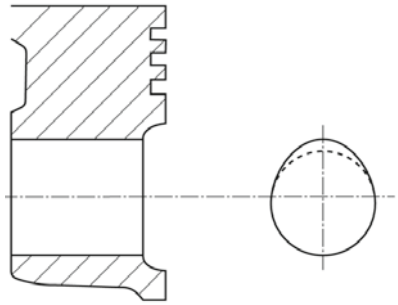

Figure 7.124:
Schematic diagram of a pin bore with single-sided vertical ovality

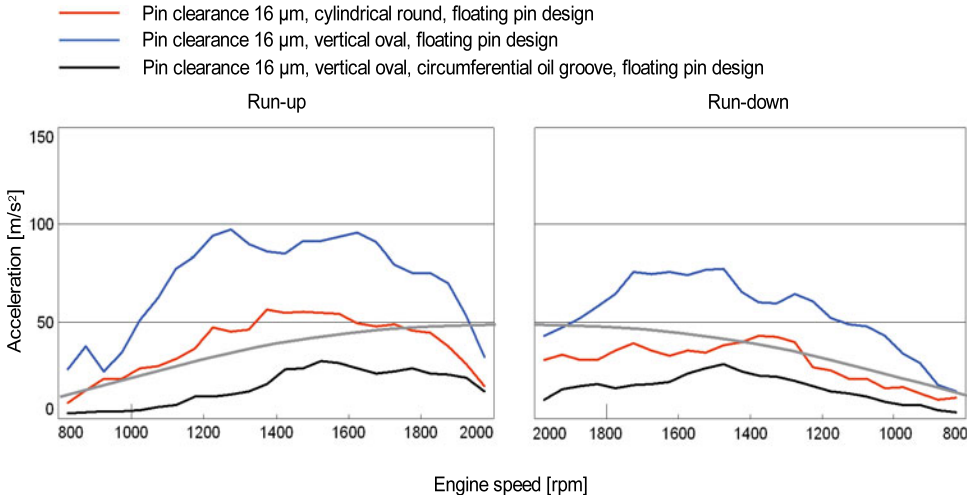

Figure 7.125: Influence of piston pin clearance on the structure-borne noise excitation in a single-sided vertical oval pin bore, with and without circumferential lubrication groove

Figure 7.125 shows the influence of a single-sided vertical oval pin bore, with and without a circumferential lubrication groove, as a potential acoustic improvement measure. In this case, with 16 µm basic installation clearance, a significant increase in structure-borne noise excitation is observed for the single-sided vertical oval pin bore relative to the round pin bore. Other clearance variations show that only a very small basic clearance can provide acceptable acoustic behavior with regard to piston pin noise. Starting at a basic fitting clearance of 8 µm, large accelerations are already evident at the structure-borne noise measurement point on the main bearing cover bolt, along with very clearly audible pin ticking.

When the single-sided vertical oval boss is combined with a circumferential lubrication groove, the test engine used showed a significant improvement in structure-borne noise excitation well below the threshold at which audible pin ticking occurs.

The vertical oval boss is a very effective means for achieving sufficient service life under high loads and can be implemented with no acoustic disadvantages, as long as it is combined with suitable design measures.

7.7.4.2.4 Shaped pin bores

A shaped pin bore is generally a trumpet-shaped expansion of the pin bore diameter, extending toward the inner or outer pin boss, **Figure 7.126**. This measure adapts the pin boss to the piston pin as it bends under the gas pressure. This reduces the maximum edge pressure in the boss area.

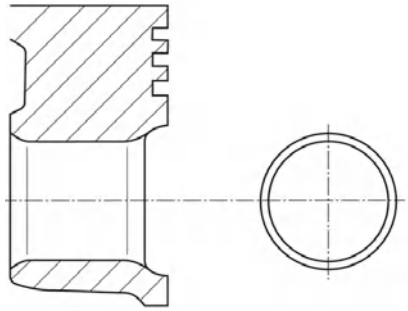

Figure 7.126:
Schematic diagram of a pin bore with inner and outer side shaped pin bore

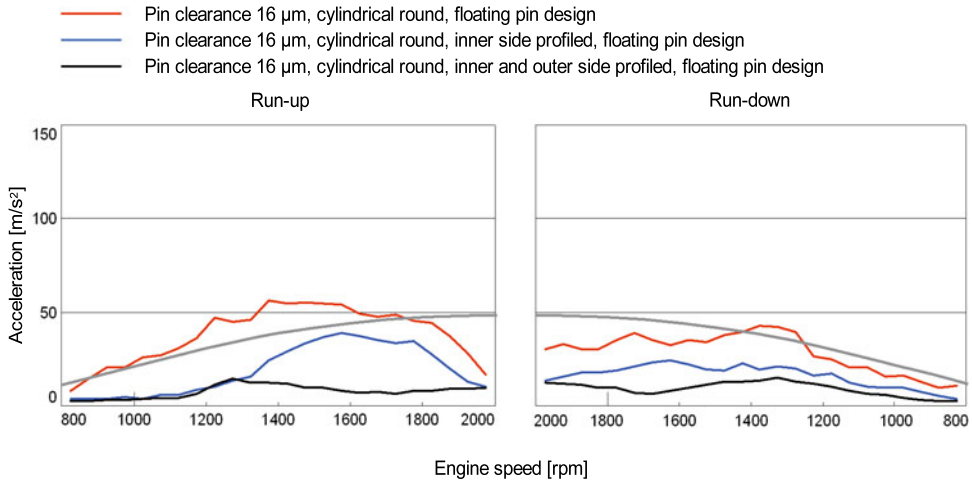

Figure 7.127: Influence of profiled pin bores on the structure-borne noise excitation

Within the noise investigation, variants with such shaped pin bores were tested. The results for this variation are shown in **Figure 7.127** for round pin bores with no ovality. The basic fitting clearance is a uniform 16 µm.

The inner side shaped bore already shows a reduction of structure-borne noise compared to the cylindrical round bore, so that no piston pin noise can be heard. The combination of inner and outer side shaped bores ultimately has the least noise excitation, comparable to that of a 5 µm installation clearance in a cylindrical round pin bore.

This also explains why increased clearance due to wear does not necessarily have to lead to increased noise, because the ovality and form of the bore can also change, thus providing the positive effects described here.

7.8 Cavitation on wet cylinder liners of commercial vehicle diesel engines

In the physical sense, cavitation means the formation, growth, and sudden implosion of vapor bubbles in fluids.

Strictly speaking, cavitation refers to the phenomenon in which vapor bubbles form as a result of a drop in pressure below the vapor pressure curve at a constant temperature; **Figure 7.128**. In contrast, boiling refers to the phenomenon in which vapor bubbles form as a result of an increase in temperature at a constant pressure. This strict view, however, applies only to chemically pure fluids, which are never encountered in practice.

Cavitation is a complex phenomenon that is influenced by many factors. Its complexity is illustrated by the fact that physical processes from hydrodynamics, thermodynamics, chemistry, plasma physics, and optics are all involved in the cavitation phenomenon [24].

Precise knowledge of the causes and effects of cavitation is a basic prerequisite for understanding complex cavitation phenomena on wet cylinder liners of commercial vehicle diesel engines. The two main causes for cavitation on the outside of the cylinder liners, which are surrounded by coolant, are the potentially adverse local flow conditions for the coolant and the vibrations of the cylinder wall caused by gas pressure and inertia forces during a four-stroke cycle.

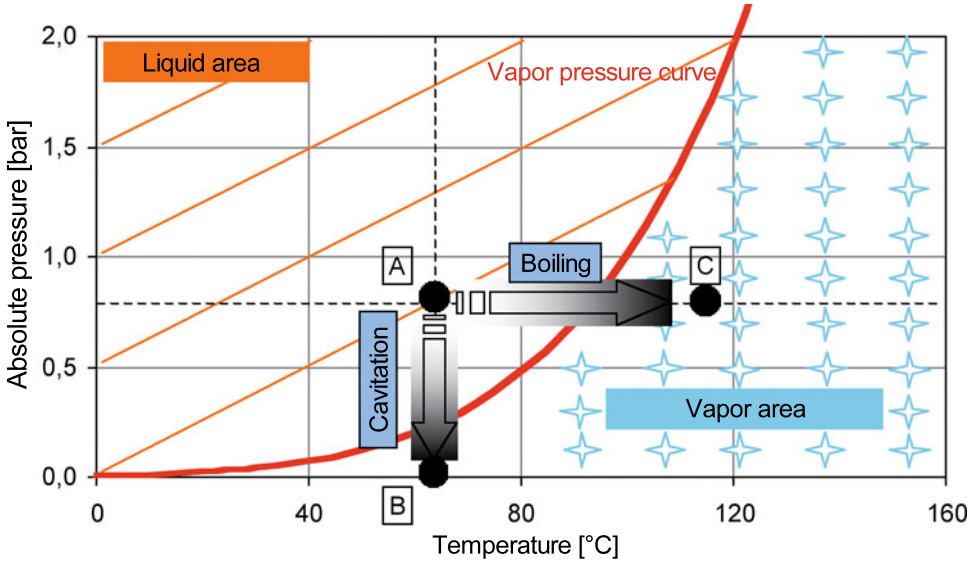

Figure 7.128: Definition of cavitation

Adverse flow conditions are found mainly around very narrow gaps in the coolant channels between the cylinder liner and engine block. Very high local flow speeds occur here, and locally cause both high dynamic pressure and low static pressure in the coolant. This promotes a tendency toward cavitation at the cylinder liner or the engine block.

During a combustion cycle, the piston performs various secondary movements. In particular, these involve multiple contact alterations on the thrust and antithrust sides, with corresponding impacts on the cylinder liner. This excites undesired, high-frequency vibrations in the cylinder liner [25].

The coolant surrounding the cylinder liner cannot keep up with these vibrations. The local static coolant pressure drops below the coolant vapor pressure. When this occurs, cavitation vapor bubbles form. If the coolant pressure rises above the vapor pressure again, then the cavitation vapor bubbles implode suddenly. Their collapsing causes physical and chemical effects, such as high pressure impulses, pressure waves, temperatures, high local flow speeds, and light effects (sonoluminescence). This results in the destruction of the material on the exterior of the cylinder liner where the coolant flows around it. Such phenomenon is known as cavitation or pitting.

Repeated occurrence of the cavitation process in each combustion cycle leads to erosion of the cylinder liner. Depending on how long the engine is operated and the intensity of the cavitation process, it is possible for eroded holes to completely penetrate the cylinder liner; **Figure 7.133**. Coolant penetrating the combustion chamber or the crankcase through these holes causes severe engine damage. Depending on their intensity, visible damage to the cylinder liner can occur due to cavitation after only a few operating hours [26].

Cavitation can occur at any point on the cylinder liner that makes contact with the coolant if the local coolant pressure drops below the coolant vapor pressure.

Two typical indications are characteristic of cavitation on cylinder liners:

- A typical pattern of damage occurs on the thrust side–or, in rare cases, on the antithrust side–in the area of piston contact alteration at the top dead center.
- Cavitation damage occurs in the area of very narrow gaps in the coolant channels between the cylinder liner and the engine block [27].

7.8.1 Basic principles of cavitation

From a theoretical point of view, cavitation occurs when the static pressure in a fluid drops below the vapor pressure associated with the ambient temperature. For flowing media, the fundamental equation for cavitation is derived from the Bernoulli equation. Bernoulli's law for flowing media states that the static pressure is reduced in a constriction, while the dynamic pressure and the associated flow speed are increased. It follows that, for the dynamic pressure of incident flow at a constriction:

$$p_d = p_{tot} - p_{st} = \frac{1}{2} \cdot \rho \cdot v^2$$

p_d: Dynamic pressure

p_{tot}: Total pressure

p_{st}: Static pressure

ρ: Density of the fluid

v: Velocity of the fluid

The characteristic factor for cavitation is the dimensionless cavitation number sigma, also known as the cavitation coefficient. It is calculated as the difference between the static pressure and the vapor pressure associated with the ambient temperature, divided by the dynamic pressure of the incident flow. If the cavitation number is negative, then cavitation will occur in a flow [28].

$$\sigma = \frac{p_{st} - p_v}{\frac{1}{2} \cdot \rho \cdot v^2}$$

σ: Cavitation number

p_v: Vapor pressure as a function of the ambient temperature

7.8.2 The physical phenomenon of cavitation

As mentioned previously, the precise physical definition of the cavitation phenomenon–vapor bubble formation due to a pressure drop below the vapor pressure of the fluid at a constant temperature–applies, strictly speaking, only to chemically pure fluids. In practice, however, chemically pure fluids are not available. Every fluid, including engine coolant, contains weak points (known as seeds), which are the source of all cavitation events. The formation of vapor bubbles due to a pressure drop thus occurs at such weak points, because the fluid breaks down preferentially at these points [29].

They include:

- Gas bubbles in the fluid
- Gas dissolved in the fluid
- Hydrophobic solid particles, known as pore seeds
- Gas formation when flowing past fine peaks of surface roughness (bubble eddies)
- Particles with gas inclusions, which often occur in recesses

7.8.3 Types of cavitation

Cavitation events depend on the behavior of the weak points. Therefore, in real fluids, the categories of

- gas cavitation;
- pseudo cavitation;
- vapor cavitation; and
- cavitation in real flows;

are differentiated; **Figure 7.129**.

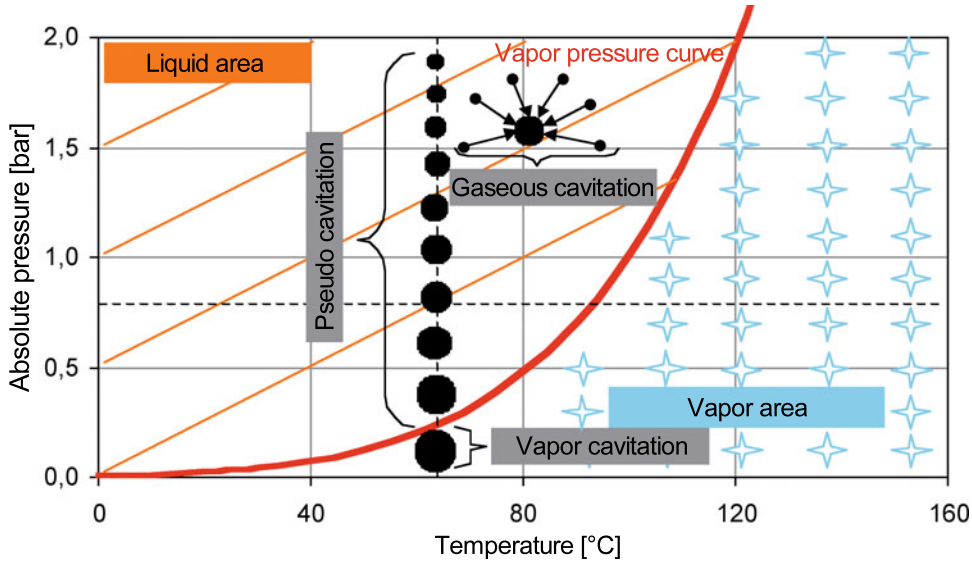

Figure 7.129: Types of cavitation

7.8.3.1 Gaseous cavitation

Gaseous cavitation is a phenomenon in which a gas dissolved in the fluid undergoes a transition to a nondissolved state due to a pressure drop; **Figure 7.129**. The bubbles that form contain the gas components, which were previously dissolved in the fluid (typically air). If the pressure rises again, the bubbles collapse and the gas components dissolve back into the fluid.

In comparison with pseudo cavitation, Chapter 7.8.3.2, and vapor cavitation, Chapter 7.8.3.3, gaseous cavitation is a relatively slow process that actually dampens the implosion of cavitation bubbles occurring with vapor cavitation. In order to minimize this dampening effect when measuring cavitation, the engine coolant is degassed in a degassing run prior to measuring. Gas cavitation can occur above the vapor pressure curve as well.

7.8.3.2 Pseudo cavitation

The expansion of gas bubbles present in the fluid due to a pressure drop is called pseudo cavitation; **Figure 7.129**. Like gaseous cavitation, pseudo cavitation can also occur above the vapor pressure curve.

7.8.3.3 Vapor cavitation

Vapor cavitation, unlike pseudo cavitation or gaseous cavitation, occurs only if the pressure drops rapidly below the vapor pressure. The cavitation bubbles that form are filled with the vapor of the surrounding fluid. If the pressure rises again, then these cavitation bubbles collapse again with an implosive reduction in volume. This phenomenon is called bubble implosion or bubble collapse; **Figure 7.129**. Very high local pressures, shock waves, flow speeds, and, briefly, very high temperatures can occur as a result of this bubble implosion. If the bubble implosion also occurs directly adjacent to a material surface, such as a cylinder liner, then fluid jets (microjets) may also occur.

These effects cause material destruction in the vicinity of material surfaces. Vapor cavitation is therefore responsible for potential material damage to material surfaces. If the bubble implosion is severe enough that the bubbles break up into many smaller bubbles, this is known as transient cavitation [28].

7.8.3.4 Cavitation in real flows

In practice, cavitation occurs as a combination of gas, pseudo, and vapor cavitation. As shown in **Figure 7.129**, bubbles first grow to a critical radius on the cavitation seeds due to gaseous and pseudo cavitation, and when this radius is reached and the pressure correspondingly drops below the vapor pressure curve, this initiates vapor cavitation [30].

7.8.4 Cavitation bubble dynamics and cavitation bubble collapse

Cavitation bubbles form at weak points, which are distributed unevenly in the fluid, often in the form of an entire bubble cloud. The individual bubbles of the bubble cloud are of different sizes. After they form, the cavitation bubbles expand if the static pressure in the surrounding fluid drops further. Substances dissolved in the surrounding fluid can then diffuse into the cavitation bubbles. Many other factors, including thermal and inertia effects, mass distribution, and compression characteristics, as well as the roughness of material surfaces, affect the growth of the cavitation bubbles and bubble implosion [31]. If the static pressure of the surrounding fluid increases again, or if the cavitation bubbles flow into areas of higher pressure, then they collapse suddenly with an implosive reduction in volume. This phenomenon is referred to as cavitation bubble collapse or cavitation bubble implosion.

Depending on the distance between the cavitation bubbles and a solid material surface, cavitation bubble implosion can be classified as either radial (or spherical) or aspherical. During bubble implosion, various effects occur, which cause material destruction in the vicinity of material surfaces.

7.8.4.1 Spherical cavitation bubble implosion

If a cavitation bubble is not near a solid material surface, then the bubble implosion is spherical; **Figure 7.130**. This also requires constant density, constant dynamic viscosity, and uniform temperature distribution in the surrounding fluid. The temperature and pressure distribution in the bubble must also be constant. The cavitation bubble grows constantly from its initial radius. In this case, the pressure in the cavitation bubble is greater than that of the surrounding fluid. The cavitation bubble implosion starts when the maximum bubble radius RM is reached. For a very brief moment, equilibrium exists between the internal bubble pressure and the external fluid pressure. If the external fluid pressure then increases above the internal bubble pressure, then the bubble volume decreases suddenly. The cavitation bubbles implode, and very high pressures and temperatures occur in them. The pressure that builds up in the surrounding fluid at the bubble boundary is emitted outward as a shock wave after passing through the minimum radius.

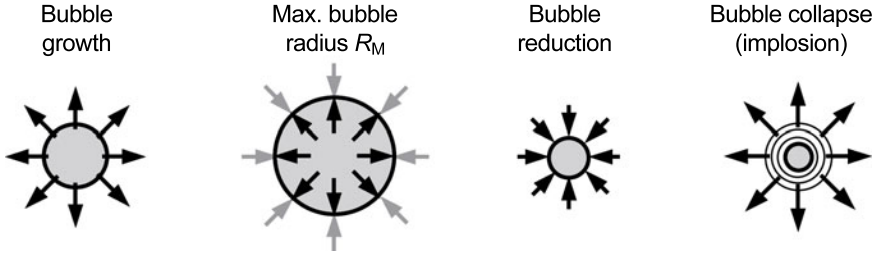

Figure 7.130: Spherical cavitation bubble collapse

7.8.4.2 Aspherical cavitation bubble collapse

If a cavitation bubble is near a solid material surface, or if there are inertia or thermal instabilities, then the cavitation bubble collapse is aspherical; **Figure 7.131** [31]. The cavitation bubble grows radially from an initial radius R_0 to the maximum bubble radius R_M. If the fluid flow in the area around the bubble is disturbed by a solid material surface, such as a wall, then the cavitation bubble becomes unstable. It implodes in a very specific manner, and creates a fluid jet. At the beginning of the implosion or bubble collapse, the side of the bubble furthest from the wall folds inward on itself. A fluid jet forms and shoots through the bubble, then impinges on the opposite bubble wall from the inside. The wall is deformed into a thin cone. After penetrating the opposite bubble wall, the fluid jet impinges on the adjacent material

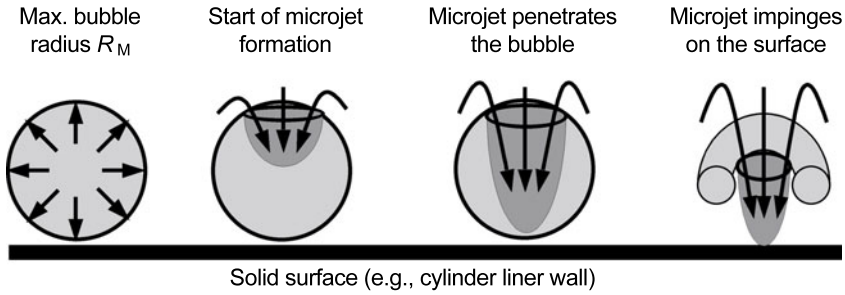

Figure 7.131: Aspherical cavitation bubble collapse

surface. The bubble, now deformed into a torus by the fluid jet, implodes further, also emitting shock waves.

If a cavitation bubble implodes in such a manner that the initial volume is reduced by a large multiple, or if the implosion is particularly severe, then the bubble can disintegrate into a whole cloud of smaller bubbles [32]. The individual bubbles in the cloud can each form fluid jets in the vicinity of the wall, and these jets can influence each other as well.

Fundamental knowledge of cavitation bubble dynamics in the vicinity of solid material surfaces is particularly crucial as they are the source of material damage [28]. For this reason, many experiments have been performed in the field of cavitation bubble dynamics in recent years [33]. Scientific studies have shown that material damage is sure to occur if the dimensional distance parameter γ is less than two. It is defined as follows:

$$\gamma = \frac{s}{R_M}$$

γ: Distance parameter

s: Distance from center of cavitation bubble to material surface

R_M: Maximum radius of cavitation bubble

The most severe damage occurs if the cavitation bubble makes direct contact with the material surface. In this case, the fluid jet reaches the material surface at full speed. The following factors are involved in material destruction by cavitation:

- Fluid jets, which impinge on the material surface with a large impulse value Very high local pressures can occur briefly
- The high internal temperature and pressures in an imploding bubble, particularly when it implodes directly on the material surface
- Shock waves induced by the bubble implosion

It is still not entirely clear which factor is dominant. New experiments have shown, however, that it is mainly the mechanical effects, such as high pressures resulting from the fluid jet, that are responsible for material damage [28]. In addition, the high temperature peaks–though they likely play a subordinate role–can contribute to material damage, despite their extremely short duration [24].

7.8.5 Cavitation damage in wet cylinder liners

Fundamentally, cavitation can occur at any point on wet cylinder liners, which makes contact with the coolant if the local coolant pressure drops below the coolant vapor pressure.

With regard to the pattern of cavitation damage, two different characteristics have been determined:

- A more planar cavitation damage, often on the thrust side of the cylinder liner, but in rarer cases also on the antithrust side.
- A more linear cavitation damage, also known as gap cavitation, which often occurs where narrow coolant channel cross sections are found between the cylinder liner and engine block. The linear cavitation damage is often identified slightly above the seal between the cooling channel and the crankcase. In a more advanced state, it can extend over almost the entire circumference of the cylinder liner.

Figure 7.132 shows a complete cylinder liner, left, with planar and linear cavitation damage. In the right part of the figure, the different types of cavitation damage are shown under magnification. As can be seen, the holes resulting in planar cavitation damage have different diameters and are not uniformly distributed. The cavitation damage shown in **Figure 7.132** occurred after 900 engine operating hours.

The cross-sectional view in **Figure 7.133** shows a magnified section through a 6 mm thick cylinder liner with cavitation damage. As is evident, the “pitting corrosion” caused by the cavitation does not propagate in a single direction; rather, the distribution is more crooked, with local broadening areas. Therefore, the cavitation damage observed on the surface of the cylinder liner is often of only limited value for evaluating the damage.

Fundamentally, the propagation of “pitting” due to cavitation is determined by the stresses arising at the material surface and are transferred to the components of the microstructure. The same applies to the internal stresses present in each material. Depending on the microstructure, grain size, and the hardness and ductility of the cylinder liner material, normal, shear, and internal stresses can arise with varying effects. For example, the microstructure of a cast iron liner contains brittle graphite and hard cementite components. The normal and shear stresses thus arising can then extend only as far as a boundary, such as a graphite lamella. This results in a change in the course of the cavitation damage [34].

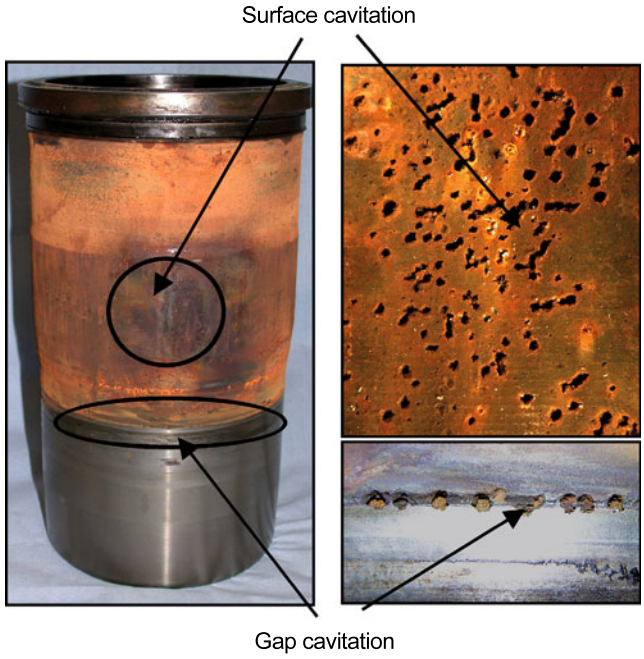

Figure 7.132:
Types of cavitation damage

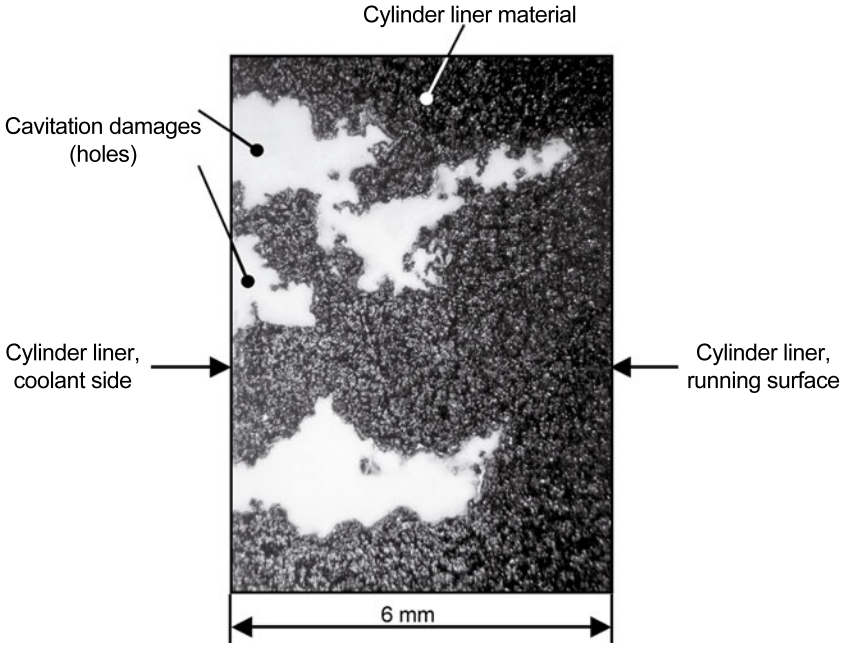

Figure 7.133: Cross section through a cylinder liner with cavitation damage

7.8.6 Cavitation measurement equipment

Cavitation is a complex and highly dynamic phenomenon, regardless of any other influences on engine operation. The entire cavitation process is therefore very difficult to detect for measurement purposes in a running combustion engine. Currently, only the effects of imploding cavitation bubbles in the coolant can be captured. The gauging method for detecting cavitation events in a running combustion engine is therefore based on the measurement of local changes in coolant pressure. Imploding cavitation bubbles lead to local high-frequency dynamic pressure peaks in the coolant. The intensity of these pressure amplitudes is correlated with the severity of the imploding cavitation bubbles. The associated pressure amplitudes can therefore be used as a measure of potential material damage resulting from cavitation.

Special pressure sensors are used for measuring high-frequency dynamic pressure peaks. Precisely determining the position of the potential cavitation damage is a prerequisite for the placement of the sensors. To this end, the engine is fitted with cylinder liners that are painted on the outside. The locations of potential cavitation damage on the cylinder liners can be determined precisely, using a special engine run program and specific cooling system conditions. Placing the sensors typically requires a great deal of machining on the engine block. Care must also be taken that the coolant flow is not significantly negatively affected. **Figure 7.134** shows a cross section through an installed pressure sensor with add-on parts.

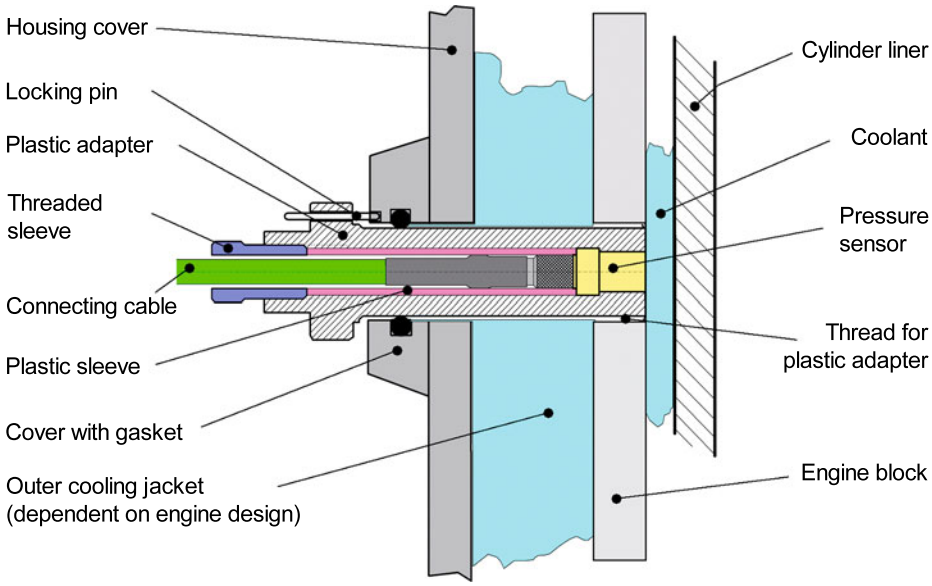

Figure 7.134: Schematic diagram of a section through an installed measurement point with sensor for measuring water pressure

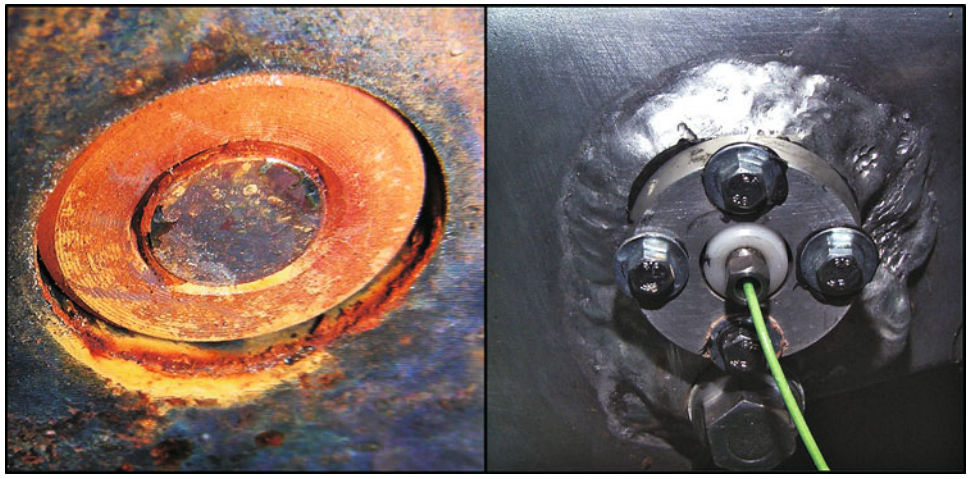

Figure 7.135: Installed pressure sensor on the engine interior where the coolant flows (left), and on the engine exterior (right)

Figure 7.135 shows an installed sensor from the interior of an engine (cooling channel side), left, and from the exterior of the engine, right.

The measurement signals are recorded and numerically processed using a computer-aided data capture unit (KI meter) specially developed for solving cavitation problems. Further processing of the measurement data is done by special PC-based software. **Figure 7.136** shows the complete measurement chain. The data capture unit is able to process the data

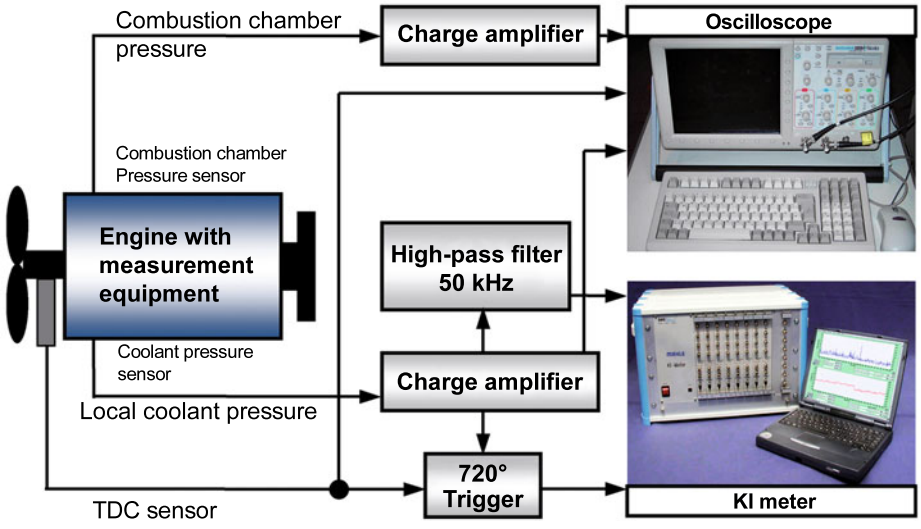

Figure 7.136: Setup of the entire measurement chain for measuring cavitation

from eight cylinders at the same time. Up to 10,000 combustion cycles can be captured for each cylinder.

7.8.7 Cavitation intensity factor and signal analysis

The data are validated on the basis of the analysis of the greatest positive high-frequency pressure amplitude, which is measured at a predetermined crank angle range in every combustion cycle; **Figure 7.137**.

The initial value of the crank angle and the length of the measurement range are determined individually for each engine–depending on the angular position of the crankshaft at which the imploding cavitation bubbles occur. The local coolant pressure curve measured for a measurement window is first conditioned by a high-pass filter so that only the pressure amplitudes that are induced by cavitation bubble implosions ultimately determine the signal curve.

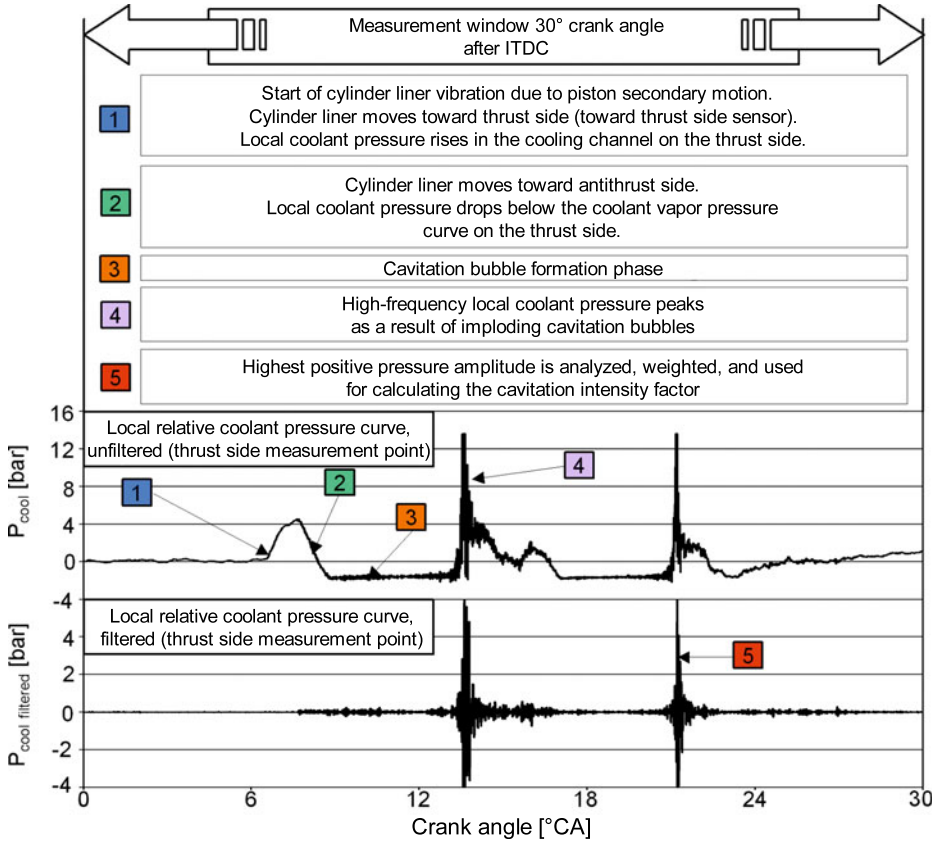

Figure 7.137: Signal analysis of the relative local coolant pressure curve

The greatest positive pressure amplitude in the high-pass filtered signal curve is captured and classified. The cavitation processes, and thus the severity of imploding cavitation bubbles, can be very different from combustion cycle to combustion cycle, even in steady-state engine operation. Therefore, several successive combustion cycles must be analyzed in order to calculate the cavitation intensity factor, KI. Every measured pressure amplitude is assigned to a pressure class based on its level. The number of events in each class is then assigned a weighting factor. The classes that represent greater pressure amplitudes are assigned a greater weighting factor. In order to compare transient and steady-state measurements with each other, the cavitation intensity factor is uniformly standardized to N combustion cycles (standardization constant). It is calculated as follows:

$$KI = N \cdot \frac{\sum_{k=0}^{m} (n_k \cdot f_k)}{c}$$

KI: Cavitation intensity factor

k: Class number

m: Maximum number of classes

n_k: Number of events per class

f_k: Weighting factor

c: Number of four-stroke cycles measured per KI factor

N: Standardization constant

7.8.8 Test bench setup for cavitation measurements

Figure 7.138 shows the test bench setup for cavitation measurements on a six-cylinder inline engine. Two pressure sensors are shown symbolically on cylinder 1 for measuring the local changes in coolant pressure. The cavitation process is influenced by many physical effects. Therefore, for a qualitative analysis of the results, it is necessary that other physical parameters be measured in addition to the local fluctuations in coolant pressure resulting from imploding cavitation bubbles. As **Figure 7.138** shows, the inlet and outlet temperatures of the coolant, the corresponding pressures, and the coolant pressure directly downstream of the water pump are captured, along with the coolant volume flow rate.

In order to influence the cooling system's system pressure and coolant volume flow, regardless of the operating condition of the engine, the test bench is also equipped with external regulators for the pressure in the cooling system. The coolant pump can be driven externally by a controlled electric motor. A coolant pump operation independent of the engine speed is therefore a prerequisite for determining various parameters.

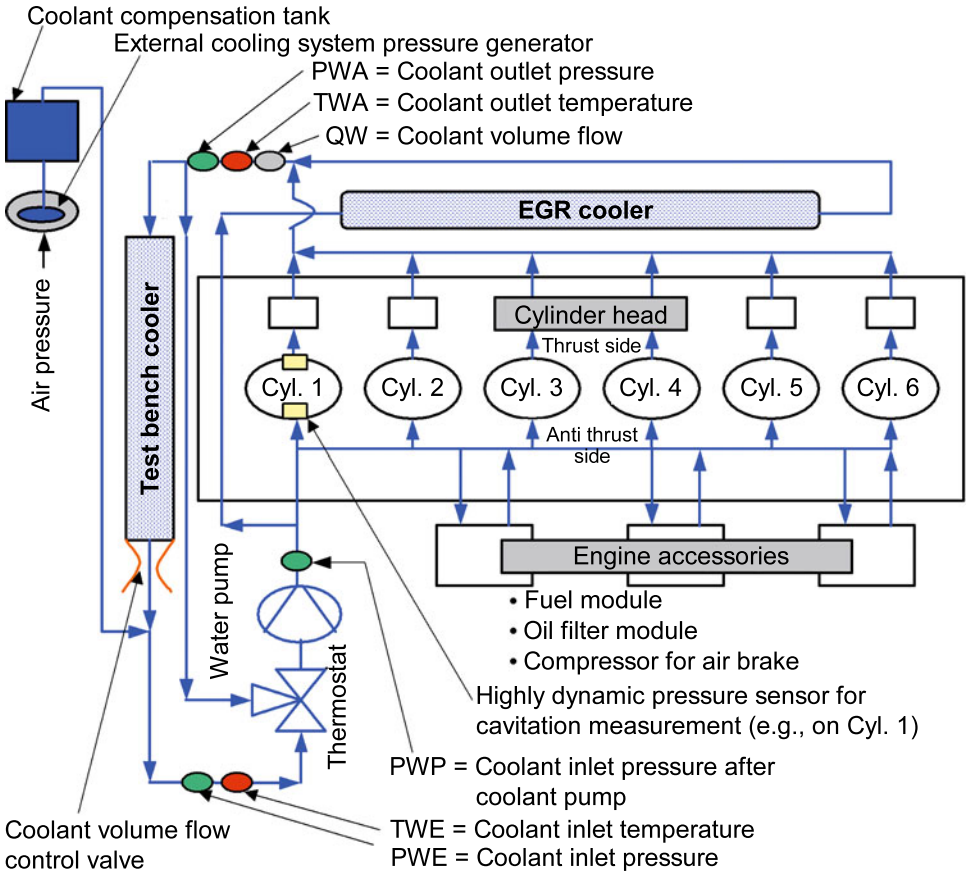

Figure 7.138: Test bench setup for cavitation measurements

The flow conditions can vary greatly within an engine from cylinder to cylinder, and depending on the type and number of engine accessories through which the coolant flows.

7.8.9 Test run programs for cavitation measurements

Cavitation measurements are particularly helpful if the effects of individual parameters can be determined. The best results are obtained with

- steady-state engine operation programs, if the influence of an individual parameter is to be determined; and with
- transient cold-warm programs, if the goal is to determine the greatest cavitation intensity under the least favorable operating conditions. Operating conditions are generated,

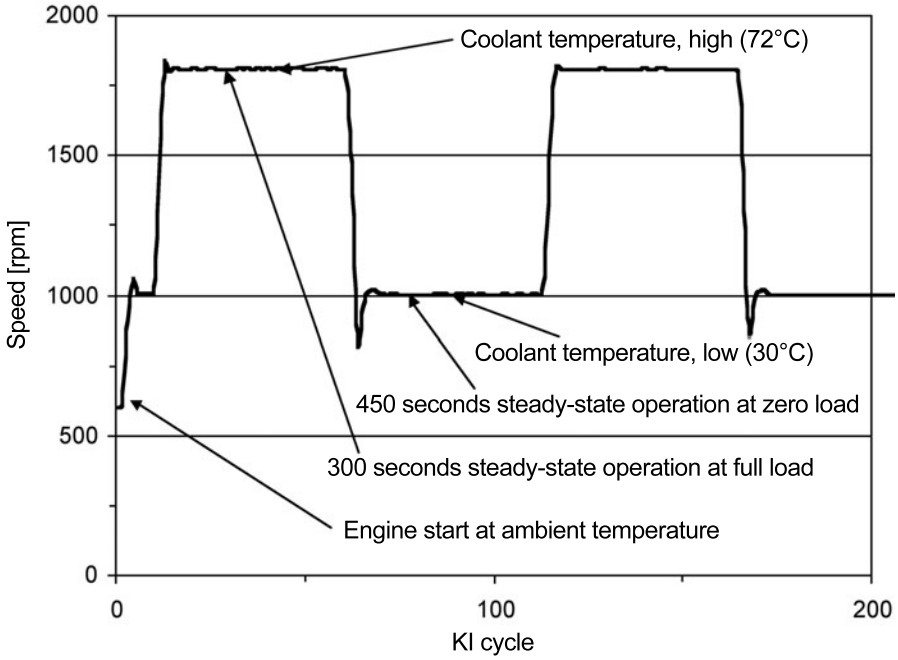

Figure 7.139: Transient test run program for cavitation measurements

in which the various factors affecting cavitation intensity overlap. **Figure 7.139** shows an example of such a program.

7.8.10 Relationship of cavitation intensity to the arrangement of the cylinder and the position on the cylinder

Depending on the design of the cooling channel in the engine and the installed engine accessories, **Figure 7.138**, which are partially integrated in the cooling circuit, the coolant's flow conditions can be very different from cylinder to cylinder. The cavitation intensities, and thus the cavitation damage, may therefore vary. Occasionally only one or two cylinder liners in an engine will show cavitation damage, whereas the others have only slight or no damage. The position of the cavitation damage can also vary from cylinder to cylinder. **Figure 7.140** shows the cavitation intensities measured on various cylinders at various positions. Furthermore it shows the measurement results from a steady-state measurement. As can be seen, the cavitation intensities determined for the lower thrust side measurement positions are significantly greater than for the upper thrust side positions or those on the antithrust side.

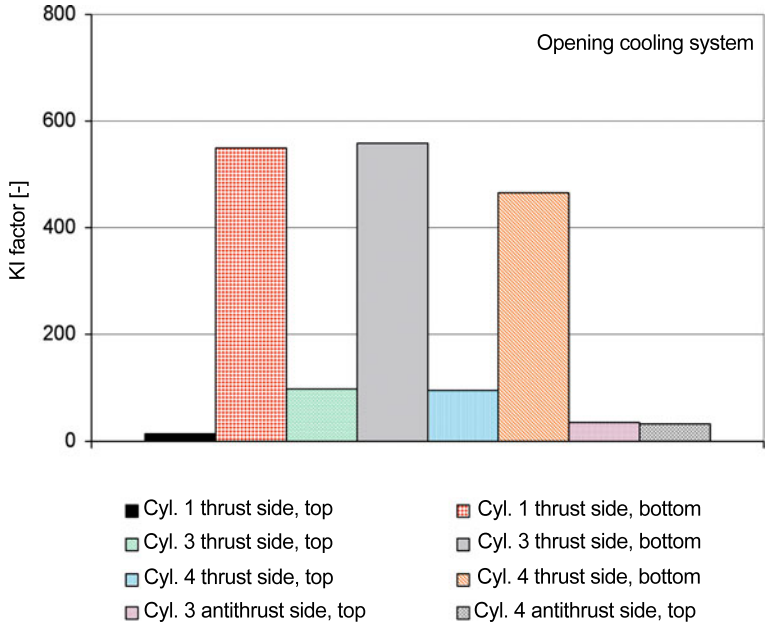

Figure 7.140: Relationship of cavitation intensity to the arrangement of the cylinders and the measurement position on the cylinder

7.8.11 Influencing parameters

Cavitation on wet cylinder liners can be affected by various parameters. The parameters can be fundamentally divided into two main groups:

- The main group of engine operating parameters includes all the parameters, which can be affected by the engine operating conditions. Engine operation parameters include, in particular:
  - Engine speed
  - Load
  - Maximum peak cylinder pressure and characteristic peak cylinder pressure curve
  - Coolant pressure
  - Coolant temperature
  - Coolant flow velocity
  - Chemical composition of the coolant
- The main group of design parameters includes all the design layout options for the piston, the cylinder liner, and the engine block, which minimize the excitation of the cylinder liners and optimize the coolant channel design with regard to cavitation. These parameters include, in particular:

– Various piston types
– Design of the piston skirt shape and the ring belt
– Piston pin offset
– Fitting clearance between the piston and the cylinder liner, and between the cylinder liner and the engine block
– Cylinder liner guidance (top stop, mid stop, bottom stop)
– Shape of the outside surface of the cylinder liners
– Shape of the cooling channel contour in the engine block

7.8.11.1 Effect of engine operating parameters on cavitation

7.8.11.1.1 Effect of engine speed

Figure 7.141 shows the effect of engine speed on cavitation propensity. Based on the fact that the experimental engine is set up on the test bench under near-series production conditions, not all of the influencing factors related to the engine speed could be completely eliminated.

The effect of the coolant pump, for example, and therefore the coolant flow behavior, also depends on the engine speed.

Another factor is that, depending on the data set in the control unit, different characteristic combustion chamber pressure curves and peak pressure values may be set. The excitation of the cylinder liner, caused by the secondary piston motion and affecting the cavitation, can therefore be different at different speeds.

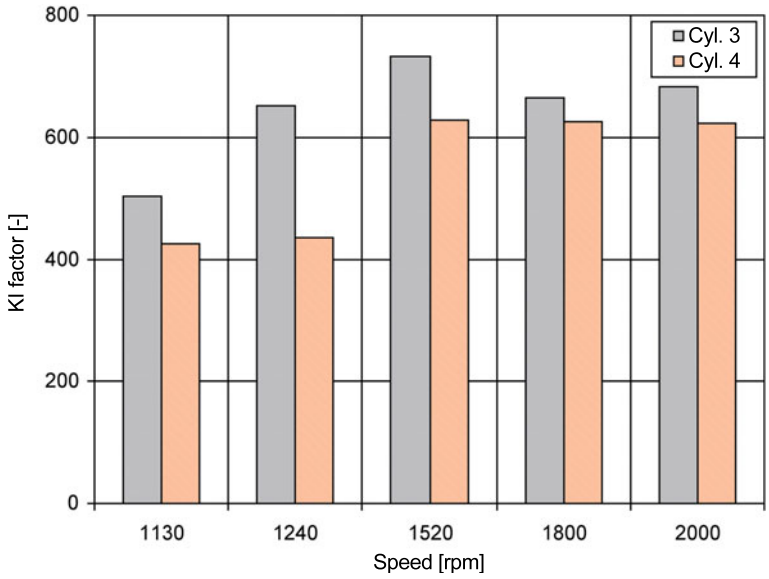

Figure 7.141: Effect of engine speed on the cavitation intensity factor (KI factor)

In the experimental engine under test, the changes in the influence variables presented were small in the higher speed range, and therefore played a secondary role. As **Figure 7.141** shows, the engine speed therefore has nearly no direct influence on the cavitation intensity. Only at low and medium engine speeds can a significant reduction in cavitation intensity be observed. This, however, is mainly the result of the significant changes in the indirect influence variables, and thus does not represent a direct effect of the engine speed.

7.8.11.1.2 Effect of engine load

Figure 7.142 shows the effect of engine load on cavitation intensity at constant engine speed. A clear correlation between load and cavitation intensity can be seen here. With increasing load, and otherwise identical operating conditions, the cavitation intensity clearly increases as well.

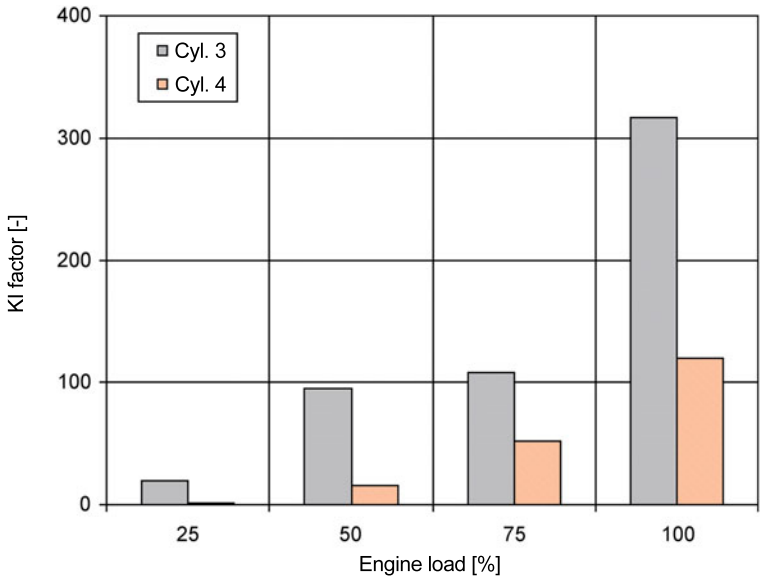

Figure 7.142: Effect of engine load on the cavitation intensity factor (KI factor) at constant engine speed

7.8.11.1.3 Effect of cooling system pressure

Based on the Bernoulli equation and the cavitation number sigma derived from it, it is clear that an increase in static cooling system pressure would theoretically reduce the cavitation intensity. This fact is also confirmed empirically; **Figure 7.143**. With increasing static cooling system pressure, a significant decrease in cavitation intensity can be observed. Depending on the severity of the cavitation that does occur, the static pressure level necessary to achieve a significant reduction may vary greatly from engine to engine. A generally applicable

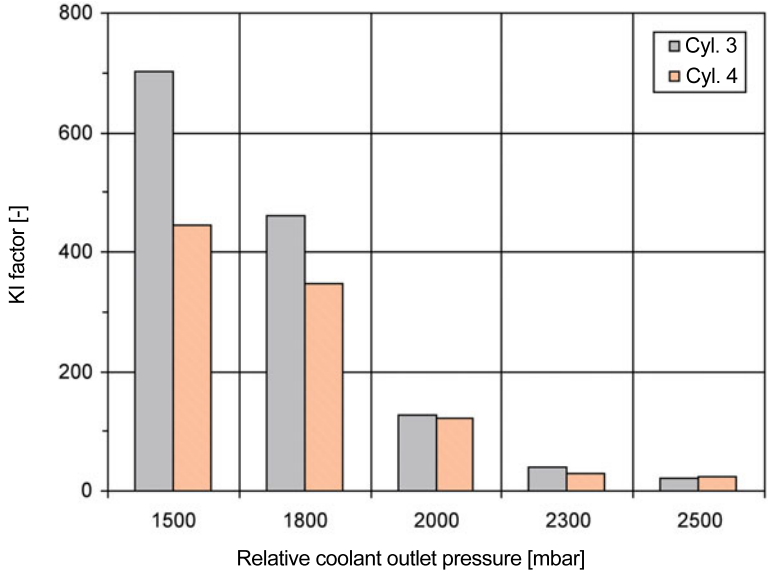

Figure 7.143: Effect of relative coolant pressure on the cavitation intensity factor (KI factor)

value from which cavitation propensity is significantly reduced can therefore not be provided. It must be determined for each engine individually. In practice, a static cooling system pressure that is higher than the pressure resulting from thermal expansion of the coolant can be achieved only with great technical effort, in the form of an additional pressurizing unit. In order to ensure operational safety of the gaskets connected to the cooling system and of the radiator, the maximum possible pressure is also limited. **Figure 7.143** shows the cavitation intensities for steady-state point measurements for various relative coolant outlet pressures at a full-load operating point.

7.8.11.1.4 Effect of coolant volume flow rate

The effect of the coolant volume flow rate, and that of the cooling system pressure, are directly related to each other. A greater coolant volume flow leads to an increase in dynamic pressure, and thus to a reduction in static pressure. This, in turn, is associated with an increase in cavitation propensity.

7.8.11.1.5 Effect of coolant temperature

If it were possible to consider coolant temperature in full isolation, then, theoretically, there would be no direct influence on cavitation. In practice, however, the coolant's temperature cannot be considered in full isolation. Indirect influence variables bring about changes in the temperature.

If the coolant temperature is increased to close to the boiling point in an open system, then vapor bubbles can form. These generally have a damping effect on the occurrence of imploding cavitation bubbles, which decreases the cavitation intensity.

If the coolant temperature is increased in a closed cooling system, then the static pressure rises in the system, due to the thermal expansion of the coolant, thus reducing the cavitation propensity.

Also to be considered is the fact that higher coolant temperatures lead to higher component temperatures, and therefore to lower operating clearances. Lower operating clearances, in turn, have a positive effect in preventing cavitation. In this context, the critical operating clearances are those between the piston and the cylinder liner, and between the engine block and the cylinder liner.

7.8.11.1.6 Effect of coolant composition

It has been empirically demonstrated that, under otherwise identical conditions, visible cavitation damage is often very different depending on the coolant used. As measurements have shown, there are no significant differences in measured cavitation intensities in experiments with different coolants. It is, however, possible that different coolants with the same measured cavitation intensity cause very different levels of cavitation damage. The reason is that a protective coating can form on the cylinder liner depending on the coolant and coolant additives used. This protective coating can have a damping effect on the imploding cavitation bubbles. Depending on the composition of the coolant additives, the damping effect of the protective coating can be more or less effective.

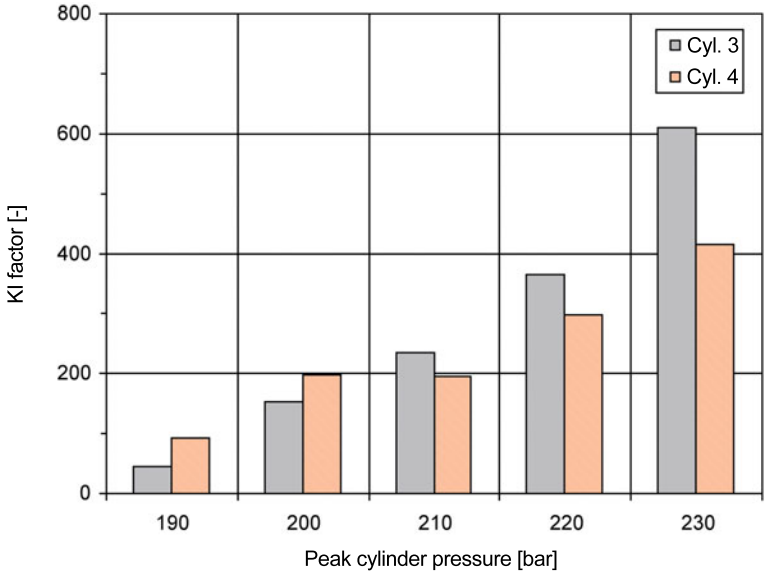

Figure 7.144: Effect of combustion chamber pressure on the cavitation intensity factor (KI factor)

7.8.11.1.7 Effect of combustion chamber pressure

There is a direct correlation between the peak combustion chamber pressure and the cavitation intensity; **Figure 7.144**. The cavitation intensity increases with increasing pressure. The peak combustion chamber pressure from which a significant increase in cavitation intensity occurs is different for every engine. Therefore, a general threshold value cannot be provided.

7.8.11.2 Effect of design parameters on cavitation

The main reason for the occurrence of cavitation is the vibrations in the cylinder liner induced by the piston and its secondary motion.

The group of design parameters, which can be used to directly or indirectly affect cavitation includes all those engine component measures that can reduce vibrations in the cylinder liner and allow optimization of the coolant circuit with regard to cavitation. These engine components include, in particular, the pistons, the cylinder liners, the coolant pump, and the engine block itself. Measures involving the guiding concept of the cylinder liners, the cooling channel shape in the engine block, and the fitting clearances between the piston and cylinder liner, and between the cylinder liner and engine block are also part of this group.

For comparisons of the effects of various design parameters on cavitation, the transient engine test program has proven to be effective.

In the transient engine test program, negative effects promoting cavitation are captured in an overlapping manner. This program allows the cavitation behavior to be analyzed very quickly at various engine speeds, loads, and coolant temperatures. Potential dynamic effects are also included in the analysis. The highest cavitation intensities can be captured using the transient engine test program.

7.8.11.2.1 Effect of piston and cylinder liner fitting clearance

There is a clear correlation between fitting clearance and cavitation intensity; **Figure 7.145**. Accordingly, a reduction in the fitting clearance leads to a lower cavitation intensity. In general, this also applies to the fitting clearance between the cylinder liner and the engine block. The reduction in fitting clearance is limited, however, by seizure resistance.

Initial stages of development serve to determine the minimum possible fitting clearance and to reduce cavitation intensity with additional design measures on the component. Potential measures include changes to the piston shape, piston skirt ovality, ovality of the piston ring land, piston pin offset, piston crown offset, and ring land clearance. Changes in material can also contribute to a reduction in cavitation intensity.

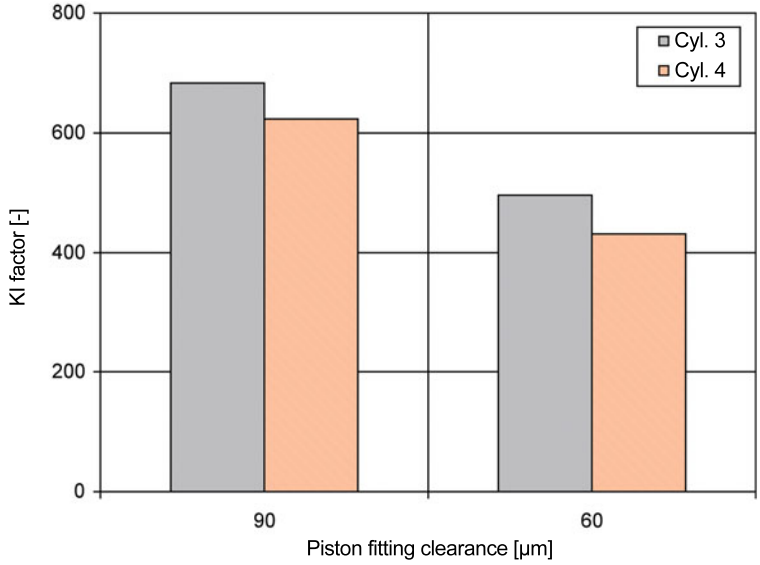

Figure 7.145: Effect of piston fitting clearance on the cavitation intensity factor (KI factor)

7.8.11.2.2 Effect of piston type and piston shape

A typical cavitation behavior can often be determined based on the piston type. **Figure 7.146** shows measurement results for an aluminum piston and an articulated piston (formerly widespread type, with steel crown and aluminum skirt). Compared to other concepts, both piston types have a relatively large fitting clearance in a cold engine due to the thermal expansion behavior of their aluminum skirts. These two piston types in particular, therefore, have very high cavitation intensities in the first stage change in the transient engine test program, immediately after starting the engine. This unfavorable set of conditions is reduced as the engine load and engine coolant temperature increase, because the operating clearances become significantly smaller. The conditions are no longer present in a warm engine. According to **Figure 7.146**, there is a fundamental difference in level between the aluminum piston and the articulated piston. It is evident in all heating stages and is not determined by the piston type here, but rather by a different level of optimization.

As **Figure 7.147** indicates, there are no significant increases in cavitation intensity for steel pistons during the first stage change, immediately after starting the engine. Among the steel pistons tested, the MONOTHERM® piston with a closed skirt had the lowest cavitation intensities. The optimized MONOTHERM® piston with the open skirt, however, also had measured cavitation intensities that were not in the critical range.

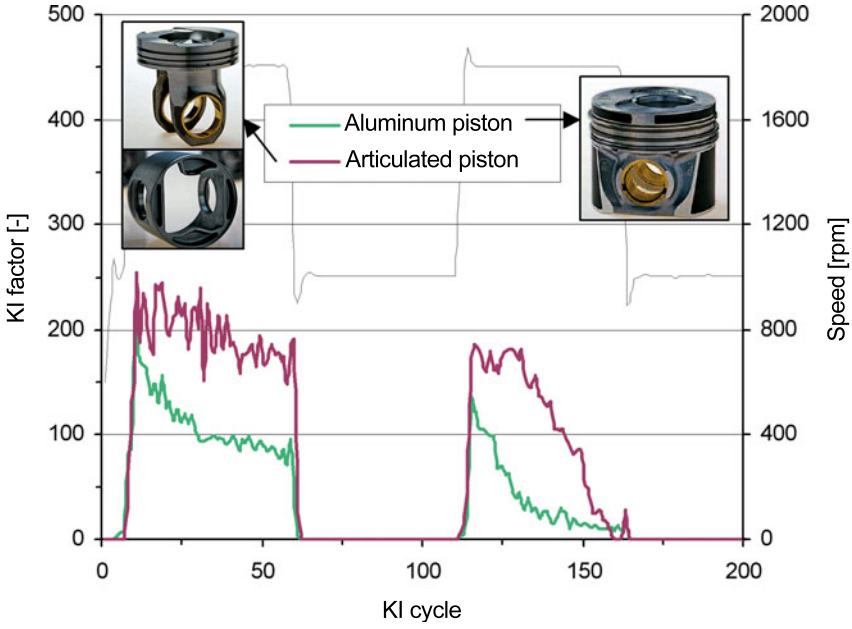

Figure 7.146: Effect of piston type on cavitation behavior

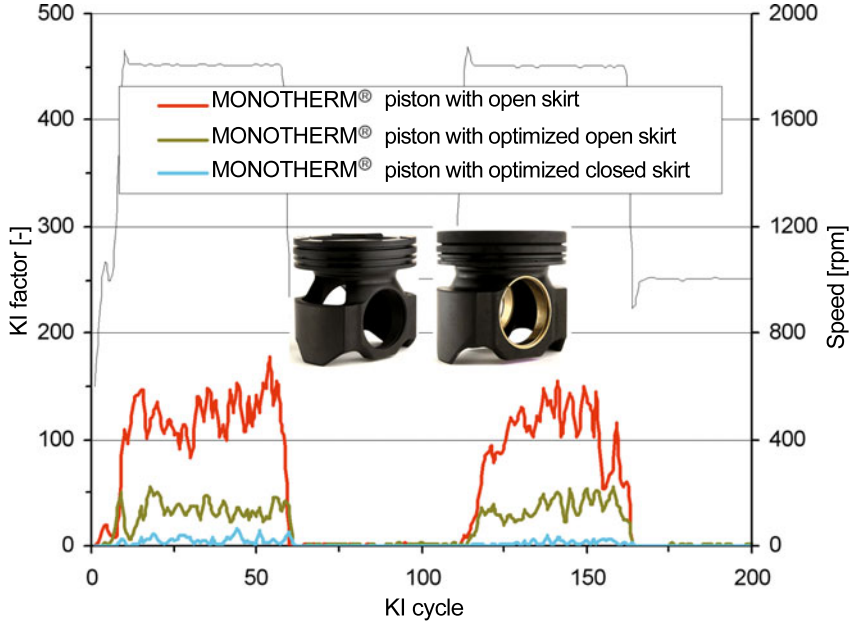

Figure 7.147: Effect of piston type and piston shape on cavitation behavior

7.8.11.2.3 Effect of other piston design adaptations

The design of the piston allows a whole series of options for positively affecting cavitation intensity. They include:

- Reducing fitting clearance (while ensuring seizure resistance)
- Altering the piston skirt (area, gating, profile, ovality)
- Piston pin offset
- Piston crown offset
- Ring land ovality
- Ring land clearance
- Material selection
- Casting process

Such changes, however, must not have any negative effects on the rigidity and deformation characteristics.

Generally applicable standard values for a cavitation-free design cannot be provided. Each change to a design parameter is a specific individual solution for the engine type being optimized. Therefore, successful optimization measures can be applied directly to a different test engine only to a limited degree.

Promising results for reducing the cavitation intensity can be obtained by adapting the ovality (piston skirt and crown), introducing piston pin offset, **Figure 7.148**, and altering the ring land.

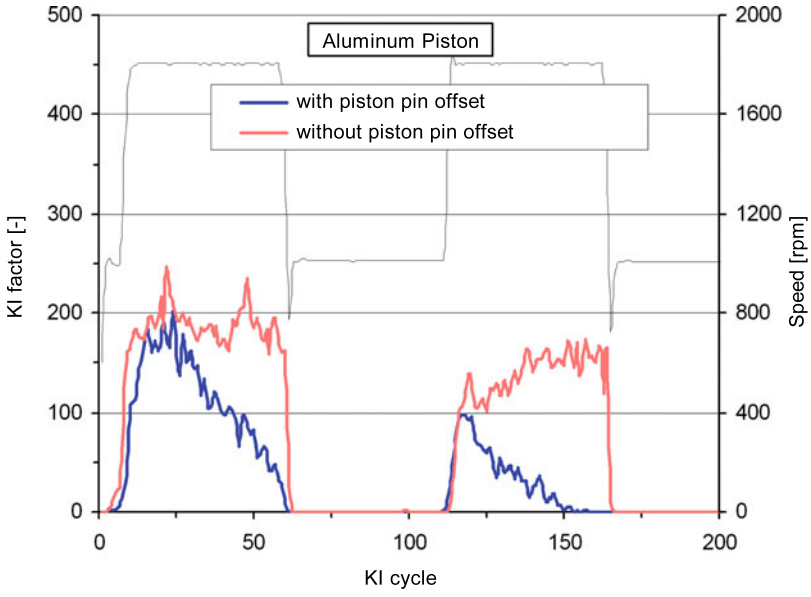

Figure 7.148: Effect of piston pin offset on cavitation behavior

7.8.11.2.4 Effect of design changes to the cylinder liner and cooling channel shape

In addition to design changes to the piston, the cavitation intensity can also be influenced by changes to the cylinder liner and cooling channel. Design parameters, which have the potential to reduce cavitation intensity include:

- Optimizing the cylinder liner guidance
- Optimizing the cylinder liner fitting clearance
- Optimizing the cylinder liner geometry with regard to reducing vibration
- Optimizing the cylinder liner geometry, in combination with changes to the engine block's cooling channel, under the aspect of optimizing coolant flow conditions
- Optimizing the coolant pump, under the aspect of optimizing coolant volume flow rates and achieving the highest possible static pressure component

7.9 Lube oil consumption and blow-by in the combustion engine

The important goals of mechanical development of a combustion engine include low blow-by and minimal lube oil consumption, and thus minimizing raw exhaust gas emissions.

The oil components entering the combustion chamber increase the particle concentration when they are carried out in the exhaust gas, which makes exhaust gas aftertreatment more difficult [35]. Further optimization of the current low levels of lube oil consumption in combustion engines absolutely requires precise understanding of the engine internal oil consumption mechanisms. Such knowledge also helps to expand simulation approaches and their validation.

This article is intended to demonstrate, with examples, the mechanisms leading to lube oil consumption and effective actions that can be taken in the development stage.

7.9.1 Lube oil consumption mechanisms in the combustion engine

The term "lube oil consumption" generally refers to the amount of engine oil by which the amount of lube oil in the engine is reduced over a specified period of time. The entry of fuel and combustion residues or products into the engine oil can give the appearance of a positive lube oil balance, despite an actual consumption of lube oil. Particularly when using biodiesel, an increased level of fuel entry into the engine oil should be expected. Heavy volatile

components in biodiesel do not sufficiently vaporize in the combustion chamber, and can therefore enter the engine oil.

Figure 7.149 shows schematically the various mechanisms as part of a lubricant balance. The exact levels of individual components cannot be provided across the board, because they vary from engine to engine, giving rise to a wide range of boundary conditions. The greatest, most definitive component of consumption, at 80 to 90%, results from the lubricating of the frictional system consisting of the piston, piston rings, and cylinder surface. It necessarily ends up in the exhaust gas in the form of unburned hydrocarbons (HC). Only a small fraction of the lube oil is burned during combustion and can contribute to particle formation with other combustion residues [35, 36].

The fraction of hydrocarbons (HC) in the exhaust gas originating from lube oil is referred to as “oil emission.” The lube oil enters the combustion chamber through various mechanisms, which are described in more detail in this chapter.

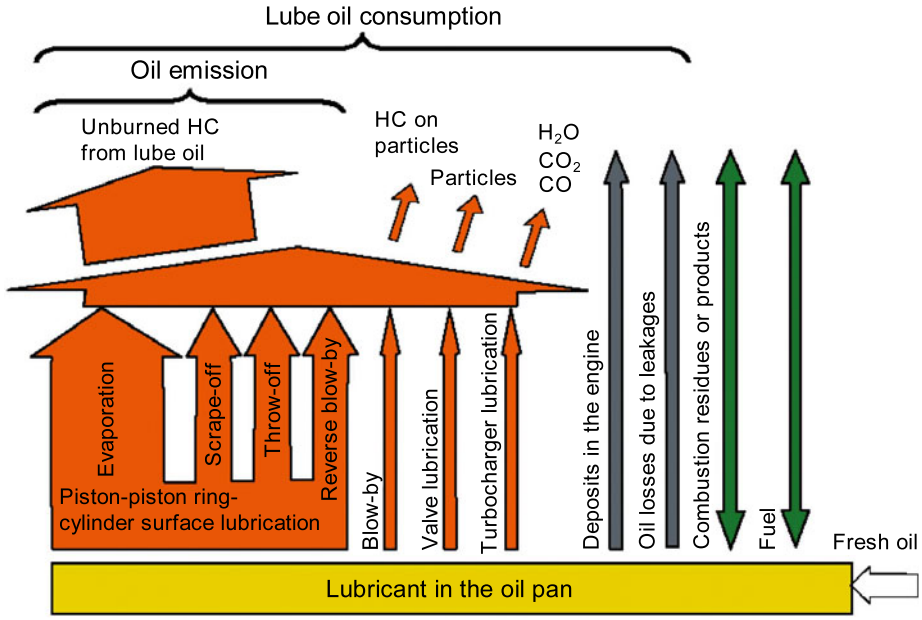

Figure 7.149: Lubricant balance in the combustion engine [36, 37]

Figure 7.150 shows paths through which engine oil enters the combustion chamber. The largest fraction comes from the cylinder surface (1), which is sealed by the piston and piston rings. Additional lube oil enters the combustion chamber through the crankcase ventilation (blow-by), and through the impeller seal in the turbocharger against the intake air (2). Another potential path for oil into the combustion chamber is through the valve stem seal (3).

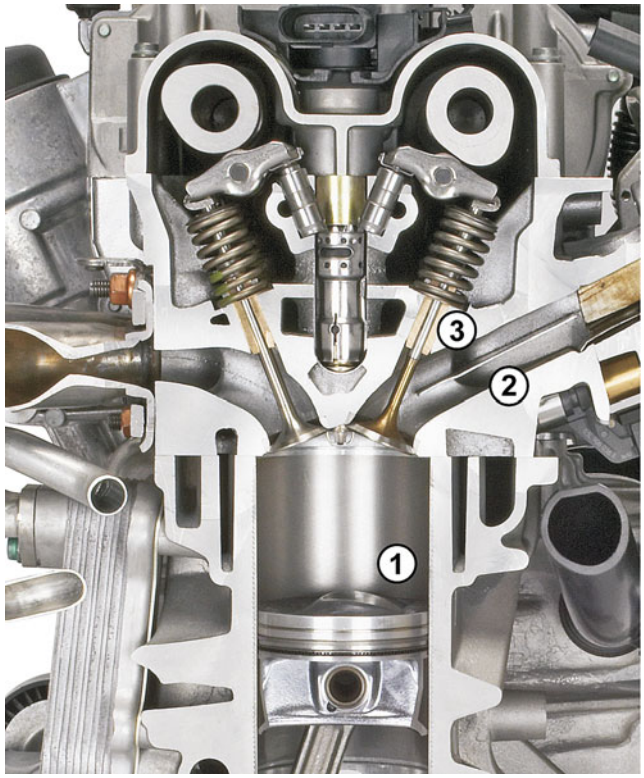

Figure 7.150:
Paths through which engine oil enters the combustion chamber [39]
① Cylinder surface-piston rings
② Crankcase ventilation
② Turbocharger, compressor side
③ Valve stem seal

The causes and mechanisms of lube oil consumption and blow-by can be very complex and interconnected. Individual interactions between oil consumption and blow-by in the area of the cylinder surface and piston rings, **Figure 7.150**, Pos. 1, are examined in the following.

- Severe cylinder distortion can lead to the piston rings sealing insufficiently during engine operation if they can no longer track the contour of the cylinder due to insufficient conformability. The results can be high lube oil consumption and/or blow-by.
- The surface roughness and honing pattern of the cylinder surface permanently affect lube oil consumption via the functional behavior of the piston rings.
- Piston ring geometries that are optimized for low oil consumption, such as sharp scraping 1st piston rings, or piston rings with very barrel-shaped running surfaces, can lead to increased blow-by–particularly under full load–if the gas pressure acting on the ring running face forces the ring away from the cylinder surface .
- Piston ring geometries that are optimally tuned for low blow-by values, such a low axial height of the 1st piston ring, have a positive effect on blow-by behavior at zero load, due to their low ring mass, but can cause increased lube oil consumption under full load, due to their lower rigidity.
- The use of compression rings with a deliberate cross-sectional perturbance, in the form of an inside bevel or an internal angle, can strongly influence the twisting behavior of

the piston rings. An additional inclined position in the ring grooves (disc-shaped or roof-shaped) and optimization of the axial ring fitting clearance can have a positive effect on blow-by behavior, in particular, as well as on lube oil consumption.

- In order to optimize lube oil consumption and blow-by, particularly during dynamic engine operation, the targeted application of chamfers to the top land and ring lands can affect the pressure build-up behind the 1st piston ring in a controlled manner.
- Brief periods of excessively high pressure between the 1st and 2nd pistons rings can cause the 1st piston ring to be forced away from the lower flank of the groove, and thereby increase the lube oil consumption due to "reverse blow-by," Chapter 7.9.1.1. A change in volume between these two rings, in the form of grooves, chamfers, or recesses, and optimization of the gap clearances can lead to faster and more uniform pressure equalization in the intermediate ring space.

7.9.1.1 Lube oil consumption in the frictional system of the piston, piston rings, and cylinder surface

As previously described, the tribological system of the piston, piston rings, and cylinder surface is mainly responsible for overall lube oil consumption in the engine, and therefore for a significant portion of oil emission. This portion is determined by the three oil consumption mechanisms depicted in **Figure 7.151**

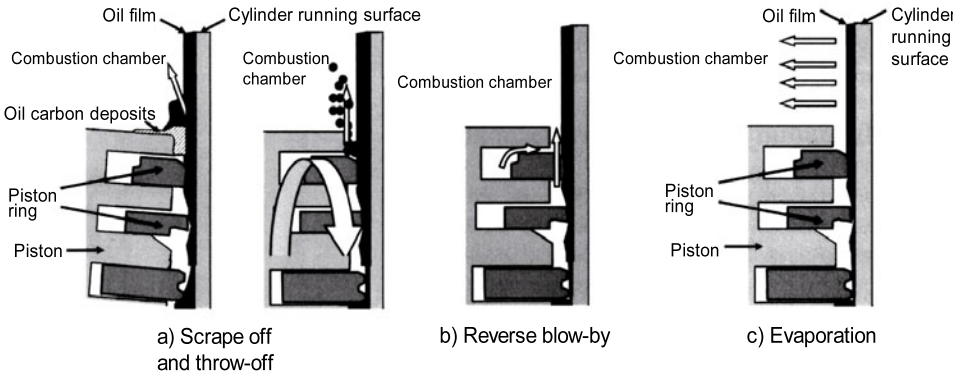

Figure 7.151: Schematic diagram of lube oil consumption mechanisms in the tribological system of the piston, piston rings, and cylinder surface [41]

At operating points with low load, the lube oil can collect on the top land and above the 1st piston ring. The high acceleration and deceleration forces "throw off" these oil droplets directly into the combustion chamber or increase the oil film thickness on the cylinder surface. Oil carbon build-up on the top land can also lead to scraping off the oil from the cylinder surface during the upward stroke; **Figure 7.151 a**.

The second way for lube oil to enter the combustion chamber is known as “reverse blow-by”; **Figure 7.151 b**. The lube oil enters the combustion chamber in the form of a liquid or a mist. The pressure in the area between the 1st and 2nd piston ring can sometimes be greater than the pressure in the top land gap or the combustion chamber. This pressure differential causes the gas to flow back through the ring gap of the 1st piston ring into the combustion chamber. This portion of lube oil can also increase the oil film thickness on the cylinder surface.

Another potential way for lube oil to enter the combustion chamber is “evaporation” of the lubricant from the hot cylinder surface; **Figure 7.151 c**. During the combustion, expansion, and exhaust strokes, the high wall temperatures in the combustion chamber briefly cause the oil film to heat up. This causes partial evaporation of the lube oil. This behavior is highly dependent on the lubricating film thickness and the condition of the lube oil on the cylinder surface. A higher fuel content in the oil film causes lube oil to be evaporated to a greater degree. This effect contributes greatly to oil emission [38].

7.9.1.2 Lube oil consumption through valve stem seals

With the development of effective and wear-resistant valve stem guides and seals, the problem of lube oil consumption in this area is of secondary significance in modern engines.

7.9.1.3 Lube oil consumption through crankcase ventilation (blow-by)

The gas entering the crankcase from the combustion chamber through the piston rings (blow-by) is partially charged with unburned fuel and lube oil from the cylinder surface. After the liquid components have largely been separated, the gas, with the remaining oil components, is fed back to the combustion cycle. This means that the lube oil consumption is directly affected by the blow-by quantity and the quality of the oil separation.

Typical lube oil consumption portions through crankcase ventilation are currently in the range of 1 to 2 g/h. They are definitely interesting because the total lube oil consumption in a modern engine can be well below 10 g/h. Further optimization of the oil separator in the blow-by recirculation systems thus remains an unchanged goal.

7.9.1.4 Lube oil consumption and blow-by in the turbocharger

Blow-by gases enter the oil return of the turbocharger due to the pressure gradient between the compressor or turbine and the crankcase, and thus collect with those from the combustion chamber; **Figure 7.152**. Lube oil consumption through the shaft seal takes place on the compressor side, where the lube oil enters the combustion chamber with the charge air, and on the turbine side, where it enters the exhaust gas. This sealing behavior is dependent on the pressure ratios at the shaft seal and the wear condition of the turbocharger.

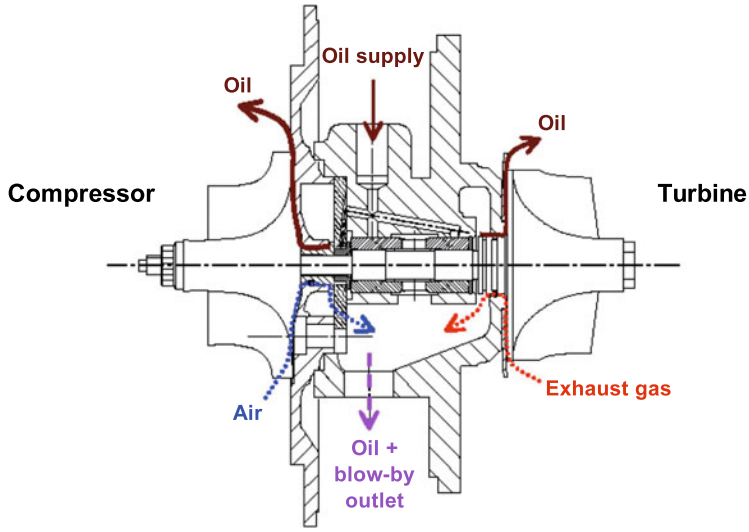

Figure 7.152: Leakage paths for lube oil and blow-by in the turbocharger

Figure 7.153 shows the results of an endurance test on a test bench, where the engine was operated with an external lubrication system for the turbocharger at the end of the endurance run. This allowed the lube oil consumption and blow-by in the turbocharger to be measured.

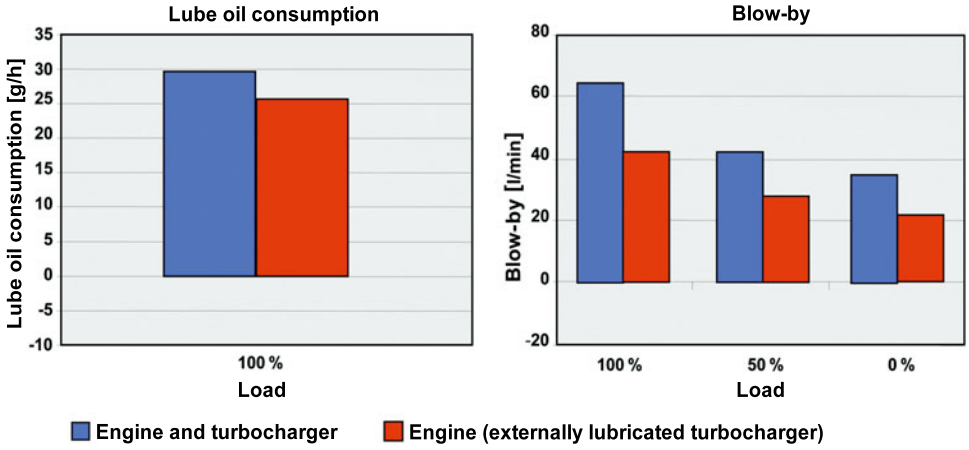

Figure 7.153: Lube oil consumption and blow-by in engine and turbocharger (2.0-liter, four-cylinder diesel engine after a 500 h endurance run)

7.9.2 Lube oil consumption measurement methods

A basic distinction is made between conventional (gravimetric and volumetric) and analytical measurement methods.

Figure 7.154 shows an overview of potential lube oil consumption measurement methods.

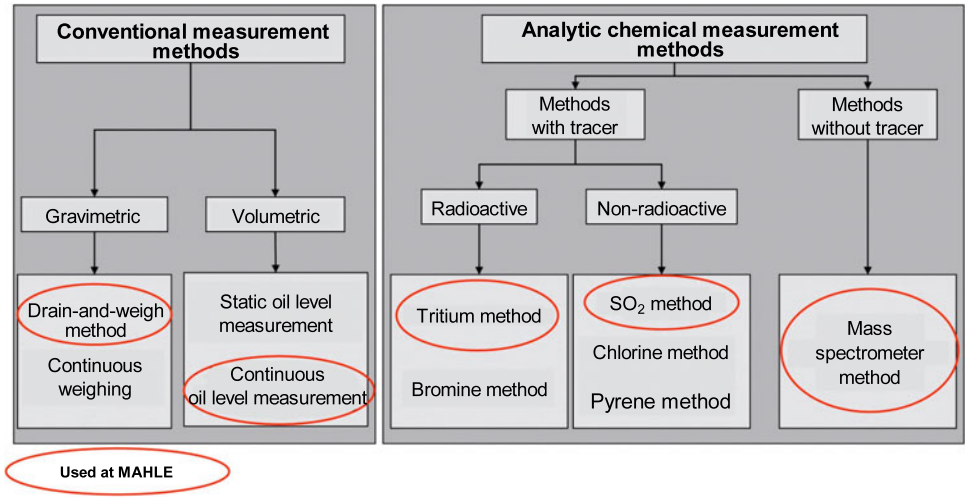

Figure 7.154: Overview and classification of lube oil consumption measurement methods

The conventional measurement methods include:

- Gravimetric:
  - Drain-and-weigh method over a specific time unit
  - Continuous weighing
- Volumetric:
  - Static oil level measurement
  - Continuous oil level measurement

The analytical measurement methods are divided into those with tracers (indicators) and those without tracers. The tracer methods can be divided into radioactive and nonradioactive:

- Radioactive:
  - Tritium method
  - Bromine method
  - ..

- Non radioactive:
  - SO_2 method
  - Chlorine method
  - Pyrene method
  - ...

In conventional measurement methods, the consumed lube oil is measured. Particularly at low levels of lube oil consumption, very long running times are needed, which means high costs.

The analytical tracer methods, in which the concentration of a tracer (marker) from the engine oil is measured in the exhaust gas, can sometimes provide high accuracy in a relatively short running time. These methods are thus ideal to generate lube oil consumption maps.

Such a system, with sulfur as tracer, is shown schematically in **Figure 7.155**, whereas an engine oil with a defined sulfur content is used. By detecting the SO_2 concentration in the exhaust gas, the lube oil consumption in the engine can be derived.

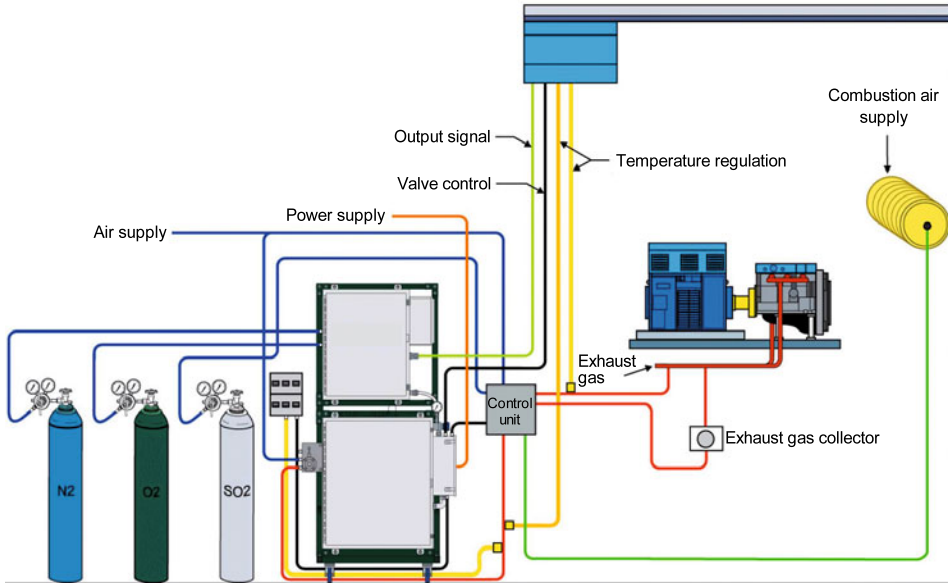

Figure 7.155: MAHLE system for lube oil consumption measurement with sulfur as tracer

Direct, fast online measurement, however, is nearly or completely impossible for transient engine operation when using tracer methods.

Experiments on modern engines show that highly dynamic operation of an engine is exactly what can lead to increased lube oil consumption, and that the most significant potential for improvement is hidden right here. Lube oil consumption maps based on steady-state

operations do not reveal this potential. Only knowledge of the effects on lube oil consumption of rapid changes in load and speed can enable correct design measures to be derived and properly implemented for the piston or piston rings, for example.

With the analytical measurement method without tracer, the oil emission in the exhaust gas can be determined directly. The underlying measurement principle is based on the condition that the hydrocarbons present in the exhaust gas, which can be associated with the fuel and the engine oil, have different molecular chain lengths. In order to measure oil emission, a mass spectrometer optimized for this application is used, and the long chain and heavy volatile HC components associated with the engine oil are separated out [36, 37]. The HC molecules from the fuel and the engine oil are then measured separately using adjustable mass filters.

Figure 7.156 schematically shows a typical mass spectrum for exhaust gas with the usable measurement ranges for gasoline and diesel fuel [36, 37]. Due to the chemical similarities between HC molecules from engine oil and diesel fuel, measurements on diesel engines are particularly challenging. Implementing suitable calibration of the measurement system using the lube oil present in the engine and a known exhaust gas mass flow rate, the lube oil concentrations measured in the exhaust gas can be converted to a mass of oil emitted per unit of time.

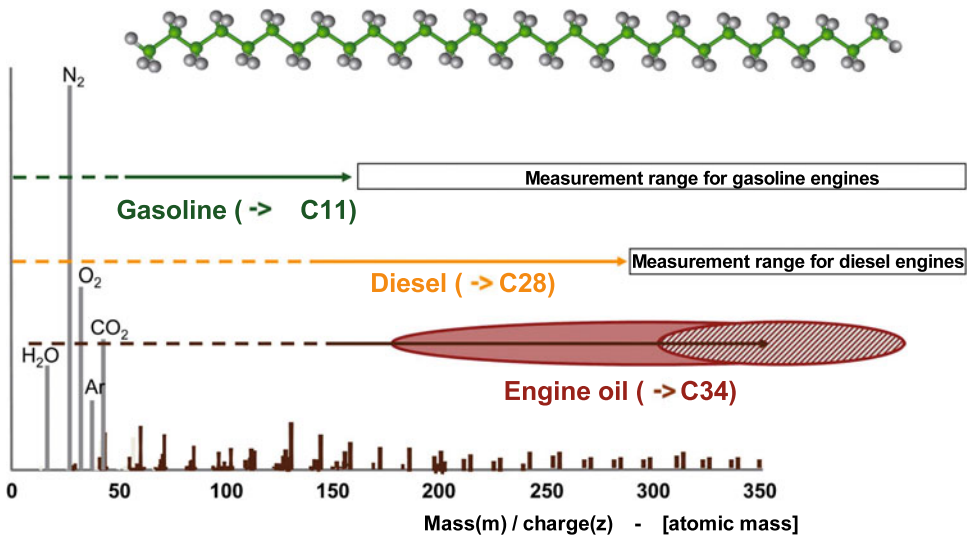

Figure 7.156: Mass spectrum of exhaust gas and usable measurement ranges for gasoline and diesel fuel [37]

The derived oil emissions indicate the amount of lube oil, which is carried off unburned in the exhaust gas. Fundamentally, however, the measured oil emission values should always be viewed in relation to the total lube oil consumption. This also includes the burned oil

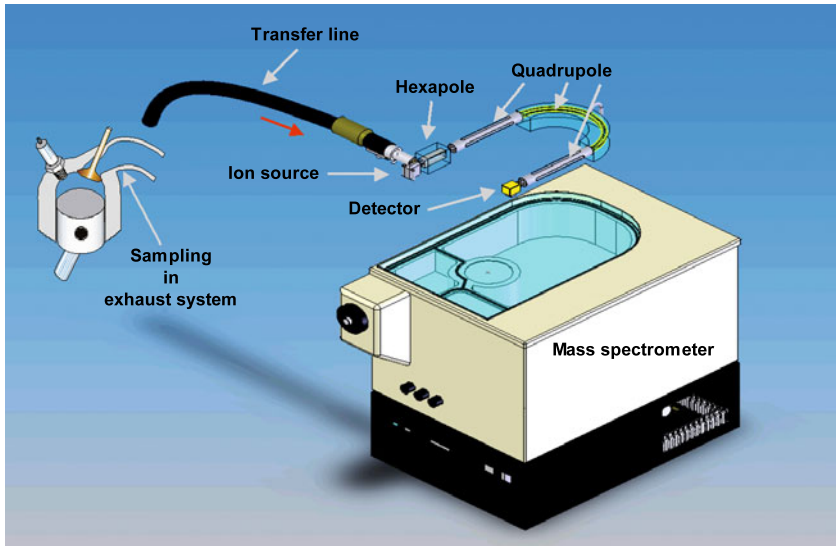

Figure 7.157: Schematic diagram of the mass spectrometer measurement system for analyzing oil emission in exhaust gas [40]

components that are not captured as well as any leakages. In the case of a lube oil quantity balance, the fuel and water components that enter the lube oil and the residues arising from combustion must also be taken into consideration [36, 37].

Figure 7.157 sketches out the Lubrisense 1200 measurement system with heated transfer line, which is used at MAHLE [40].

Since the exhaust gas can be collected immediately downstream of the exhaust valve, it is possible to determine oil emission selectively for each cylinder, and thus to detect cylinder-specific lube oil consumption problems. This fast, online measurement of oil emission can capture the lube oil mass, which is carried off in near real time, even for transient run programs with rapid load and speed changes.

MAHLE has developed special dynamic run programs for such online lube oil consumption measurements, which are used in engine development to reliably identify the operating ranges that are critical for lube oil consumption.

7.9.3 Lube oil consumption maps and dynamic oil consumption behavior

Figure 7.158 shows an example of the lube oil consumption map of a four-cylinder gasoline engine. Lube oil consumption was determined using the described fast oil emission measurement system based at 42 quasi-steady state measurement points (2 to 4 minutes per operating point).

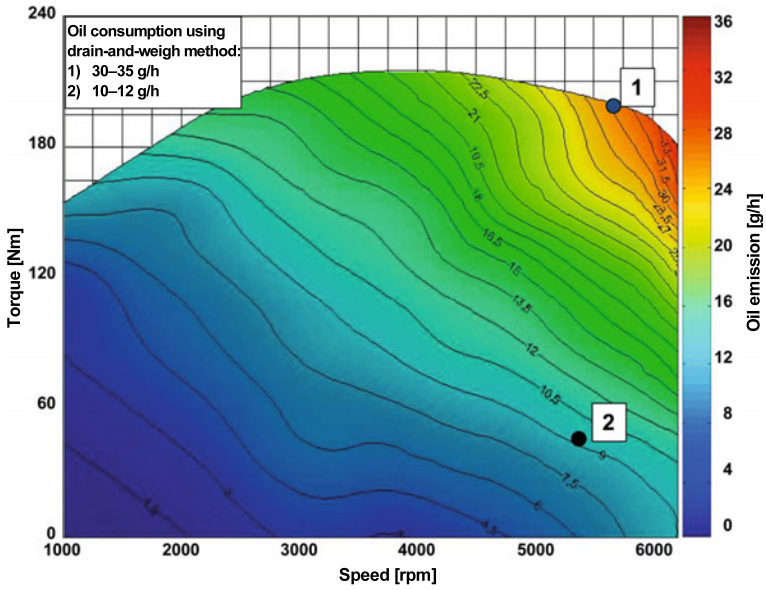

Figure 7.158: Lube oil consumption map for a 2.0-liter, four-cylinder gasoline engine, using fast lube oil consumption measurement; measurement points 1 and 2 measured conventionally

Lube oil consumption was also determined during an endurance test using the drain-and-weigh method at two selected operating points. In order to make definitive statements about the actual quantity of lube oil consumption, the engine was subjected to a steady-state endurance test for 3 times 5 hours at each operating point. This established a good correlation between the oil consumption values measured through the drain-and-weigh method and the lube oil consumption map.

Precise matching of these values cannot be achieved in principle, because the drain-and-weigh method collects not only the lube oil emitted with the exhaust gas but also all the components from the entire lubricating oil balance, including all the fuel components that enter the engine oil.

This relationship between oil emission and actual lube oil consumption can be influenced by a number of external boundary conditions. They include the admixture of biocomponents to fuels, which affect the evaporation behavior and therefore the action mechanisms that are most critical for lube oil consumption. Combustion methods with associated mixture preparation can also play a decisive role in evaporation behavior due to different fuel component levels at the cylinder surface or in the oil film. A correlation between the air-fuel mixture and the measured oil emission has already been demonstrated [38].

Figure 7.159 shows the oil emission of individual cylinders over time during a transient test program. Here again, the lube oil consumption as measured by the drain-and-weigh method matches the cylinder-selective oil emission very well, and no concrete lube oil consumption problem can be detected.

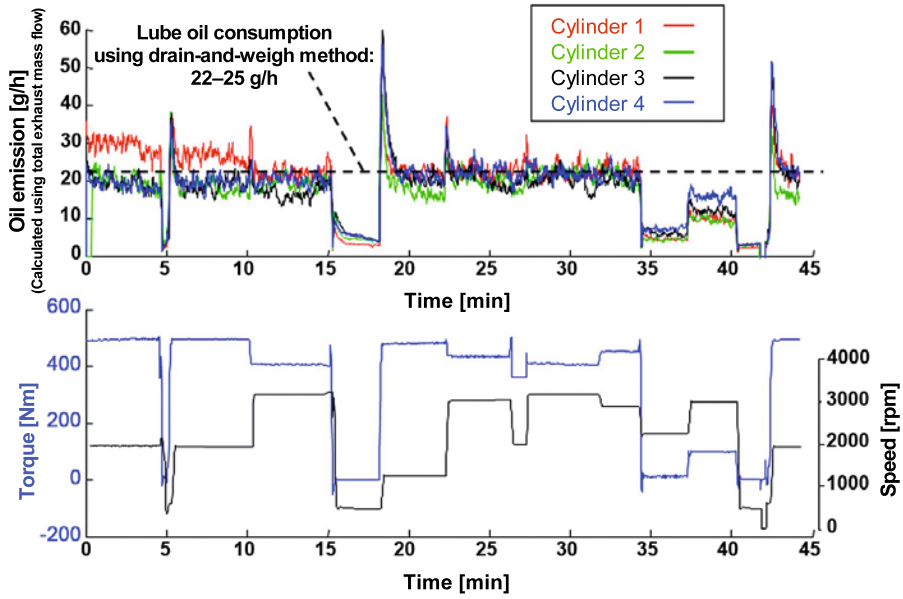

Figure 7.159: Oil emission of individual cylinders over time during a transient test program

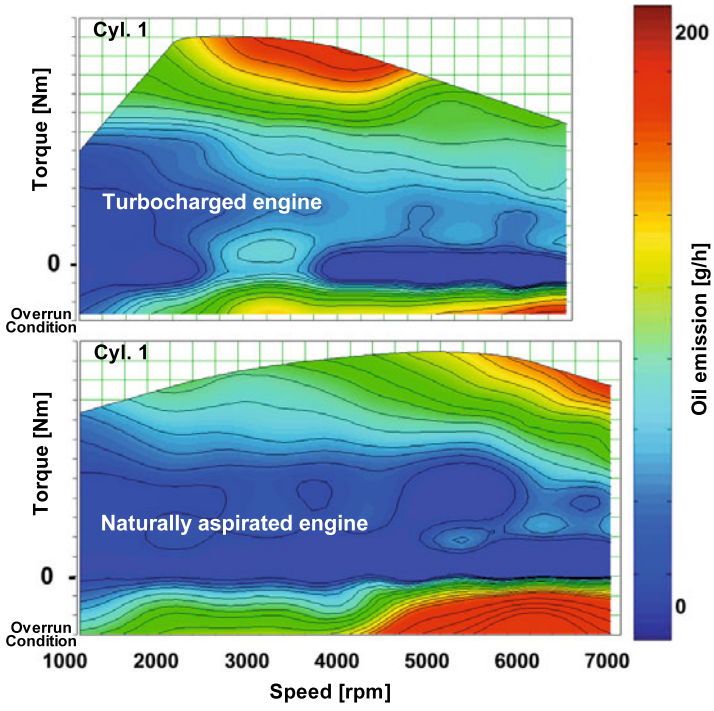

Figure 7.160: Cylinder-selective lube oil consumption maps for a turbocharged (top) and non turbocharged (bottom) gasoline engine–oil emission levels relative to the exhaust gas mass of the entire engine

Figure 7.160 shows additional typical lube oil consumption maps, as they can be measured for gasoline engines with and without turbocharging. These cylinder-selective measurements were performed on engines of similar types and with similar displacements.

Turbocharged engines typically reach their maximum lube oil consumption at medium speeds in the range of maximum torque. Naturally aspirated engines, on the other hand, generally reach their maximum lube oil consumption at full load in the range of maximum engine speed. These phenomena can be observed with measurements of various turbocharged and naturally aspirated engines with different displacements, and are presumably best explained by the location of the maximum cylinder pressures in the characterization map.

Another maximum point for lube oil consumption is often found during overrun condition at higher speeds and, as a rule, is significantly more distinct for naturally aspirated engines than for turbocharged engines due to the different pressure ratios in the intake duct.

For engines with concrete lube oil consumption problems, experience often shows that it is difficult to identify an operating range that is most responsible for the average lube oil consumption. Indications from actual vehicle operation can typically be helpful here.

Critical operating ranges can be clearly identified in a transient lube oil consumption measurement run using the online oil emission measurement system presented here.

Figure 7.161 shows the results of measurements from such a transient lube oil consumption measurement run on a naturally aspirated gasoline engine, which was performed with different piston ring sets. The measurement in the initial state (piston ring pack 1) shows extremely high lube oil consumption in overrun mode and at low speeds; **Figure 7.161**, see operating range B). In this case, this knowledge allowed targeted changes to be made to the ring pack. A direct comparison of the results of both test variants, running the same measurement program, shows that the optimized piston ring pack 2 no longer shows any significant lube oil consumption in operating range B.

The increased lube oil consumption that occurred in overrun mode and at high speeds, **Figure 7.161**, operating range A), is present at the same level in the measurements for both piston ring packs. The changes made to the piston rings did not lead to any significant reduction in lube oil consumption for the indicated operating range A, and must be addressed with other measures.

The average total oil consumption calculated from the oil emission curves does, however, show a significant decrease in lube oil consumption for piston ring pack 2. This result was confirmed in actual vehicle operation.

Beyond such quasi-steady state phenomena, there is a further potential for improvement by analyzing dynamic oil consumption processes. Spikes in lube oil consumption can often be found under highly dynamic changes in load and speed, and their amplitudes and damping times also affect the average lube oil consumption.

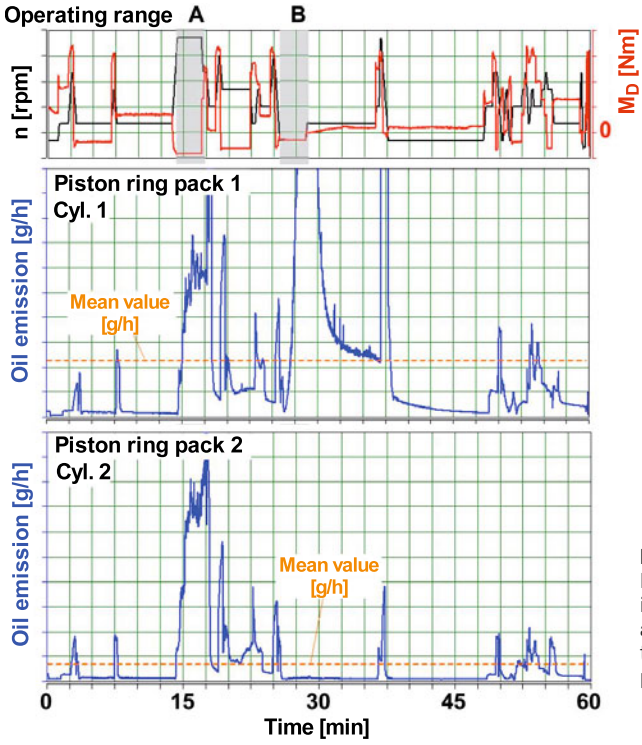

Figure 7.161:
Lube oil consumption curve in one cylinder of a naturally aspirated gasoline engine in a transient program using different piston ring sets

The online lube oil consumption measurement system presented here allows extensive parameter studies to be performed systematically. Suitable measures can be derived from these results, allowing the lube oil consumption to be minimized through targeted changes to the piston and piston rings, optimizing them as a system.

7.9.4 Effect of intake manifold vacuum on lube oil consumption in the gasoline engine

In the past, the effect of intake manifold vacuum on lube oil consumption was typically marked by visible blue smoke in vehicles without exhaust gas aftertreatment systems. In overrun phases at high speed, the intake manifold vacuum extends into the combustion chamber during the valve overlap phase, which increases “reverse blow-by” and thus the quantity of lube oil drawn into the combustion chamber.

Figure 7.162 shows the result of a series of tests in which the lube oil consumption behavior of a naturally aspirated V8 engine was measured as a function of the intake manifold vacuum occurring in the overrun phase of a dynamic deceleration/acceleration engine program. The intake manifold vacuum is varied by the throttle valve position in the overrun phase.

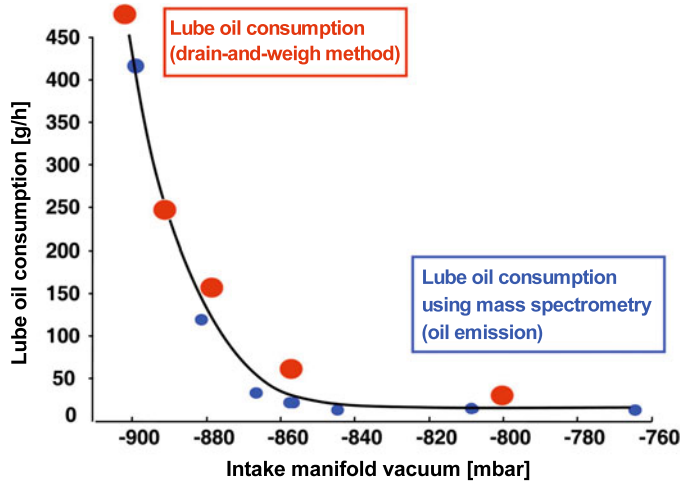

Figure 7.162: Effect of intake manifold vacuum on lube oil consumption and oil emission for a deceleration/acceleration engine program on a naturally aspirated V8 gasoline engine

The lube oil consumptions shown here were determined using two different measurement methods. In order to measure the lube oil consumption using the conventional drain-and-weigh method, the engine ran the deceleration/acceleration program for a long period of time. In parallel, the oil emission in the exhaust gas was captured online using mass spectrometer method.

In this case, a strong increase in oil consumption occurred at very low intake manifold vacuum levels. This relationship was confirmed by further measurements on other naturally aspirated engines.

The advantage of the online oil emission measurement system is the online support for the application engineer responsible for the characterization map, who can thus make appropriate changes with regard to lube oil consumption levels, such as the throttle valve control in this example. The necessary boundary conditions can thereby be established for further reductions in lube oil consumption in order to meet future requirements.

Literature references

[1] Aluminium-Taschenbuch, 14. Auflage, Düsseldorf 1983

[2] Böhm, H.: Aushärtung. In: Aluminium Heft (1963), Nr. 12

[3] Wellinger, K.; Stähli G.: Verhalten von Leichtmetallkolben bei betriebsähnlicher Beanspruchung. In: VDI Z (1978), Nr. 6

[4] Koch, E.: Charakteristik von Kolbenmaterialien unter Berücksichtigung des Verschleißwertes, TH Aachen 1931

[5] Müller-Schwelling, D.; Röhrle, M.: Verstärkung von Aluminiumkolben durch neuartige Verbundwerkstoffe. In: MTZ (1988), Nr. 2

[6] Zustandsschaubild Eisen-Kohlenstoff und die Grundlagen der Wärmebehandlung des Stahles. Neu bearbeitet von D. Horstmann, 4. Auflage, Düsseldorf 1961

[7] Nickel, O.: Austenitische Gusseisenwerkstoffe. In: Gießerei (1969), Nr. 18

[8] Kaluza, E.: Die Wärmebehandlung von Baustählen. In: Industrieanzeiger (1964), Nr. 67/72

[9] Frodl, D.; Gulden, H.: Neue mikrolegierte Stähle für den Fahrzeugbau. In: Der Konstrukteur (1989, Mai)

[10] Informationsschrift des Musashi Institute of Technology, Japan

[11] MAHLE Vortrag: Klopfregelung für Ottomotoren. HDT-Tagung, Berlin 2003

[12] MAHLE Broschüre „KI-Meter“

[13] FVV-Vorhaben Nr. 816: Extremklopfer. Abschlussbericht, Heft 836 (2007)

[14] FVV-Vorhaben Nr. 931: Vorentflammung bei Ottomotoren (2009)

[15] Künzel, R.; Essers, U.: Neues Verfahren zur Ermittlung der Kolbenbewegung in Motorquer- und Motorlängsrichtung. In: MTZ 55 (1994), Nr. 11: S. 636 – 643

[16] Künzel, R.; Tunsch, M.; Werkmann, M.: Piston Related Noise with Spark Ignition Engines – Characterization, Quantification and Mechanisms of Excitation. 9. Congresso SAE Brasil, SAE Paper 2000-01-3311

[17] Gabele, H.: Beitrag zur Klärung der Entstehungsursachen von Kolbengeräuschen bei Pkw-Ottomotoren. Dissertation, Universität Stuttgart (1994)

[18] Künzel, R.; Werkmann, M.; Tunsch M.: Piston Related Noise with Diesel Engines – Parameters of Influence and Optimization. ATT Congress Barcelona 2001, SAE Paper 2001-01-3335

MAHLE GmbH (Ed.), *Pistons and engine testing,* DOI 10.1007/978-3-8348-8662-0,

[19] Künzel, R.: Die Kolbenquerbewegung in Motorquer- und Motorlängsrichtung, Teil 2: Einfluss der Kolbenbolzendesachsierung und der Kolbenform. In: MTZ 56 (1995), Nr. 9, S. 534 – 541

[20] Haller, H.; Spessert, B.; Joerres, M.: Möglichkeiten der Geräuschquellenanalyse bei direkteinspritzenden Dieselmotoren. In: VDI-Berichte Nr. 904 (1991)

[21] Helfer, M.: Zur Anregung und Ausbreitung des vom Kolben erregten Geräusches. Dissertation, Universität Stuttgart (1994)

[22] Gabele, H.: Beitrag zur Klärung der Entstehungsursachen von Kolbengeräuschen bei Pkw-Ottomotoren. Dissertation, Universität Stuttgart (1994)

[23] Werkmann, M.; Tunsch, M.; Künzel, R.: Piston Pin Related Noise – Quantification Procedure and Influence of Pin Bore Geometry. Congresso SAE Brasil, São Paulo, 2005, SAE Paper 2005-01-3967

[24] N.N.: Von der Kavitation zur Sonotechnologie, Department Future Technology of the VDI Technology Center (2000)

[25] Hosny, D. M. et al.: A System Approach for the Assessment of Cavitation Corrosion Damage of Cylinder Liners in Internal Combustion Engines, 1993, SAE Paper 930581

[26] Steck, B.: Cavitation on Wet Cylinder Liners of Heavy Duty Diesel Engines, 2006, SAE Paper 2006-01-3477

[27] Steck B.: Kavitation an nassen Zylinderlaufbuchsen in Nutzfahrzeug-Dieselmotoren – mögliche Einflussparameter zur Vermeidung. 9. Internationales Stuttgarter Symposium Automobil- und Motorentechnik (2009)

[28] Brennen, C. E.: Cavitation and Bubble Dynamics; chap. 1, pp. 1 – 33, chap. 3, pp. 80 – 106. Oxford University Press (1995)

[29] Sauer, J.: Instationär kavitierende Strömungen – Ein neues Modell, basierend auf Front Capturing (VoF) und Blasendynamik, S. 4 – 5. Dissertation, Technische Universität Karlsruhe (2000)

[30] Katragadda, S.; Bata, R.: Cavitation Problem in Heavy Duty Diesel Engines: A Literature Review. In: Heavy Vehicle Systems, International Journal of Vehicle Desgin, vol. 1 (1994), no. 3, pp. 324 – 346

[31] Benjamin, T. B.; Ellis, A. T.: The Collapse of Cavitation Bubbles and the Pressures thereby Produced against Solid Boundaries. In: Phil. Trans. Roy. Soc. London, Ser. A, 260 (1966), pp. 221 – 240

[32] Frost, D.; Stuetevant, B.: Effects of Ambient Pressure on the Instability of a Liquid Boiling Explosively at the Superheat Limit. In: ASME Journal of Heat Transfer, 108 (1986), pp. 418 – 424

[33] Knapp, R. T.; Daily, J. W.; Hammitt, F. G.: Cavitation. McGraw-Hill, New York (1970)

[34] Tandara, V.: Beitrag zur Kavitation an Zylinderlaufbuchsen von Dieselmotoren, S. 13 – 17. Dissertation, Technische Universität Berlin (1968)

[35] Tritthart, P.: Dieselpartikelemissionen: Analysetechniken und Ergebnisse. In: Mineralöltechnik, hrsg. von der Beratungsgesellschaft für Mineralöl-Anwendungstechnik mbH, Hamburg, (1994), Heft 8

[36] Gohl, M.; Ihme, H.: Massenspektrometrische Bestimmung des Ölverbrauchs von Verbrennungsmotoren und dessen Einfluss auf die HC-Emission. FVV Abschlussbericht, Vorhaben Nr. 707, Heft 691 (2000)

[37] Gohl, M.: Massenspektrometrische Bestimmung der Ölemission im Abgas von Otto- und Dieselmotoren. FVV Abschlussbericht, Vorhaben Nr. 758, Heft 764 (2003)

[38] Krause, S.; Stein, C.; Brandt, S.: Beeinflussung der Schmierölemission durch die Gemischbildung im Brennraum von Verbrennungsmotoren. FVV Abschlussbericht, Vorhaben Nr. 933, Heft 901 (2010)

[39] Püffel: Eine neue Methode zur schnellen Ölverbrauchsmessung In: MTZ 60 (1999)

[40] Fa. Airsense Automotive: Informationsbroschüre zum System Lubrisense 1200. Schwerin (2005)

[41] Krause, S.: Massenspektrometrisches Verfahren zur Charakterisierung der Ölverdampfung im Brennraum von Ottomotoren. Dissertation, Technische Universität Hamburg-Harburg (2009)

Dictionary/Glossary

Piston designations and dimensions

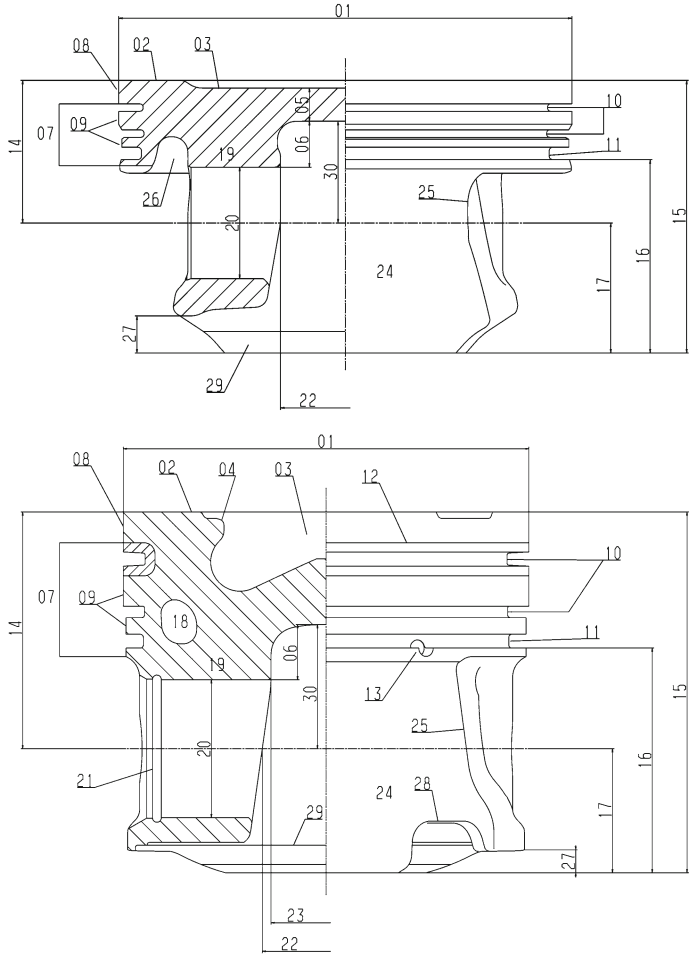

01 Piston diameter
02 Piston crown
03 Combustion bowl
04 Bowl rim
05 Crown thickness
06 Elongation length
07 Ring belt
08 Top land
09 Ring land
10 Compression ring groove
11 Oil ring groove
12 Ring carrier
13 Oil drain (hole)
14 Compression height
15 Total height
16 Skirt length
17 Lower height
18 Cooling gallery
19 Pin boss
20 Pin bore
21 Piston pin circlip groove
22 Pin boss spacing (on pin centerline)
23 Upper pin boss spacing
24 Piston skirt
25 Window
26 Cast undercut
27 Skirt bottom recess
28 Fuel injector cut out
29 Register
30 Inner height

MAHLE GmbH (Ed.), *Pistons and engine testing,* DOI 10.1007/978-3-8348-8662-0,

Shapes of piston crowns

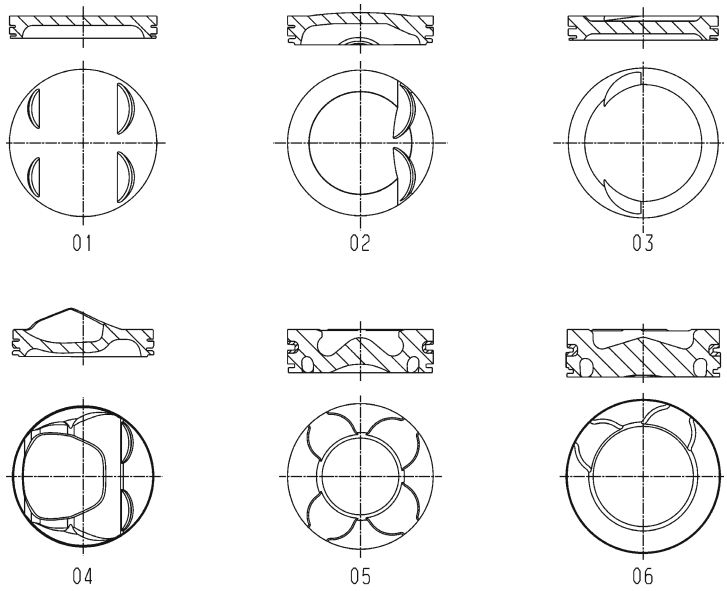

01 Flat crown with valve pockets
02 Cap
03 Flat cavity
04 Cavity for direct gasoline injection piston with stratified charge
05 Direct diesel injection piston with deep, undercut cavity
06 Direct diesel injection piston with flat, open cavity

Top land, ring belt

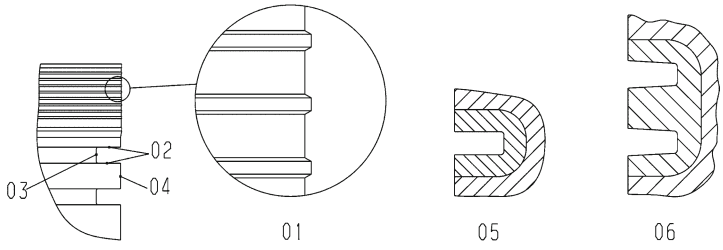

01 Scuff band of top land
02 Groove flank
03 Groove root
04 Ring land
05 Single ring insert
06 Double ring insert

Pin boss support

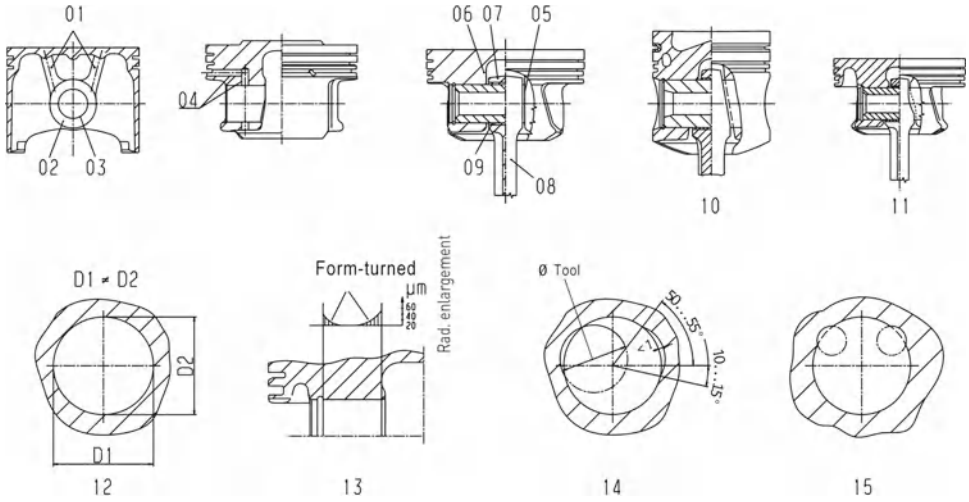

01 Supporting ribs
02 Pin boss
03 Pin bore
04 Pin lubricating holes
05 Parallel boss support
06 Solid boss support
07 Connecting rod small end (small end bore)
08 Connecting rod shank
09 Connecting rod bushing
10 Tapered support
11 Stepped support
12 Oval pin bore
13 Shaped pin bore, convex expansion at one or both sides
14 Pin bore side reliefs
15 Oil slots (generally deeper than side relief, made with a smaller tool and larger tolerances), only for improved lubrication

Piston pins, piston pin circlips

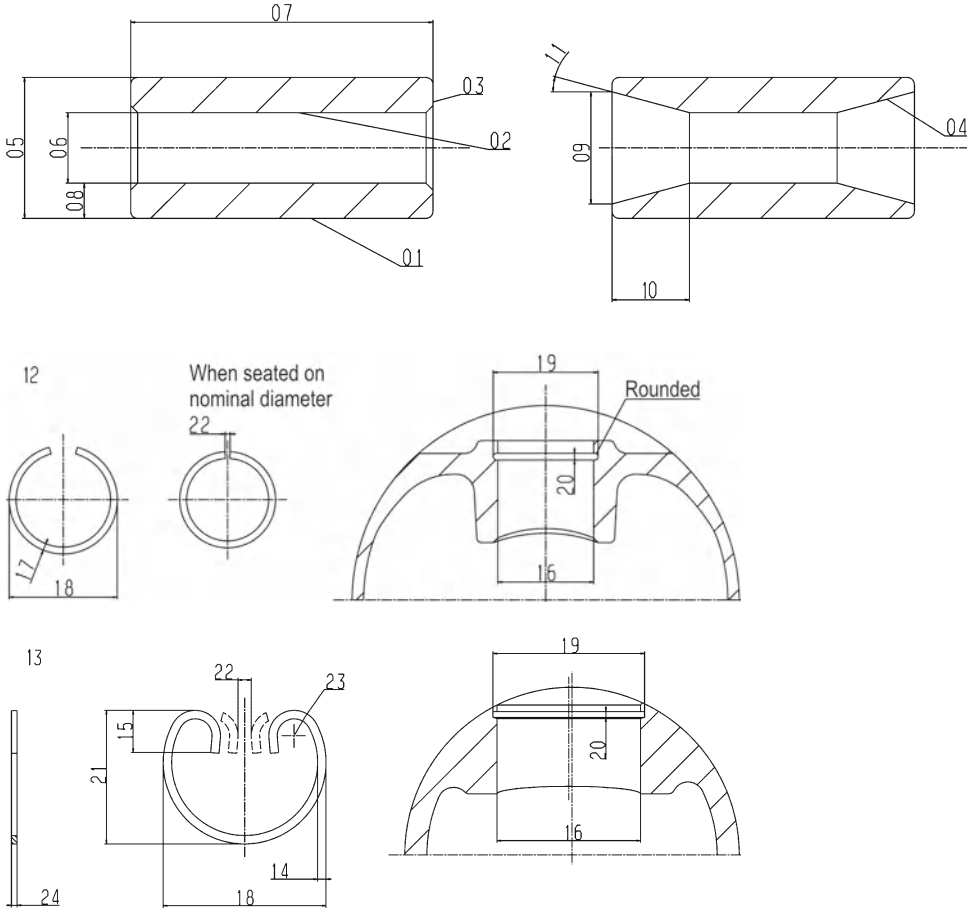

01 Outer surface
02 Inner surface
03 End surface
04 Taper
05 Outer diameter
06 Inner diameter
07 Length
08 Wall thickness
09 Taper diameter
10 Taper length
11 Taper angle
12 Circlip made of round wire, no hook, wire snap ring with no hook
13 Circlip made of flat wire, with hook, square wire snap ring with hook
14 Radial wall thickness
15 Hook length
16 Pin bore diameter
17 Wire diameter
18 Circlip diameter, unassembled
19 Circlip groove diameter
20 Circlip groove width
21 Circlip height
22 Gap width when assembled to nominal diameter (16)
23 Hook radius
24 Thickness

Piston types

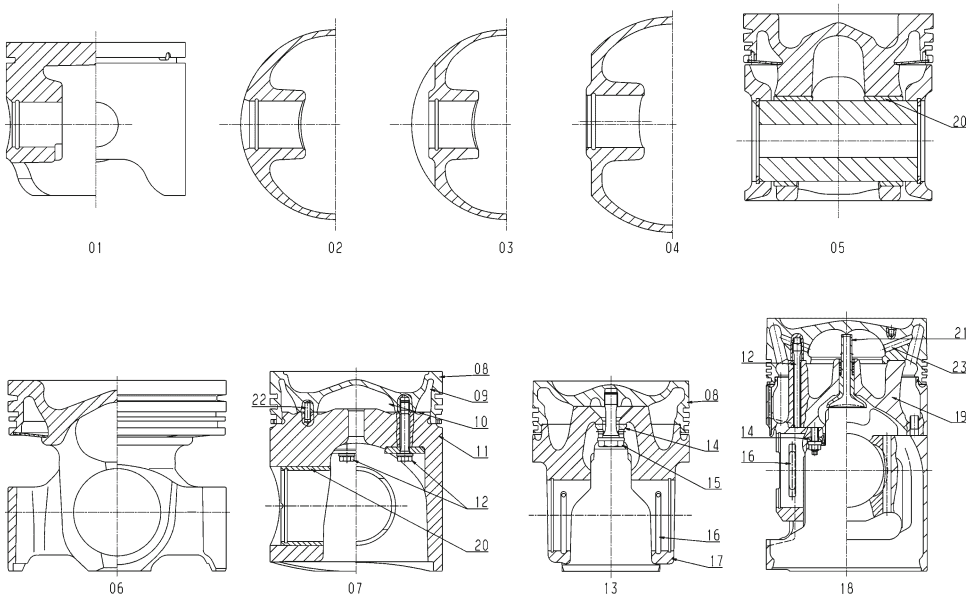

01 Solid-skirt piston
The single-piece piston has no interruptions in its supporting cross sections between the piston crown, ring belt, and skirt, except for any oil return notches.

02 Full-skirt piston
The skirt has a continuous circular surface.

03 Window-type piston
Skirt has a recess near the pin bores.

04 Box-type piston
Skirt recess outside of the pin bores, all the way to the end of the skirt.

05 FERROTHERM® piston
Articulated piston, multi-component piston; piston crown and skirt are connected by the piston pin.

06 MONOTHERM® piston
Single-piece steel piston

07 Composite piston (St/Al)
A multicomponent piston; the piston crown (made of forged steel) is connected to the piston skirt (made of aluminum alloy) using high-strength bolts.

08 Steel crown

09 Outer cooling gallery

10 Inner cooling gallery

11 Aluminum skirt

12 Antifatigue bolt
Multiple screw connection

13 Composite piston (St/St)
A multicomponent piston; the piston crown (made of forged steel) is connected to the piston skirt (made of forged steel) using high-strength bolts.

14 Thrust piece

15 Antifatigue bolt
Central screw joint

16 Oil groove
Provides oil supply from the piston pin to the gallery

17 Steel skirt

18 Composite piston (St/NCI)
A multicomponent piston; the bore-cooled piston crown (made of forged steel) is connected to the piston skirt (here made of nodular cast iron) using high-strength bolts.

19 Nodular cast iron skirt

20 Pin bore bushing

21 Slide shoe
Provides cooling oil supply from the connecting rod small end to the inner gallery

22 Locator pin
Locates crown with respect to the skirt

23 Crossflow holes
Oil passage between outer and inner cooling galleries

Piston cooling

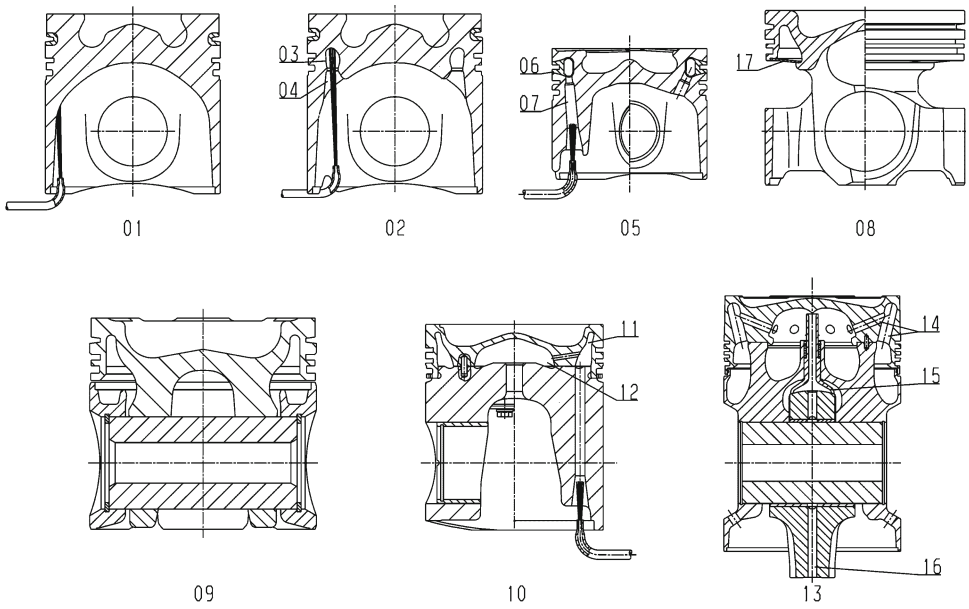

01 Spray jet cooling
Oil is fed via nozzle from the crankcase oil gallery, or via conrod and bore in the small end bore

02 Piston with salt core cooling gallery
Inlet through cast bore; oil is fed via nozzle from the crankcase oil gallery

03 Salt core cooling gallery

04 Funnel (cast)

05 Piston with cooled ring carrier
Drilled inlet bore; oil is fed via nozzle from the crankcase oil gallery

06 Cooled ring carrier

07 Drilled oil inlet

08 MONOTHERM® piston
With closed cooling channel

09 FERROTHERM® piston
With shaker pockets in the skirt

10 Composite piston
Oil is fed via nozzle from the crankcase oil gallery

11 Outer cooling gallery

12 Inner cooling gallery

13 Bore-cooled piston (composite piston)
Cooling oil is fed via conrod and slide shoe to the inner piston cooling gallery

14 Cooling oil bore

15 Slide shoe

16 Pressure oil bore

17 Cover plate

Pin bore offset (schematic)

Offset of the pin axis from the longitudinal piston axis

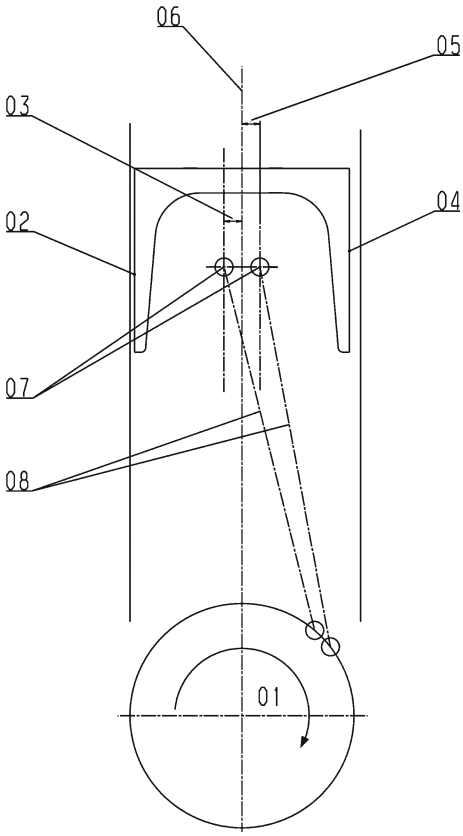

01 Crankshaft rotation, as seen from the control side
02 Thrust side
03 Offset toward the thrust side; typically noise offset and/or to prevent wet liner cavitation
04 Antithrust side
05 Offset toward the antithrust side; typically thermal offset
06 Longitudinal piston axis (cylinder axis)
07 Offset piston pin axis
08 Connecting rod

Technical terminology

Blow-by — see *Blow-by gas*

Blow-by gas — Gas that passes from the combustion chamber, past the piston rings, into the crankcase

Burning mark — Piston ring face marks indicative of local overheating between the piston ring and the cylinder running surface due to lack of oil

Catching efficiency — For evaluating piston cooling, indicates the percentage of the oil delivered by the cooling oil nozzle that flows back into the crankcase from the drain hole(s) of the piston

Cavitation — Local material loss on the water-side of a wet cylinder liner due to the interaction of several physical processes

Cold-start scuffing	Local wear between the piston and the cylinder liner, due to lack of clearance or lubricating oil when the engine is started
Compression height	Distance between the centerline of the piston pin and the edge of the piston crown (top edge of the top land)
Compression ring	First (and second) piston ring
Conformability	Ability of a piston ring to adapt to the noncircularity of the cylinder surface
Cooling gallery	Cooling oil duct(s) in the piston crown/ring belt area for thermally relieving the piston
Crankcase ventilation	Gas passage for the combustion gases that enter the crankcase
Cylinder liner	Liner inserted in the engine block
Cylinder surface	Inner surface of the cylinder bore
First piston ring	First piston ring toward the combustion chamber side
Gap clearance	Spacing of the piston ring ends in the installed condition
Honing	Machining process to produce a defined topographical structure of the cylinder surface
Installation clearance	Difference between the inner diameter of the cylinder liner and the largest piston diameter at room temperature
Keystone ring	Piston ring with tapered side faces on one or both sides
KI factor	Knock intensity factor
KI meter	Device for quantitatively evaluating extreme variations in pressure, such as knocking intensity in the combustion chamber or during a cavitation attack
Knock control	Dynamic control of the ignition point to prevent knocking combustion
Knocking	Irregular combustion of the fuel-air mixture, with some high pressure peaks
Knocking damage	Damage, particularly to the piston top land, due to knocking combustion
Lateral force	Part of the combustion force exerted on the piston that acts perpendicularly on the cylinder via the piston skirt
Normal force	see *Lateral force*
Offset	Offset of the piston pin axis relative to the longitudinal piston axis
Oil control ring	Piston ring designed to remove oil from the cylinder running surface in a defined manner
Ovality	Shape of the relaxed piston ring, such that the contact pressure on the cylinder surface is uniform in the installed state see also *Skirt ovality*

Pin bore	Bore for supporting the piston pin in the piston
Piston	Movable part of the combustion chamber
Piston coating	Coating on the piston skirt, tribologically matched to the cylinder bore
Piston cooling	Heat dissipation and temperature reduction of the piston using engine oil
Piston crown	The part of the piston that bounds the combustion side
Piston pin	Connecting member between the piston and the connecting rod
Piston ring	Slotted, self-tensioning ring
Rectangular ring	Basic shape of a piston ring with a rectangular cross section
Ring carrier	Cast-in insert made of Ni-resist in the area of the 1st piston ring groove in diesel pistons in order to improve the ring groove wear resistance
Ring gap	Open ends of the piston ring
Secondary piston motion	Motion of the piston transverse to its longitudinal axis during a combustion cycle
Shaped pin bore	Pin bore with defined convex end(s)
Shrink-fit connecting rod	Also called fixed-pin connecting rod; connecting rod with a piston pin that is firmly seated in the small end of the connecting rod due to a controlled interference fit
Side faces	Axial surfaces of the piston ring or piston ring grooves
Skirt collapse	Permanent deformation of the piston skirt
Skirt ovality	Noncircular shape of the piston skirt surface, so that a defined contact behavior is achieved in the cylinder
Top dead center wear	Wear on the cylinder surface at the top reversal point (combustion chamber side) of the 1st piston ring
Top land	Area between the edge of the piston crown and the top side of the 1st piston ring groove
Twist	Torsional deformation of a piston ring cross section due to a groove or chamfer on one ring side of the inner diameter

Index

MAHLE GmbH (Ed.), *Pistons and engine testing,* DOI 10.1007/978-3-8348-8662-0,